

UNIVERSITE DE STRASBOURG

2010

THESE

Présentée pour l'obtention du grade de

DOCTEUR DE L'UNIVERSITE DE STRASBOURG

par

Mei-Jin LIN

**Molecular Tectonics: Porous Networks Based on
Hexafluorosilicate Pillars**

UMR CNRS n°7140 : Tectonique moléculaire du solide

Soutenue le 22 Janvier 2010

devant la commission d'examen composée de:

Pr. A. Proust (IUF, Université Pierre et Marie CURIE)	Rapporteur externe
Pr. A. Marsura (Université de Nancy)	Rapporteur externe
Dr. J.-P. Sauvage (CNRS, Université de Strasbourg)	Examineur
Dr. N. Avarvari (Université d'Angers)	Examineur
Pr. M.W. Hosseini (IUF, Université de Strasbourg)	Co-Directeur de thèse
Dr. A. Jouaiti (Université de Strasbourg)	Co-directeur de thèse

“Research is to see what everybody else has seen, and to think what
nobody else has thought”

Albert Szent-Gyorgyi, *Hungarian Biochemist, 1937 Nobel Prize for Medicine*

To my family

Table of Content

Acknowledgements.....	i
Abstract.....	iii
Résumé.....	v
Chapter I: General Introduction.....	1
1.1. Supramolecular Chemistry.....	1
1.2. Molecular self-assembly.....	1
1.3. Molecular tectonics.....	3
1.3.1. The molecular tectons and their designs.....	3
1.3.2. The intermolecular interactions and their energies.....	5
1.3.3. The molecular networks and their geometries.....	6
1.3.4. The molecular packing and interpenetration in solid state.....	14
1.3.5. The conclusions and some comments on the molecular networks.....	19
1.4. Coordination networks.....	19
1.5. The challenges and trends for the coordination network design.....	22
1.6. Design of the project.....	24
1.6.1. Choice of the inorganic anion.....	24
1.6.2. Choice of the metallic cation.....	25
1.6.3. The overview of this PhD thesis.....	25
1.7. References.....	26
Chapter II: Design and Study of the Coordination Networks Based on Rigid Organic Tectons and SiF ₆ ²⁻ Pillars.....	31
2.1. Introduction.....	31
2.2. Design organic tectons (T2).....	32
2.2.1. The choice of donor atom and solvent.....	32
2.2.2. The role of H-bond donor group located within the framework of the tectons (T2) on the formation of the network.....	33
2.3. Construction and modulation of cuboid 3-D coordination networks.....	35
2.3.1. Design and synthesis of rigid organic tectons T2.....	35
2.3.2. Structural studies of cuboid 3-D networks.....	36

2.3.3. Stability and thermal properties of cuboid 3-D networks.....	42
2.4. Changing the central metals of the cuboid 3-D coordination networks.....	44
2.4.1. Structural studies of cobaltic cuboid 3-D networks.....	44
2.4.2. Stability and thermal properties of cobaltic cuboid 3-D networks.....	46
2.5. Functionalization of cuboid 3-D coordination networks.....	47
2.5.1. Design and synthesis of functionalized organic tectons T2.....	47
2.5.2. Structural studies of functionalized cuboid 3-D networks.....	48
2.5.3. Stability and thermal properties of functionalized cuboid 3-D networks.....	50
2.6. Transformation of cuboid 3-D coordination networks.....	52
2.6.1. Design and synthesis of rigid zigzag organic tectons T2.....	53
2.6.2. Structural studies of transformed cuboid 3-D networks.....	53
2.6.3. Stability and thermal properties of transformed cuboid 3-D networks.....	55
2.7. Conclusions.....	56
2.8. References.....	57

Chapter III: Design and Study of the Coordination Networks Based on Semi-rigid Organic Tectons and ZnSiF_6 Pillars.....

3.1. Introduction.....	59
3.2. The coordination networks based on the naphthalene core.....	60
3.2.1. Design and synthesis of naphthalene based organic tectons T2.....	60
3.2.2. Attempt to build coordination networks based on MSiF_6 and naphthalene based tectons.....	61
3.2.3. The coordination networks based on other metallatectons and tecton E2.....	61
3.2.4. The coordination networks based on other metallatectons and naphthalene based tectons.....	70
3.3. The coordination networks based on the spirobiindane core.....	73
3.3.1. Design and synthesis of spirobiindane based organic tectons T2.....	73
3.3.2. Attempt to build coordination networks based on MSiF_6 and spirobiindane based tectons.....	74
3.3.3. The coordination networks based on HgCl_2 and spirobiindane based tectons.....	74
3.4. The coordination networks based on the 1,3,5-triazine core.....	79
3.4.1. Design and synthesis of 1,3,5-triazine based organic tectons T2.....	79
3.4.2. Attempt to build coordination networks based on MSiF_6 and 1,3,5-triazine based tectons.....	79
3.4.3. The coordination networks based on HgCl_2 and 1,3,5-triazine based tectons.....	80
3.5. Conclusions.....	81

3.6. References	81
Chapter IV: Design and Study of the Coordination Networks Based on Flexible Organic Tectons and ZnSiF ₆ Pillars	83
4.1. Introduction	83
4.2. Construction and modulation of tubular 2-D coordination networks	83
4.2.1. Design and synthesis of the flexible organic tectons T2	83
4.2.2. Structural studies of tubular 2-D coordination networks.....	84
4.2.3. Stability and thermal properties of tubular 2-D coordination networks	88
4.3. Functionalization of tubular 2-D coordination networks.....	89
4.3.1. Design and synthesis of functionalized flexible organic tectons T2	89
4.2.2. Structural studies of functionalized 2-D tubular coordination networks.....	90
4.2.3. Stability and thermal properties of functionalized tubular 2-D coordination networks	93
4.4. Design and Construction of helical 2-D tubular coordination networks	93
4.4.1. Design and synthesis of chiral flexible organic tectons T2.....	93
4.4.2. Structural studies of helical 2-D tubular coordination networks.....	94
4.4.3. Stability and thermal properties of helical 2-D tubular coordination networks	98
4.5. From discrete molecular cages to the infinite caged chains	100
4.5.1. Design and synthesis of flexible organic tectons (T2) of specific lengths	100
4.5.2. Structural studies of 1-D caged chain.....	101
4.5.3. Stability and thermal properties of 1-D caged chain	103
4.6. From 2-D to 3-D tubular porous frameworks.....	104
4.6.1. Design and synthesis of the muti-dentate flexible tectons	104
4.6.2. Structural studies of 3-D tubular coordination networks.....	105
4.6.3. Stability and thermal properties of 3-D tubular coordination networks	106
4.7. Conclusions	107
4.8. References	108
Chapter V: General Conclusions and Perspectives.....	109
References	112
Chapter VI: Experimental Part.....	115

6.1. General	115
6.1.1. Solvents and Reagents.....	115
6.1.2. Instruments.....	115
6.2. Syntheses of Organic Tectons	116
6.2.1. The reported tectons	116
6.2.2. The unreported tectons	118
6.3. Crystallization and crystallographic data.....	127
6.3.1. General condition and method	127
6.3.2. The crystallographic data for the products for preparative experiments	128
6.3.3. The crystallographic data for the networks from rigid organic tectons.....	129
6.3.4. The crystallographic data for the networks from semi-rigid organic tectons	139
6.3.5. The crystallographic data for the networks from flexible organic tectons	152
6.4. References	166
Publications	167

ACKNOWLEDGEMENTS

Acknowledgements

I would like to thank...

The members of the jury: Dr. Jean-Pierre Sauvage, Prof. Anna Proust, Prof. Alain Marsura and Dr. Narcis Avarvari who have accepted to evaluate my thesis work.

Prof. Mir Wais Hosseini for giving me the opportunity to work on a fascinating research project and for keeping his door open for discussion at any time.

Dr. Abdelaziz Jouaiti for his patient helps in chemistry and everyday living during these three years.

The work presented here would not have been possible without the help of our excellent crystallographer Nathalie Kyritsakas, who performed all X-ray crystallographic analyses. I also would like thank Dr. M. Coppe for his help concerning NMR spectroscopy.

Dr. Sylvie Ferlay-Charitat for reading and correcting the proof of this manuscript and Dr. Mohammed Kurmoo for his help to prepare administrative documents for entering France.

All my lab colleagues, past and present: Prof. Jean-Marc Planeix, Prof. Véronique Bulach, Dr. Ernest Graf, Dr. Stéphane Baudron, Dr. Domingo Salazar, Dr. Aurélie Guenet, Dr. Marina Kozlova, Dr. Pierre Dechambenoit, Dr. Jérôme Ehrhart, Dr. Yusuke Yoshida, Dr. Cory Black, Dr. Elisabeth Kühn, Dr. Fabrice Eckes, Cristina Carpanese, Dmitry Pogozhev, Thomas Lang, Catherine Bronner, Nicolas Delcey, Katia Nchimi Nono, Nicolas Zigon, Alexandre Gehin and Arnaud Poirel as well as our secretary Valérie Rey and Françoise Rothhut. Thanks you for your help and advices, as well as for the nice atmosphere in the lab.

All my friends who help me during the last three years, in particular my Chinese friends: Xiao-Yu, Jia-Wei, Gao-Ju, Zheng Yuan, Chen Zhang and Yun-Hui, *et al.* Thank you for your help to deal with my French works which made my living in Strasbourg easier.

Marie Curie EST Actions, FuMaSSEC program (Contract N° MEST-CT-2005-020992) for financial support.

Last but not least, I also thank my family, and especially my wife, parents, and parents-in-law for their unconditional support and encouragements.

ABSTRACT

Abstract

In this PhD work, the strategy called molecular networks, which combines molecular recognition processes with iterative self-assembly events, has been used for the design and formation of coordination networks.

With the aim of forming porous materials in the crystalline state offering tailored cavities and avoids, the self-assembly strategy based on combinations of SiF_6^{2-} anion, Zn^{2+} dication and a variety of organic tectons has been studied. These combinations are based on two inorganic tectons (SiF_6^{2-} anion, Zn^{2+} dication) and different organic tectons. The Zn^{2+} cation is used as a metallic structural node and SiF_6^{2-} anion is served as a connector bridging consecutive Zn^{2+} cations into an inorganic pillar. The latter event takes place through the formation of F-Zn bonds by the two F atoms occupying the two apical positions. Finally, the organic tectons are used to interconnect consecutive pillars into a variety of new architectures. In summary, the new approach developed during this thesis consists in considering the (SiF_6^{2-} , Zn^{2+}) couple not as two separate entities but as a pillar and the latter as an infinite tecton for the design of 1-D, 2-D and 3-D architectures.

Depending on the nature (rigidity, length, chirality and denticity) of the bridged organic tectons bridging the pillars, the formation of 1-D, 2-D and 3-D architectures offering inner cavities and different topologies was demonstrated. The new architectures generated have been characterized by physical-chemical methods, including XRD techniques (Single crystal and Powder). The stability of crystals has been investigated by TGA technique and improved by several approaches, including using other metal cations, functionalizing rigid organic tectons, designing new rigid tectons serving as diagonal of cuboid 3-D architecture as well as controlling the packing of 2-D networks.

Keywords: Molecular Tectonics, Coordination Network, SiF_6^{2-} Pillar, Structure Analysis

RESUME (IN FRENCH)

Tectonique Moléculaire: Réseaux poreux à base de pilier ZnSiF_6

La conception et la synthèse de nouveaux réseaux moléculaires de coordination ou MOFs (metal-organic frameworks) connaissent un intérêt très important ces dernières années. Cette classe de matériaux à l'état solide offre plusieurs applications dans différents domaines, tels que le stockage, la séparation et la catalyse. Par conséquent, l'exploration de différentes stratégies permettant de générer de nouvelles architectures jamais décrites est justifiée. Dans ce domaine, l'utilisation de l'approche nommée tectonique moléculaire,¹ centrée sur la conception et les combinaisons de briques moléculaires ou tectons, est d'un intérêt particulier. Ce travail nous permettra d'étendre cette stratégie à l'utilisation du complexe ZnSiF_6 comme tecton inorganique. Il sera centré sur la conception, la synthèse et la caractérisation des réseaux de coordination poreux à base de ZnSiF_6 comme pilier de construction.

L'anion SiF_6^{2-} est une unité intéressante pour la conception des réseaux de coordination moléculaires. En effet, sa combinaison avec les dications tels que Zn^{2+} , Co^{2+} , Cu^{2+} et des ligands organiques entraîne la formation de colonnes résultant d'un « pont » entre deux centres métalliques à travers les deux atomes de fluor qui occupent les positions axiales.² Pour cette stratégie, au lieu de regarder Zn^{2+} et SiF_6^{2-} comme deux entités distinctes, on peut envisager leur association en tant que pilier (Fig. 1a) pouvant être considéré comme un tecton neutre et infini offrant la possibilité de

¹ (a) M. Simard, D. Su, J. D. Wuest, *J. Am. Chem. Soc.*, 1991, **113**, 4696; (b) S. Mann, *Nature*, 1993, **365**, 499; (c) M. W. Hosseini, *Acc. Chem. Res.*, 2005, **38**, 313; (d) M. W. Hosseini, *Cryst. Eng. Comm.*, 2004, **6**, 318.

² (a) R. A. J. Driessen, F. B. Hulsbergen, W. J. Vermin, J. Reedijk, *Inorg. Chem.*, 1982, **21**, 3594; (b) L. R. MacGillivray, S. Subramanian, M. J. Zaworotko, *Chem. Commun.*, 1994, 1325; (c) S.-I. Noro, S. Kitagawa, M. Kondo, K. Seki, *Angew. Chem.*, 2000, **39**, 2082; (d) M.-C. Suen, J.-C. Wang, *Struct. Chem.*, 2006, **17**, 315; (e) M.-C. Suen, Z.-K. Chan, J. -D. Chen, J.-C. Wang, C. H. Hung, *Polyhedron.*, 2006, **25**, 2325.

construire des architectures de dimensionnalité 1-D (Fig. 1b), 2-D (Fig. 1c) ou 3-D (Fig. 1d) possédant des cavités internes. Ces dernières sont obtenues *via* la sphère de coordination autour du métal Zn^{2+} (quatre sites disponibles occupant les coins d'un carré) répartis régulièrement (tous les *ca* 7,5 Å) le long du pilier. Ainsi, selon la nature du tecton organique pontant entre les piliers, on peut contrôler à la fois la dimensionnalité (1-3 D) du réseau ainsi que la forme, la taille et la nature des cavités et canaux. Basé sur la diversité des tectons organiques utilisés, ce travail est subdivisé en trois parties.

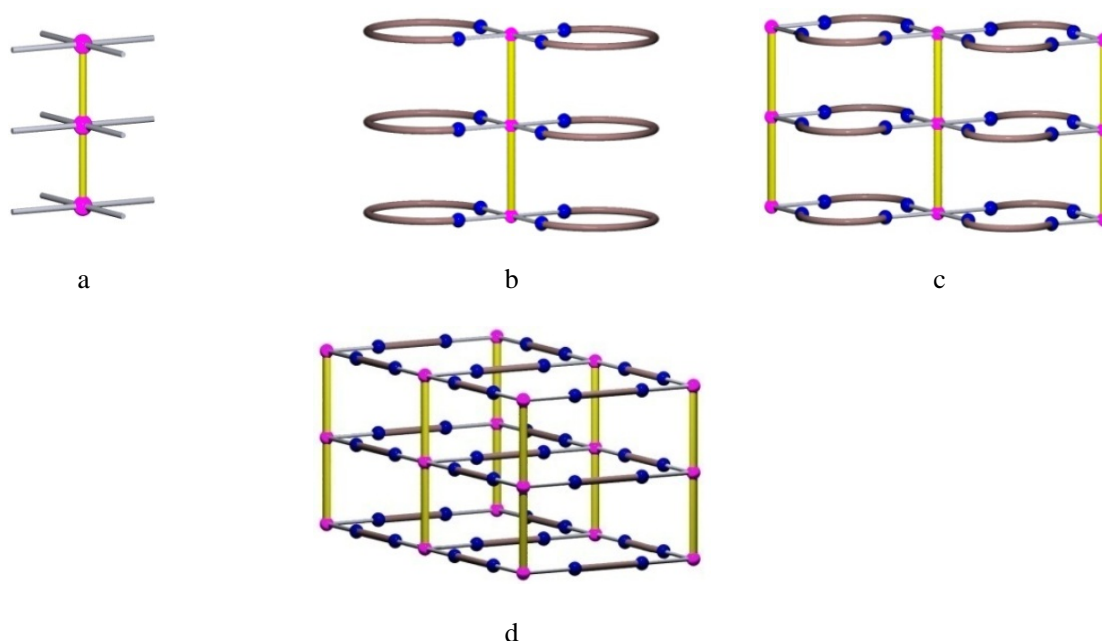


Fig.1: architectures résultant de la combinaison de $ZnSiF_6$ avec des tectons organiques : schéma d'un pilier (a), réseau 1-D (b), réseau 2-D (c) et réseau 3-D (d) tubulaires.

Tout d'abord, nous avons étudié le rôle joué par des tectons organiques rigides et linéaires de longueur variable portant deux unités 4-pyridyl (position *para* par rapport à l'atome d'azote de la pyridine) orientées de façon divergente. La combinaison de ces tectons organiques avec le complexe inorganique $ZnSiF_6$, conduit à la formation d'architectures infinies (3-D) de type cubique (Fig. 2a-b). Nous avons pu montrer que, la taille des cavités poreuses, l'interpénétration des réseaux moléculaires, ainsi que leur stabilité thermique dépendent de la longueur de l'unité organique. Afin

d'améliorer la stabilité de ces architectures, d'autres cations métalliques et / ou d'autres tectons organique fonctionnalisés (Fig. 2c) ont été utilisés.

En utilisant l'unités 3-pyridyl (connexion en position *mé*ta) comme entité de coordination, ou 5-pyrimidinyl (tectons rigides de type zigzag), d'autres types d'architectures 3-D cubiques ont été obtenus (Fig. 2d). Encore une fois, il a été montré que la forme et la taille des cavités et des canaux peuvent être contrôlées par la longueur de l'unité organique.

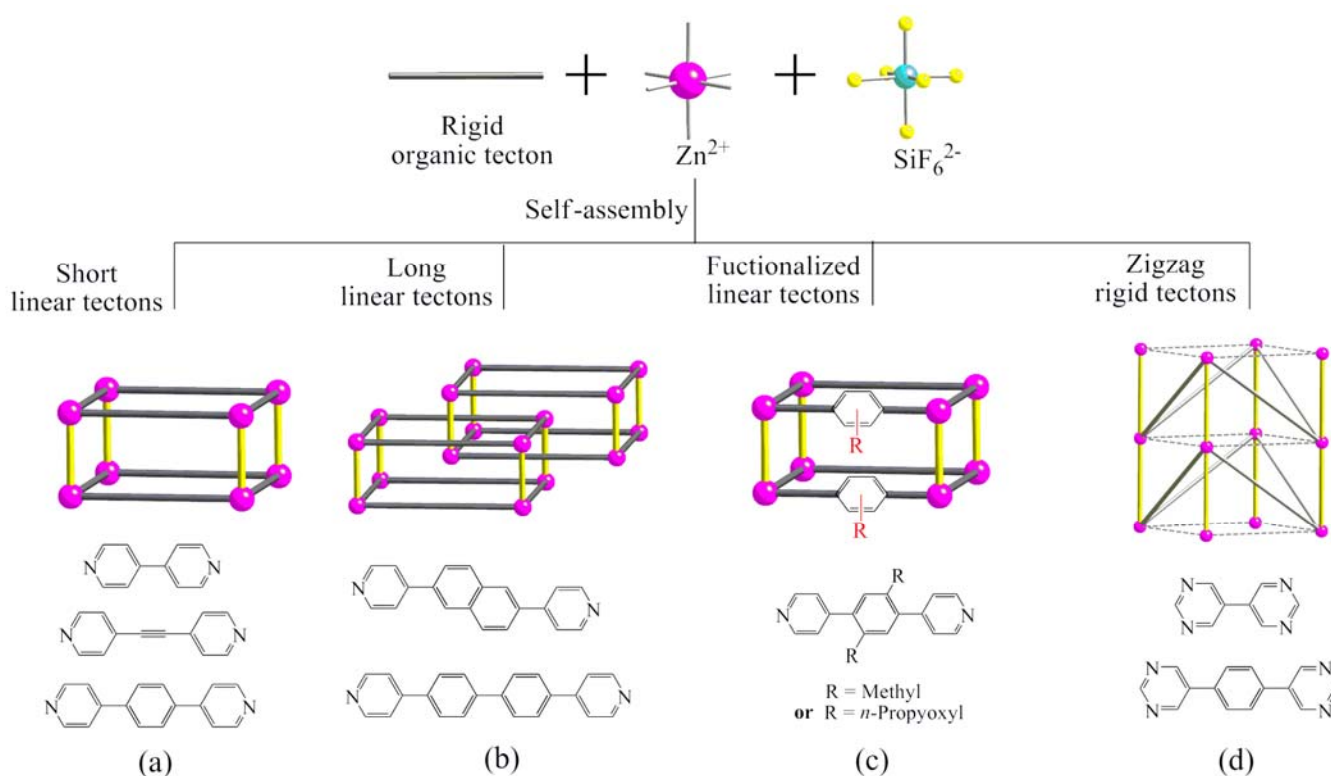


Fig. 2 : représentation schématique des architectures 3-D résultant de la combinaison de ZnSiF₆ avec différents tectons organiques rigides. Pour plus de clarté, les anions SiF₆²⁻ sont représentés par des cylindres jaunes

Nous avons étendu nos investigations aux combinaisons du complexe ZnSiF₆ (généralisé in situ à partir de Zn(BF₄)₂) avec des tectons semi-rigides basés sur des noyaux comme naphthalène, spirobiindane ou le 1,3,5-triazine. La restriction partielle de la conformation du tecton organique a conduit à la formation de réseaux 3-D de type parallélépipède. En raison de la distorsion du tecton organique donnant naissance à des unités de construction possédant différentes longueurs, des

architectures de type parallélépipède à quatre composants de longueur différente ont été obtenues (Fig. 3).

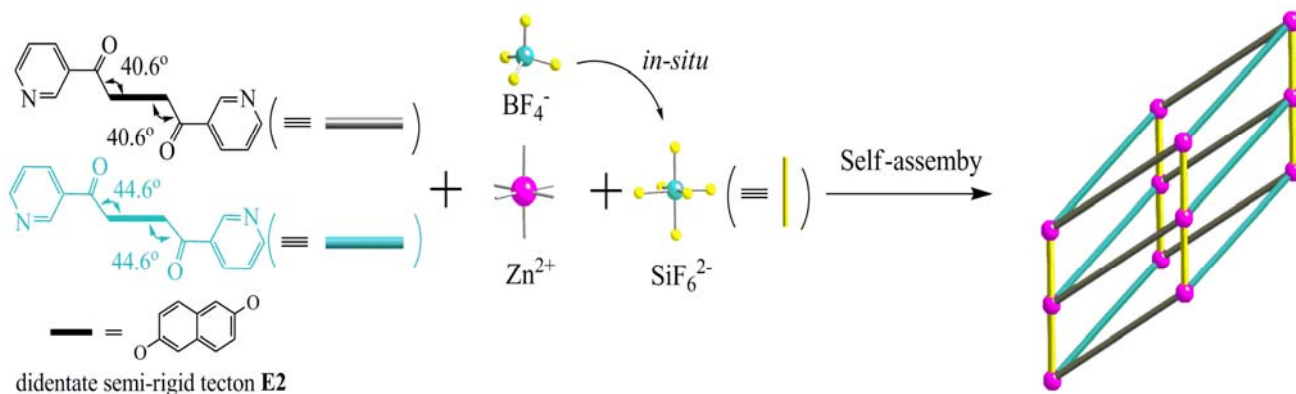


Fig. 3: représentation schématique de l'architecture (3-D) parallélépipédique qui résulte de la combinaison de ZnSiF_6 avec un tecton semi rigide à base de naphthalène. Pour plus de clarté, dans la représentation topologique (à droite), l'anion SiF_6^{2-} et le tecton organique sont représentés respectivement par les cylindres jaune et bleus.

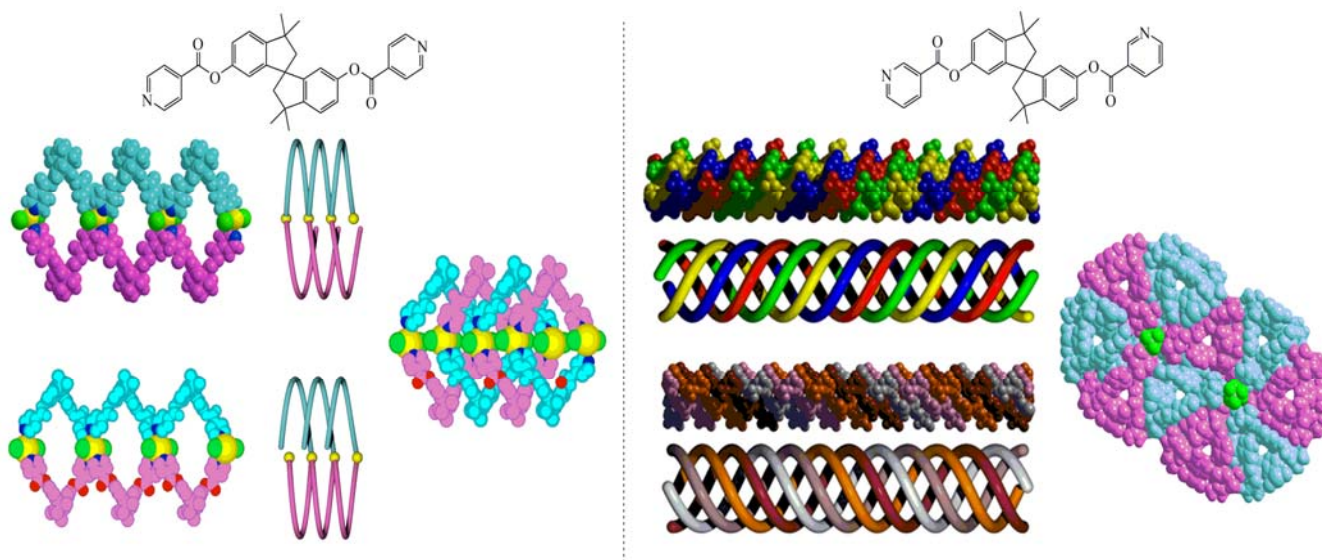


Fig. 4: Représentation schématique d'arrangement en double hélices entrelacées ou quadruple hélices obtenues en associant le tecton à base de 1,1'-spirobi(indane) organique avec HgCl_2 .

En outre, une série de réseaux moléculaires de coordination hélicoïdaux de dimension 1-D et 2-D ont été générés et caractérisés structurellement. La combinaison du mélange racémique du

tecton à base de 1,1'-spirobi(indane) avec HgCl_2 , dépendant de la position de jonction de l'unité coordinante au squelette (*para* ou *mé*ta), conduit respectivement à la formation d'un réseau hélicoïdal à double brins entrelacés et à un réseau hélicoïdal à quadruple hélices (Fig. 4).

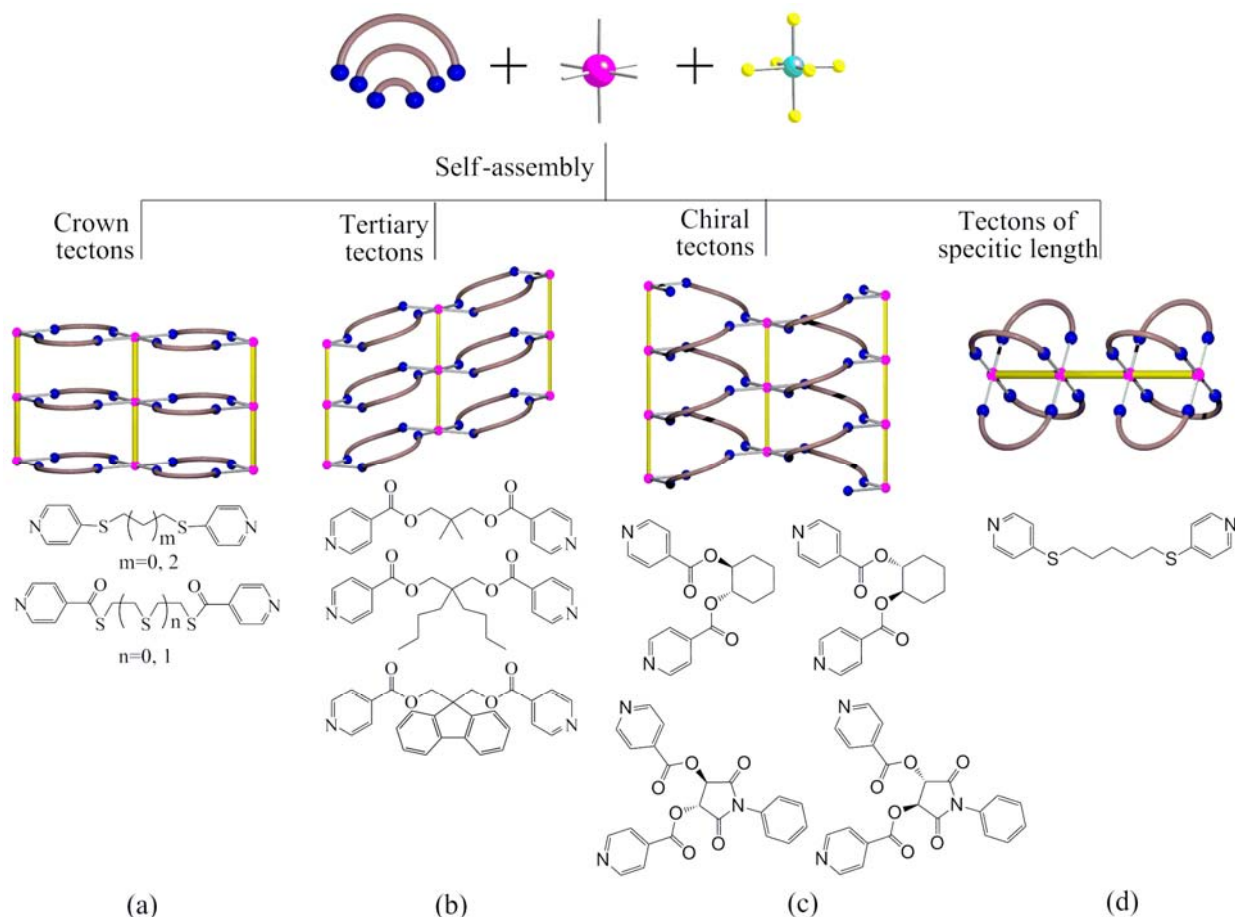


Fig. 5 : Représentation schématique d'architectures 1-D et 2-D résultant de la combinaison de ZnSiF_6 avec différents tectons organiques flexibles. Pour plus de clarté, les anions SiF_6^{2-} sont représentés par des cylindres jaunes.

Des tectons organiques flexibles ont également été explorés. Une nouvelle série de réseaux 2-D tubulaires a été obtenue en combinant ces tectons avec ZnSiF_6 (Fig. 5a-c). Il a été constaté que la forme et la géométrie (perpendiculaire, incliné ou hélicoïdal) de l'architecture dépendent de la nature de l'unité reliant les deux sites de coordination au sein du tecton organique. Les tectons organiques pour lesquels le connecteur ne possède que des groupes méthylène conduisent à

arrangement perpendiculaire (Fig. 5a), tandis que ceux contenant des centres carbonés tertiaires conduisent à une organisation inclinée (Fig. 5b). Enfin, l'utilisation des tectons organiques chiraux conduisent à la formation d'architectures hélicoïdales (Fig. 5c). Pour toutes ces architectures, la forme ainsi que la taille des canaux tubulaires peuvent être moduler par la longueur et la nature des tectons organiques.

Un réseau de coordination mono dimensionnel sous forme de "brochette" basé sur l'interconnexion par des SiF_6 de cages métallamacrotétracycliques binucléaires au zinc a été obtenu (Fig. 5d). A notre connaissance, aucun exemple de ce type de réseau moléculaire de coordination n'a été décrit dans la littérature.

Enfin, en s'inspirant du modèle de réseaux moléculaires décrit précédemment (réseaux tubulaires bidimensionnels), nous avons utilisé un ligand tétradentate. Ceci a permis d'étendre la dimensionnalité en interconnectant les plans 2-D pour former un réseau tubulaire tridimensionnel (Fig. 6). Cependant, à notre grande surprise, dans ce cas, le complexe MSiF_6 ($\text{M} = \text{Co}^{2+}, \text{Zn}^{2+}$) ne forme pas un polymère (pilier infini) comme dans les cas décrits précédemment.

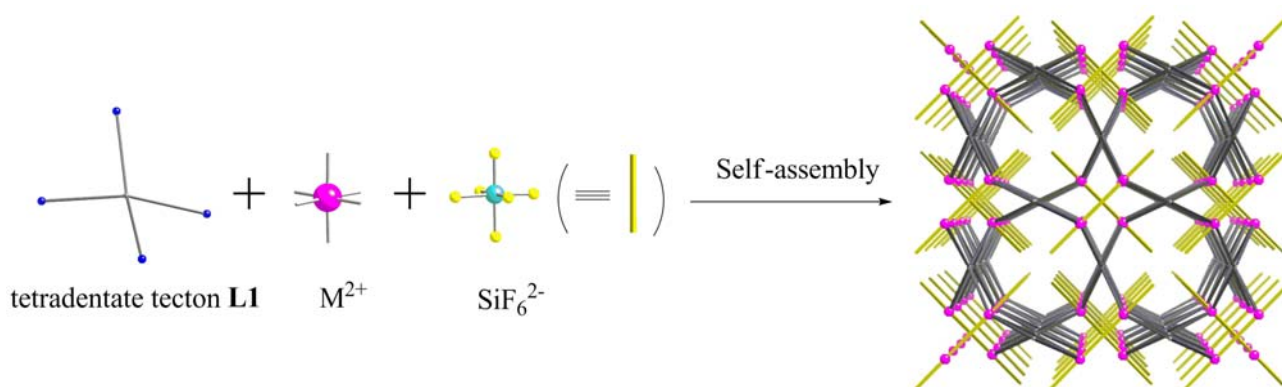


Fig. 6 : Représentation schématique de la 3-D des réseaux de coordination résultant de la combinaison de MSiF_6 ($\text{M} = \text{Co}^{2+}, \text{Zn}^{2+}$) avec ligand tétradentate

CHAPTER I : GENERAL INTRODUCTION

Chapter I: General Introduction

Nature is an inexhaustible source of inspiration for mankind when designing novel materials. The symmetry of natural structures, the complexity of biological pathways and the efficiency of natural photochemical processes are reasons to wonder. When fascinated by the beautiful natural structures, such as the hexagonal crystal of snowflakes (Figure 1-1a), the highly symmetric structure of virus molecules (Figure 1-1b) or the double helical structure of DNA (Figure 1-1c), one may have the same question on how they are formed spontaneously. In order to approach the answer to this pertinent question, chemists, for decades, conceive artificial systems based on abiotic molecules and tackle the very complex self-assembly and self-organization processes.

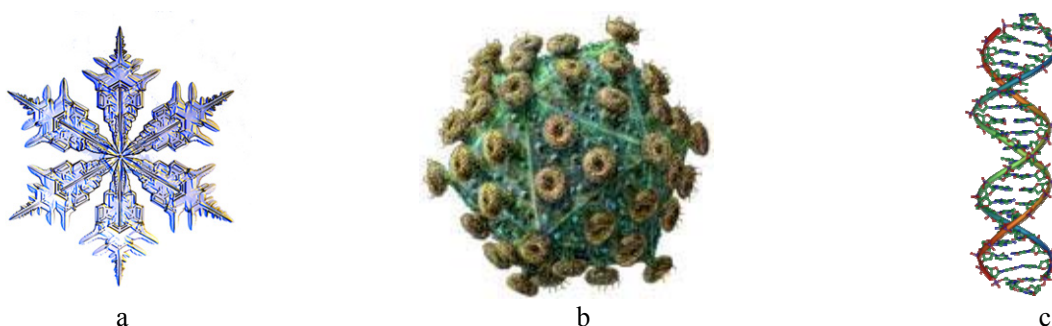


Figure 1-1: the snowflake crystal (a)¹, the structure of HIV virus molecule (b)² and the double-helical structure of DNA (c)³

As a result, new interdisciplinary branches of chemistry, biology, physics and mathematics, such as supramolecular chemistry⁴, molecular biology⁵ and molecular physics⁶ emerged over the last decades.

1.1. Supramolecular Chemistry

The terms of supramolecular chemistry^{4,7,8} was introduced in 1978 by Professor Jean-Marie Lehn⁹, referring to the area of “chemistry beyond the molecules, bearing on the organized entities of higher complexity that result from the association of two or more chemical species held together by intermolecular forces”. Different from traditional chemistry focusing on the covalent bonds, supramolecular chemistry examines the weak and reversible non-covalent interactions between molecules, including Van der Waals forces, hydrophobic forces, electrostatic effects, π - π interactions, hydrogen bonding and metal coordination bonding. In the field of supramolecular chemistry, molecular self-assembly, molecular recognition, mechanically-interlocked molecular architectures, dynamic covalent chemistry and molecular machinery are six core concepts. Among them, molecular self-assembly is an important approach to generate supramolecular materials.

1.2. Molecular self-assembly

Molecular self-assembly is a spontaneous process that involves assembly of pre-organized

substances obtained by classical covalent synthesis into ordered, stable aggregates *via* weak and reversible interactions. Compared with traditional covalent synthesis, there are at least two distinctive features that make molecular self-assembly an approach of interest.

Firstly, the molecular self-assembly is a **spontaneous and thermodynamic process**. In order to make self-assembly take place without guidance or management from an outside source, the process must lead to a lower Gibbs free energy, thus self-assembled structures are thermodynamically more stable than the single, unassembled components. The driving power of self-assembly is based on the enthalpy-entropy compensation and solvophobic effects.

Secondly, the molecular self-assembly is a **reversible and self-repairing process**. It is known that for traditional covalent bond formation processes, owing to the high activation barrier, the system may be trapped in several states (multiple energy minima) and consequently many different structures may be generated (the products **A-D** illustrated in Figure 1-2b). For the self-assembly, the low activation energy barrier of the non-covalent interactions leads to the reversible events and are governed by equilibrium processes. Although some intermediates (**A-C** in Figure 1-2a) with different moderate energy states (**A-C** in Figure 1-2b) may be generated during the self-assembly, the self-assembled complex who hold the lowest energy (**D**) is the only final product according to the minimum total potential energy principle. If we look the intermediates (**A-C**) as defect products, the self-assembly, through self-repairing processes resulting from the reversible nature of the interactions involved, will eliminate them.

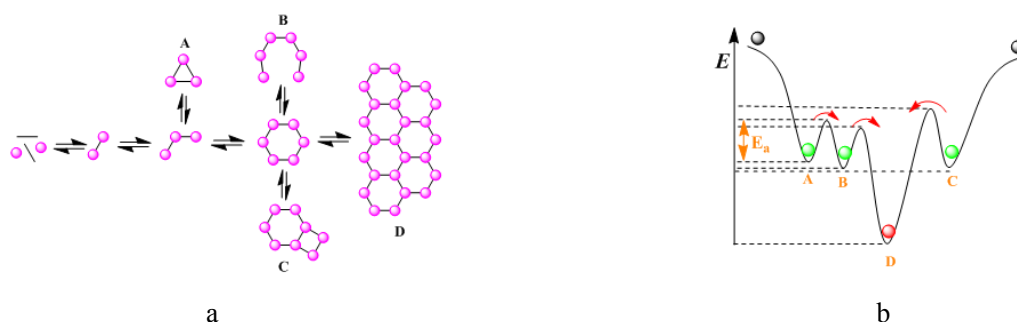


Figure 1-2: Schematic representation of a self-assembly process highlighting the phenomenon of self-repairing (a) and its energy representation of reversible interactions (b)

However, the often uncontrollability and unpredictability of molecular self-assembly lead to the unexpected final architectures (serendipity). Although, in traditional covalent synthesis, chemists are able to link atoms together in any desired configuration and conformations, for self-assembly approach, it is so far impossible to control and predict precisely the formation of the final product because of the limited knowledge on all intermolecular interactions governing the molecular self-assembly processes. At present, the only way to gather knowledge is to collect more data about different interactions in different environments.

Currently, molecular tectonics¹²⁻¹⁴, an important sub-branch of supramolecular chemistry is

intensively under investigation. This approach deals with the programming of recognition processes at the molecular level. Its aim is to design and form high-order architectures (molecular networks^{10, 11}) by self-assembly process through the mastering of intermolecular interactions.

1.3. Molecular tectonics

The term “molecular tectonics” has been introduced by Prof. S. Mann¹² in 1993 and defined as a process of chemical construction of high-order architectures (molecular networks) from molecular tectons¹⁵ (from Greek: *tekton*) by self-assembly process through non-covalent interactions. The two core concepts of molecular tectonics are molecular recognition between construction units and the iteration of the process leading to periodic architectures.

- ✧ Molecular recognition, in the context of molecular tectonics, can be defined as selective association processes between two complementary interactions sites. These complementarities not only deal with energy (the strength of the attractive interactions), but also with geometry (size and orientation of the interactions). Thus, for the self-assembled architectures, the first step is the formation of supramolecular synthons or structural nodes resulting from molecular recognition events between complementary recognition sites.
- ✧ The repeating recognition process (iterative event) leads to the translation of recognition pattern and generates the molecular network. The dimensionality of the latter (one, two or three-dimensional molecular networks) depends on the number of translation in different directions of space taking place during the iterative processes.

Molecular tectonics deals with several features such as tectons (construction units), intermolecular interactions between tectons, recognition events and their iteration, the formation of molecular networks, and finally their packing in the crystalline phase. These aspects are discussed below.

1.3.1. The molecular tectons and their designs

Molecular tectons are structurally and energetically defined active molecular building blocks bearing recognition sites and thus capable of recognizing each other. As the basic elements of molecular networks, the features coded within the tectons framework run through all architecture. Thus, for the molecular tectonics approach, intermolecular interactions, formation of networks, their packing and generation of crystals may, in principle, be monitored by the design of molecular tectons.

As stated above, for the design of tectons, two features must be taking into account:

First of all, from the viewpoint of energy and geometry, the molecular tectons should be self-complementary or complementary. In principle, molecular networks may be generated through self-assembly processes engaging either a self-complementary or several complementary tectons

(Figure 1-3). Although a mono-component system composed of a single self-complementary tecton (Figure 1-3a) would be the most attractive situation in terms of atoms and synthetic economy, actually such a system often produces insoluble powders difficult to characterize structurally. The use of a poly-component system composed of several complementary tectons (Figure 1-3b) is a more viable strategy. Indeed, for poly-component systems, both thermodynamic and kinetic parameters leading to the formation of the crystalline material may be monitored. Consequently, one may use X-ray diffraction on single crystal or powder to achieve their structural investigations.

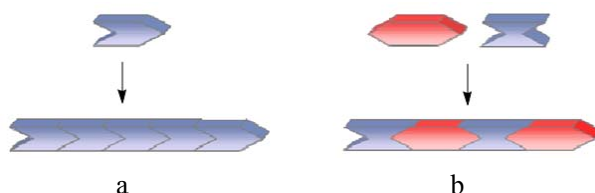


Figure 1-3: Schematic representation of the formation of supramolecular structures by a self-complementary tecton (a) or two complementary tecton (b).

Secondly, the geometry of molecular tectons should allow iterative recognition process. Dealing with tecton's geometry, one may differentiate two categories: *endo*-receptor and *exo*-receptor¹⁶. An *endo*-receptor is a molecular species bearing convergent recognition sites inwardly oriented. In the presence of suitable substrates, discrete receptor-substrate complexes are formed through molecular recognition processes (Figure 1-4). These discrete complexes are also called inclusion complexes. Therefore, *endo*-receptors are suitable entities for host-guest chemistry but of no interest for the generation of molecular networks.

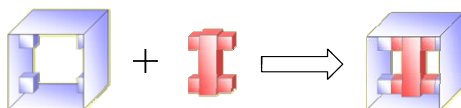


Figure 1-4: Schematic representation of an inclusion complex formed by the combination of an *endo*-receptor with a suitable substrate.

Conversely, the recognition sites of *exo*-receptor are outwardly oriented. Depending on the geometry of the nature of the associated substrates or connectors, either discrete complexes or infinite entities may be formed. If the substrate possesses only a single recognition site, it will not allow the iterative recognition process to take place and consequently discrete entities called capped complexes will be generated (Figure 1-5a). On the other hand, if the substrate offers at least two divergent interactions sites, through the iteration self-assembly events will lead to the formation of infinite molecular networks (Figure 1-5b, c, d).

The dimensionality of molecular networks depends on the number and the localization of recognition sites within the structure of tectons (*exo*-receptors and corresponding substrates). For example, the combination of an *exo*-receptor with two divergent sites oriented at 180° combine with a substrate with the same shape (two divergent sites oriented at 180°) leads to the formation of

α -networks or 1-D linear networks (Figure 1-5b). Indeed in such a case, the iteration of the recognition process leads to a single translation into one direction of space. Similarly, β - (2-D) and γ -networks (3-D) networks can be generated, among many other possibilities, when combining tectons bearing four divergently oriented recognition sites in planar arrangement (Figure 1-5c) or six recognition sites occupying the apices of an octahedron (Figure 1-5d).

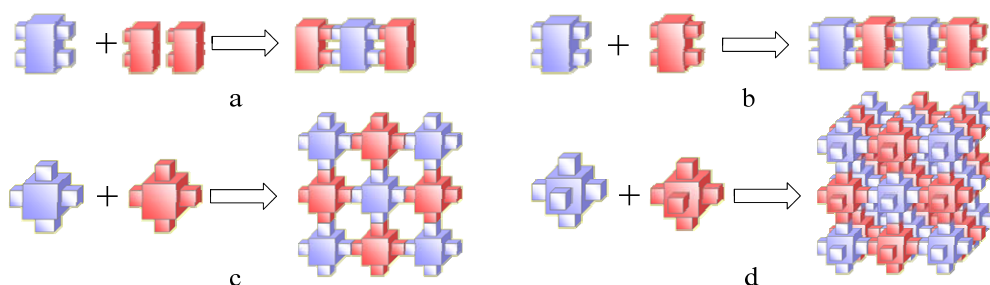


Figure 1-5: Schematic representation of a capped complex or 1-D, 2-D and 3-D molecular network formed by *exo*-receptors.

It is worth noting that the divergent orientation of the recognition sites within the *exo*-receptors and their corresponding substrates, does not necessarily imply the formation of infinite networks. Indeed, as analyzed by P. J. Stang¹⁷ for a “molecular library” (Figure 1-6), the combination of the ligands bearing two recognition sites at 60° angles with linear (180°) ditopic entities leads indeed exclusively to the formation of discrete triangular cyclic architectures. The reason proposed is enthalpy-entropy compensation¹⁸.

Ditopic Subunit \ Ditopic Subunit	60°	90°	109.5°	120°	180°
60°					
90°					
109.5°					
120°					
180°					

Figure 1-6: “Molecular Library” of cyclic molecular polygons created *via* the systematic combination of ditopic building blocks with predetermined angles¹⁷.

To sum up, for the design of molecular tectons for the formation of molecular networks, one needs to consider both the energetic and geometrical factors.

1.3.2. The intermolecular interactions and their energy

As mentioned above, the recognition event between complementary sites may take place through

a variety of reversible attractive intermolecular interactions (Figure 1-7). The toolbox available to supramolecular chemists is composed of van der Waals interactions, charge assisted electrostatic interactions, π - π interactions, charge transfer interactions, metal-metal interactions, H-bonding and coordination bonding.

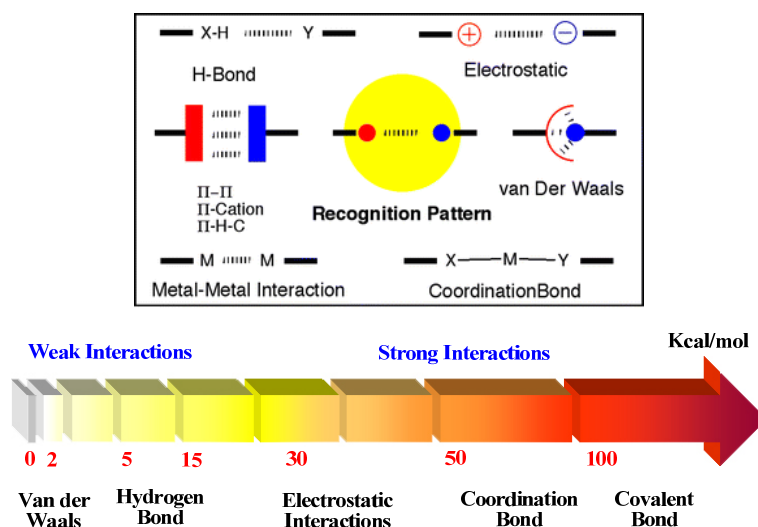


Figure 1-7: Schematic representation of the toolbox of reversible intermolecular interactions (top) and their energy (bottom)

In terms of energy, van der Waals interactions are among the weakest (*ca* 0.5-2 kcal/mol) and for that reason are rather difficult to master. H-bonding, one of the most used attractive interaction, ranges from weak to rather strong (*ca* 2-10 kcal/mol). Metal-metal interactions such as aurophilic interactions may be as strong as H-bonding (*ca* 10 kcal/mol). Electrostatic charge/charge interactions may be substantially strong (up to 50 kcal/mol). Finally, coordination bonding which is another commonly used interaction ranges from weak to rather strong (30-70 kcal/mol). The terminology used so far, defines molecular networks in roughly three categories: inclusion networks mainly based on van der Waals interactions; H-bonded networks; charge-assisted H-bonded networks (combination of H-bonding and charge-charge electrostatic interactions); and finally coordination networks or coordination polymers mainly based on the use of coordination bonds.

Although in principle any type of reversible intermolecular interactions may be used for the design of molecular networks, to date, the majority of the reported cases are either based on hydrogen bonding¹⁹ or on coordination bonds²⁰⁻²¹. A few examples of inclusion networks mainly based on van der Waals interactions in the solid state between concave and convex tectons have been also reported¹¹⁶.

The research project developed during three years in the context of this PhD thesis was mainly concerned with the design and formation of coordination networks. For that reason, examples discussed below deal with this category of architectures.

1.3.3. The molecular networks and their geometries

As stated above, molecular networks may be generated through self-assembly processes engaging either a self-complementary or several complementary tectons. Their topology (dimensionality) and geometry (size, shape...etc) depend on the nature and geometry of molecular tectons. Few examples of 1-D, 2-D and 3-D molecular networks reported in the literature will be discussed in this section.

1) 1-D molecular networks

The formation of 1-D networks requires tectons bearing at least two interaction sites arranged in a divergent fashion. The divergent orientation is essential for avoiding the formation of discrete species. As enumerated by Prof. Hosseini¹³ in Figure 1-8, a 1-D network may be generated using a self-complementary tecton (Figure 1-8a). Such a network may also be designed using a two-component system based on a combination of two complementary tectons (Figure 1-8b and c). For this design principle, one may use two centric tectons leading thus to a single recognition pattern (Figure 1-8b) or two non-centric tectons generating two different assembling nodes (Figure 1-8c). One may increase the number of tectons. For example, one may use a combination of three different tectons leading to two different recognition patterns (Figure 1-8d) or a four-component system based on four different tectons generating two different assembling nodes (Figure 1-8e, f). The analysis given here is not exhaustive. One may indeed imagine a large variety of cases. The only limitation is the imagination and the synthetic ability of chemists to conceive and prepare the tectons.

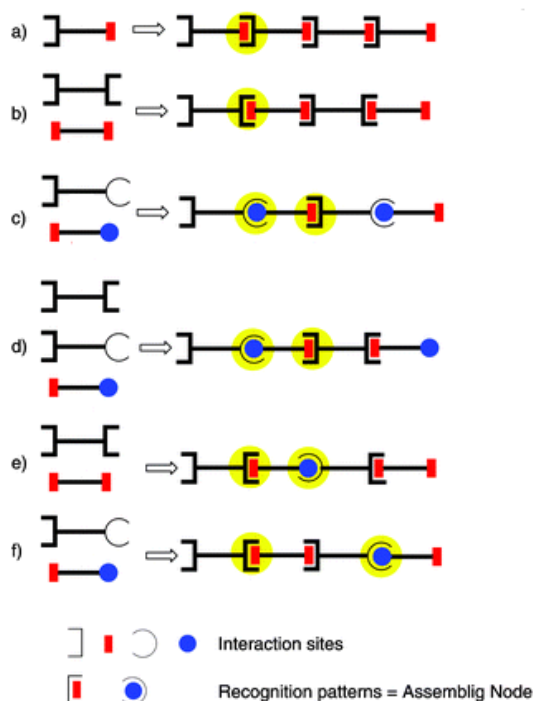


Figure 1-8: A non-exhaustive schematic representation¹³ of a variety of 1-D molecular networks based on self-assembly of either self-complementary (a) or complementary tectons (b-f).

Using these self-assembly strategies, a variety of 1-D molecular networks have been obtained and their single crystal structures have been determined. The analysis of reported examples reveals

several geometries ranging from linear²², zigzags²³, slot²⁴, wavy²⁵ and helical²⁶ (Figure 1-9). It is worth noting that the shapes of the linear 1-D networks may be a cylinder, a ladder²⁷, a ring ribbon²⁸, ring-rod chain²⁹ (chain alternating rings and rods) or tube³⁰ (Figure 1-10).



Figure 1-9: Schematic representation of varieties of 1-D molecular networks: linear (a), zigzag (b), slot (c), wavy (d) and helix (e)

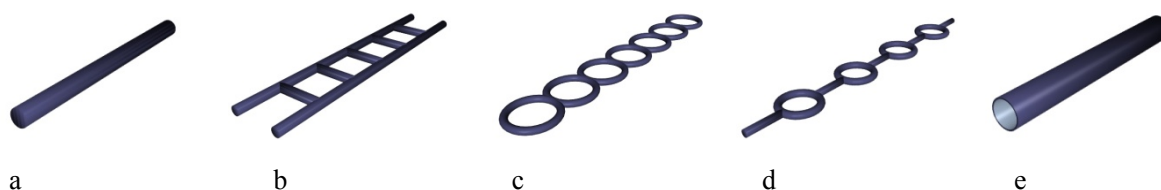


Figure 1-10: Schematic representation of the shapes of linear 1-D networks presented in in Figure 1-10: cylinder (a), ladder (b), ring ribbon (c), ring-rod chain (d) or tube (e).

To better understand these geometries, one of the previous results³⁰ obtained in our group is given as an example. The combination of a divergent organic tecton of the tetracyanocyclophane (TCC) type with silver cations leads to an infinite 1-D coordination network (Figure 1-11). Its geometry is a linear tubular chain composed of Ag^+ and TCC tectons.

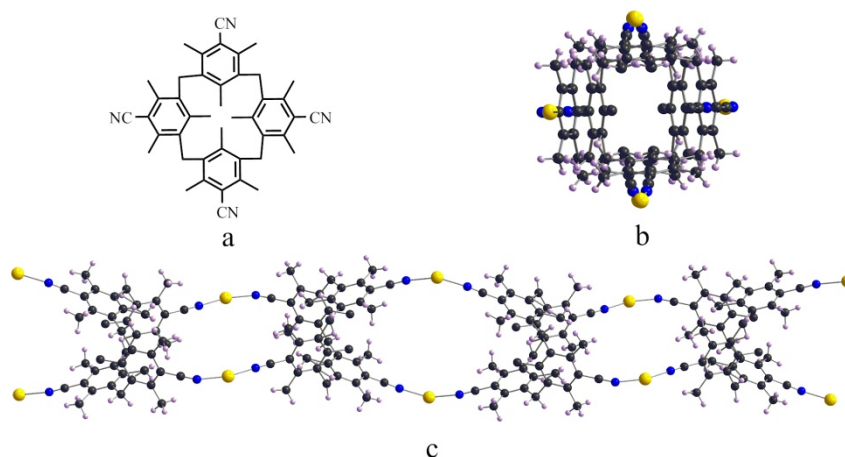


Figure 1-11: Portions of a linear tubular 1-D coordination network³⁰: the organic tecton TCC (a) and the structure of its combination with Ag^+ viewed along (b) and perpendicular to the tube axis (c).

Among the reported 1-D molecular networks, most of them are not directional networks. Since the exploitation of directional physical properties requires vectorial arrangements of the building blocks, the control of directionality remains a challenging issue. Using an acentric tecton, the

formation of directional molecular networks (an example is illustrated in Figure 1-3a) may be envisaged. For example, Dr. A. Jouaiti³¹ in our laboratory obtained a directional linear 1D directional network by combining a hetero-L (1, 3) (a tecton composed of two coordination poles each containing 1 and 3 coordination sites of different nature) with a Co^{2+} ion bearing two chloride ions occupying the two apical positions (Figure 1-12).

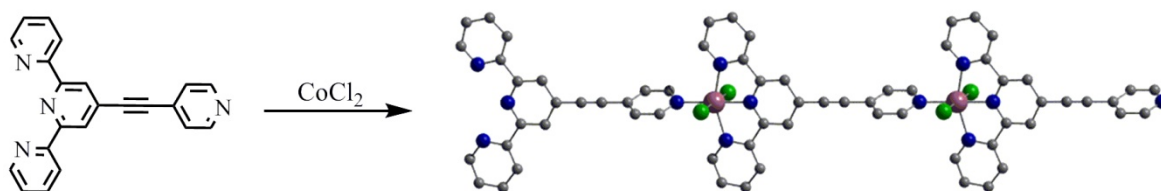


Figure 1-12: Portions of the single crystal structure of directional coordination networks formed upon combining an acentric tecton with CoCl_2 .³¹

2) 2-D molecular networks

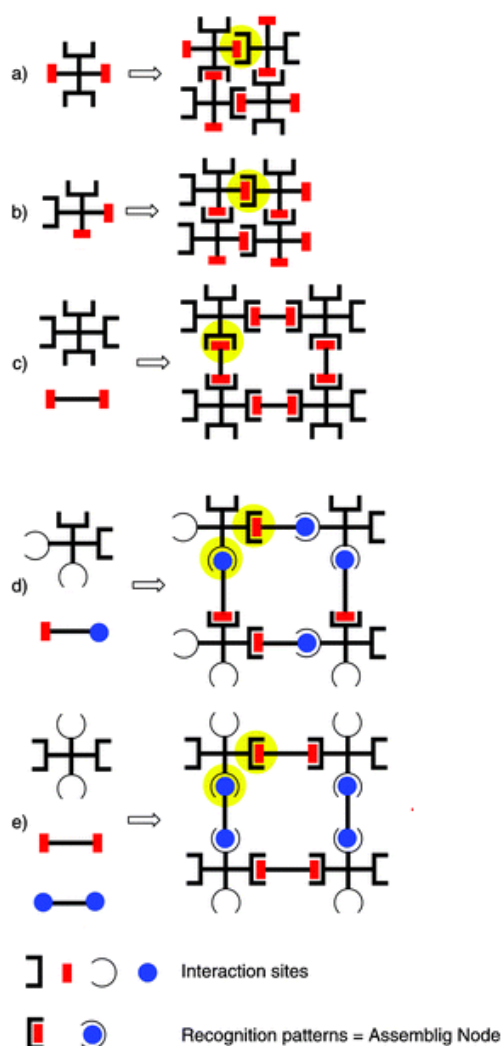


Figure 1-13: A non-exhaustive schematic representation of a variety of 2-D molecular networks based on self-assembly of either self-complementary (a, b) or complementary tectons (c-e).

Similar to the formation strategy of the 1-D molecular network, for the design of 2-D networks, tectons bearing at least three divergently oriented coplanar recognition sites are required. Again using the illustration enumerated by Prof. Hosseini¹³ in Figure 1-13, two dimensional networks may either be generated using a single component system based on a unique self-complementary tecton (Figure 1-13a and 1-13b) or poly-component systems based on combinations of complementary tectons (Figure 1-13c-e). For example, depending on the number of recognition sites, a two-component system may be based on two complementary tectons leading to one assembling node (Figure 1-13c) or generating two different recognition patterns (Figure 1-13d). As in the case of 1-D networks mentioned above, one may also increase the number of components. For example, one may design a combination based on three tectons generating two different assembling nodes (Figure 1-13e). The formal analysis presented here is not exhaustive and only some selected examples are given here. Again, as mentioned for 1-D networks, the increase in the number of tectons might generate diversity (several connectivities) if the design of different tectons is not accurately done.

Using these strategies, a variety of 2-D molecular networks with planar, zigzag³², slot or wavy³³ plane geometries have been reported (Figure 1-14). The plane type arrangement may be a grid, ring plane or tubular plane (Figure 1-15, none actually observed). Further, according to the angle of the grid, it will be classified into square, rhombus, rectangle, or hexagon types, *etc.*

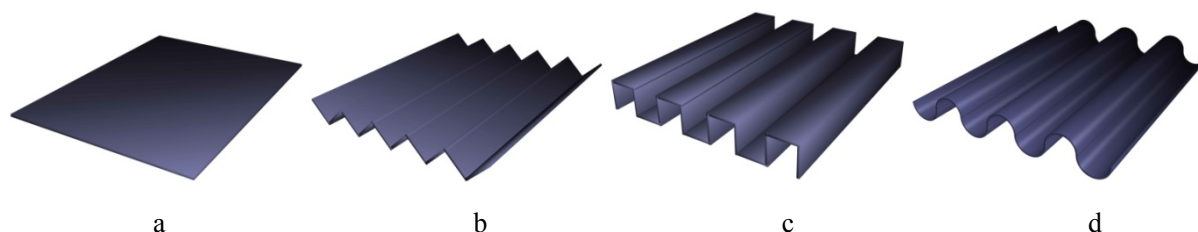


Figure 1-14: Schematic representation of geometries of 2-D molecular networks: planar plane (a), zigzag plane (b), slot plane (c) and wavy plane (d)

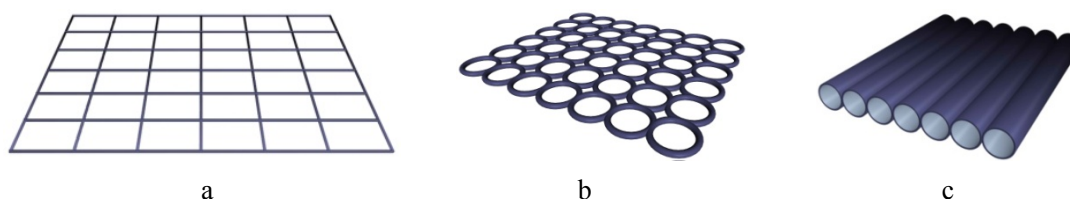


Figure 1-15: Schematic representation of different type of the plane architecture presented in Figure 1-15 composed of grid (a), ring plane (b) or catenation tube (c).

In the following section, we shall present two reported examples.

The first example³⁴ is a square (rhombus) grid plane, as shown in Figure 1-16. The combination of divergent organic tecton **T1** with nickel cations adopting the square planar coordination geometry (here Ni²⁺ adopts the octahedral coordination with two nitrate anions on the axial positions, omitted in the figure for clarity) leads to grid plane. The shapes of the cavities within the grid are square or

rhombus depending on the solvents encapsulated within the cavities. These grids can be stacked in the solid state to form channels and thus offering porosity. For that reason such structures may be considered as analogues of zeolites.

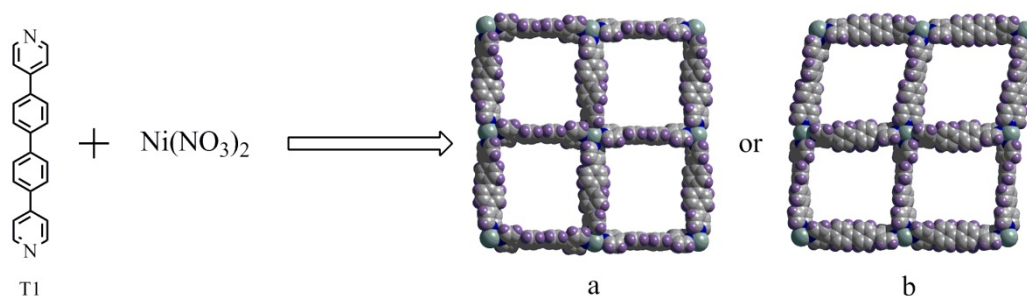


Figure 1-16: Representation of a 2-D network with square (rhombus) grid obtained by Fujita and coworkers³⁴. For clarity, the nitrate ions as well as solvent molecules are omitted.

The second example is a 2-D zigzag molecular network with hexagonal grid³⁷. Self-assembly of a self-complementary tecton (benzene-1,3,5-tricarboxylic acid) leads to the formation of a 2-D grid-type network with honeycomb structure ((6, 3) nets)^{34,35} by hydrogen bonds (Figure 1-17a). In the space, this network adopts a zigzag geometry (Figure 1-17b), which is quite unusual in molecular tectonics.

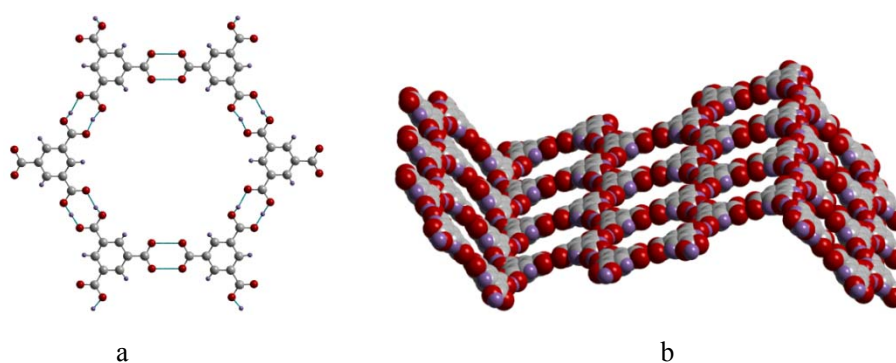


Figure 1-17: Representation of a 2-D zigzag network³⁷ with hexagonal grid generated from trimesic acid by H-bonds: the basic hexagonal pattern (a) and the 2-D zigzag networks based on it (b).

In a broad sense, one may include interpenetrated structures based on 0-D or 1-D network, however, for these architectures, the interpenetration does not result from specific recognition but rather imposed by packing. For that reason, these assemblies will be discussed in the section dealing with packing.

3) 3-D molecular networks

For the design of 3-D networks, tectons bearing at least four non-planar divergently oriented recognition sites are required. The recognition sites can be distributed at the vertices of a tetrahedron, hexahedron, octahedron, *etc.* Hereafter, we shall discuss the use of an octahedral tectons for the formation of 3-D cuboid molecular architectures (Figure 1-18).

Again, the three dimensional networks may either be generated using a single component system based on a unique self-complementary tecton (Figure 1-18a, b) or by poly-component systems based on combinations of complementary tectons (Figure 1-18c, d). For example, a two-component system may be based on two complementary hexahedral tectons (Figure 1-18c) or one hexahedral tecton and one complementary linear tecton (Figure 1-18d). Of course, one may also increase the number of components or recognition patterns. But in the case of 3-D networks, the connectivity between tectons in all three dimensions of space is programmed. Because of this lack of freedom, the generation of 3-D networks requires rather precise tecton design both in terms of geometry and metrics.

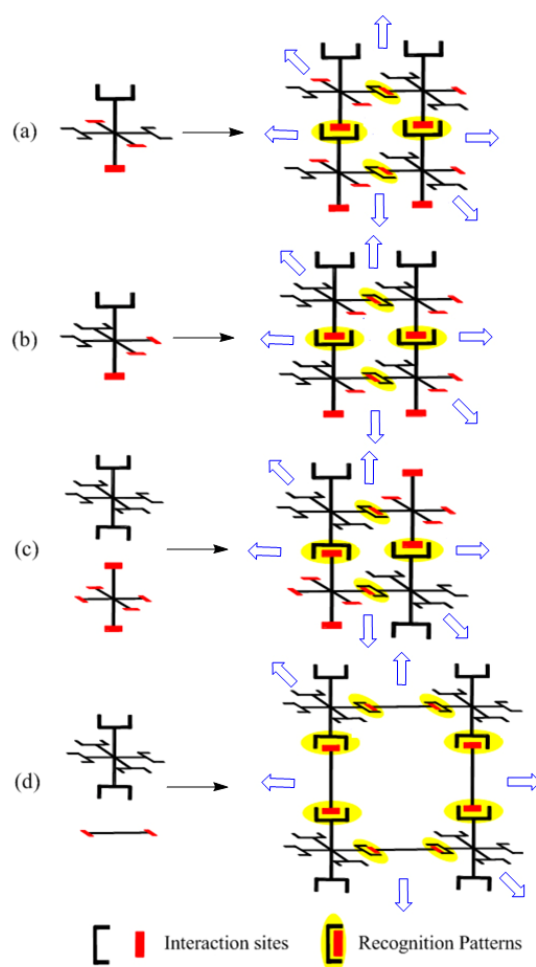


Figure 1-18: A non-exhaustive schematic representation of a variety of 3-D molecular networks based on self-assembly of either self-complementary (a, b) or complementary tectons (c, d). For clarity, **only 2-D** connectivity is shown.

Using similar strategies as those illustrated in Figure 1-18, a variety of 3-D molecular network with different shapes (tetrahedron, cuboid, octahedron, *etc*) have been reported in the past two decades. As Prof. O. M. Yaghi and his co-workers³⁸ summing up in his review of reticular chemistry, nine polyhedra are popular (Figure 1-19) in the context of 3-D coordination networks. They include the familiar regular solids (first row in the Figure 1-19) and the quasi-regular polyhedra, the

cub-octahedron and icosidodecahedron. When the recognition patterns at vertices of the polyhedra are replaced by the corresponding secondary building units³⁹ (SBUs, which are molecular complexes and cluster entities in which ligand coordination modes and metal coordination environments can be utilized in the transformation of these fragments into extended porous networks using polytopic linkers), some 3-D molecular networks with more complicated truncated polyhedra are generated (Figure 1-20). In the following paragraph, two examples will be given to explain the formation of such polyhedra from individual tectons and truncated polyhedra from SBU.

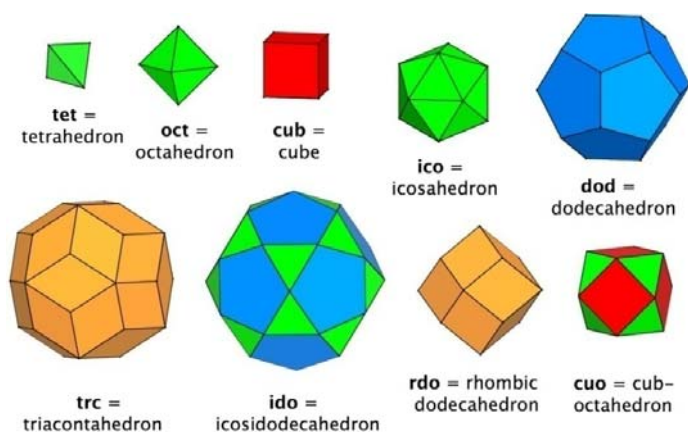


Figure 1-19: Representation of the nine popular convex polyhedra in 3-D molecular networks.

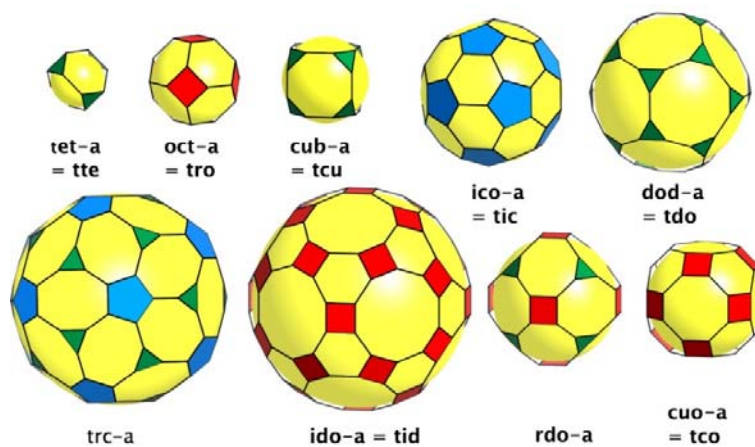


Figure 1-20: Representation of some truncated polyhedra extending from the nine polyhedra.

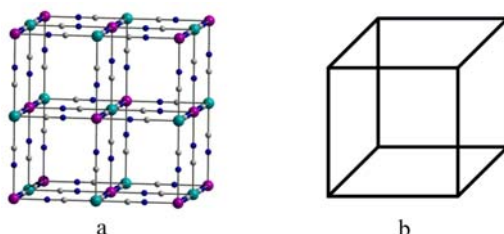


Figure 1-21: a Prussian-type classic cubic structure⁴¹ (a) and schematic representation of polyhedral shape (b)

As the most famous cubic networks, the Prussian blue and its analogues (Figure 1-21), assembled from individual CN⁻ tectons and metal cation, have been widely studied⁴⁰⁻⁴¹ in the last

century. However, concerning 3-D networks based on truncated cubic shape, the carboxyl-zinc metal-organic frameworks (MOFs) have been widely studied recently. O. M. Yaghi⁴³⁻⁴⁴ and other researchers⁴⁵⁻⁴⁷ have prepared a series of MOFs with truncated cubic shape (Figure 1-22b-c) using $Zn_4(CO_2)_6(O)$ as SBUs (Figure 1-22a)⁴². They found that these architectures are good candidates for the absorption and storage of hydrogen.

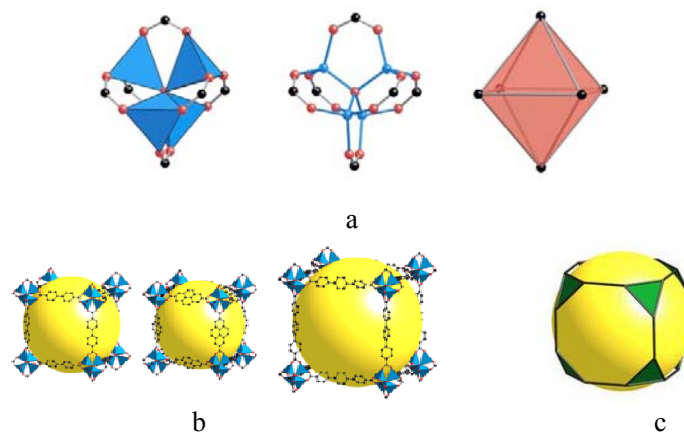


Figure 1-22: Representation of the octahedral geometry of SBUs $Zn_4(CO_2)_6(O)$ (a), some examples with truncated cubic structure (b) and the polyhedral shape of truncated cube (c).

Similarly to 2-D networks, in a broad sense, the 3-D molecular networks, formed by the interpenetration of 0-D, 1-D or 2-D molecular networks, should also be included in this section. However, they will be discussed in the section dealing with packing.

1.3.4. The molecular packing and interpenetration in solid state

As mentioned above, the interpenetration is a special packing pattern, which has attracted many attentions because of their novel topology and their super-strong stabilities. In view of such interests, here the interpenetrations of 1-D, 2-D and 3-D molecular networks will be discussed independently from normal packing (using *packing* in the following content).

1) The packing of 1-D molecular networks

As stated above, for 1-D molecular networks, the information coded within the structure of tectons concerns only the recognition event generating the assembling nodes and the iteration of the process leading to its translation into one direction of space. In principle, the arrangements in the other two directions of space leading thus to the crystal are not *a priori* controlled by chemists. In other words, the system is free to find its own way to pack the 1-D networks in the other two directions.

But during the self-assembly (crystallization), the stack of networks in space also require to reach a thermodynamic minimum in terms of the electronic distribution and steric hindrance. As a result, the geometry of the molecular packing may be adopted in many different ways.

For the packing of rigid 1-D networks in one plane, one must consider the relative position of structural nodes. The consecutive parallel strands may be packed in an eclipsed (as shown in [Figure 1-23a](#)) or staggered ([Figure 1-23b](#)) fashions.

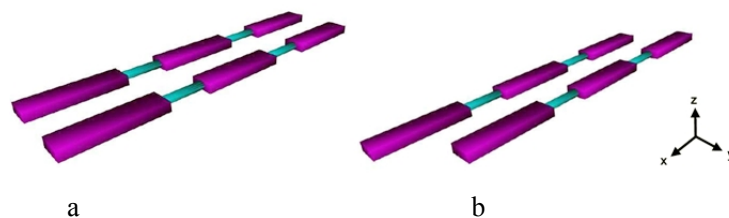


Figure 1-23: Schematic representation of the relative position between the neighboring two parallel networks: parallel absolutely (a) or slipped each other along the axis the network (b).

For simplification, 1-D networks with different geometries (linear, zigzag, slot, wavy or helical geometry) and relative positioning of the nodes (presented in [Figure 1-23](#)) will be considered as cylindrical rods. The different possibilities of packing cylinders in the crystalline phase (condensed phase) are represented in [Figure 1-24](#). All rod can be packed in a parallel fashion ([Figure 1-24 a](#) (tetragonal), [b](#) (hexagonal)) or in the plane all the rods may be arranged in a parallel mode but consecutive planes may be packed with 90° angle between the cylinders ([Figure 1-24c](#)). Finally, a rather rare example of packing, orthogonal arrangement of cylinders) is given by [Figure 1-24d](#).⁴⁸

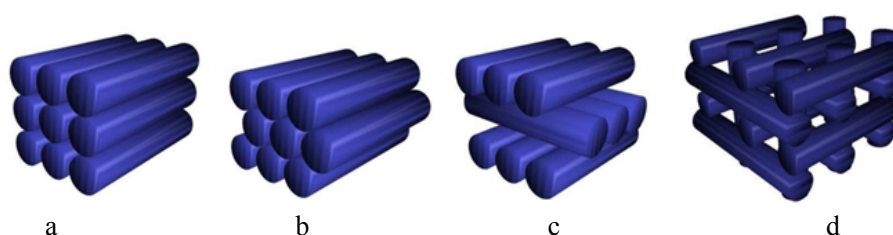


Figure 1-24: Representation of different possibilities of packing of 1-D molecular networks.

Last but not at least, the helical 1-D networks may adopt molecular entanglement in the crystal. As G. Ciani described⁴⁹, an entangled system is an extended array more complex than its constituents, “that is comprised of individual motifs forming, *via* interlocking or interweaving, a periodic architecture infinite in at least one dimension”. The entanglement of the molecular networks *via* interlocking is named as *interpenetration*, which will be discussed in the following content. Here we only describe interweaving ([Figure 1-25](#)).

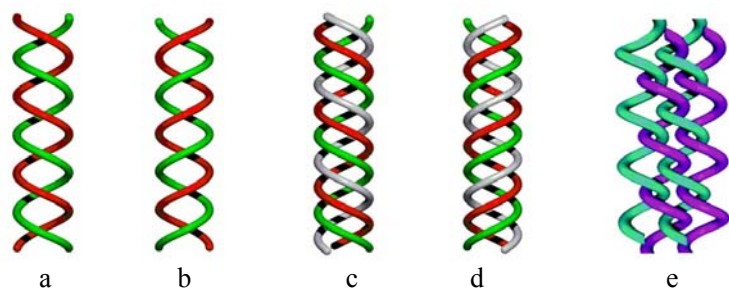


Figure 1-25: Representation of some possible interweaving of 1-D molecular networks.

A familiar example is provided by the entangled strands in the DNA double helix. This and other helical biological molecules have provided the inspiration for a rapidly expanding range of double-, triple-helical⁵⁰⁻⁵¹ and interwoven helical coordination compounds⁵², as shown in Figure 1-25 (none actually observed).

Moreover, it is worth noting that the molecular packing plays an important role in the properties of the crystalline materials, especially those of the non-centrosymmetric materials (NLO, piezoelectric and pyroelectric properties). Indeed, for instance, the molecular network formed upon combining acentric tecton shown in Figure 1-12 (page 10) is directional and non-centrosymmetric, but its stacking in the space is *antiparallel* and thus leads to the formation of a centrosymmetric crystal³¹ (Figure 1-26a). However, using the similar hetero-L (1, 3) tecton bearing chiral groups within the coordinating poles containing 3 coordination sites, directional 1-D molecular networks and crystalline solid can be obtained (Figure 1-26b)⁵³. Other techniques also allow the growth of polar crystals, such as the addition of the additives⁵⁴ (e.g. chiral additives) or epitaxial growth on metallic or inorganics surfaces⁵⁵.

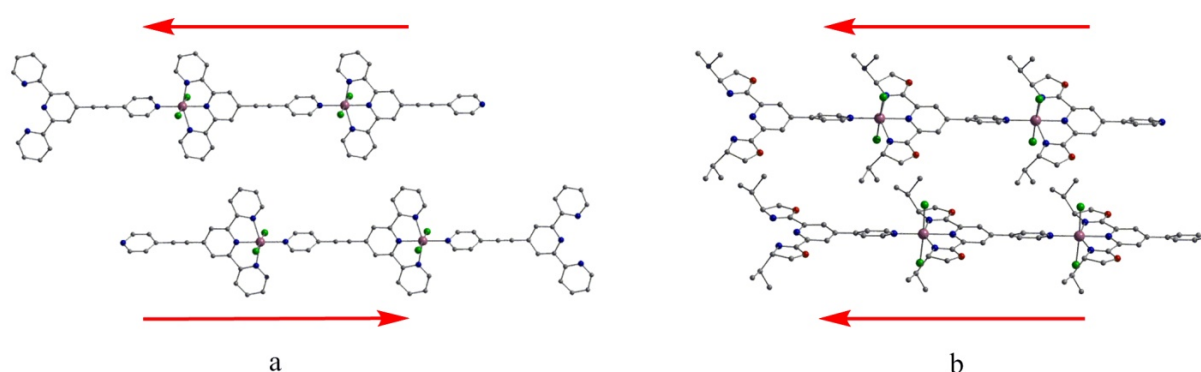


Figure 1-26: Representation of the packing of two directional 1-D molecular networks: *antiparallel* packing³¹(a) and *parallel* packing⁵³(b).

2) The interpenetration of 1-D molecular networks

As previously stated, the interpenetration is the entanglement of the molecular networks *via* interlocking. That is, the interpenetrating structures, which “can be disentangled only by breaking internal connections”, are characterized by the presence of infinite structurally regular motifs that must contain rings “through which independent components are inextricably entangled”⁵⁶.

In principle, 1-D molecular networks such as ring-rod chains, ring ribbons and ladders (Figure 1-10, page 9) may give interpenetration. However, only few cases based on the interpenetration of ring-rod chain or ring ribbon type networks have been reported. For instance, the first architecture based on interpenetrating sheets illustrated in Figure 1-27a was reported by R. Robson²⁸. This arrangement is obtained by combining 1,4-bis(imidazol-1-yl-methyl) benzene with silver nitrate. The second one (Figure 1-27b) was obtained by K. S. Suslick and his co-workers²⁹ using the free base 5,10,15,20-*tetrakis*-(4-carboxyphenyl) porphyrin with calcium(II) ions under hydrothermal conditions.

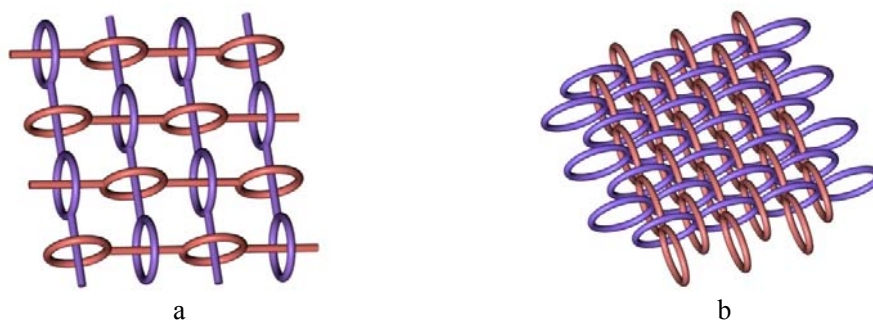


Figure 1-27: Schematic representation of two reported examples of 2-D polyrotaxane sheets formed by interpenetration of ring-rod chains²⁸ (a) or ring ribbons²⁹ (b).

The majority of examples reported are exclusively based on 1-D infinite molecular ladders. As shown in [Figure 1-28](#), the 1-D, 2-D or 3-D structures can be constructed by the interpenetration of the ladders^{27, 57-60}.

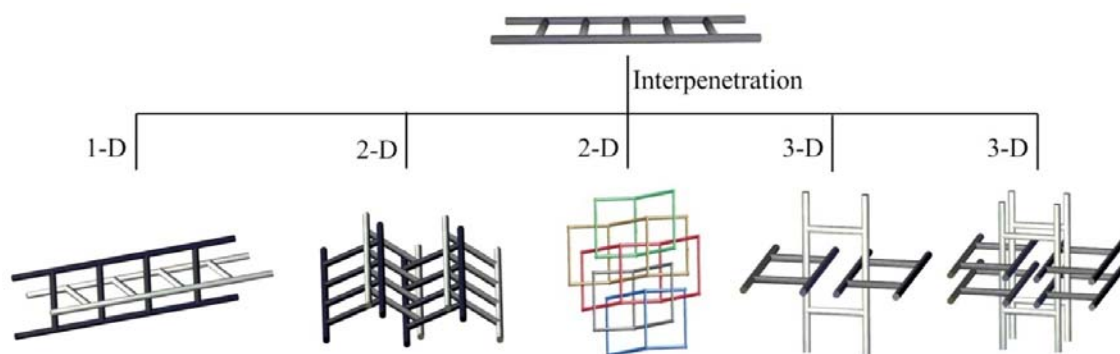


Figure 1-28: Representation of the reported 1-D, 2-D or 3-D structures constructed by the interpenetration of the ladders^{27, 57-60}.

3) The packing of 2-D molecular networks

As in the case of 1-D networks, 2-D networks possess lower dimensionality than the crystal. The information coded within the structure of tectons concerns in that case the formation of two-dimensional architecture (control of two space dimensions). Consequently, the arrangement in the third dimension, *i.e.* the packing of 2-D sheets, in principle, is not programmed and thus cannot be predicted.

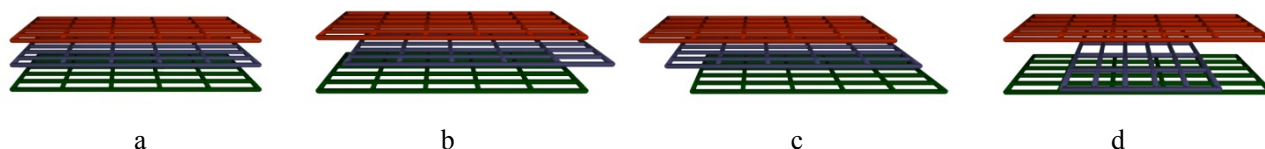


Figure 1-29: Schematic representation of four possible modes of packing of 2-D molecular networks.

However, during the crystallization process, the stacking of 2-D networks in the third dimension follows the seek for a thermodynamic minimum. Considering electronic distribution and steric hindrance, etc, some possible stacking modes of planes, for example those of grid plane, are illustrated in [Figure 1-29](#). The neighboring planes may be parallel and eclipsed (a), parallel and

staggered (b and c) or parallel and rotated with some angle (d), etc.

4) The interpenetration of 2-D molecular networks

If the neighboring planes are not parallel, they will generate interpenetration. Of course, for the zigzag, slot and wavy plane, even if the relative orientations of their planes are parallel, it is still possible to obtain interpenetrated architectures. For a given geometry, even when considering a single interpenetration (parallel or inclined), there are many different possibilities. For example, there are at least 4 modes for the parallel interpenetration of (4, 4) nets (Figure 1-30)⁶¹⁻⁶³.

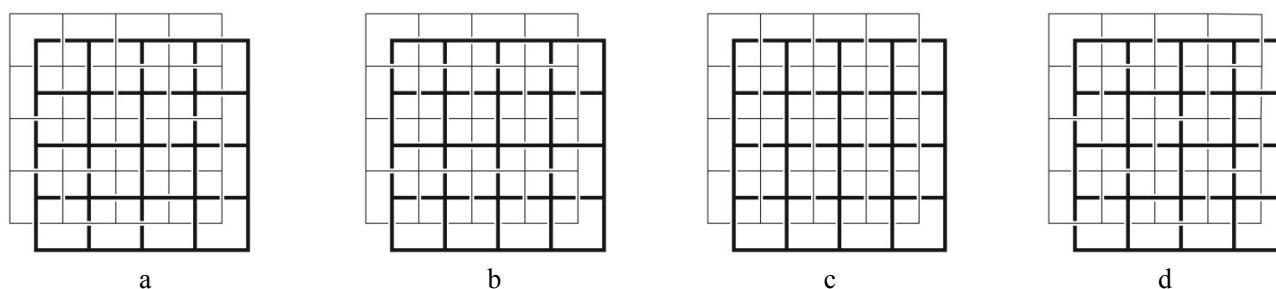


Figure 1-30: Schematic representation of four topological modes for parallel interpenetration of (4,4) nets.

Thus, for 2-D molecular networks, many interpenetrated architectures may be obtained and it is not possible to draw any general rules allowing any prediction.

5) The interpenetration of 3-D molecular networks

Different from the 1-D or 2-D molecular networks, the connectivity of the 3-D networks between tectons in all three dimensions of space is programmed within the structure of tectons (the dimensionality of 3-D networks is identical to the dimensionality of the crystal) and thus the packing concerns only the possible interpenetration. Indeed, for 3-D networks containing large volumes, in some cases, the empty space may be occupied by one or several other independent networks through interpenetration. The interpenetrating mode depends on the shape of 3-D frameworks (Figure 1-19 and 1-20, page 14). Two examples are illustrated in Figure 1-31.

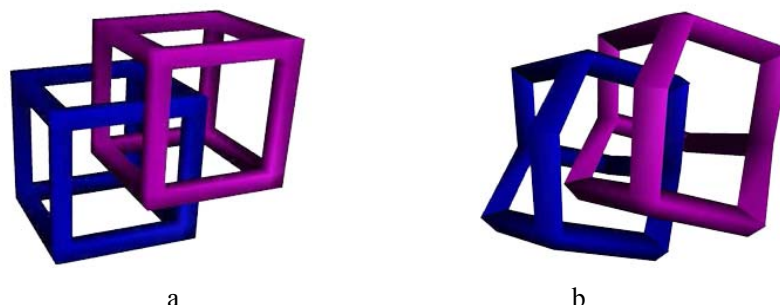


Figure 1-31: Schematic representation of two interpenetration modes based on cubic (a) and diamondoid frameworks.

Other types of structures based on other modes of interpenetration of 3-D networks will not be given here. If interested, one can consult the review papers of S. R. Batten^{56, 64} and G. Ciani^{49, 65, 66}

or a *precious* list of the interpenetrations summarized by Batten¹¹⁷.

1.3.5. The conclusions and some comments on the molecular networks

In general, the dimensionality and geometry of molecular networks may be controlled by the design of molecular tectons. However, some other parameters may influence their assembly, such as the rigidities of tectons, the experimental environments (solvents, concentration, temperature and stoichiometry), the possible interpenetrations *etc*, and thus make it very difficult to predict the final architectures¹¹⁸.

In order to control the construction of predefined self-assembled architectures, one must take into accounts the following four features:

- Firstly, for the design of tectons, one should analyze all possible modes of interactions and thus supramolecular tectons and structural nodes. This information (geometric: nature, number and arrangement of recognition sites, and energy: strength of interactions) is encoded within the structure of tectons.
- Secondly, one must, through a retrosynthetic approach, propose a synthetic strategy and synthesize the desired tectons by the classic chemical methods.
- Thirdly, one should search, select and implement the suitable experimental conditions allowing the self-assembly (solvents, concentration, temperature, *etc*) to take place and generate crystalline materials.
- Finally, one must characterize the formed supramolecular structures by the modern techniques. The single crystal X-ray diffraction is the most direct and powerful method since it is capable of determining the relative position of each component with high precision, thus giving a complete picture of the architecture. Other analytical techniques may be used, such as powder X-ray diffraction, neutron diffraction, elemental analysis, NMR, IR, UV-Vis, mass spectrometry, *etc*.

1.4. Coordination networks

A coordination network (also called coordination polymer), as stated above, contains metal ions linked by coordinated tectons (including organic or inorganic tectons) into infinite arrays⁶⁷. These infinite nets must be generated mainly by coordination bonds. Molecular species linked only by hydrogen bonding, such as those shown in [Figure 1-32a](#) are elegant examples of H-bonded networks but are not coordination networks⁶⁸. In the contrary, a structure linked by both coordination bonds in one direction and hydrogen bonds in another two directions is a 1-D coordination polymer⁶⁹ ([Figure 1-32b](#)). However, when taking into accounts the different types of recognition events (coordination and H-bonding), the overall architecture is a 3-D network.

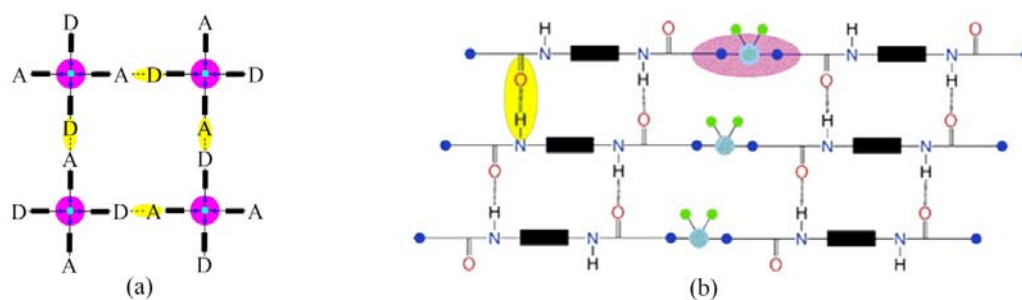


Figure 1-32: Schematic representation of two molecular networks constructed using exclusively H-bonding (a) or coordination bonds in addition to H-bonding (b). The purple recognition pattern represents the coordination bond and the yellow one H-bonding.

Although the first man-made coordination network, Prussian Blue, was accidentally discovered as early as 1704 by a Berlin artist⁷⁰, little attention was paid to coordination networks until a short communication reported by R. Robson in 1989⁷¹, and a subsequent full paper in 1990⁷². After that, reports on coordination networks, in particular, those containing organic tectons (MOFs), have increased at an exponential rate with nearly 4000 papers reported in 2006 only (Figure 1-33)⁷³.

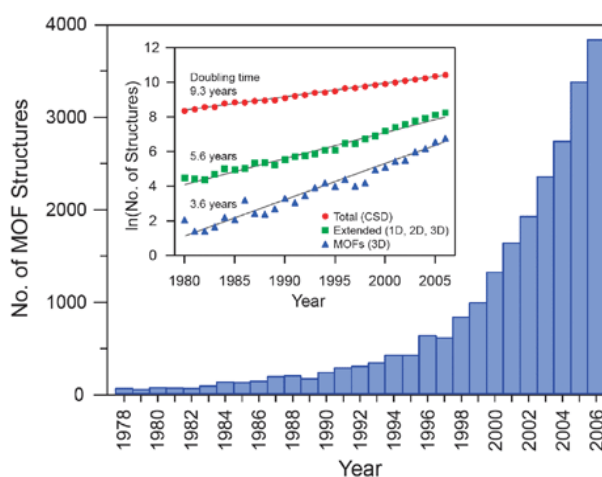


Figure 1-33: Number of metal-organic framework (MOF) structures reported in the Cambridge Structural Database (CSD) from 1978 through 2006. The bar graph illustrates the recent dramatic increase in the number of reports, while the inset shows the natural log of the number of structures as a function of time, indicating the extraordinarily short doubling time for MOF structures compared to the total number of structures archived in the database⁷³.

Indeed, according to the statistical results obtained by O. M. Yaghi and co-workers^{73,74}, since 1978 the number of reported MOF structures has doubled every 3.9 years for 3-D periodic structures and every 5.7 years for all MOFs (1-D, 2-D, and 3-D structures). This is compared to a doubling time of 9.3 years for the entire structures in CSD. It is so much so that one might say that MOF chemistry is in a “runaway” mode, in that it is leading to an abundance of breakthroughs and discoveries rarely accomplished in such a brief period of time. What is the excitement about? Why has this area captured the attention and imagination of so many? And, most importantly, what is so intrinsically different about MOF chemistry that causes it to be ubiquitous in the literature?

The strong point of metal-organic frameworks in synthesis, structure, property and application provides some answers to these questions.

First of all, the chemistry of the MOF components *i.e.*, of the individual organic molecules (organic tectons) and the metal coordination sites is so highly developed, we can have great confidence in our ability to formulate and execute a plan of how to produce a related material with specific changes in chemical functionality and metrics. As exemplified above, the organic tectons can be any organic molecules containing coordination sites, such as pyridyl, imidazole, nitrile or carboxylate functional groups. The metal can be any "free" metal, capped complexes (some coordination sites in the metal have been capped by other atoms and thus inactive for construction Figure 1-34) or any secondary building units (SBUs) with different geometries (Figure 1-22)³⁹.

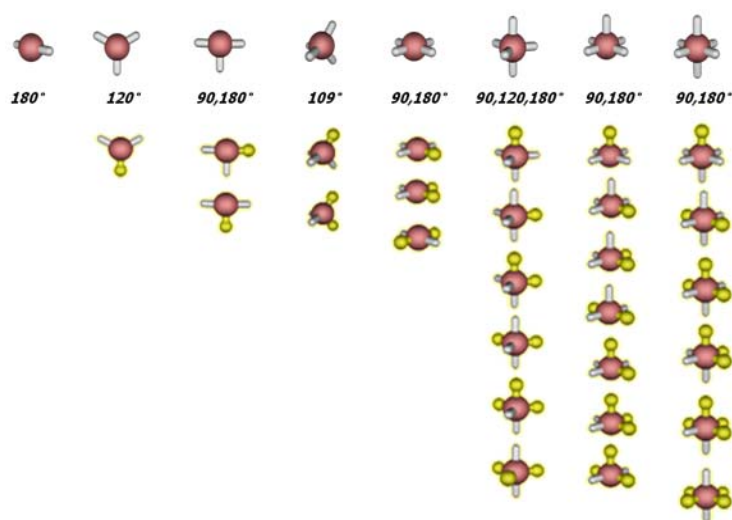


Figure 1-34: Schematic representation of the geometries of metals and capped metal complexes, where the gray points are the active coordination sites but yellow ones are inactive.

Secondly, for the synthesis of MOFs, it is now a matter of routine to use solution chemistry to link inorganic “joints” with organic “struts” by strong bonds to make robust and often porous MOFs featuring extended network architectures^{74, 75}. These materials are crystalline, so we know exactly where the atoms are and how they are connected, and the measured properties of the system can be correlated with the structure.

Thirdly, it is possible for one to first formulate a hypothesis of what structural attributes should give rise to the best performance for a specific application (Figure 1-35), and then to synthesize a variety of MOFs that test the hypothesis, and ultimately, by reiterating this process, to achieve truly exceptional properties. In this way, MOFs have been generated that exhibit the highest known surface areas, the lowest crystal densities, a high hydrogen storage capacity⁷⁷, selective heterogeneous catalysis⁷⁸⁻⁷⁹, magnetic ordering⁸⁰, channels for regulating polymerizations⁸¹, selective carbon dioxide capture^{82, 83}, and guest-dependent luminescence⁸⁴.

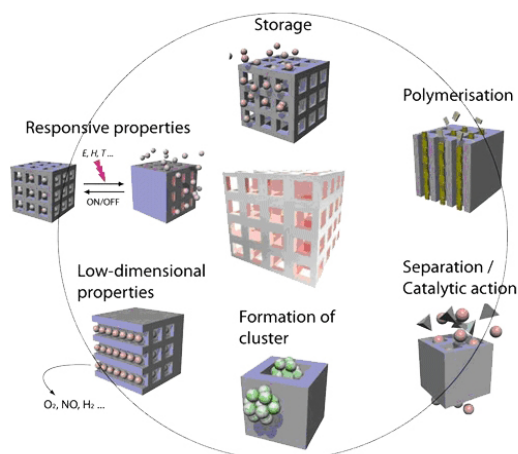


Figure 1-35: Schematic representation of some properties and corresponding applications of MOFs summarized by S. Kitagawa and co-workers⁸⁵.

The last but not least, the drive for utilizing these multi-functional materials in applications has led to development of new chemical methodologies for functionalizing their internal surfaces (Figure 1-36)⁸⁶, and for obtaining them in flexible⁸⁷, thin film⁸⁸, and nanoparticle forms⁸⁹. Thus, the stage is set for this new class of materials to have the diversity, multiplicity, and exceptional properties that are required to solve some of our most pressing societal problems, including for example the creation and deployment of clean, sustainable sources of energy. Their widespread implementation will be significantly aided by the simple methods that have been developed to scale up the production of certain MOFs to ton-quantities⁹⁰.

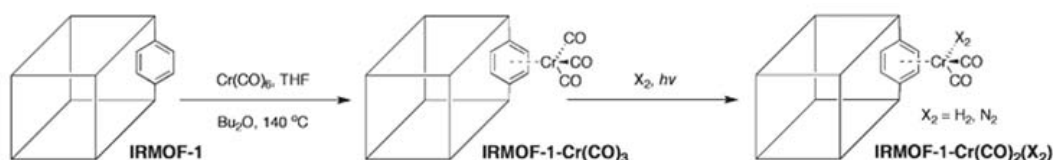


Figure 1-36: Schematic representation of an example about the postsynthetic modification of each of these MOFs with metal ion complexes⁹¹.

In other words, on a fundamental level, MOFs combine chemistry and geometry to produce technology-generating properties in a way that is rarely experienced in science. These aspects are contributing to both the intellectual and the practical foundations of the field. The vast expanse of possibilities that MOF chemistry offers has without doubt allowed many chemists from around the world to emerge as important leaders for their own unique contributions.

1.5. The challenges and trends for the coordination network design

Although the coordination network, in particular, MOF study is in a “runaway” mode now, at least three important challenges in this area have not yet been resolved. First, as stated above, framework design still remains a challenge today due to the inability to control all the orientation and stereochemistry of the tectons during crystallization in order to achieve a desired topology. Second,

the self-assembled products are often obtained as poorly crystalline materials making single crystal x-ray structural characterization difficult or impossible. Third, the porosity is the base of most application of MOFs, but access to the channels of MOFs is often precluded due to the phenomena of self-inclusion or interpenetration.

Generally, the normal MOFs have been made by linking metal cations with multi-topic nitrogen (oxygen, sulfur, *etc*) donor organic tectons to generate 1-D, 2-D or 3-D cationic structures. For these networks, the porosity is a natural and desirable outcome of design. However, the self-inclusion of their counter anions always precludes their porosities. For example, a cubic cationic framework have been produced upon combining a 1,2-di(pyridin-4-yl)ethane with a Cd^{2+} cation whose porosity is occupied by the counter anion ClO_4^- ⁹² (Figure 1-37).

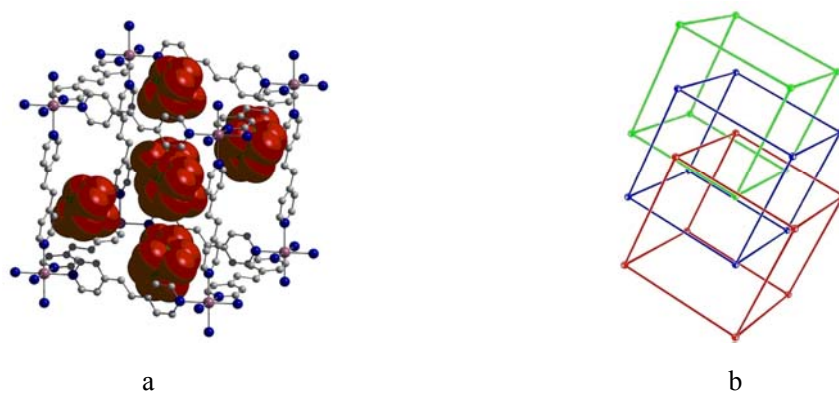


Figure 1-37: Schematic representation of one example about the cubic cationic MOFs: the cube with the space-filling ClO_4^- anions⁹² (a) and its three-fold interpenetration (b).

In order to avoid such self-inclusion, the use of coordinating anions is advisable. So far, the vast majority of examples reported deal with either the capped anions⁹³⁻⁹⁵ or bridged organic anions^{39, 96-98}. For the former ones, the decrease of the active coordination sites by capped anions always lead to the low dimensional networks that frequently contain no channels. For the latter ones, such as carboxylate³⁹, sulfonate⁹⁶, dipyrin⁹⁷, Imidazolate⁹⁸, are insoluble in common solvents, and thus the final crystalline architectures are not easy to be obtained.

However, the bridged inorganic anions exhibit an advantage in spite of few reports. In the CSD, bifluoride (HF_2^-)⁹⁹⁻¹⁰⁰, hexafluorometallates (MF_6^- or MF_6^{2-})¹⁰¹⁻¹¹⁰, thiocyanate (SCN^-)¹¹¹⁻¹¹², nitrate (NO_3^-)^{95,103} and sulfate (SO_4^{2-})^{113, 114} have been reported to be bridged to the metallic cations (Figure 1-38).

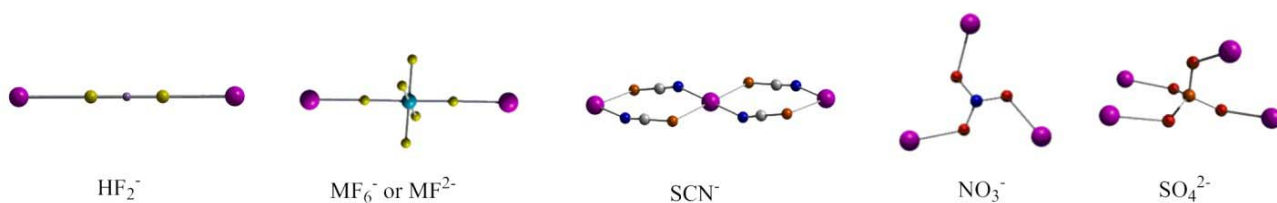


Figure 1-38: Schematic representation of reported multi-coordinating inorganic anions and their geometries.

1.6. Design of the project

As described above, we are rather far from the level of predicting the structures of molecular networks at present. However, we do believe in *Rome was not built in a day* and with this faith, over past two decades, we have pursued our effort in the area of molecular networks¹³⁻¹⁴, in particular, coordination networks using the principles of molecular tectonics. In the present thesis, I will expand on this idea to the porous coordination networks based on SiF_6^{2-} pillars.

1.6.1. Choice of the inorganic anion

In order to avoid the self-inclusion of counter-anions in generated cavities and difficult crystallization, this work was aimed at the inorganic coordinating anions. Compared with other inorganic anions, there are at least three advantages for SiF_6^{2-} anion.

- ◆ First, SiF_6^{2-} anion is a linear tecton: Among the reported multi-coordinating inorganic anions shown in Figure 1-38 and Table 1-1, only bifluoride (HF_2^-) and hexafluorometallates (MF_6^- or MF_6^{2-}) are linear. They bridge octahedral divalent metal centers⁹⁹⁻¹⁰⁴ and the interconnections takes place through the two fluorine atoms occupying the apical positions on the metal cation to serve as a pillar (Figure 1-39). It is known that a linear tecton is more flexible to connect any shape of metal cations, and thus leads to a variety of novel topologies.

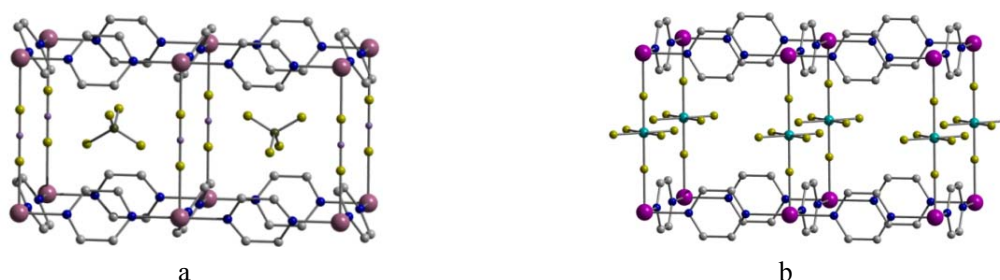


Figure 1-39: Portions of two examples based on linear inorganic anion pillars: $[\text{Cu}(\text{HF}_2)(\text{pyz})_2]\text{BF}_4$ (a) and $[\text{Zn}(\text{SiF}_6)(\text{pyz})_2]$ (b).

Table 1-1: Comparison of Cu-F distances in selected networks bridged by linear inorganic anions

Compounds ^[a]	Cu-F distances/Å	CSD code	Ref.
$[\text{Cu}(\text{HF}_2)(\text{pyz})_2]\text{BF}_4$	2.208	CETPIB	[99]
$[\text{Cu}(\text{SiF}_6)(2,6\text{-Me}_2\text{pyz})_4]_n$	2.313	LIQLED	[101]
$[\text{Cu}(\text{SiF}_6)(\text{ppzH})_4]_n$	2.251, 2.245	JJKIO	[106]
$\{[\text{Cu}(\text{SiF}_6)(\text{pyz})_3] \cdot 2\text{H}_2\text{O}\}_n$	2.402	700686	[110]
$[\text{Cu}(\text{SiF}_6)(4,4'\text{-bpy})_2]_n$	2.336	AFEKAX	[102]
$[\text{Cu}(\text{GeF}_6)(4,4'\text{-bpy})_2]_n$	2.421	AFEHUO	[103]
$[\text{Cu}_2(\text{PF}_6)(\text{NO}_3)(4,4'\text{-bpy})_4]_n$	2.585	AFEJOK	[103]
$[\text{Cu}_2(\text{TiF}_6)(\text{py})_4]_n$	2.511	JOLQAC	[104]

^[a] Abbreviations: pyz = pyrazine, 2,6-Me₂pyz = 2,6-dimethylpyrazine, 4,4'-bpy = 4,4'-bipyridine, py = pyridine.

- ◆ Second, the coordination ability of SiF_6^{2-} anion is moderate: Table 1-1 summarized all the reported cupric coordination networks bridged by linear inorganic anions (HF_2^- , MF_6^- and MF_6^{2-}). The lengths of Cu-F bonds are sorted with an order of $\text{HF}_2^- < \text{SiF}_6^{2-} < \text{GeF}_6^{2-} < \text{TiF}_6^{2-} < \text{PF}_6^-$, which presents their bond energies are sorted in a converse order. Considering the electrostatic matching, dianion SiF_6^{2-} was chosen.
- ◆ Thirdly, SiF_6^{2-} anion is a H-bond acceptor¹¹⁵, which leads to a possible selective site for H-bond donor molecules, such as H_2 ¹¹⁰.

1.6.2. Choice of the metallic cation

So far, the reported coordination networks bridged by SiF_6^{2-} (totally 9 structures, Table 1-2) are based on octahedral transitional divalent metallic cations (Co^{2+} , Cu^{2+} and Zn^{2+}). From the distances of M-F bonds listed in Table 1-2, it is found that the Zn-F bond length is shortest resulting in a strong bond energy theoretically. Considering its loose electronic cloud (large cationic radius) and possible flexible coordination, Zn^{2+} dication was chosen in this work.

Table 1-2: Comparison of distances in all reported networks bridged by SiF_6^{2-} anions

Compounds ^[a]	M	M-F distances/Å	M-N distances/Å	CSD code	Ref.
$[\text{Co}(\text{SiF}_6)(\text{viz})_4]_n$	Co	2.143	2.097	BOHFAF	[105]
$[\text{Cu}(\text{SiF}_6)(2,6\text{-Me}_2\text{pyz})_4]_n$	Cu	2.313	2.023	LIQLED	[101]
$[\text{Cu}(\text{SiF}_6)(\text{ppzH})_4]_n$	Cu	2.251, 2.245	1.992-2.009	JAJKIO	[106]
$\{[\text{Cu}(\text{SiF}_6)(\text{pyz})_3] \cdot 2\text{H}_2\text{O}\}_n$	Cu	2.402	2.054	700686	[110]
$[\text{Cu}(\text{SiF}_6)(4,4'\text{-bpy})_2]_n$	Cu	2.336	2.011	AFEKAX	[102]
$[\text{Zn}(\text{SiF}_6)(4,4'\text{-bpy})_2]_n$	Zn	2.082	2.157	ZESFUY	[107]
$\{[\text{Zn}(\text{SiF}_6)(\text{bbp})_2] \cdot 4\text{H}_2\text{O} \cdot 2\text{MeOH}\}_n$	Zn	2.135	2.145, 2.170	GELJEN	[109]
$\{[\text{Zn}(\text{SiF}_6)(4\text{-PDS})_2] \cdot 3\text{MeOH}\}_n$	Zn	2.135	2.007-2.170	LEMMAS	[108]
$\{[\text{Zn}(\text{SiF}_6)(\text{pyz})_2] \cdot 2\text{MeOH}\}_n$	Zn	2.057	2.172	700687	[110]

[^a] Abbreviations: viz = N-vinylimidazole, 2,6-Me₂pyz = 2,6-dimethylpyrazine, ppzH = 3(5)-phenylpyrazool, pyz = pyrazine, 4,4'-bpy = 4,4'-bipyridine, bbp = 1,3-bis(4-pyridyl)propane, 4-PDS = 4,4'-dipyridyldisulfide.

1.6.3. The overview of this PhD thesis

In this work, based on the molecular tectonics strategy, we will focus on the design, synthesis and characterization of porous coordination networks based on SiF_6^{2-} pillars and the study of their properties. Based on the nature of organic tectons, the manuscript is subdivided into three parts:

In Chapter II, we will start with some simple mono-dentate organic tectons bearing nitrogen, oxygen or sulfur atoms as coordinating sites and study their propensity for the design of SiF_6^{2-} pillar based coordination networks by a self-assembly method, and then focus on the rigid organic tectons bearing two extreme pyridine units. The influence of their length on the geometry and stability of final networks will be investigated by X-ray diffraction on single crystals (XRD) and powders

(PXRD) as well as by thermal analysis (TGA). In order to improve the stability of architectures, the same strategy was also applied using other metal cations, other functionalized organic tectons or by designing new tectons serving as diagonal of cuboid architecture.

In Chapter III, we will extend our investigations to semi-rigid naphthalene, spirobiindane and 1, 3, 5-triazine based tectons. A four-component parallelepiped 3-D architecture based on SiF_6^{2-} pillars as well as a series of 1-D to 3-D networks with different topologies based on other metallatectons were studied by XRD and TGA techniques. The influence of crystallizations on the conformations of semi-rigid tectons will be presented.

In Chapter IV, the last part of this work, we will explore the influence of flexible organic tectons. The tectons with different denticity, spacer (containing only methylene, tertiary carbon or chiral unit) and length will be involved. The coordination networks based on SiF_6^{2-} pillars will be generated using self-assembly methods and their topology and geometry will be investigated by XRD technique and thermal stability will be investigated by TGA technique.

References

1. K. G. Libbrecht, *Ken Libbrecht's Field Guide to Snowflakes*, Voyageur Press, **2006**.
2. <http://www.rkm.com.au/imagelibrary/index.html>
3. http://en.wikipedia.org/wiki/Wikipedia:Featured_picture_candidates/DNA_Overview
4. J.M. Lehn, *Supramolecular Chemistry: Concepts and Perspectives*, Wiley-VCH, **1995**.
5. L. A. Allison, *Fundamental Molecular Biology*, Blackwell Publishing, **2006**.
6. W. Demtröder, *Molecular Physics: Theoretical Principles and Experimental Methods*, Wiley-VCH, **2006**.
7. J.M. Lehn, *Angew. Chem. Int. Ed. Engl.*, **1990**, 29(11): 1304–1319.
8. J.M. Lehn, *Angew. Chem. Int. Ed. Engl.*, **1988**, 27 (11): 89-121.
9. J. M. Lehn, *Pure & Appl. Chem.*, **1978**, 50: 871-892.
10. M. C. Etter, *Acc. Chem. Res.*, **1990**, 23:120-126.
11. Y. L. Chang, M. A. West, F. W. Fowler, J. W. Lauher, *J. Am. Chem. Soc.* **1993**, 115:5991-6000.
12. S. Mann, *Nature*, **1993**, 365: 499-505.
13. M. W. Hosseini, *CrystEngComm*, **2004**, 6(56): 318-322.
14. M. W. Hosseini, *Acc. Chem. Res.*, **2005**, 38:313-323.
15. M. Simard, D. Su, J. D. Wuest, *J. Am. Chem. Soc.*, **1991**, 113: 4696-4698.
16. D. G. Hilmey, L. A. Paquette, *J. Org. Chem.*, **2004**, 69 (10):3262-3270.
17. S. Leininger, B. Olenyuk, and P. J. Stang, *Chem. Rev.*, **2000**, 100: 853-908.

18. J. L. Atwood, J. W. Steed, *Encyclopedia of Supramolecular Chemistry*, Taylor & Francis, **2004**: 1248-1256
19. D. S. Lawrence, T. Jiang, M. Levett, *Chem. Rev.*, **1995**, 95 (6): 2229-2260.
20. G. F. Swiegers, T. J. Malefetse, *Chem. Rev.*, **2000**, 100 (9): 3483-3538.
21. B. Moulton and M. J. Zaworotko, *Chem. Rev.*, **2001**, 101 (6):1629-1658.
22. F. Hajeck, E. Graf, M. W. Hosseini, X. Delaigure, A. De Cian, J. Fischer, *Tetrahedron Lett.*, **1996**, 37:1401-1404.
23. C. Klein, E. Graf, M. W. Hosseini, N. Kyritsakas-Gruber, *Transactions ACA*, **2005**, 39:1-7.
24. M. A. Beswick, C. Lopez-Casideo, M. A. Paver, P. R. Raithby, C. A. Russell, A. Steiner, D. S. Wright, *J. Chem. Soc., Chem. Comm.*, **1997**, 109-110.
25. M. J. Irwin, J. J. Vittal, G. P. A. Yap, R. J. Puddephatt, *J. Am. Chem. Soc.*, **1996**, 118:13101-13102.
26. P. Grosshans, A. Jouaiti, V. Bulach, J.-M. Planeix, M. W. Hosseini, J.-F. Nicoud, *Cryst. Eng.Comm.* **2003**, 5: 414-416.
27. A. J. Blake, N. R. Champness, A. Khlobystov, D. A. Lemenovskii, W. S. Li, M. Schroder, *Chem. Commun.* **1997**: 2027-2028.
28. B. F. Hoskins, R. Robson, and D. A. Slizys, *J. Am. Chem. Soc.*, **1997**, 119 (12): 2952-2953.
29. M. E. Kosal, J. H. Chou and K. S. Suslick, *J. Porphyrins Phthalocyanines*, **2002**, 6: 377-381.
30. C. Klein, E. Graf, M. W. Hosseini, A. De Cian, J. Fischer, *J. Chem. Soc., Chem. Commun.*, **2000**, 239-240.
31. A. Jouaiti, V. Jullien, M. W. Hosseini, J.-M. Planeix, A. De Cian, *Chem. Commun.*, **2001**, 1114-1115.
32. S. Ferlay, T. Mallah, J. Vaissermann, F. Bartolomé, P. Veillet, M. Verdaguer, *Chem. Commun.* **1996**, 2481-2842.
33. B. F. Abrahams, T. A. Hudson, R. Robson, *J. Mol. Struct.*, **2006**, 796: 2-8.
34. K. Biradha, Y. Hongo, M. Fujita, *Angew. Chem. Int. Ed. Engl.*, **2000**, 39 (21): 3843-3845.
35. A. F. Wells, *Three-dimensional Nets and Polyhedra*, Wiley-Interscience, New York, **1997**.
36. V. A. Blatov, A. P. Shevchenko, V. N. J. Serezhkin, *J. Appl. Cryst.*, **2000**, 33, 1193.
37. D. J. Duchamp, R. E. Marsh, *Acta. Cryst.* **1969**, B 25, 5-19.
38. D. J. Tranchemontagne, Z. Ni, M. O'Keeffe, O. M. Yaghi, *Angew. Chem. Int. Ed.*, **2008**, 47 (28):5136-5147.
39. O. M. Yaghi, M. O'Keeffe, N. Ockwig, H. K. Chae, M. Eddaoudi, J. Kim, *Nature*, **2003**, 423:705-714.
40. S. M. Holmes, G. S. Girolami, *J. Am. Chem. Soc.* **1999**, 121:5593-5594.
41. W. Dong, L. N. Zhu, H. B. Song, D. Z. Liao, Z. H. Jiang, S. P. Yan, P. Cheng, S. Gao, *Inorg.*

- Chem.*, **2004**, 43 (8): 2465-2467
42. H. Kovama, Y. Saito, *Bull. Chem. Soc. Jpn.*, **1954**, 27:112-114.
 43. N. Rosi, M. Eddaoudi, D. Vodak, J. Eckert, M. O'Keeffe, O. M. Yaghi, *Science*, 2003, 300: 1127-1129
 44. J. Rowsell, O. M. Yaghi, *Micro- and Mesoporous Mater.*, **2004**, 73:3-14.
 45. G Férey, *Acc. Chem. Res.* **2005**, 38: 217-225
 46. D. Maspoch, D. Ruiz-Molina, J. Veciana, *Chem. Soc. Rev.*, **2007**, 36: 770-818.
 47. G Férey, *Chem. Soc. Rev.*, **2008**, 37:191-241.
 48. A. Jouaiti, M. W. Hosseini, N. Kyritsakas, P. Grosshans, J.-M. Planeix, *Chem. Comm.*, **2006**, 3078-3080.
 49. L. Carlucci, G. Ciani, D. M. Proserpio, *Coord. Chem. Rev.*, **2003**, 246:247-289.
 50. K. T. Potts, C. P. Horwitz, A. Fessak, M. Keshavarz-K, K. E. Nash, P. J. Toscano, *J. Am. Chem. Soc.* **1993**, 115:10444 -10445.
 51. J. M. Lehn, A. Rigault, *Angew. Chem. Int. Ed.*, **1988**, 27:1095-1097.
 52. J. Bourlier, M. W. Hosseini, J.-M. Planeix, N. Kyritsakas, *New. J. Chem.*, **2007**, 31:25-32.
 53. A. Jouaiti, M. W. Hosseini, N. Kyritsakas, *J. Chem. Soc., Chem. Commun.*, **2002**, 1898-1899.
 54. I. Weissbuch, R. Popovitz-Biro, M. Lahav, L. Leiserowitz, *Acta Crystallogr.* **1995**, B51:115-148.
 55. S. M. Barlow, R. Raval, *Surf. Sci. Rep.*, **2003**, 50: 201-341.
 56. S.R. Batten and R. Robson, *Angew. Chem. Int. Ed.*, **1998**, 37:1460-1494.
 57. H.F. Zhu, J. Fan, T. Okamura, W.Y. Sun and N. Ueyama, *Chem. Lett.*, **2002**, 898-899.
 58. M. Maekawa, H. Konaka, Y. Suenaga, T. Kuroda-Sowa and M. Munakata, *J. Chem. Soc., Dalton Trans.*, **2000**, 4160-4166.
 59. L. Carlucci, G. Ciani and D.M. Proserpio, *J. Chem. Soc., Dalton Trans.*, **1999**, 1799-1804.
 60. M. Fujita, Y. J. Kwon, O. Sasaki, K. Yamaguchi, K. Ogura, *J. Am. Chem. Soc.*, **1995**, 117 (27): 7287-7288.
 61. T. Soma, T. Iwamoto, *Chem. Lett.*, **1994**, 821-824.
 62. S.R. Batten, B.F. Hoskins, R. Robson, *Chem. Eur. J.*, **2000**, 6:156-161.
 63. S.B. Copp, S. Subramanian, M.J. Zaworotko, *Angew. Chem. Int. Ed.*, **1993**, 32:706-709.
 64. S. R. Batten, *CrystEngComm*, **2001**, 3:67-72.
 65. L. Carlucci, G. Ciani, D. M. Proserpio, *CrystEngComm*, **2003**, 5: 269-279.
 66. V.A. Blatov, L. Carlucci and D.M. Proserpio, *CrystEngComm*, **2004**, 6:377-395.
 67. S. R. Batten, S. M. Neville, D. R. Turner, *Coordination Polymers: Design, Analysis and Application*, RSC publishing, **2009**.
 68. C. B. Aakeröy, A. M. Beatty and D. S. Leinen, *Angew. Chem., Int. Ed.*, **1999**, 38:1815-1819.

69. J. Pansanel, A. Jouaiti, S. Ferlay, M. W. Hosseini, J.M. Planeix, N. Kyritsakas, *New J. Chem.*, **2006**, 30:71-76.
70. K. Dunbar, R. A. Heintz, In *Progress in Inorganic Chemistry*, K. D. Karlin Ed.; John Wiley and Sons Inc. **1997**, Vol. 45, pp283-391, and the references there in.
71. B.F. Hoskins, R. Robson, *J. Am. Chem. Soc.*, **1989**, 111:5962-5964.
72. B. F. Hoskins, R. Robson, *J. Am. Chem. Soc.*, **1990**, 112:1546-1554.
73. J. R. Long, O. M. Yaghi, *Chem. Soc. Rev.*, **2009**, 38:1213-1214.
74. N. Ockwig, O. D. Friedrichs, M. O'Keeffe, O. M. Yaghi, *Acc. Chem. Res.* **2005**, 38:176-182.
75. D. J. Tranchemontagne, J. L. Mendoza-Cortes, M. O'Keefe, O. M. Yaghi, *Chem. Soc. Rev.*, **2009**, 38: 1257-1283.
76. J. J. Perry IV, J. A. Perman, M. J. Zaworotko, *Chem. Soc. Rev.*, **2009**, 38:1400-1417.
77. L. J. Murray, M. Dinca, J. R. Long, *Chem. Soc. Rev.*, **2009**, 38:1294-1314.
78. J. Y. Lee, O. K. Farha, J. Roberts, Joseph T. Hupp, *et al*, *Chem. Soc. Rev.*, **2009**, 38:1450-1459.
79. L. Q. Ma, C. Abney, W. B. Lin, *Chem. Soc. Rev.*, **2009**, 38:1248-1256.
80. M. Kurmoo, *Chem. Soc. Rev.*, **2009**, 38:1353-1379.
81. T. Uemura, N. Yanai, S. Kitagawa, *Chem. Soc. Rev.*, **2009**, 38:1228 -1236.
82. J.-R. Li, R. J. Kuppler, H.-C. Zhou, *Chem. Soc. Rev.*, **2009**, 38:1477 -1504.
83. T. Düren, Y. S. Bae, R. Q. Snurr, *Chem. Soc. Rev.*, **2009**, 38:1237 -1247.
84. M. D. Allendorf, C. A. Bauer, R. K. Bhakta, R. J. T. Houk, *Chem. Soc. Rev.*, **2009**, 38:1330 -1352.
85. S. Kitagawa, R. Kitaura, and S. Noro, *Angew. Chem. Int. Ed.*, **2004**, 43:2334-2375.
86. Z.Q. Wang, S. M. Cohen, *Chem. Soc. Rev.*, **2009**, 38:1315-1329.
87. G. Férey, C. Serre, *Chem. Soc. Rev.*, **2009**, 38:1380 -1399.
88. D. Zacher, O. Shekhan, C. Wöll, R. A. Fischer, *Chem. Soc. Rev.*, **2009**, 38:1418-1429.
89. A. M. Spokoyny, D. Kim, A. Sumrein, C. A. Mirkin, *Chem. Soc. Rev.*, **2009**, 38:1218-1227.
90. A. U. Czaja, N. Trukhan, Ulrich Müller, *Chem. Soc. Rev.*, **2009**, 38:1284-1293.
91. S. S. Kaye and J. R. Long, *J. Am. Chem. Soc.*, **2008**, 130: 806-807.
92. M. J. Plater, M. R. St J. Foreman, J. M. S. Skakle, *Crystal Engineering*, **2001**, 4, 293-308.
93. E. Deiters, V. Bulach, M. W. Hosseini, *New J. Chem.*, **2006**, 30:1289 -1294.
94. E. Deiters, V. Bulach, M. W. Hosseini, *New J. Chem.*, **2008**, 32:99-104.
95. M. N. Kozlova, S. Ferlay, N. Kyritsakas, M. W. Hosseini, *et al*, *Chem. Commun.*, **2009**, 2514-2516.
96. R. G. Xiong, J. Zhang, Z. F. Chen, X. Z. You, *et al*, *J. Chem. Soc., Dalton Trans.*, **2001**, 780-782.
97. D. Salazar-Mendoza, S. A. Baudron, M. W. Hosseini, *Inorg. Chem.*, **2008**, 47:766-768.

98. B. Wang, A. P. Côté, H. Furukawa, M. O'Keeffe, O. M. Yaghi, *Nature*, **2008**, 453: 201-211.
99. J. L. Manson, M. M. Conner, J. A. Schlueter, T. Lancaster, *et al*, *Chem. Commun.*, **2006**, 4894-4896.
100. S. Brown, J. Cao, J. L. Musfeldt, M. M. Conner, *et al*, *Inorg. Chem.*, **2007**, 46:8577-8583.
101. M. Conner, A. McConnell, J. Schlueter, J. Manson, *J. Low. Temp. Phys.* **2006**, 142: 273-278.
102. S.I., Noro, S. Kitagawa, M. Kondo, K. Seki, *Angew. Chem. Int. Ed.*, **2000**, 39:2081-2084.
103. S.I., Noro, R. Kitaura, M. Kondo, S. Kitagawa, *et al*, *J. Am. Chem. Soc.*, **2002**, 124:2568-2583.
104. A. J. Norquist, K. R. Heier, C. L. Stern, K. R. Poeppelmeier, *Inorg. Chem.*, **1998**, 37:6494-6501.
105. R. A. J. Driessen, F. B. Hulsbergen, W. J. Vermin, J. Reedijk, *Inorg. Chem.*, **1982**, 21:3594-3597.
106. F. S. Keij, R. A. G. De Graaff, J. G. Haasnoot, J. Reedijk, *Inorg. Chim. Acta*, **1989**, 156: 65-70.
107. S. Subramanian, M. J. Zaworotko, *Angew. Chem. Int. Ed.*, **1995**, 34: 2127-2129.
108. M.C. Suen, J.C. Wang, *Struct. Chem.*, **2006**, 17:315-322.
109. M.C. Suen, Z.K. Chan, J. D. Chen, J.C. Wang, C. H, Hung, *Polyhedron*, **2006**, 25:2325-2332.
110. K. Uemura, A. Maeda, T. K. Maji, P. Kanoo, H. Kita, *Eur. J. Inorg. Chem.* **2009**, 16: 2329-2337.
111. A. J. Blake, N. R. Brooks, N. R. Champness, M. Crew, *et al*, *J. Chem. Soc. Dalton Trans*, **1999**, 2813-2817.
112. M. G. Barandika, M. L. Hernandez-Pino, M. K. Urtiaga, R. Cortes, *et al*, *J. Chem. Soc. Dalton Trans*, **2000**, 1469-1473.
113. W. Ouellette, B. S. Hudson, J. Zubieta, *Inorg. Chem.*, **2007**, 46 (12): 4887-4904.
114. C. H. Springsteen, R. D. Sweeder, R. L. LaDuca, *Crystal Growth & Design*, **2006**, 6 (10): 2308-2314.
115. A. Waskowska, *Acta Cryst.* **1997**, C53: 128-130.
116. W. Jaunky, M. W. Hosseini, J.-M. Planeix, A. De Cian, N. Kyritsakas, J. Fischer, *Chem. Comm.*, **1999**, 2313-2314.
117. <http://www.chem.monash.edu.au/staff/sbatten/interpen/index.html>
118. J. D. Dunitz, *Chem. Commun.*, 2003, 545-548.

**CHAPTER II : DESIGN AND STUDY OF THE
COORDINATION NETWORKS BASED ON RIGID
ORGANIC TECTONS AND HEXAFLUOROSILICATE
PILLARS**

Chapter II: Design and Study of the Coordination Networks Based on Rigid Organic Tectons and SiF_6^{2-} Pillars

In this chapter, the constructions of cuboid 3-D coordination networks based on SiF_6^{2-} pillars are described. A series of rigid organic tectons of different length bearing two pyridines oriented in a divergent fashion were chosen to modulate the size and shape of cuboid 3-D networks. In the meantime, the stabilities of the cuboid 3-D architectures were improved by several approaches, such as changing the central metal and the functionalization of the rigid tectons.

2.1. Introduction

The rational design and synthesis of coordination networks with cubic or cuboid shape are of great interest because of their porosity and applications that they might offer¹⁻³. Prussian blue, a cubic arrangement of iron and cyanide entities and its analogues have been widely studied in past decades and their properties were shown to depend on the metal cations (homonuclear or heteronuclear) in their structures⁴⁻⁷.

Herein, let us focus on the design of homonuclear cubic networks. Such architecture can be defined by a single metal centre (M) as a structural node adopting the octahedral coordination geometry and three organic tectons (T) behaving as connectors. As shown in Figure 2-1, when three identical tectons (T), are used, geometrically the architecture is defined as a cube (M, 3T) (Figure 2-1left). When the tectons are different, the assembly is of the cuboid (M, T1, 2T2, Figure 2-1middle) or rectangular prismatic type (M, T1, T2, T3, Figure 2-1right).

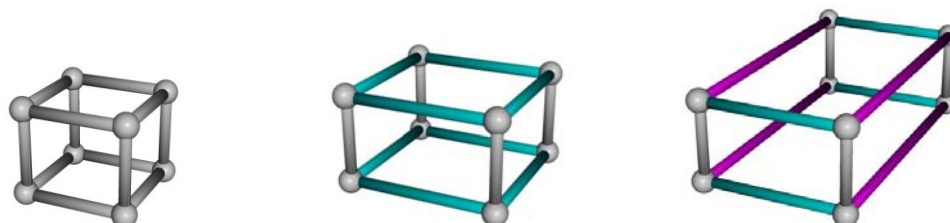


Figure 2-1: Schematic representation of homonuclear cubic ($a = b = c$), cuboid ($b, a \neq b = c$) and rectangular prismatic ($a \neq b \neq c$) coordination networks.

For the design of cubic networks, a two components system (M, 3T) is rather trivial and the majority of reported example belongs to that category^{3, 8}. However, the design and controlled generation of cuboid architectures by self-assembly processes require a more sophisticated strategy. The simplest cuboid case (Figure 2-1b), a three components system (M, T1, 2T2) requires to combine a metal centre with two different tectons. In order to avoid homo self-assembly processes to take place leading to two independent cubic networks (M, 3T1) and (M, 3T2) networks, one needs to differentiate both tectons through their binding mode towards the metal. The last case (Figure 2-1c), not yet reported, is even more complicated to achieve since it requires a metal and three differentiated tectons (a four components system).

The design principle developed in the context of this work fits with the second type cuboid networks. Using octahedral Zn^{2+} (M) as a structural node, its counter anion SiF_6^{2-} as first inorganic tecton T1 and a rigid organic ligand as the second tecton T2, depending on the different types of connectivity of T1 and T2, a series of 3-D cuboid coordination networks of the type ($a \neq b = c$) can be constructed. The metrics of cuboid networks can be controlled by the length of organic tectons T2. The control of the metrics is pertinent since it allows tuning the size and shape of channels and thus the porous properties of the materials.

When dealing with rigid organic tectons, one needs to define several features such as the choice of the donor atom (the coordinating site of organic tecton), the choice of solvent used for self-assembly, and the possible role played by H-bond donor/acceptor groups present within the organic tectons. Thus, as a first step, we have explored the formation of networks using simple commercially available organic tectons in the presence of SiF_6^{2-} anion and metal dications.

2.2. Design of organic tectons (T2)

2.2.1. The choice of donor atom and solvent

In previously reported examples⁹⁻¹¹, organic tectons (T2) based on imidazole or pyridine have been used for the generation of cuboid SiF_6^{2-} pillared based coordination networks. We have extended these systems to other organic tectons containing oxygen or sulfur donor atoms. Some commercially available, mono-dentate organic solvents, such as methanol, ethanol, acetone, THF, DMSO and ligand such as thiophene were combined with ZnSiF_6 using a liquid-liquid diffusion method.

Unfortunately, no crystalline materials have been obtained. Indeed, evaporation of the solutions containing the mixture afforded colorless prism type crystals composed of $\text{ZnSiF}_6 \cdot 6\text{H}_2\text{O}$. The crystalline material was analyzed by the X-ray diffraction on single crystal.

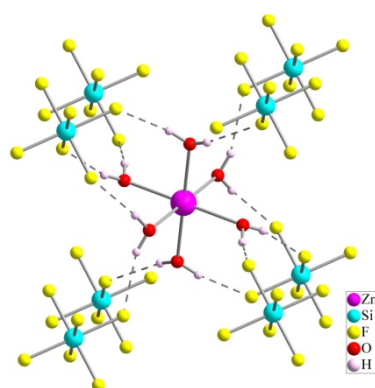


Figure 2-2: Portions of the crystal structure of $\text{ZnSiF}_6 \cdot 6\text{H}_2\text{O}$.

As reported by S. Ray and his co-worker in 1973¹², the crystal system for $\text{ZnSiF}_6 \cdot 6\text{H}_2\text{O}$ is monoclinic with $R\bar{3}$ as the space group. In the crystal (Figure 2-2), each zinc cation adopt the octahedral coordination geometry with six waters coordinating at six vertices. Each water molecule

links the neighboring two F atoms of SiF_6^{2-} by the strong hydrogen bonds ($d_{\text{H-F}} = 1.85\text{-}1.98\text{\AA}$) thus leading to the formation of a 3-D molecular network.

The coordination ability of the tectons bearing oxygen or sulfur atoms was found to be inexistent since the pK_a value for their protonated species in aqueous solution is much lower than the one of water (Table 2-1). According to Lewis acid-base concepts, the coordinated waters in $\text{ZnSiF}_6 \cdot 6\text{H}_2\text{O}$ are not easily substituted by a weak Lewis base (methanol, ethanol and THF *etc*) with pK_a lower than that of water (-1.7)¹³. For this reason, these tectons will be used as linkers and solvents during the self-assembly.

Table 2-1: Comparison of protonated pK_a for some selected organic tectons¹³

Name	pK_a	Name	pK_a	Name	pK_a
Acetone	-3.8	Methanol	-2.2	THF	-2.05
DMSO	-1.8	Water	-1.7	Pyrazine	0.65
4,4'-Bipyridine	4.4	Pyridine	5.21	Imidazole	6.95
4-cyanopyridine	1.6	Acridine	5.6		

Thus, we have to design an organic tecton T2 bearing coordination units behaving as a strong Lewis base ($pK_a > -1.7$). For that reason, pyridine and imidazole groups are candidates of choice. Dealing with the spacer connecting the coordinating sites, they can be any fragment containing C, O and S atoms whose pK_a are lower than the one of water. For the same reasons, solvents, such as CHCl_3 , ethanol and THF *etc*, possessing low pK_a values may be used.

2.2.2. The role of H-bond donor group located within the framework of the tectons (T2) on the formation of the network

The SiF_6^{2-} anion is a good H-bond acceptor. For the design of the network, it is necessary to consider how to use or to prevent this event.

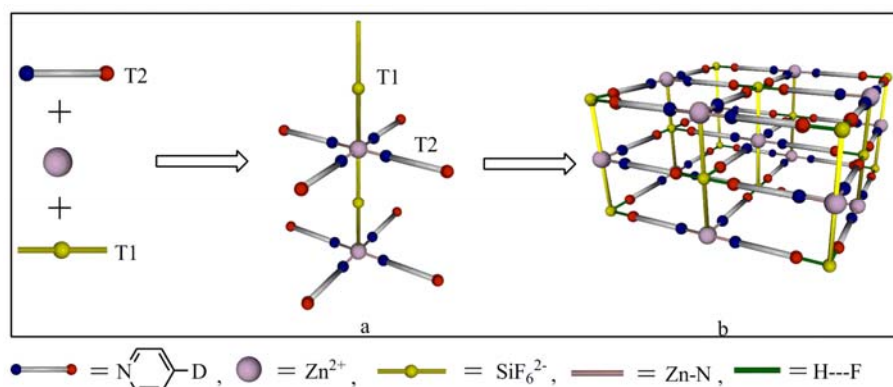
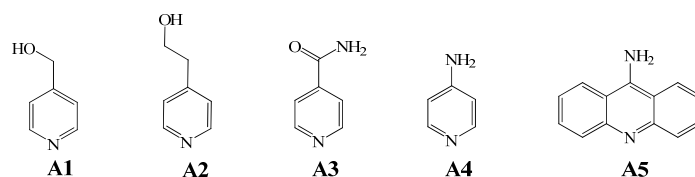


Figure 2-3: Schematic representation of a possible routine to build 3-D molecular networks by H-bonds..

For example, the combination of a monodentate tecton T2 bearing a unit bearing a H-bond donor site (*e.g.* OH, CONH_2 , NH_2 , *etc*) with ZnSiF_6 can lead to the formation of 1-D pinwheel-type

coordination networks with four free hydrogen bond donor sites (Figure 2-3a). Through hydrogen bonding interactions of the D--F type with SiF_6^{2-} anion, the neighboring 1-D networks may be connected into a 3-D molecular network (Figure 2-3b).

Consequently, some commercially available pyridine-based tectons substituted with hydroxyl, carboxamide or amine moieties (series **A**, Scheme 2-1) have been chosen to illustrate this design principle. With respect 4-cyanopyridine¹⁴ ($pK_a=1.9$), the pK_a of tectons should be higher than 1.9 in order to build pillared type complexes.



Scheme 2-1

For all chosen tectons, colorless crystalline materials were obtained upon slow diffusion of an EtOH solution of $\text{ZnSiF}_6 \cdot 6\text{H}_2\text{O}$ into a CHCl_3 or DMSO solution of the tectons. Unfortunately, in the majority of cases, crystals obtained were of poor quality.

Only in the case of 9-aminoacridine (**A5**), the colorless prismatic crystals were suitable for X-ray single crystal diffraction studies. The structural study revealed the formation of a 3-D hydrogen-bonded network composed of protonated 9-aminoacridine and SiF_6^{2-} anion ($2(\text{HA5})\text{SiF}_6$, abbreviated as **A5**· H_2SiF_6 , Figure 2-4). Within the network, each protonated 9-aminoacridine is linked by two neighboring SiF_6^{2-} anions and each SiF_6^{2-} anion is connected to five protonated 9-aminoacridine through three types of N--H--F H-bonds ($d_{\text{H-F}} = 2.05\text{-}2.10\text{\AA}$) and two types of weak C--H--F H-bond ($d_{\text{H-F}} = 2.30\text{-}2.50\text{\AA}$).

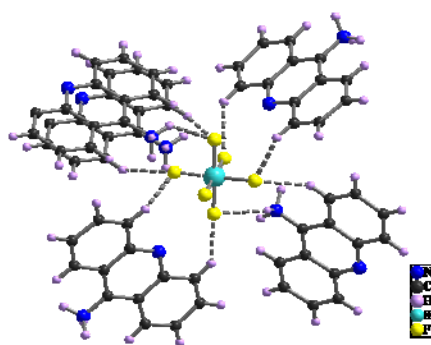


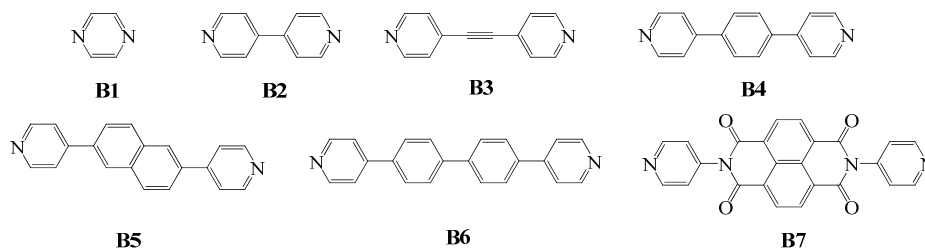
Figure 2-4: Portions of the crystal structure of **A5**· H_2SiF_6 .

In order to avoid the competition between the generation of H-bonded networks through hydrogen bonds between the protonated self-complementarities tecton and SiF_6^{2-} anion and coordination networks containing both SiF_6^{2-} anion and Zn^{2+} cation, we decided to avoid organic tectons T2 possessing hydrogen-bond donor units.

2.3. Construction and modulation of cuboid 3-D coordination networks

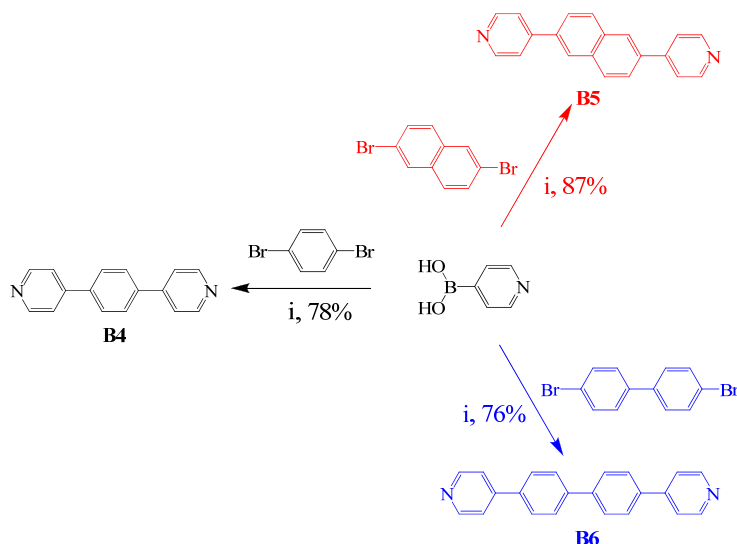
2.3.1. Design and synthesis of rigid organic tectons T2

Based on above observations concerning the tecton design, in order to build and modulate the size of 3-D cuboid SiF_6^{2-} pillared frameworks, seven rigid organic tectons (series **B**, Scheme 2-2) of different length bearing two pyridines oriented in a divergent fashion have been chosen.



Scheme 2-2

Among them, pyrazine (**B1**) and 4, 4'-bipyridine (**B2**) were commercially available and used without further purification. 1, 2-di(pyridin-4-yl)ethyne (**B3**) has been prepared following reported procedures¹⁵⁻¹⁷ by coupling 4-bromopyridine with 4-ethynylpyridine in the presence of catalytic amounts of $\text{PdCl}_2(\text{PPh}_3)_2$ and CuI . 1,4-di(pyridine-4-yl)benzene (**B4**), 2,6-di(pyridine-4-yl)naphthalene (**B5**) and 4,4'-di(pyridin-4-yl)biphenyl (**B6**) have been prepared in high yields by the Suzuki coupling reaction¹⁸⁻¹⁹ of 4-pyridylboronic acid with the required dibromo aromatic compounds under anaerobic in the presence of $[\text{Pd}(\text{PPh}_3)_4]$ as catalyts (Scheme 2-3) (*see experimental section*).



Scheme 2-3: Reaction conditions: (i) Cs_2CO_3 , $[\text{Pd}(\text{PPh}_3)_4]$, deoxygenated DMF under N_2 for 48 h.

The last tecton, N, N'-Di-(4-pyridyl)-1, 4, 5, 8-naphthalenetetracarboxydiimide (**B7**) has been prepared in high yield (82%) from 1, 4, 5, 8-naphthalenetetracarboxylic dianhydride and 4-aminopyridine using the same procedure as described in the literature²⁰.

2.3.2. Structural studies of cuboid 3-D networks

Upon slow diffusion of an EtOH solution of $\text{ZnSiF}_6 \cdot 6\text{H}_2\text{O}$ (5 mg) into a CHCl_3 solution (1 mL) of tectons **B1**, **B2**, **B3**, **B4** and **B7** (3mg), DMSO solution (1 mL) of **B5** (3mg) or $\text{CHCl}_2\text{CHCl}_2$ solution (1 mL) of **B6** (3mg) at room temperature, colorless (red for **B7**) prismatic crystalline materials were obtained in the crystallization tubes after several days. For all combinations of six tectons (**B1-B6**), the crystalline material obtained was structurally investigated by X-ray diffraction technique on single crystals. Unfortunately, for tecton **B7**, the quality of the crystal was too poor to be structurally characterized by X-ray diffraction on single crystal.

Since the unit cell parameters for **B1**· ZnSiF_6 ($a = b = 7.1409\text{\AA}$, $c = 7.6068\text{\AA}$) were identical to those reported in the literature¹¹, the structural study was not further pursued. Interestingly, for **B2**· ZnSiF_6 the unit cell parameters ($a = b = 16.049\text{\AA}$, $c = 15.368\text{\AA}$, Table 2-2) were found to be different from published one ($a = b = 11.396\text{\AA}$, $c = 7.677\text{\AA}$)¹⁰ and thus its structure was investigated. In the following section, we describe the crystal structures of the five new networks generated and compare them with published architectures¹⁰⁻¹¹.

Table 2-2: Selected crystallographic parameters for cuboid 3-D coordination networks

Compound	Chemical formula	Crystal system	Space group	a(Å)	b(Å)	c(Å)
B2 · ZnSiF_6	$[\text{Zn}(\text{B2})_2\text{SiF}_6]_4 \cdot 22\text{H}_2\text{O}$	Tetragonal	<i>I4/mcm</i>	16.049	16.049	15.368
B3 · ZnSiF_6	$[\text{Zn}(\text{B3})_2\text{SiF}_6] \cdot 6\text{CHCl}_3$	Tetragonal	<i>I4/mcm</i>	19.594	19.594	15.067
B4 · ZnSiF_6	$[\text{Zn}(\text{B4})_2\text{SiF}_6]_4 \cdot 8\text{CHCl}_3 \cdot \text{H}_2\text{O}$	Tetragonal	<i>I4/mcm</i>	22.059	22.059	15.094
B5 · ZnSiF_6	$[\text{Zn}(\text{B5})_2\text{SiF}_6] \cdot 2\text{DMSO} \cdot \text{C}_2\text{H}_5\text{OH}$	Tetragonal	<i>P4/ncc</i>	17.789	17.789	15.047
B6 · ZnSiF_6	$[\text{Zn}(\text{B6})_2\text{SiF}_6] \cdot 4\text{C}_2\text{H}_4\text{Cl}_2$	Tetragonal	<i>P4/ncc</i>	19.918	19.918	15.289

The X-ray diffraction study revealed that all five crystals are composed of organic tecton T2, Zn^{2+} dication and SiF_6^{2-} anion however with different crystallization solvents (Figure 2-5). The crystallographic data shows that crystals based on three short tectons **B2**, **B3** and **B4** are isostructural (tetragonal system and *I4/mcm* space group). The Zn atoms are located on sites with 42 symmetry and the Si atoms are located at sites with 4/m symmetry. For all three cases, no interpenetration is observed.

Crystals based on two long tectons **B5** and **B6** are isostructural (tetragonal system and *P4/ncc* space group) and form another category. In this category, a homo second-order interpenetration is observed. Interestingly, all architectures generated offer channels filled with different crystallization solvent molecules, more specifically, H_2O for **B2**· ZnSiF_6 , CHCl_3 for **B3**· ZnSiF_6 , CHCl_3 and H_2O for **B4**· ZnSiF_6 , DMSO and $\text{CH}_3\text{CH}_2\text{OH}$ for **B5**· ZnSiF_6 and $\text{CHCl}_2\text{CHCl}_2$ for **B6**· ZnSiF_6 (Figure 2-5).

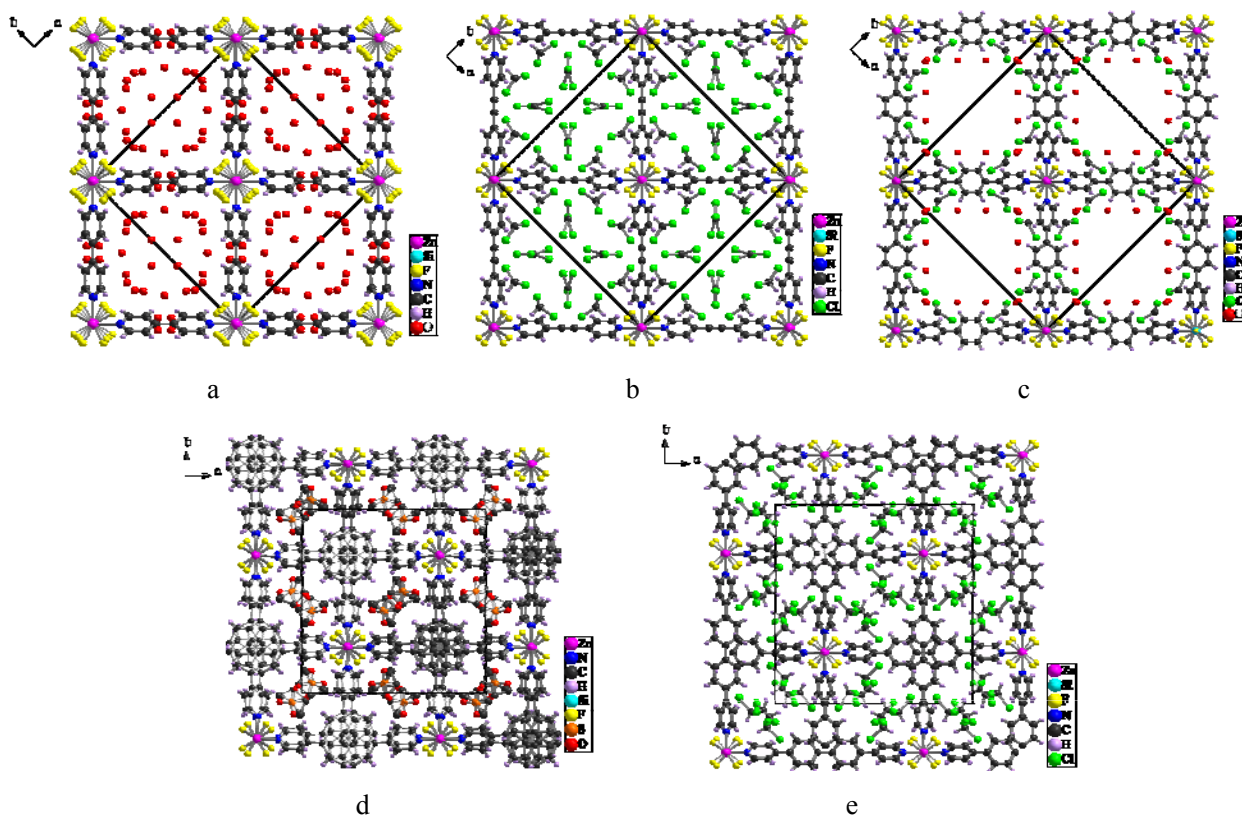


Figure 2-5: top views of the crystal structure of architectures based on the tecton **B2** (a), **B3** (b), **B4** (c), **B6**(d) and **B7** (e) with $\text{ZnSiF}_6 \cdot 6\text{H}_2\text{O}$

As expected from the design principle mentioned above, the combination of three compounds composed of the organic tectons (**B2-B6**), Zn^{2+} cation and SiF_6^{2-} dianion (octahedral geometry with F-Si-F angles of 180 and 90°), behaving as a linear inorganic tecton, leads to the formation of neutral cuboid type architectures (Figure 2-6).

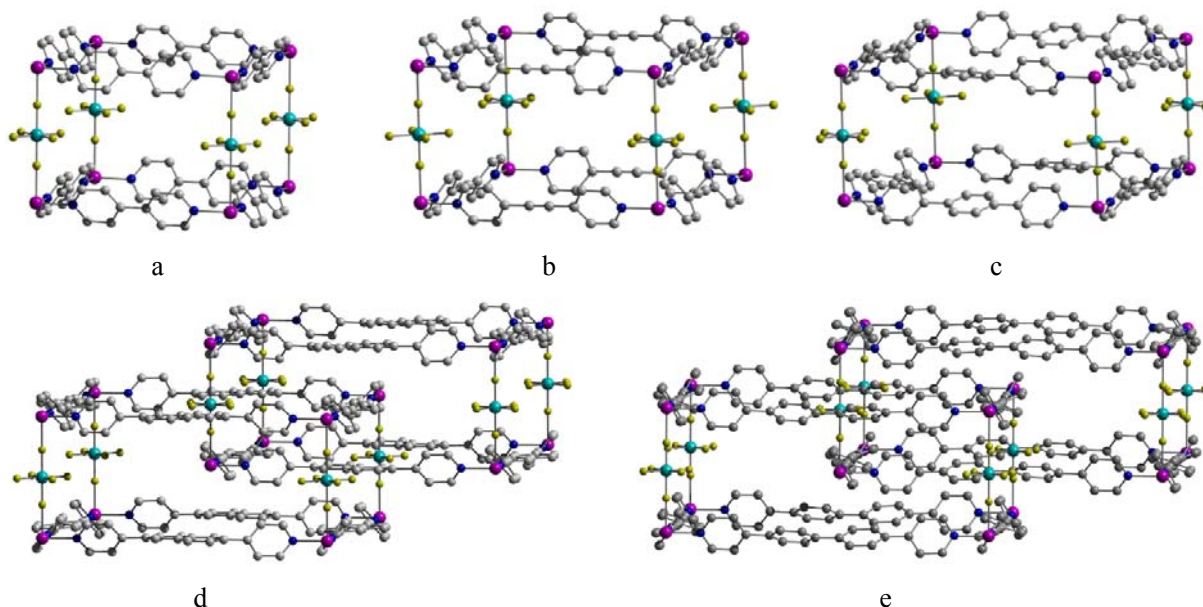


Figure 2-6: Portions of the X-ray structures of cuboid neutral 3-D networks **B2**· ZnSiF_6 (a), **B3**· ZnSiF_6 (b), **B4**· ZnSiF_6 (c), **B5**· ZnSiF_6 (d) and **B6**· ZnSiF_6 (e). For clarity, the solvents and H atoms are omitted.

Despite the different crystal space groups, the five structures present the same connectivity. Each Zn^{2+} cation, adopting an octahedral coordination geometry (N-Zn-N and F-Zn-F angles of 90° and 180° , details listed in Table 2-3), is connected to four rigid organic tectons T2 through the formation of Zn-N bonds ($d_{\text{Zn-N}} = 2.11\text{-}2.14 \text{ \AA}$) in the square plane of the octahedron around the metal and the other two axial positions are bridged by the SiF_6^{2-} counter-anion ($d_{\text{Si-F}} = 1.59\text{-}1.67 \text{ \AA}$ for unbound fluorine atoms and $d_{\text{Si-F}} = 1.70\text{-}1.73 \text{ \AA}$ for bridging F atoms) with Zn-F bonds ($d_{\text{Zn-F}} = 2.07\text{-}2.15 \text{ \AA}$). As a result, along the direction of Zn-F bond (c axis in these structures), a neutral 1-D network ZnSiF_6 is formed (Figure 2-7a), which can be regarded as a pillar imposing one of the parameters of the cuboid architecture. Each organic tecton T2, offering two coordination sites, serves as a connector to link the neighboring two ZnSiF_6 pillars and leads to the final 3-D cuboid networks (Figure 2-7b and c). The long connectors of **B5** and **B6** lead to the interpenetration of 3-D cuboid architectures (Figure 2-7c). Similar observations have been reported for MOF-5 analogues by Yaghi and his co-workers²¹.

Table 2-3: Selected bonds and angles for cuboid 3-D coordination networks

Compound	Zn-F(SiF_6^{2-}) distances/ \AA	Zn-N distances/ \AA	Si-F (unbound) distances/ \AA	Si-F (bridge) distances/ \AA	N-Zn-N angles/ $^\circ$	F-Zn-F angles/ $^\circ$
B2 · ZnSiF_6	2.122, 2.123	2.137	1.592	1.714	90	180
B3 · ZnSiF_6	2.069	2.124	1.667	1.697	90	180
B4 · ZnSiF_6	2.074	2.112	1.669	1.699	90	180
B5 · ZnSiF_6	2.064, 2.066	2.135	1.669	1.698	90	180
B6 · ZnSiF_6	2.097	2.129	1.675	1.704, 1.712	90, 90.25	180

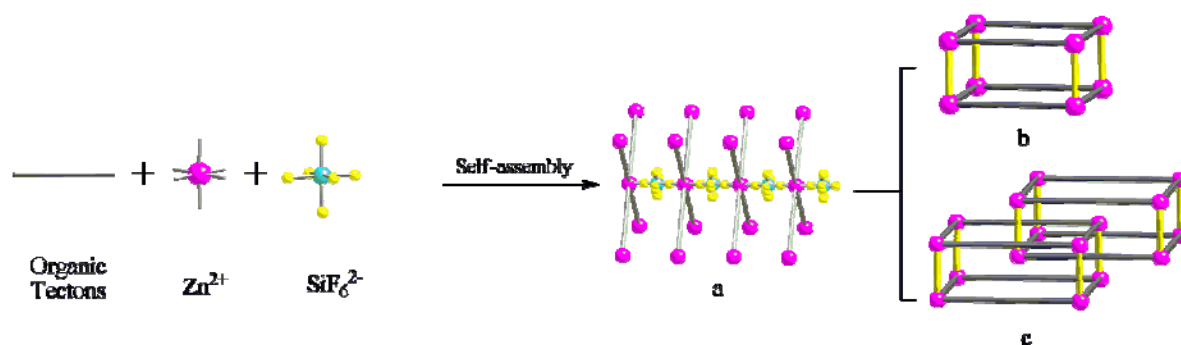


Figure 2-7: The illustration of the possible construction process leading to the formation of the cuboid 3-D networks. In **b** and **c**, the yellow cylindrical rods are used to illustrate the SiF_6^{2-} pillars

For the non-interpenetrated networks (**B2**· ZnSiF_6 , **B3**· ZnSiF_6 and **B4**· ZnSiF_6), the pyridine rings of three tectons **B2**, **B3** and **B4** are parallel and coplanar (dihedral angle of 0.0°). In the case of **B4**, the central aromatic moiety is tilted by *ca.* 37.8° with respect to the pyridine units. On the contrary, in the interpenetrated architectures, the pyridine rings of two tectons **B5** and **B6** are intersecting with dihedral angle of 80.2° and 61.6° . For the tecton **B5**, the central naphthalene moiety is tilted by *ca.* 49.9° and 49.8° to the two adjacent pyridine units respectively. For the tecton **B6**, the dihedral angle between the benzene ring and its neighboring pyridine ring are *ca.* 38.7° and

39.5° respectively and thus that between the central two benzene rings is *ca.* 40.7°.

Concerning the solvents presented in networks, for **B2**·ZnSiF₆, each cuboid unit is filled with 22 crystallization H₂O molecules. Four of them are interconnected forming a square ring by hydrogen bonds and located at the center of Zn-4,4'-bpy layer as illustrated in Figure 2-8. The remaining 18 H₂O molecules are hydrogen bonded and form tetradecagon water crown type arrangement and located between Zn-4,4'-bpy layer *via* hydrogen bonds with the F atoms of the SiF₆²⁻ anions (Figure 2-8b). The tetradecagon water crowns in the neighboring two units are linked together forming a plane of water molecules (Figure 2-8a).

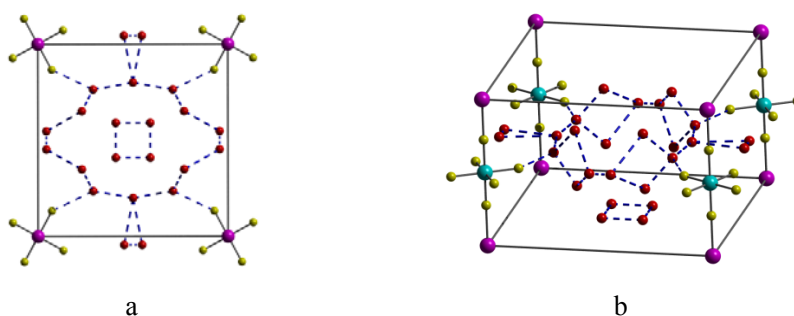


Figure 2-8: views of square four-ring and tetradecagon crown of guest H₂O molecules. The tecton 4,4'-bpy is omitted and illustrated with a line for clarity.

For the **B3**·ZnSiF₆, the channels are filled with 6 crystallization chloroform molecules per cuboid unit. Among them, four chloroform molecules are hydrogen bonded to the F atoms of the SiF₆²⁻ anions. The remaining molecules are disordered and located at the center of two pillars along *a* or *b* axis without any specific interactions (Figure 2-9a). For the **B4**·ZnSiF₆, the cuboid unit is occupied by 1/2 water and 4 chloroform molecules (Figure 2-9b). Some solvent molecules are disordered and unfortunately not all of them could be refined. For that reason, the quality of the structural determination is rather poor.

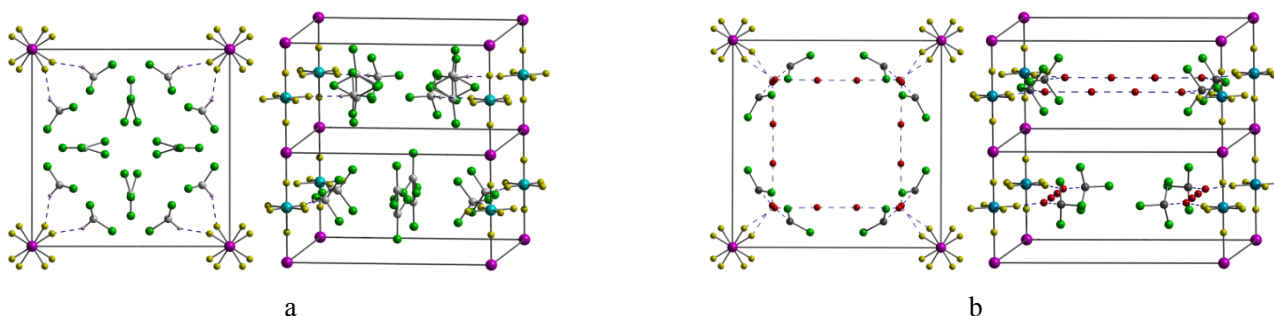


Figure 2-9: top and side views of solvent packing for the **B3**·ZnSiF₆ (a) and **B4**·ZnSiF₆ (b). The tectons are omitted and illustrated with a line for clarity.

For the two interpenetrating complexes, the channels are taken up by the two DMSO and one ethanol molecules for **B5**·ZnSiF₆, and four CHCl₂CHCl₂ molecules for **B6**·ZnSiF₆. They are located at the plane of Zn-tecton without any specific interactions with the network skeletons (Figure 2-10).

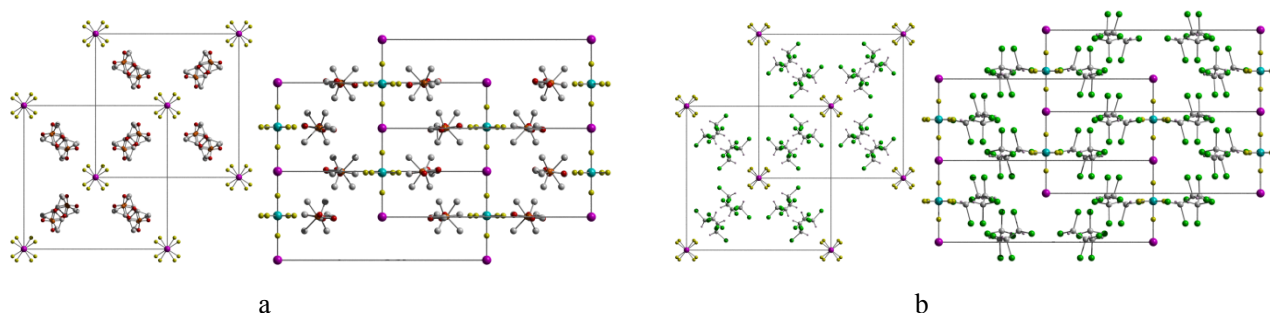


Figure 2-10: top and side views of solvent packing for the **B5**·ZnSiF₆ (a) and **B6**·ZnSiF₆ (b). The tectons are omitted and illustrated with a line for clarity.

To a great extent, the included guest molecules in the cuboid 3-D networks are depending on the nature of the diffusion solvents. However, much to our surprise, the analogous **B2**·ZnSiF₆, **B3**·ZnSiF₆ and **B4**·ZnSiF₆ present a selectivity towards the included solvents.

Moreover, another unclear but important fact for this type cuboid 3-D networks is their formation mechanism. In contrast with the crystal structure of ZnSiF₆·6H₂O for which each Zn²⁺ cation is coordinated to six water molecules and thus no Zn-F bonds is found, in the cases of cuboid 3-D networks, the pyridine units of rigid organic tectons T2 play an important role in the formation of Zn-F bonds. The possible step is that the substitution of equatorial four water molecules by pyridine groups may lead to the construction of the 2-D network and then the axial two water molecules could be substituted by SiF₆²⁻ anions.

One may wonder why the pyridine groups do not substitute all the six waters around Zn²⁺ cation, but only four in the equatorial plane? For metal centers adopting the octahedral coordination geometry, case of hexacoordination by six pyridine groups (not chelate type ligands, such as 2, 2'-bipyridine²³, 1, 10-Phenanthroline²⁴, etc.) are rather rare. A search in the CCDC database revealed only one example of a network¹, as shown in Figure 1-37. In support of our observation, in most cases reported, pyridine groups indeed occupy the four coordinating sites of octahedral metal cation in the equatorial plane and the axial two positions are always occupied by anions or solvents. Another question which remains to be answered is why the two axial water molecules are replaced by the fluorine atoms of SiF₆²⁻? A possible explanation may relate to the fact that the presence of four pyridine groups in equatorial plane lead to the weakening of H₂O-Zn interactions. Indeed, the Zn-O distance in ZnSiF₆·6H₂O (2.05-2.08Å), is shorter than the one observed (2.13Å) for 2-D coordination networks {[Zn(H₂O)(4,4'-bpy)₂] SiF₆}_n²⁵. Furthermore, owing to the anionic nature of SiF₆²⁻, electrostatic interactions and the formation of a neutral node also favor the replacement of water molecules.

In order to achieve the minimum of steric interactions, the octahedron of SiF₆²⁻ anions are staggered with respect to octahedron around Zn²⁺, as listed Table 2-4 and Figure 2-11. Compared to the published **B1**·ZnSiF₆ and **B2**·ZnSiF₆-2 with *P4/mmm* space group, the stagger angles of our networks are much smaller (28.6 - 38.3°), which may be attributed to the smaller canting angles

between the plane of pyridine group in the xy coordination plane (square plane of octahedral Zn^{2+} , $49-60^\circ$ for our compounds, 90° for reported compounds). The latter is possibly caused by the hydrogen bonding type interactions between included solvents and organic tectons.

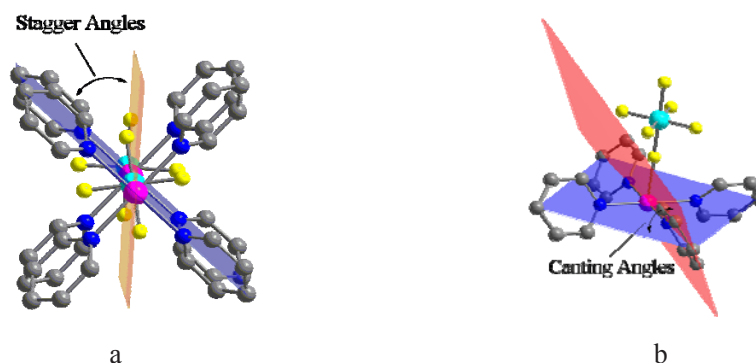


Figure 2-11: The illustrations of stagger angles (a) and canting angles (b).

Table 2-4: Comparison of angles.

Compound	B2 ·ZnSiF ₆	B3 ·ZnSiF ₆	B4 ·ZnSiF ₆	B5 ·ZnSiF ₆	B6 ·ZnSiF ₆	B1 ·ZnSiF ₆ ^[11]	B2 ·ZnSiF ₆ - 2 ^[10]
Stagger angles/ ^o [^a]	28.63	32.52	31.07	35.56	38.29	45	45
Canting angles/ ^o [^b]	58.75	57.08	54.52	49.93	59.36	90	90

[^a] Angles between the plane FFFF and NNNN along the direction of pillars, as illustrated in Figure 2-11a; [^b] Angles between xy coordination plane and coordination pyridine plane, as illustrated in Figure 2-11b

It is worth noting that, as mentioned above, for **B2**·ZnSiF₆, the space group $I4/mcm$ observed is different from the published case (**B2**·ZnSiF₆-**2**, $P4/mmm$)^[10]. The analysis of their unit cell parameters reveals that their skeletons are nearly same however with different translation, as shown in Figure 2-12a. This is substantiated by the nearly same simulated powder X-ray diffraction (PXRD) patterns from their single crystal structure data upon removal of solvent molecules (Figure 2-12b) The lower space group for **B2**·ZnSiF₆-**2** is attributed the lower symmetries of their included solvents (DMF).

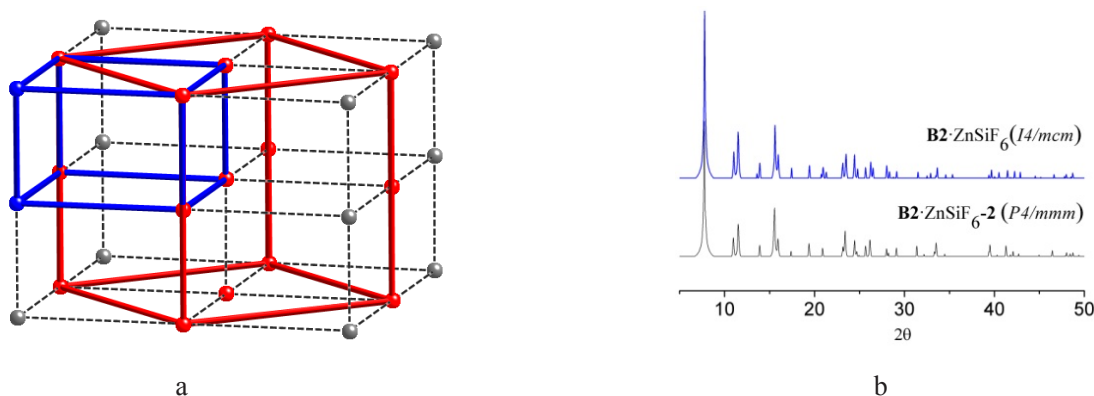


Figure 2-12: The illustration of the unit cell of **B2**·ZnSiF₆ ($I4/mcm$, red) and **B2**·ZnSiF₆-**2** ($P4/mmm$, blue) (a), and their simulated PXRD patterns upon removal of solvent molecules (b).

2.3.3. Stability and thermal properties of cuboid 3-D networks

Owing to the difference in the length of the rigid organic tectons T2, the five networks differ by the distance between two consecutive zinc cations (11.35, 13.85, 15.60, 17.79 and 19.92 Å for **B2-B6**, respectively) (Table 2-5 and Figure 2-13). Consequently, by modulating the length of the organic moiety, one may control the size of the cavities (cross sections along the *c* axis of 7.68×11.35 Å for **B2**, 7.53×13.85 Å for **B3**, 7.55×15.60 Å for **B4**, 7.52×17.79 Å for **B5** and 7.65×19.92 Å for **B6**) generated upon the formation of the cuboid architecture of the type ($a \neq b = c$) (Figure 2-14).

Owing to the length of tectons **B5** and **B6**, the cuboid architectures in both cases are interpenetrated (two fold homo interpenetration) and consequently offer cavities with smaller size. For networks based on **B5**·ZnSiF₆ and **B6**·ZnSiF₆, the side windows of the channels are close (Figure 2-11d, e) leading to 1-D square channels with side lengths of 8.90 and 9.96 Å respectively. It is worth noting that because of the height (7.60 Å, near the double thickness value of normal aromatic system (2×3.50 Å)), only two-fold interpenetration may occur in this type cuboid even if its side length is long enough to allow multiple-fold interpenetration.

Table 2-5: Comparison of parameters and porous data for the cuboid compounds.

Compound	B1 ·ZnSiF ₆ ¹⁰	B2 ·ZnSiF ₆	B3 ·ZnSiF ₆	B4 ·ZnSiF ₆	B5 ·ZnSiF ₆	B6 ·ZnSiF ₆
Side lengths of top square ($b=c$)/Å	7.141	11.35	13.86	15.60	17.79	19.92
Heights (<i>a</i>)/Å	7.61	7.68	7.53	7.55	7.52	7.65
Solvent accessible void volume/Å ³	114.7	2259.0	3913.2	5063.3	1791.0	2859.7
Unit cell volume/ Å ³ [*]	387.9	3958.5	5784.4	7344.8	4761.8	6066.1
Occupancy percents/%	29.6	57.1	67.7	68.9	37.6	47.1

[*] Calculated with the Platon software²⁶

As listed in Table 2-5, the potential solvent accessible volumes, calculated with the Platon software, are 2259.0, 3913.2, 5063.3, 1791.0 and 2859.7 Å³, corresponding to 57.1%, 67.7%, 68.9%, 37.6% and 47.1% of the total unit cell volume for **B2**·ZnSiF₆, **B3**·ZnSiF₆, **B4**·ZnSiF₆, **B5**·ZnSiF₆ and **B6**·ZnSiF₆ respectively. As expected, in spite of the longer parameters for the latter two structures, their solvent accessible volumes are smaller due to the interpenetration.

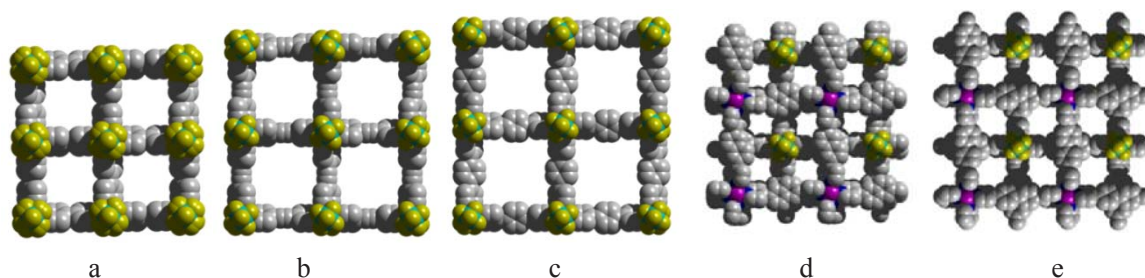


Figure 2-13: Top views of cuboid neutral 3-D networks upon removal the solvent molecules: **B2**·ZnSiF₆ (a), **B3**·ZnSiF₆ (b), **B4**·ZnSiF₆ (c), **B5**·ZnSiF₆ (d) and **B6**·ZnSiF₆ (e).

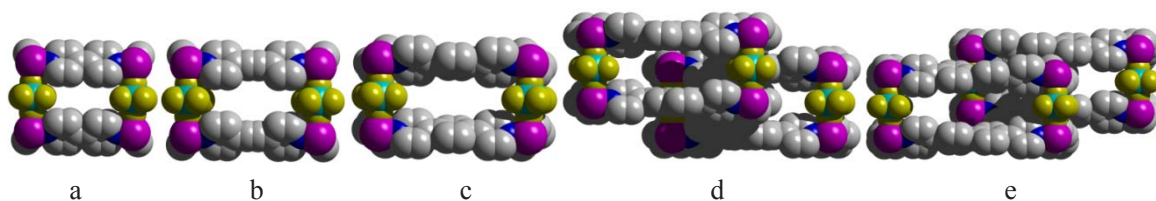


Figure 2-14: Side views of cuboid neutral 3-D networks upon removal the solvent molecules: **B2**·ZnSiF₆ (a), **B3**·ZnSiF₆ (b), **B4**·ZnSiF₆ (c), **B5**·ZnSiF₆ (d) and **B6**·ZnSiF₆ (e).

Among the five combinations, the non-interpenetrated three crystalline materials (**B2**·ZnSiF₆, **B3**·ZnSiF₆ and **B4**·ZnSiF₆) obtained are rather unstable upon standing in air and upon removal of the solvent molecules. They irreversibly collapse in a few seconds. However, both interpenetrated networks (**B5**·ZnSiF₆ and **B6**·ZnSiF₆) are relatively stable in air. This was confirmed by their PXRD patterns (Figure 2-15), wherein only a single set of diffraction peaks implying a single phase.

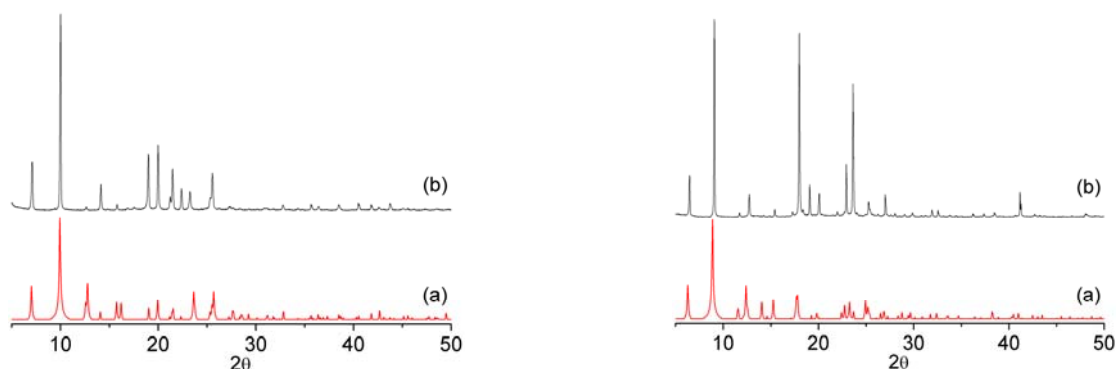


Figure 2-15: Comparison of the simulated (a) and recorded (b) PXRD for the crystalline material of **B5**·ZnSiF₆ (left) and **B6**·ZnSiF₆ (right).

The thermal behavior of the crystalline materials based on **B5**·ZnSiF₆ and **B6**·ZnSiF₆ was investigated using TGA technique. As shown in Figure 2-16, their stability was investigated from room temperature to 600°C under the nitrogen atmosphere.

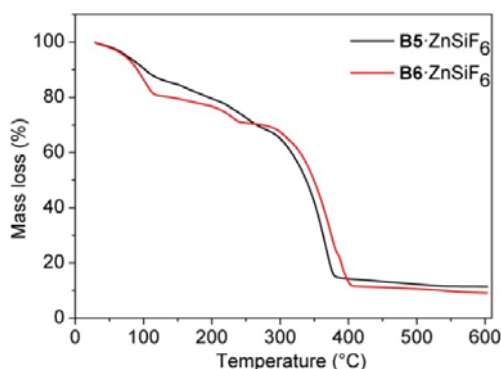


Figure 2-16: The TGA traces of **B5**·ZnSiF₆ and **B6**·ZnSiF₆ under the N₂ with the speed of 5°C/min.

The TGA trace revealed two intermediate mass losses for both networks. The first one between 30 and 120 °C and the second one between 120 and 280 °C, prior to decomposition of the sample, which appeared at *ca.* 300°C. The first loss of mass corresponds to the release of the ethanol molecules and the second one to the release of high-boiling solvents (DMSO for **B5**·ZnSiF₆ and

CHCl₂CHCl₂ for **B6**·ZnSiF₆). In the case of **B6**·ZnSiF₆, owing to the lower boiling point of CHCl₂CHCl₂ with respect to DMSO present in crystals based on **B5**·ZnSiF₆ networks, the solvent release is achieved at lower temperature as expected. Compared to non-interpenetrating networks, the higher stability observed may be attributed to the close side windows of their channels resulting from interpenetration.

In conclusion, we have demonstrated that upon combining a rigid bimonodentate organic tecton with zinc dication and SiF₆²⁻ anion as an inorganic tecton, a series of 3-D cuboid type architectures may be designed. The interpenetration, the cross section of the faces as well as the size of the channels may be tuned by the length of the organic unit. Whereas the non-interpenetrated architectures are rather unstable in air, several approaches (*e.g.* replacing the center metal, functionalized the organic tectons T2) were explored in order to improve stability of the architecture (see the following section).

2.4. Changing the central metals of the cuboid 3-D coordination networks

According to the Irving-Williams sequence²⁷, for the exchange of water by other ligands, the general stability sequence of high spin octahedral metal complexes is: Fe(II) < Co(II) < Ni(II) < Cu(II) > Zn(II). This trend is essentially independent of the nature of the ligand. By replacing Zn²⁺ dication by other transition metal cations, the stability of the porous cuboid 3-D coordination network could be increased. Actually, the cupric analog of **B2**·ZnSiF₆, **B2**·CuSiF₆, has been already generated by Kitagawa and his co-workers²⁸ through mixing Cu(BF₄)₂·6H₂O, (NH₄)₂SiF₆, and tecton **B2** in a water/ethylene glycol (1:3) mixture. The architecture obtained was found to be robust. Because of the coexistence of 2-D grid byproduct with two axially coordinated water molecules²⁹, the above procedure is unsuitable to prepare high quantity crystalline material. We turned our attention to the pure MSiF₆ (M = Fe²⁺, Co²⁺, Ni²⁺ and Cu²⁺).

The metallic hexafluorosilicate salts, FeSiF₆, CoSiF₆, NiSiF₆ and CuSiF₆ have been prepared in large scale by the double decomposition reaction between the MCO₃ and H₂SiF₆^{12, 29}. Unfortunately, the poor solubility of most salts in common organic solvents (*e.g.* glycol, DMSO, THF) prevents to use them as metallatectons. Only CoSiF₆ slightly dissolves in methanol (MeOH) and thus could be used to build the cuboid 3-D network.

2.4.1. Structural studies of cobaltic cuboid 3-D networks

Similarly, upon slow diffusion of an MeOH solution of CoSiF₆·xH₂O (3 mg) into a CHCl₃ solution (1 mL) of the rigid tectons **B1**-**B6** (3 mg) at room temperature, in most cases, only pink powders are generated despite many attempts by modifying the crystallization conditions. Fortunately, when a solution of the tecton **B2** or **B4** in CH₂ClCH₂Cl was layered with DMSO and then a MeOH solution of CoSiF₆ was carefully, pink prismatic crystalline materials suitable for X-ray single crystal diffraction studies were obtained in crystallization tubes after several days.

The structural determination in the case of tecton **B4** revealed the formation of a DMSO solvated CoSiF_6 without any tecton **B4** ($\text{CoSiF}_6 \cdot 6\text{DMSO}$, Figure 2-17). The structure is similar to the one observed for ZnSiF_6 hydrate (Figure 2-2). Each cobalt cation adopts the octahedral coordination geometry with six DMSO molecules located at the six vertices. The counter anion SiF_6^{2-} links with coordinated DMSO by the by strong hydrogen bonds ($d_{\text{H-F}} = 2.2\text{-}2.5\text{\AA}$) leading thus to a 3-D hydrogen-bonded molecular network.

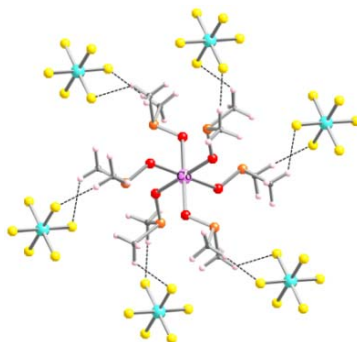


Figure 2-17: Portions of the crystal structure of $\text{CoSiF}_6 \cdot 6\text{DMSO}$.

The crystals generated by the combination of the tecton **B2** with CoSiF_6 ($[\text{Co}(\text{B2})_2\text{SiF}_6]_4$, abbreviated as $\text{B2} \cdot \text{CoSiF}_6$) is isostructural with $\text{B2} \cdot \text{ZnSiF}_6$. As shown in Figure 2-18, the structure of $\text{B2} \cdot \text{CoSiF}_6$ can be simply regarded as the replacement of the zinc cations by cobalt cations. That is, each Co^{2+} cation is coordinated to the four pyridine groups of four different tectons **B2** through the formation of Co-N bonds ($d_{\text{Co-N}} = 2.12\text{ \AA}$, Table 2-6) in the square plane and the other two axial positions are bridged by the SiF_6^{2-} counter-anions ($d_{\text{Si-F}} = 1.66\text{ \AA}$ for unbound fluorine atoms and $d_{\text{Si-F}} = 1.71\text{ \AA}$ for bridging F atoms) *via* Co-F bonds ($d_{\text{Co-F}} = 2.08\text{ \AA}$) to form a CoSiF_6 pillar. Tectons **B2** are connected to consecutive pillars generating thus the 3-D cuboid frameworks. The crystallization solvent molecules occupy the cavities of the network. Owing to large disorder of the solvents and could not be refined and thus SQUEEZE command was used for the refinement of structure.

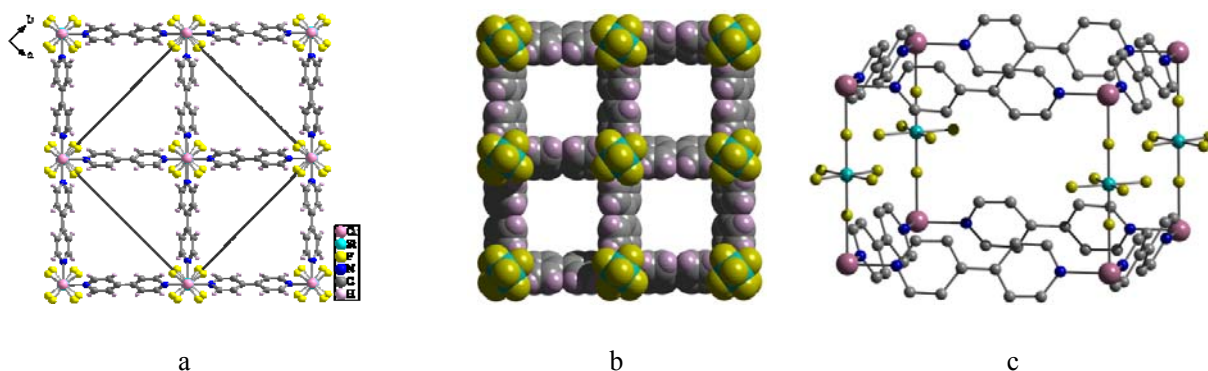


Figure 2-18: Top views (a, b) and smallest cuboid units (c) for the crystal structure of $\text{B2} \cdot \text{CoSiF}_6$. For clarity, the H atoms are omitted in (c).

Table 2-6: Selected bonds and angles for the three isostructural coordination networks

Compound	M-F(SiF ₆ ²⁻) distances/Å	M-N distances/Å	Si-F (unbound) distances/Å	Si-F (bridge) distances/Å	N-M-N angles/°	F-M-F angles/°
B2 ·ZnSiF ₆	2.122, 2.123	2.137	1.592	1.714	90	180
B2 ·CuSiF ₆ ²⁸	2.357	2.009	1.616	1.698	90	180
B2 ·CoSiF ₆	2.082	2.124	1.662	1.707	90	180

When analyzing in detail bonds and angles in the three isostructural networks **B2**·MSiF₆ (M = Zn²⁺, Cu²⁺ and Co²⁺), it is found that the bond length of M-F in cobalt complex is much shorter than those of other two architectures. However, the bond lengths of M-N are sorted in the order of Cu²⁺ < Co²⁺ < Zn²⁺, however, the M-F bond length follows the Irving-Williams sequence. As a result, the volume of the smallest units for these three cuboid networks and the possible solvent accessible volume are in the order of Cu²⁺ < Co²⁺ < Zn²⁺ (Table 2-7).

Table 2-7: Comparison of parameters and porosity data for the three isostructural networks.

Compound	B2 ·ZnSiF ₆	B2 ·CuSiF ₆ ²⁸	B2 ·CoSiF ₆
Side lengths of top square (b=c)/Å	11.35	11.11	11.33
Heights (a)/Å	7.68	8.11	7.58
Solvent accessible void volume/Å ³	2259.0	513.3	2199.9
Unit cell volume/ Å ³ [*]	3958.5	1000.8	3891.9
Occupancy percents/%	57.1	51.3	56.5

[*] Calculated with the Platon software²⁶

2.4.2. Stability and thermal properties of cobaltic cuboid 3-D networks

The stability of crystals of **B2**·CoSiF₆ in air is rather high and thus its purity could be established by PXRD (Figure 2-19 left) which revealed a single set of diffraction peaks implying a single phase.

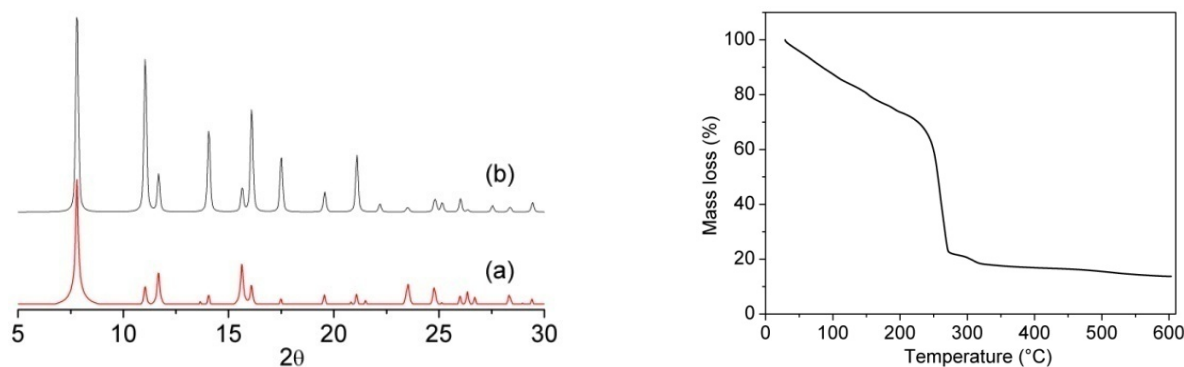


Figure 2-19: Comparison of the simulated (a) and recorded (b) PXRD (left) and TGA (right) traces for the **B2**·CoSiF₆.

The thermal stability of **B2**·CoSiF₆ was investigated from room temperature to 600°C under nitrogen atmosphere by the TGA technique (Figure 2-19 right). The TGA analysis revealed that

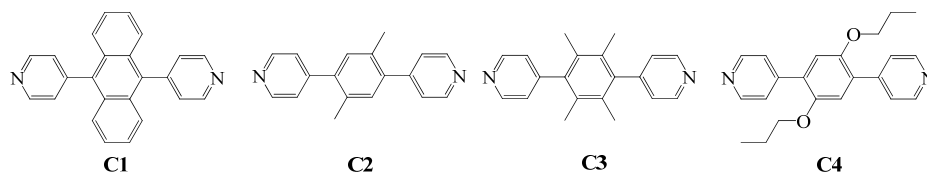
crystallization solvents (possibly methanol, $\text{CH}_2\text{ClCH}_2\text{Cl}$ and DMSO) are slowly released prior to decomposition of the framework at *ca.* 250°C, much higher than for **B2**·CuSiF₆ (decomposition of the frameworks at 150°C)²⁸. The much smaller recorded solvent volume (*ca.* 25%) than the calculated one by the PLATON software (56.5%) may be attributed to the partial filling and even partial release of solvent molecules during the filtration of the sample.

In conclusion, we have demonstrated that by replacing the Zn^{2+} by Co^{2+} cation, the stability of non-interpenetrated 3-D cuboid architecture is improved. However, the low solubility of CoSiF_6 in organic solvents prevents it to be generated in good quality and high quantities. Extension to other approaches (*e.g.* functionalized the organic tectons T2) will be discussed below.

2.5. Functionalization of cuboid 3-D coordination networks

2.5.1. Design and synthesis of the functionalized organic tectons T2

The low stability of crystalline materials of **B4**·ZnSiF₆ possessing large cavities motivated us to improve its stability. As described above, the close side windows of the interpenetrated networks based on **B5**·ZnSiF₆ and **B6**·ZnSiF₆ may account for their stability. Inspired by this, we replaced the tecton **B4** by functionalized rigid analogues **C_i** (*i*=1, 2, 3, 4; Scheme 2-4 and Figure 2-20).



Scheme 2-4

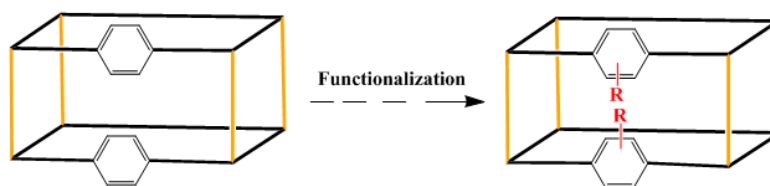
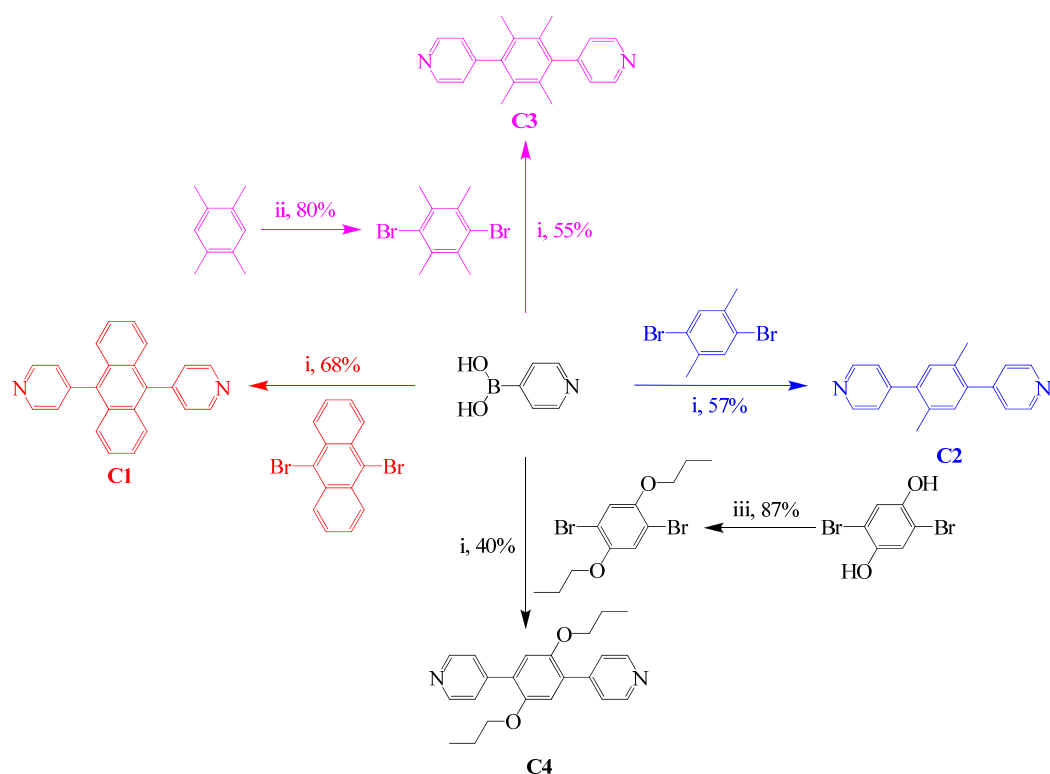


Figure 2-20: Schematic representation of the functionalized cuboid architecture. For clarity, only one face exhibits the functionalized groups (R).

As shown in Scheme 2-5, all the functionalized tectons T2 were obtained by palladium-catalyzed cross coupling reactions between 4-pyridylboronic acid and dibromo aromatic compounds under anaerobic conditions in 68%, 57%, 55% and 40% yields for tectons **C1-C4** respectively. The starting materials, 4-pyridylboronic acid, 9, 10-dibromoanthracene and 1,4-dibromo-*p*-xylene were commercially available. 1,4-dibromodurene was obtained in 80% yield by bromination of durene at the low temperature (below 0 °C)^{30, 33}, and 1,4-dibromo-2,5-di(*n*-prooxy)benzene was easily generated in 87% yields by nucleophilic substitution of 1-iodopropane by 2, 5-Dibromohydroquinone under basic condition. All the intermediates and final

products were fully characterized (*see experimental section*).



Scheme 2-5: Reaction conditions: (i) Cs_2CO_3 , $[\text{Pd}(\text{PPh}_3)_4]$, deoxygenated DMF under N_2 for 48h; (ii) Br_2 , below 0°C for 8h; (iii) K_2CO_3 , RI, DMF under N_2 for 48h.

2.5.2. Structural studies of functionalized cuboid 3-D networks

Again, upon slow diffusion of an EtOH solution of $\text{ZnSiF}_6 \cdot 6\text{H}_2\text{O}$ (5mg) into a CHCl_3 solution (1 mL) and the organic tecton (3mg) at room temperature, colorless prismatic crystalline materials suitable for X-ray diffraction on single crystal were obtained for **C2** and **C4** in crystallization tubes after several days (Table 2-8). For tecton **C1** and **C3**, the obtained crystals were twinned in spite of many attempts.

Table 2-8: Selected crystallographic parameters for functionalized cuboid 3-D coordination networks

Compound	Chemical formula	Crystal system	Space group	a(Å)	b(Å)	c(Å)
B4 · ZnSiF_6	$[\text{Zn}(\mathbf{B4})_2\text{SiF}_6]_4 \cdot 8\text{CHCl}_3 \cdot \text{H}_2\text{O}$	Tetragonal	$I4/mcm$	22.059	22.059	15.094
C2 · ZnSiF_6	$[\text{Zn}(\mathbf{C2})_2\text{SiF}_6]_4$ (SQUEEZE)	Tetragonal	$I4/mcm$	22.078	22.078	15.119
C4 · ZnSiF_6	$[\text{Zn}(\mathbf{C2})_2\text{SiF}_6]_4$ (SQUEEZE)	Tetragonal	$I4/m$	22.058	22.058	15.179

The structural studies revealed that the network based on tecton **C2** (**C2**· ZnSiF_6 , Table 2-8) is isostructural to **B4**· ZnSiF_6 with tetragonal system and $I4/mcm$ space group, but the space group for the combination of tecton **C4** (**C4**· ZnSiF_6) is $I4/m$. The difference in the space group is related to the difference in the symmetry of the central benzene ring (Figure 2-21). For **C2**· ZnSiF_6 , in the crystal, the two methyl groups are statistically distributed on four sites on the benzene unit and the

latter is disordered because of rotation. As a result, the final cuboid 3-D network, due to the disorder, appears as the one observed for $\mathbf{C3}\cdot\text{ZnSiF}_6$ (Figure 2-21b, f). Due to the large steric hindrance of *n*-propoxy groups, there are no disorders found in the frameworks based on $\mathbf{C4}\cdot\text{ZnSiF}_6$ (Figure 2-21c, g). The channels of both networks are filled with chloroform and ethanol molecules. Some of the solvent molecules are disordered and unfortunately not all of them could be refined. Consequently, the SQUEEZE command was used during the refinement.

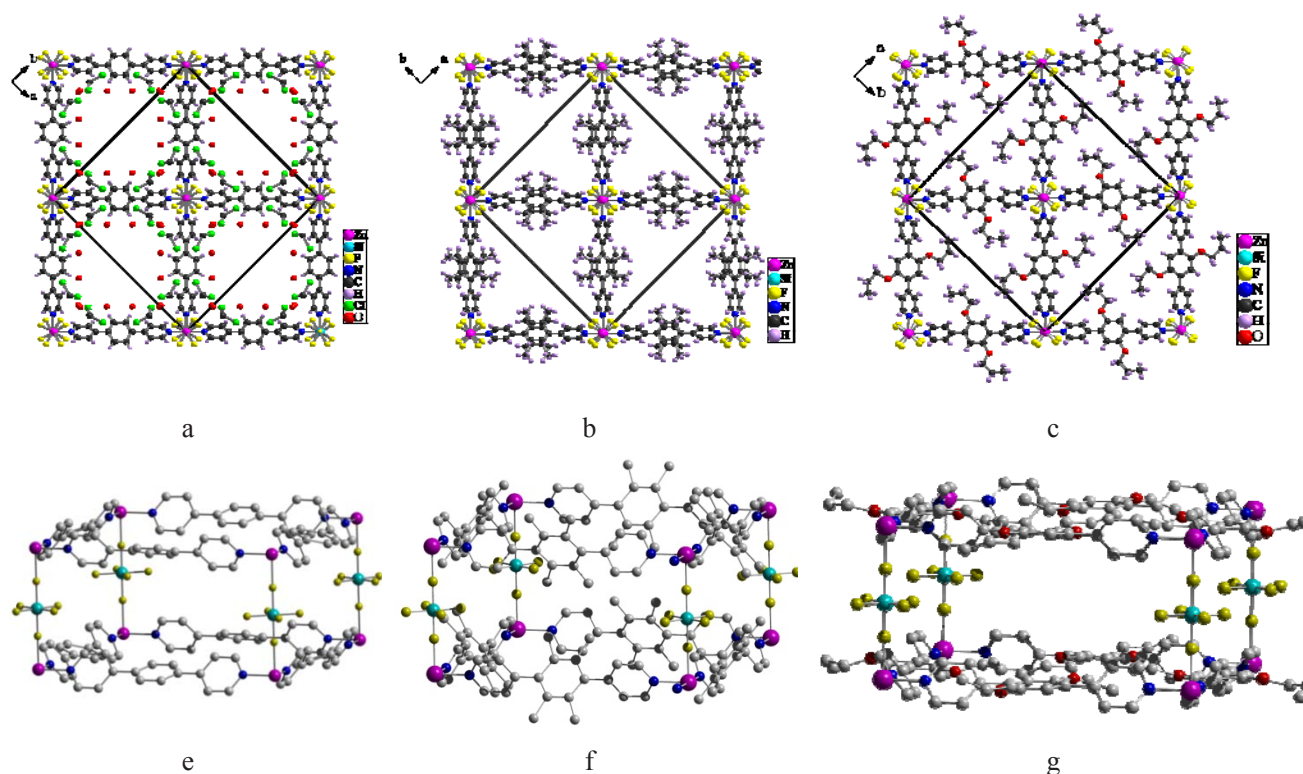


Figure 2-21: the top views and cuboid units for the $\mathbf{C2}\cdot\text{ZnSiF}_6$ (b, f) and $\mathbf{C4}\cdot\text{ZnSiF}_6$ (c, g), and those of $\mathbf{B4}\cdot\text{ZnSiF}_6$ is given for comparison (a, e). For clarity, the hydrogen atoms in the representation of smallest cuboid unit (e, f, and g) and the disordered benzene moieties are omitted.

The coordination connectivity of $\mathbf{C2}\cdot\text{ZnSiF}_6$ and $\mathbf{C4}\cdot\text{ZnSiF}_6$ is analogous to one which was observed for $\mathbf{B4}\cdot\text{ZnSiF}_6$. Each Zn^{2+} cation coordinated to four pyridine groups of four different rigid organic tectons through the formation of Zn-N bonds in the square plane, and the other axial positions are bridged by the SiF_6^{2-} counter-anions *via* Zn-F bonds to form a ZnSiF_6 pillar. The functionalizations of the benzene moiety of 1,4-di(pyridine-4-yl)benzene slightly influence the bond lengths and angles (Table 2-9).

Table 2-9: Selected bond distances and angles for the functionalized cuboid 3-D coordination networks

Compound	Zn-F(SiF_6^{2-}) distances/Å	Zn-N distances/Å	Si-F (unbound) distances/Å	Si-F (bridge) distances/Å	N-Zn-N angles/ $^\circ$	F-Zn-F angles/ $^\circ$
$\mathbf{B4}\cdot\text{ZnSiF}_6$	2.074	2.112	1.669	1.699	90	180
$\mathbf{C2}\cdot\text{ZnSiF}_6$	2.083	2.135	1.661	1.697	90	180
$\mathbf{C4}\cdot\text{ZnSiF}_6$	2.073	2.120	1.660	1.690	90	179.45

For both networks, the pyridine rings are parallel and coplanar (dihedral angle of 0.0 °) and they coordinate to the central zinc cations with a dihedral angle of 62.01° or 51.89° in the *xy* coordination plane (NNNN square plane, Table 2-10) respectively. The central aromatic moieties are tilted by *ca.* 59.6 ° (63.91°) and 48.4 ° with respect to the two pyridine units respectively, which is much larger than the one observed for of tecton **B4** (37.8 °).

Table 2-10: Comparison of some angles in functionalized complexes.

Compound	Tilted angles/° ^[a]	Canting angles/°	Stagger angles/°
B4 ·ZnSiF ₆	37.80	54.52	31.07
C2 ·ZnSiF ₆	59.61/63.91	62.01	33.34
C4 ·ZnSiF ₆	48.43	51.89	30.93/44.55

^[a] the angle between the central aromatic moiety and pyridine units

In both networks, in order to minimize the steric hindrance, the octahedron of SiF₆²⁻ anions are staggered and connected with a stagger angle of 33.3 ° and 30.9 ° (44.5 °) with respect to the octahedron of Zn²⁺.

2.5.3. Stability and thermal properties of functionalized cuboid 3-D networks

Despite the considerable steric congestion of substituents in the structures of **C2**·ZnSiF₆ and **C4**·ZnSiF₆, the distances between two consecutive zinc cations are not enlarged markedly and thus the sizes of generated cuboid architectures of the type (*a* ≠ *b* = *c*) are nearly equivalent with cross sections along the *c* axis of 7.55 × 15.60 Å for **B4**·ZnSiF₆, 7.56 × 15.61 Å for **C2**·ZnSiF₆ and 7.63 × 15.60 Å for **C4**·ZnSiF₆ respectively (Table 2-11 and Figure 2-22). However, the introduction of substituents decreases the size of the actual cavities as expected by the introduction of bulky substituents. The potential solvent accessible volumes, calculated with the Platon software²⁶, are 4318.9 and 3746.9 Å³, thus 58.6% and 50.7% of the total unit cell volume for **C2**·ZnSiF₆ and **C4**·ZnSiF₆ respectively, much smaller than that of **B4**·ZnSiF₆ (68.9%).

Table 2-11: Comparison of parameters and porous data for the functionalized cuboid 3-D networks.

Compound	B4 ·ZnSiF ₆	C2 ·ZnSiF ₆	C4 ·ZnSiF ₆
Side lengths of top square (<i>b=c</i>)/Å	15.60	15.61	15.60
Heights (<i>a</i>)/Å	7.55	7.56	7.63
Solvent accessible void volume/Å ³	5063.3	4318.9	3746.9
Unit cell volume/ Å ³ [*]	7344.8	7370.1	7385.9
Occupancy percents/%	68.9	58.6	50.7

[*] Calculated with the Platon software²⁶

As expected from the design principle, for **C2**·ZnSiF₆ the side windows of the channel are close (Figure 2-22b and Figure 2-23b). In contrast, for **C4**·ZnSiF₆, the bulky and long substituents cannot spread along the direction of ZnSiF₆ pillar and the channels are almost filled with the chains

(Figure 2-22c and Figure 2-23c).

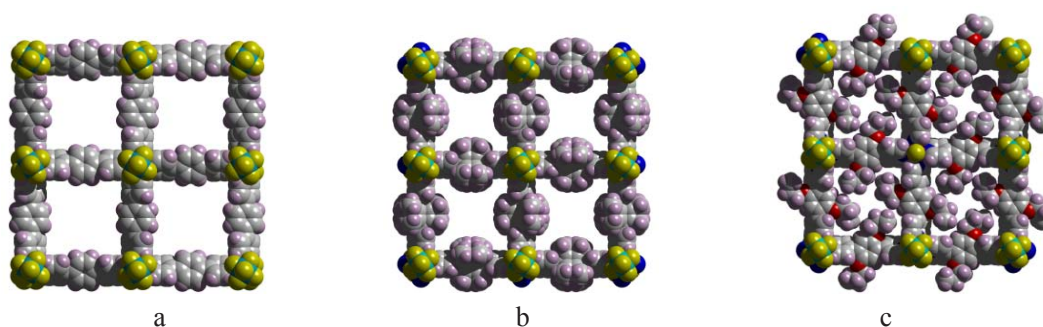


Figure 2-22: Top views of functionalized cuboid 3-D networks upon removal the solvent molecules: **B4**·ZnSiF₆ (a), **C2**·ZnSiF₆ (b) and **C4**·ZnSiF₆ (c).

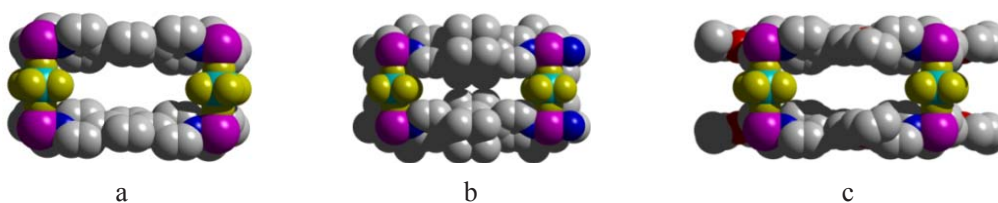


Figure 2-23: Side views of functionalized cuboid 3-D networks upon removal the solvent molecules: **B4**·ZnSiF₆ (a), **C2**·ZnSiF₆ (b) and **C4**·ZnSiF₆ (c).

As a result of the decrease of channels size and accessibility, the stability in air of the first functionalized networks (**C2**·ZnSiF₆) is found to be distinctly improved. The purity of its crystalline phases was established by PXRD which revealed only a single set of diffraction peaks implying a single phase (Figure 2-24). However, for the second one (**C4**·ZnSiF₆), crystals were found to be rather unstable in air and upon removal of the solvent molecules which caused irreversible collapse of the architecture in a few seconds.

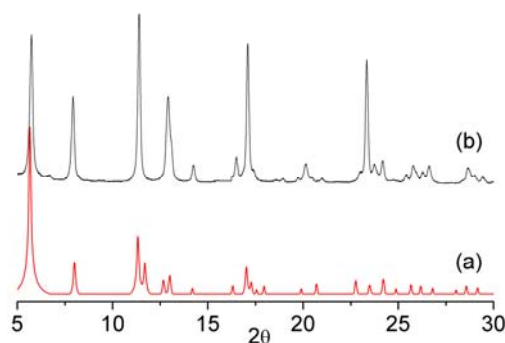


Figure 2-24: Comparison of the simulated (a) and recorded (b) PXRD for the crystalline material of **C2**·ZnSiF₆.

Subsequently, the thermal stability of **C2**·ZnSiF₆ was investigated from room temperature to 600°C under the nitrogen atmosphere using the TGA technique (Figure 2-25). The TGA analysis reveals very slow weight loss between 30-200°C prior to decomposition of the sample, which appeared at *ca.* 230°C. Considerably fewer amounts of solvents were estimated from the TGA curve than the calculated solvent accessible void volume (58.6%). This may be attributed to the partial filling of the cavities by solvents and even partial release during the filtration of the sample.

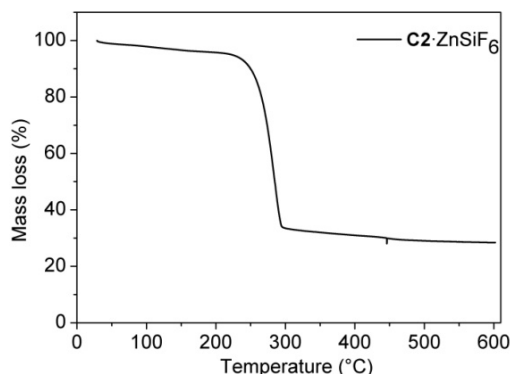


Figure 2-25: The TGA trace of $C2 \cdot ZnSiF_6$ under N_2 with the speed of $5^\circ C/min$.

As expected from the design of the ligands **C1-C4**, the better stability of the 3-D cuboid architecture is anticipated through “closing” the side window. However, the stability of $C4 \cdot ZnSiF_6$ is not improved distinctly by “closing” the top window. Thus, an assumption can be made that the improved stability may be attributed to the strong support from the neighboring two organic tectons T2 and SiF_6^{2-} pillars who “close” the side window. In other words, the weak Zn-F bonds seem to be broken upon removal of the solvent molecules and the close side window may act as a brace to help the SiF_6^{2-} pillars to support Zn-tecton grid plane (top square plane for the cuboid architecture shown in [Figure 2-1b](#)).

In conclusion, we have demonstrated that the stability of non-interpenetrated 3-D cuboid architectures may be improved by the addition of a support to SiF_6^{2-} pillars by substituent at faces bearing SiF_6^{2-} units. Along this line, the stability of the networks could be further improved by design of a new series of organic tectons T2 which will discuss below.

2.6. Transformation of cuboid 3-D coordination networks

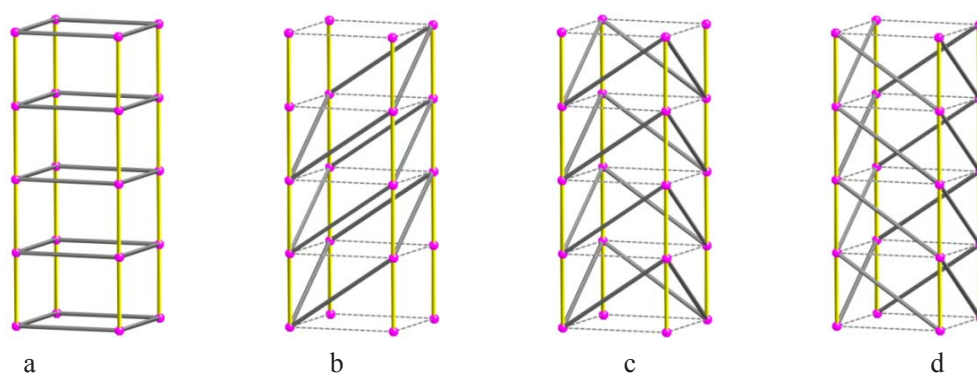


Figure 2-26: Schematic representation of homonuclear cuboid coordination networks based on $ZnSiF_6$ pillars where the organic tectons act as side (a) or diagonal (b-d). For clarity, the yellow and gray cylindrical rods are used to illustrate the SiF_6^{2-} pillars (T1) and organic tectons (T2) respectively.

When designing the cuboid networks based on $ZnSiF_6$ pillars, the organic tectons T2, the latter not only may act as a side to connect the neighboring two pillars to form the above mentioned

cuboid architecture (Figure 2-26a), but may also serve as a diagonal to link the adjacent pillars to generate other types of cuboid architectures (Figure 2-26b-d). From a mechanical viewpoint, the diagonal organic tecton will directly support SiF_6^{2-} pillars to stabilize the cuboid 3-D networks.

2.6.1. Design and synthesis of the rigid zigzag organic tectons T2

To act as diagonal in cuboid architectures, *i.e.* interconnecting zinc cations in the equatorial plane, the organic tecton T2 must bear two coordination sites divergently oriented and located at the two extremities of a zigzag type backbone (Figure 2-26). Among the possible rigid skeletons, those bearing two *meta*-connected pyridines with a linear spacer offer the required zigzag arrangement.

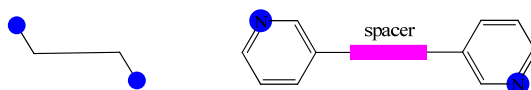
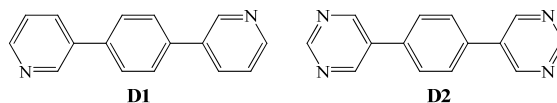


Figure 2-26: Schematic representation of zigzag type tectons.

Taking into account the fact that the distance between the two nitrogen atoms in the tectons (diagonal) should be larger than the height of cuboid imposed by SiF_6^{2-} (*ca.* 7.5 Å), two rigid tectons shown in Scheme 2-6 have been chosen. Both tectons are also obtained by the Suzuki coupling from the 1,4-phenylenediboronic acid and 3-bromopyridine or 5-bromopyrimidine under anaerobic condition and palladium (0) as catalyst according to the published procedure³¹⁻³².



Scheme 2-6

2.6.2. Structural studies of transformed cuboid 3-D networks

Again, upon slow diffusion of an EtOH solution (1 mL) of $\text{ZnSiF}_6 \cdot 6\text{H}_2\text{O}$ (5 mg) into a $\text{CH}_2\text{ClCH}_2\text{Cl}$ solution (1 mL) of above two organic tectons (3 mg) respectively at room temperature, colorless prismatic crystalline material suitable for X-ray diffraction on single crystal was obtained for **D2** in crystallization tubes after several days (Figure 2-27). For tecton **D1**, the obtained crystals were twinned because of the existence of two possible configurations (*anti* and *syn*).

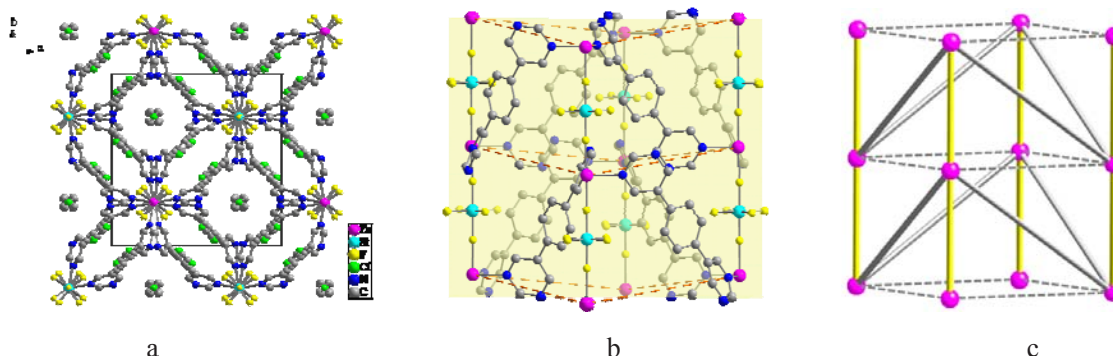


Figure 2-27: the top views (a), smallest cuboid units (b) and the schematic representation of its topological geometry for the **D2**· ZnSiF_6 . For clarity, the hydrogen atoms in both and solvents in (b) are omitted.

As expected, the X-ray analysis (tetragonal, $P4/ncc$) revealed the formation of a transformed cuboid 3-D network ($[\text{Zn}(\mathbf{D2})_2\text{SiF}_6]_4 \cdot 3\text{C}_2\text{H}_4\text{Cl}_2$, abbreviated as $\mathbf{D2} \cdot \text{ZnSiF}_6$, [Figure 2-27](#)) resulting from the interconnection of ZnSiF_6 pillars by the tecton $\mathbf{D2}$ along the diagonals. To the best of our knowledge, no example with the same connectivity has been previously reported.

The transformed cuboid 3-D network can also be regarded as a pillared arrangement composed of “lumpy” planes, $[\text{Zn}(\mathbf{D2})_2]_n$, interconnected by the SiF_6^{2-} pillars. In the structure, each Zn^{2+} cation, adopts the octahedral coordination geometry, connecting four pyrimidine groups (only one N-donor site participate to the coordination, and the other one remains unbound) of four $\mathbf{D2}$ molecules in the equatorial plane through the formation of Zn-N bonds ($d_{\text{Zn-N}} = 2.14 \text{ \AA}$) and the four tectons around each zinc cation, adopt a distorted zigzag shape, extended upwardly or downwardly to form a “lumpy” plane as shown in [Figure 2-28](#). Two consecutive planes are stacked by *concave-convex* mosaic and bridged by the SiF_6^{2-} pillars ($d_{\text{Si-F}} = 1.66 \text{ \AA}$ for unbound fluorine atoms and $d_{\text{Si-F}} = 1.73 \text{ \AA}$ for bridging F atoms) through Zn-F bonds ($d_{\text{Zn-F}} = 2.07\text{-}2.08 \text{ \AA}$) at the remaining two axial positions of each Zn^{2+} cations, which leads to final transformed cuboid 3-D network.

In detail, for a $\mathbf{D2}$ tecton, the dihedral angle between two pyridine rings is 71.7° and the central aromatic moiety is tilted by 37.6° and -38.0° with respect to both pyridine units. Owing to such distortion, the $\mathbf{D2}$ tecton adopts an “arch-like” zigzag shape, coordinating to the neighboring two zinc ions with a dihedral angle of 69.4° . The four tectons around each zinc cation are bent towards the same direction and thus look likes a clockwise or counterclockwise pinwheel ([Figure 2-28a](#)). Each pinwheel of given direction makes contact with six pinwheel of opposite direction ([Figure 2-28b](#)).

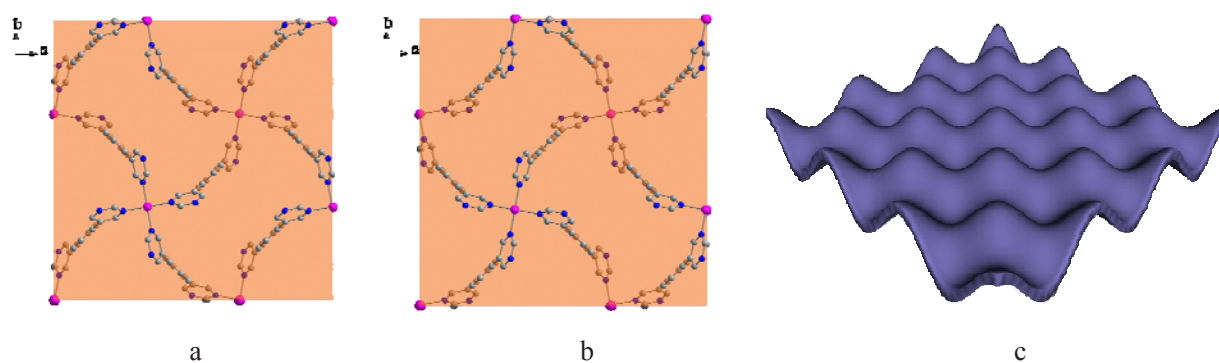


Figure 2-28: Top views of two neighboring lumpy plane along the direction of ZnSiF_6 pillar (a, b) and schematic representation of the “lumpy” plane. For clarity, the hydrogen atoms and solvents are omitted.

The *concave-convex* mosaic of the neighboring two consecutive planes leads to the transformed cuboid 3-D network with channels of “double wedding rings” type along the c axis ([Figure 2-29a](#)). The latter are composed of two crossed “double-hatchet-like” cavities stacked alternately. The cross section of each double-hatchet-like cavity perpendicular to c axis is $15.34 \times 7.35 \text{ \AA}$ for $d_1 \times d_2$ as illustrated in [Figure 2-29b](#). As a result, for the “double-wedding-ring-like” channels, cross section of the central arc square is $7.35 \times 16.04 \text{ \AA}$ for $d_2 \times d_3$ and that of

surrounding ellipse is $11.34 \times 4.00 \text{ \AA}$ for $d_4 \times d_5$ as illustrated in Figure 2-29c.

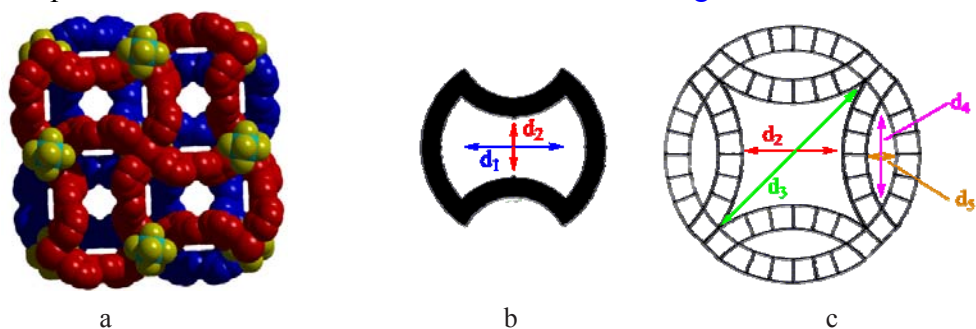


Figure 2-29: the “double-wedding-ring-like” channels for $D_2 \cdot ZnSiF_6$ along the c axis (a) and schematic representation of the “double-hatchet-like” cavity (b) and “double-wedding-ring-like” channel. For clarity, the hydrogen atoms and solvents are omitted.

In the channels, each double-hatchet-like cavity is filled with 3 crystallization CH_2ClCH_2Cl molecules, as shown in Figure 2-30. One is in the center and the other two are close to the convex sides without any specific interactions. Each CH_2ClCH_2Cl molecule adopts upstanding shape along the direction of $ZnSiF_6$ pillars.

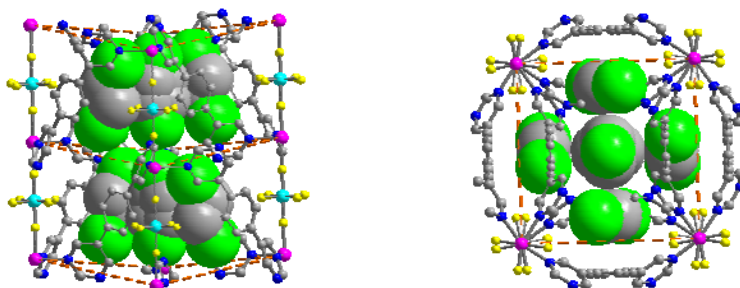


Figure 2-30: Solvents filled in the channels of $D_2 \cdot ZnSiF_6$: side view (left) and top view (right). For clarity, the hydrogen atoms are omitted and the solvents are displayed with spacefilling style.

2.6.3. Stability and thermal properties of transformed cuboid 3-D networks

The stability of $D_2 \cdot ZnSiF_6$ in air is rather high. In order to investigate the reproducibility of the formation of the above mentioned crystalline architecture, the crystallization process was repeated several times (checked by PXRD, Figure 2-31left). The purity of the crystalline phase was also established by PXRD which revealed a single set of diffraction peaks implying a single phase.

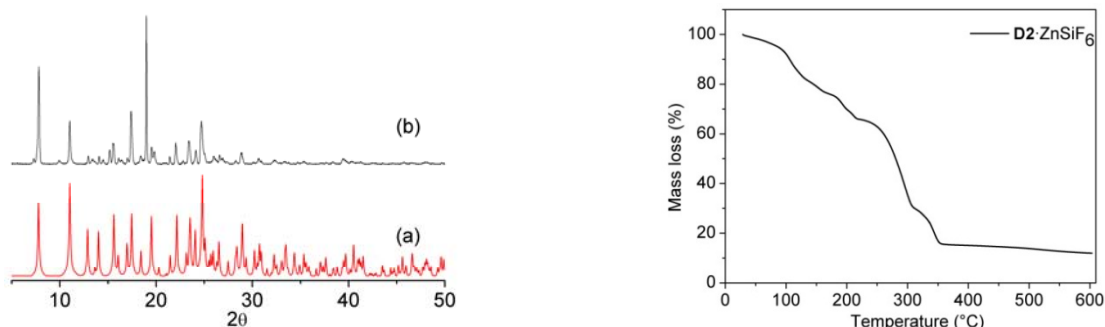


Figure 2-31: Comparison of the simulated (a) and recorded (b) PXRD (left) and TGA (right) trace for the $D_2 \cdot ZnSiF_6$.

The thermal stability of $\mathbf{D2} \cdot \text{ZnSiF}_6$ is investigated from room temperature to 600 °C under the nitrogen atmosphere by the TGA technique (Figure 2-31right). The TGA analysis revealed two intermediate weight losses. The first one between 30 and 100 °C and the second one between 120 and 200 °C, prior to decomposition of the sample, which appeared at *ca.* 250 °C. The first loss of mass corresponds to the release of the ethanol molecules and the second one to the release of high-boiling solvents ($\text{CHCl}_2\text{CHCl}_2$). The observed 35-40% of solvent proportion is close to the theoretical porosity (41.6%) calculated by PLATON software. As expected, the increased stability may be attributed to the additional connectivity in the diagonal direction.

In conclusion, we have demonstrated that the stability of non-interpenetrated 3-D cuboid architectures may be improved by using organic tectons T2 capable of connecting the pillars in the diagonal direction of cuboid architectures.

2.7. Conclusions

In this chapter, we have demonstrated that upon using octahedral M^{2+} ($\text{M}=\text{Co}$ and Zn) as a structural node, its counter anion SiF_6^{2-} as an inorganic tecton T1 and rigid linear organic tecton of various length as the second tecton T2, depending on the binding propensity of T1 and T2, a series of 3-D cuboid coordination networks of the type ($a \neq b = c$) have been designed and generated. The cross section of the faces, the size of the channels as well as the geometry and topology (interpenetration or non-interpenetration) may be finely tuned by the length of the organic tecton T2. For short tectons ($\leq 15.60 \text{ \AA}$), the networks do not interpenetrate and the empty space is occupied by the solvent molecules. The encapsulation of the solvent seems to depend on the nature and metrics of the channels and a selectivity of uptake between different solvents has been observed. Unfortunately, the formed networks were found to be rather unstable in air in the case of $\text{M} = \text{Zn}$. However, when tectons are long enough to allow interpenetration ($\geq 17.79 \text{ \AA}$), the networks are stable even in the case of $\text{M} = \text{Zn}$. In order to improve the stability of non-interpenetrated 3-D cuboid architectures, three approaches have been explored:

- ✧ By replacing Zn^{2+} dication by Co^{2+} , the stability of non-interpenetrated 3-D cuboid architecture was found to be improved.
- ✧ By introducing substituents within the framework of the organic tecton T2, the cuboid architecture obtained are congested and their stability is improved.
- ✧ By designing zigzag type tectons, the connectivity of the cuboid architecture was further increased through diagonal interconnection. Consequently, the stability of the architecture was enhanced.

References

1. M. J. Plater, M. R. St J. Foreman, J. M. S. Skakle, *Crystal Engineering*, **2001**, 4:293-308.
2. N. Rosi, M. Eddaoudi, D. Vodak, J. Eckert, M. O'Keeffe, O. M. Yaghi, *Science*, **2003**, 300: 1127-1129
3. J. Rowsell, O. M. Yaghi, *Micro- and Mesoporous Mater.*, **2004**, 73:3-14.
4. S. M. Holmes, G. S. Girolami, *J. Am. Chem. Soc.* **1999**, 121:5593-5594.
5. W. Dong, L. N. Zhu, H. B. Song, D. Z. Liao, Z. H. Jiang, S. P. Yan, P. Cheng, S. Gao, *Inorg. Chem.*, **2004**, 43: 2465-2467
6. M. V. Bennett, M. P. Shores, L. G. Beauvais, J. R. Long, *J. Am. Chem. Soc.* **2000**, 122: 6664-6668
7. S. S. Kaye, H. J. Choi, J. R. Long, *J. Am. Chem. Soc.* **2008**, 130:16921-16925
8. G. Férey, *Acc. Chem. Res.* **2005**, 38: 217-225
9. S.I., Noro, S. Kitagawa, M. Kondo, K. Seki, *Angew. Chem. Int. Ed.*, **2000**, 39:2081-2084.
10. S. Subramanian, M. J. Zaworotko, *Angew. Chem. Int. Ed.*, **1995**, 34: 2127-2129.
11. K. Uemura, A. Maeda, T. K. Maji, P. Kanoo, H. Kita, *Eur. J. Inorg. Chem.* **2009**, 16: 2329-2337.
12. S. Ray, A. Zalkin, D. H. Templeton, *Acta Cryst.* **1973**, B29:2741-2747.
13. <http://www.chem.wisc.edu/areas/reich/pkatable/>
14. T. Yoshimura, K. Umakoshi, Y. Sasaki, S. Ishizaka, H.-B. Kim, N. Kitamura, *Inorg. Chem.*, **2000**, 39:1765-1772
15. L. D. Ciana, and A. Haim, *J. Heterocyclic Chem.*, **1984**, 21:607-608.
16. N. R. Champness, A. N. Khlobystov, A. G. Majuga, M. Schröder, N. V. Zyk, *Tetrahedron Lett.*, **1999**, 40:5413-5416.
17. A.-C. Ribou, T. Wada, H. Sasabe, *Inorg. Chim. Acta*, **1999**, 134-141.
18. K. Biradha, M. Fujita, *J. Chem. Soc., Dalton Trans.*, **2000**, 3805-3810.
19. K. Biradha, Y. Hongo, M. Fujita, *Angew. Chem. Int. Ed. Engl.*, **2000**, 39:3843-3845.
20. P. H. Dinolfo, M. E. Williams, C. L. Stern, J. T. Hupp, *J. Am. Chem. Soc.*, **2004**, 126: 12989-13001.
21. M. Eddaoudi, J. Kim, N. L. Rosi, D. T. Vodak, J. Wachter, M. O'Keeffe, O. M. Yaghi, *Science*, **2002**, 295:469-472.
22. G. Chevrier, A. Goukassov, *Acta Cryst.* **1996**. C52:2121-2123.
23. C. Kaes, A. Katz, M. W. Hosseini, *Chem. Rev.*, **2000**, 100: 3553-3590.
24. P. G. Sammes, G. Yahiolglu, *Chem. Soc. Rev.*, **1994**, 28: 327-334.
25. R. W. Gable, B. F. Hoskins, R. Robson, *Chem. Commun.*, **1990**, 1677-1678.

26. A. L. Spek, Platon, the University of Utrecht, Utrecht, the Netherlands, **1999**.
27. H. Irving, R. J. P. Williams, *J. Chem. Soc.*, **1953**, 3192-3210.
28. S.-I., Noro, R. Kitaura, M. Kondo, S. Kitagawa, T. Ishii, H. Matsuzaka, M. Yamashita, *J. Am. Chem. Soc.*, **2002**, 124: 2568-2583.
29. W. C. Hamilton, *Acta Cryst.* **1962**, 15, 353-360.
30. Y. -H. Kim, S. -K. Ahn, H. S. Kim, S. -K. Kwon, *J. Polymer Sci. A. Polymer Chem.*, **2002**, 40: 4288-4296.
31. D. K. Chand, K. Biradha, M. Kawano, S. Sakamoto, K. Yamaguchi, M. Fujita, *Chem. Asian. J.*, **2006**, 1: 82-90.
32. J.-P. Bourgeois, M. Fujita, M. Kawano, S. Sakamoto, K. Yamaguchi, *J. Am. Chem. Soc.*, **2003**, 125: 9260-9261.
33. K. Yamashita, K. Sato, M. Kawano, M. Fujita, *New J. Chem.*, **2009**, 33: 264 - 270.

**CHAPTER III : DESIGN AND STUDY OF THE
COORDINATION NETWORKS BASED ON SEMI-RIGID
ORGANIC TECTONS AND ZINC
HEXAFLUOROSILICATE PILLARS**

Chapter III: Design and Study of Coordination Networks Based on Semi-rigid Organic Tectons and ZnSiF_6 Pillars

In this chapter, the constructions of new coordination networks based on MSiF_6 infinite tecton T1 and semi-rigid organic tecton T2 will be presented. The symmetrical tecton T2 based on naphthalene, spirobiindane and 1,3,5-triazine bearing pyridine groups as coordinating sites were designed. Several coordination networks based on these tectons with other metallatectons will also be discussed.

3.1. Introduction

SiF_6^{2-} anion is an interesting unit for the design of coordination networks. In the chapter II, we have demonstrated that its combinations with dications such as Zn, Co, Cu and organic tectons T2 leads to the formation of pillars resulting from the bridging of metal centres through the two fluorine atoms occupying the axial positions (Figure 3-1a). In terms of design strategy, instead of looking at MSiF_6 as two separated entities, one may consider the pillar as an infinite tecton T1. Depending on the rigidity of the organic tecton T2 bridging the pillars, 1-D (Figure 3-1b), 2-D (Figure 3-1c) or 3-D (Figure 3-1d) architectures with controlled inner cavities may be designed. These features have been already demonstrated in Chapter II for rigid tectons.

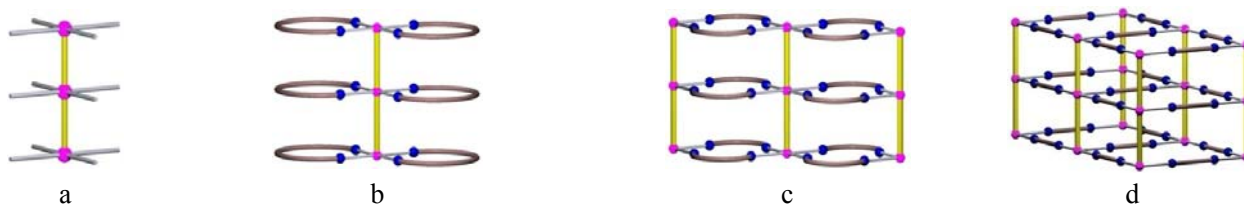


Figure 3-1: Schematic representation of a pillar (a), 1-D (b) chain, 2-D (c) tubular and 3-D (d) architectures resulting from the combination of MSiF_6 with flexible or rigid organic tectons

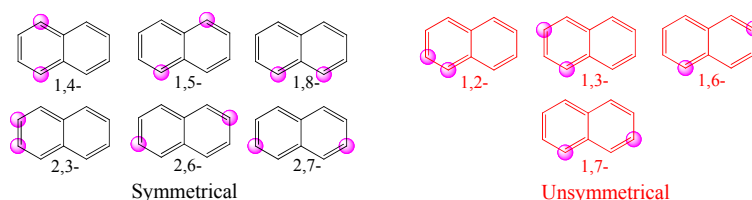
For the semi-rigid tectons T2, all three possible connectivities (from 1-D to 3-D) illustrated in Figure 3-1 may be achieved by controlling the angles between the two extremities of tectons. For example, a semi-rigid tecton offering the appropriate curvature should lead to the formation of 1-D tubular networks resulting from the binding of the cation by both extremities of the tecton (Figure 3-1b). The use of a curved semi-rigid tecton unable to bite on the same Zn^{2+} cation may generate 2-D tubular systems for which the cyclic cavities are oriented perpendicular to the pillar's axis (Figure 3-1c) and finally, a linear semi-rigid tecton may afford a 3-D cuboid architecture (Figure 3-1d) or transformed 3-D cubic architecture (Figure 2-26).

In order to design the semi-rigid tectons with different angles between two extremities, the naphthalene core¹⁻² and chiral spirobiindane scaffold³⁻⁴ were chosen as building blocks for bidentate tectons. Moreover, 1,3,5-triazine⁵ was chosen as a core for the design of a tridentate tectons. This chapter will be subdivided into three parts based on naphthalene, spirobiindane and 1,3,5-triazine based tectons.

3.2. Coordination networks based on the naphthalene core

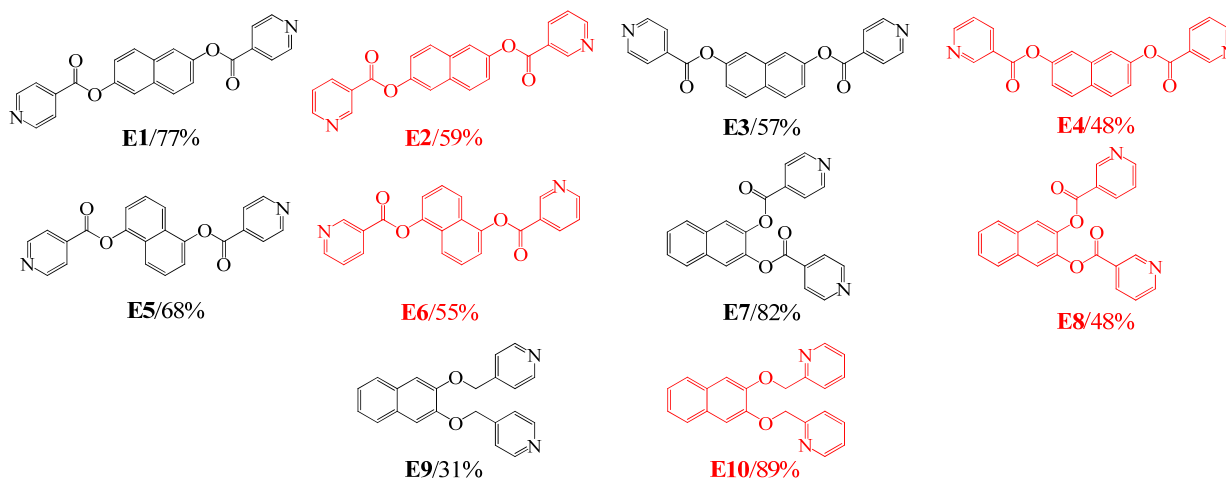
3.2.1. Synthesis of naphthalene based organic tectons T2

As stated above, the functionalization of the eight available positions around the naphthalene core leads to ten possible disubstitution patterns (Scheme 3-1). Among them, six have the two substituents symmetrically related, while the other four isomers are unsymmetrical.



Scheme 3-1: Ten possible disubstitution patterns with naphthalene core

To avoid the possibility of diversity due to isomer formation during the self-assembly process, the symmetrical isomers are preferable to be used as tectons. Due to the asymmetry of 1,4-isomer along the 1,4 positions and the similar shape between 2,3- and 1,8-isomers, only four symmetrical isomers (2,6-, 2,7-, 1,5-, and 2,3-) have been chosen in this work. Another factor to be considered is how to link the coordination sites to the naphthalene core. As shown in Scheme 3-2, the *para*-, *meta*-, *ortho*-pyridine or imidazole moieties have been attached to the backbone of naphthalene in 2,6-, 2,7-, 1,5- or 2,3- positions *via* the flexible ether, ester or methylene connectors.

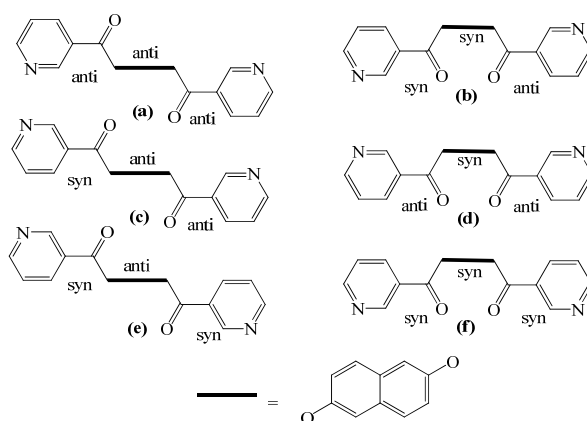


Scheme 3-2: The structures of naphthalene based tectons and the yields for their final steps.

The tectons **E1-E10** are easily prepared (yields shown in Scheme 3-2, see also experimental part) from the corresponding dihydroxynaphthalene derivatives by reaction with isonicotinoyl chloride, nicotinoyl chloride, 4-bromomethylpyridine or 2-bromomethylpyridine under basic condition (in the presence of triethylamine) and under nitrogen atmosphere. Because of the easy oxidation of dihydroxynaphthalene and poor solubility of the target tectons in most organic solvents, the reaction mixtures have been chromatographed to obtain the pure target products.

3.2.2. Attempt to build coordination networks upon combinations of $MSiF_6$ and naphthalene based tectons

Following the design principle already exposed, upon slow diffusion of an EtOH solution of infinite inorganic tecton $MSiF_6 \cdot 6H_2O$ ($M=Zn^{2+}$, Co^{2+} , 5 mg) into a $CHCl_3$ solution (1 mL) of naphthalene based organic tectons **E1-E10** (3 mg) respectively at room temperature. Unfortunately, no suitable crystals for X-ray structural studies on single crystals were obtained in spite of many attempts by modifying the solvents (DMSO, $CHCl_3/DMSO$, $CH_2ClCH_2Cl /DMSO$). The main reason for the bad crystallization behavior may be attributed to the unfavorable initial conformations of the tectons **E1-E10** that were difficult to adjust during the crystallization process. Indeed, because of the rotation of the two coordinating sites (ester and carboxyl group), each tecton offers several possible initial conformations. For example, tecton **E2** may adopt 6 possible conformations, as shown in [Scheme 3-3](#).



Scheme 3-3: Representation of six possible conformations for the tecton **E2**, supposing that the naphthalene ring is in a different plane with respect to the pyridine moiety and the amide group.

In order to gather some evidences, these tectons are combined with metallic tectons ($M(BF_4)_2$, $M(SCN)_2$, $Cu(OAc)$, $HgCl_2$, $M = Fe^{2+}$, Co^{2+} , Zn^{2+}). In some cases, single crystals were obtained and their structures have been investigated by X-ray diffraction technique. Because 7 networks based on tecton **E2** have been obtained, we will discuss them together to show the role played by the rotational processes.

3.2.3. Coordination networks based on other metallatectons and tecton **E2**

3.2.3.1 The crystal structure of the free tecton **E2**

Colorless crystals of the free tecton **E2** were obtained by slow evaporation of its $CHCl_3/EtOH$ solution at room temperature. The single-crystal X-ray structural study revealed the presence of an inversion centre at the midpoint of the central C-C bond of naphthalene moiety and the molecule adopts the *anti-anti-anti* conformation ([Scheme 3-3a](#)). For the compound **E2**, the two pyridine rings are opposite and parallel but tilted with respect to the naphthalene plane with an angle of 50.41° . In the crystal, the packing results from stacking of molecules along the b axis without any π - π

interactions, and both planes (naphthalene and nicotinoyl) of two neighbor molecules are parallel with distances of 3.07 Å and 1.64 Å. The molecular packing is stabilized by the intermolecular C=O--H-C and N--H-C hydrogen bonds ($d_{O1--H2} = 2.68$ Å, $d_{O1--H11} = 2.49$ Å and $d_{N1--H3} = 2.71$ Å, Figure 3-2) to form a 2-D molecular network. Due to the disposition (coplanar and zigzag arrangement) of the two nicotinoyl moieties, this tecton might be of interest as a diagonal connector (see chapter II).

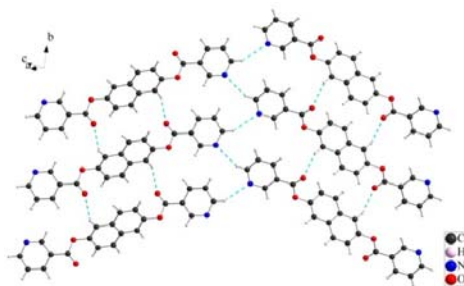


Figure 3-2: The crystal structure of the free tecton **E2**.

3.2.3.2 The crystal structure of $E2 \cdot HBF_4$

The colorless crystals of the protonated tecton **E2** (Figure 3-3) was obtained accidentally upon slow diffusion of an EtOH solution of $Fe(BF_4)_2 \cdot xH_2O$ into a CH_2Cl_2 solution of tectons **E2** at room temperature.

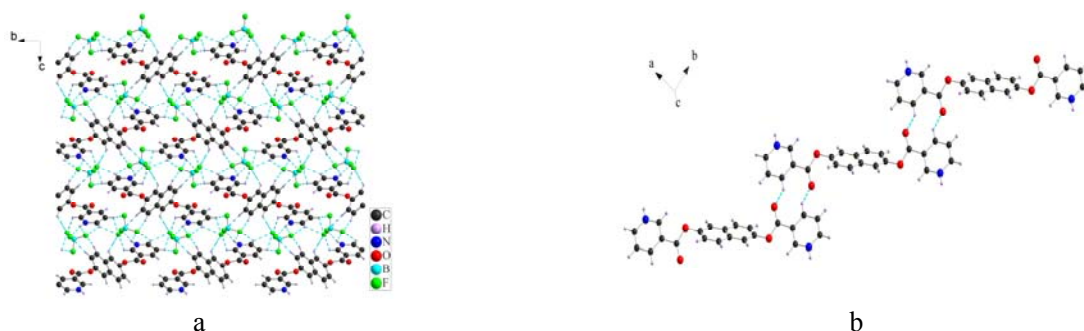


Figure 3-3: The crystal structure of $E2 \cdot HBF_4$ (a) and its H-bonded connection between protonated **E2**

The single-crystal X-ray structural study revealed that the crystal is composed of protonated **E2** and BF_4^- anion ($(HE2)BF_4$, abbreviated as $E2 \cdot HBF_4$). The protonated tecton **E2** adopts the *anti-anti-anti* conformation with the OCCO dihedral angle of 180° (Figure 3-3). The dihedral angle between the parallel pyridine rings and naphthalene moiety is *ca.* 40.9° , much smaller than the one observed for the free tecton. Along the *b* axis, the neighboring two tectons are connected by C--H--O hydrogen bonds ($d_{O--H} = 2.42$ Å) to form a 1-D molecular network (Figure 3-3b). The 1-D hydrogen-bonded networks are stabilized by strong N--H--F and C--H--F hydrogen bonds ($d_{H(N)--F} = 1.90$ Å and $d_{H(C)--F} = 2.31$ Å) with BF_4^- anions (Figure 3-3a). The proton H^+ present in the structure is possibly originated from traces of water.

3.2.3.3 In-situ generation of $ZnSiF_6$ pillared coordination networks from $Zn(BF_4)_2$ and tecton **E2**

a. Structural studies of E2·ZnSiF₆

At the very beginning, we intended to build 2-D zinc coordination networks containing tecton **E2**. For doing that, weak coordinating BF₄⁻ anion was chosen as the counter-ion. Using a conventional method, upon slow diffusion of an EtOH solution of Zn(BF₄)₂·xH₂O into a CH₂Cl₂ solution of **E2**, colorless prismatic crystalline materials were formed in the crystallization tube after *ca.* one month.

Surprisingly, the X-ray diffraction analysis on single crystal revealed the formation of SiF₆²⁻ based pillared type network (*Triclinic, P-1*, [Figure 3-4](#)) composed of the tecton **E2**, Zn²⁺ dication, SiF₆²⁻ anion generated in-situ from BF₄⁻ anion, solvents CH₂Cl₂ and H₂O with a formula [Zn(**E2**)₂SiF₆]⁺·CH₂Cl₂·H₂O (Abbreviated as **E2**·ZnSiF₆). So, it confirms a classic proverb “*many things grow in the gardens that were never sown there (Thomas Fullers, 1732)*”.



Figure 3-4: Top views (a) and cuboid units (b) of the coordination networks **E2**·ZnSiF₆. For clarity, the hydrogen atoms and solvents are omitted.

As previously described for cuboid 3-D networks obtained with rigid tectons (*Chapter II*), the combinations of zinc cations (octahedral geometry with FZnF angles of 180° and NZnN angles of 90 °) with SiF₆²⁻ anion ($d_{\text{Si-F}} = 1.65 \text{ \AA}$ for unbound fluorine atoms and $d_{\text{Si-F}} = 1.76 \text{ \AA}$ for bridging F atoms) leads to the formation of a infinite 1-D pillared tecton resulting from the bridging of metal centres through the two fluorine atoms occupying the axial positions ($d_{\text{Zn-F}} = 2.14 \text{ \AA}$). Each organic tecton **E2**, adopting an *anti-anti-anti* conformation, bridges consecutive ZnSiF₆ pillars with a “staircase-like” mode ([Figure 3-5](#)) to form a transformed cuboid 3-D network ([Figure 3-4b](#)).



Figure 3-5: the positive staircase like plane composed of organic tectons and zinc cations (a) and its schematic representation (b). For clarity, the hydrogen atoms and solvents are omitted in (a).

However, the adjacent two **E2** tectons around each zinc dication present two different distortions. Although the pyridine rings in both tectons are parallel, the dihedral angle between the naphthalene and pyridine moieties is 40.6° and 44.6° respectively. As a result, they could be regarded as two units with different parameters in terms of lengths ($b = 20.48\text{\AA}$ and $c = 17.63\text{\AA}$) in the parallelepiped units (Figure 3-6 right) with a third parameter of 7.80\AA (a , SiF_6^{2-} pillar).

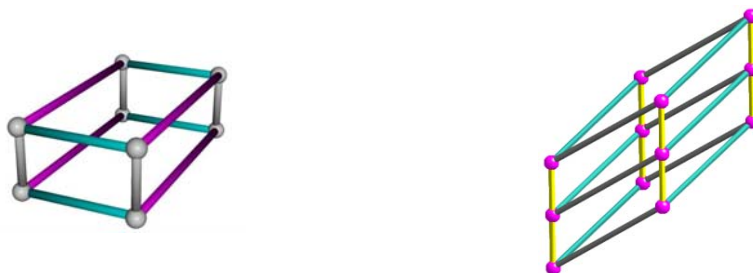


Figure 3-6: Schematic representation of the four-component cuboid 3-D architecture (left, $a \neq b \neq c$, $\alpha = \beta = \gamma = 90^\circ$) and the parallelepiped geometry of **E2**· ZnSiF_6 (right, $a \neq b \neq c$, $\alpha \neq \beta \neq \gamma \neq 90^\circ$).

In the parallelepiped type network, the channel presents a rectangular shape with cross section of $8.72 \times 8.88\text{\AA}$, as shown in Figure 3-7a. Each channel is filled by one dichloromethane molecule and one water molecule per zinc cation (Figure 3-7b), with strong hydrogen bonds towards F atom of the SiF_6^{2-} anions ($d_{\text{H-F}} = 2.30\text{-}2.50\text{\AA}$, Figure 3-7c). The void of the crystalline materials was analyzed using the PLATON software and a free volume per unit cell of *ca.* 18% was calculated.

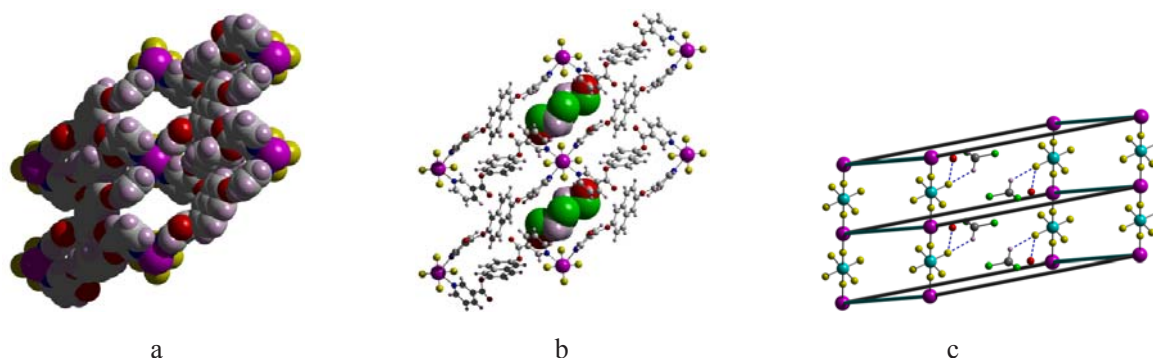


Figure 3-7: The top views of **E2**· ZnSiF_6 to highlight the channels (a) and solvents (b), and the solvent packing in channels (c). For clarity, the solvents in (a) and the organic tectons in (c) are illustrated with a line.

b. Stability and thermal properties of **E2**· ZnSiF_6

The crystalline phase in air is rather stable. In order to investigate the reproducibility of the formation of the above mentioned crystalline architecture, the crystallization process was repeated several times (checked by PXRD). The purity of the crystalline phase was also established by PXRD which revealed that **E2**· ZnSiF_6 forms a pure phases, *i.e.* matching between observed (Figure 3-8 left) and simulated peaks.

The thermal stability of **E2**· ZnSiF_6 is investigated from room temperature to 600°C under nitrogen atmosphere using TGA technique (Figure 3-8 right). The TGA analysis revealed only one

intermediate regime between 30 and 200°C prior to decomposition of the sample, which appeared at *ca.* 300°C. In the TGA curve, the first loss of mass corresponds to the release of the dichloromethane and water molecules and the *ca* 18-20% solvent released is close to the theoretical porosity calculated by PLATON software. As expected, the better stability is attributed to the additive support of organic tectons in the diagonal directions.

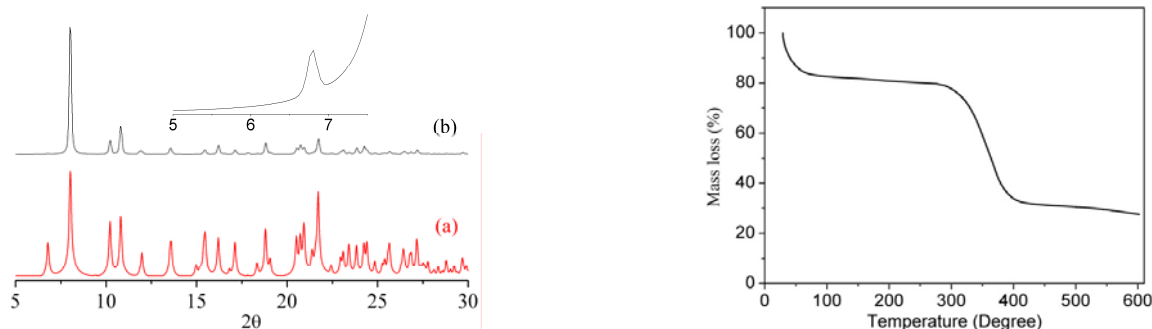


Figure 3-8: The Comparison of the simulated (a) and recorded (b) PXRD patterns (left) and TGA trace under the N_2 (right) for the $E2 \cdot ZnSiF_6$.

c. Some comments on the *in-situ* generation of SiF_6^{2-} from BF_4^- during the crystallization

With respect to the *in-situ* generation of SiF_6^{2-} anions from BF_4^- anion, several papers have also reported similar phenomena (transformation of BF_4^- anion to SiF_6^{2-} during crystallization in glass tube⁶⁻⁸). However, no one give a mechanism for the formation. Herein, in combination with the above structure of protonated tecton **E2**, a convincing conjecture on the generating process of SiF_6^{2-} anion will be presented.

As stated in *section 3.2.3.2*, firstly, the residual water (trace) present in the solvents would be split into a proton and $Zn(OH)_2$ induced by the presence of Zn^{2+} cations. The proton upon protonation of BF_4^- anion would generate HF and neutral BF_3 , which is confirmed by the different lengths of B--F bonds for BF_4^- anions in the above $E2 \cdot HBF_4$ structure. The bond length ($d_{B-F(H)} = 1.41 \text{ \AA}$) is much longer than of B-F ($d_{B-F} = 1.36-1.38 \text{ \AA}$). The generated H, by attacking the glass surface, forms SiF_6^{2-} anion. The latter, a larger anion, preferentially crystallizes. Furthermore, most likely due to the more pronounced propensity of SiF_6^{2-} anion, its stronger interaction with Zn^{2+} is another factor in favor of the pillar formation.⁶ To exclude the possible action of organic tectons, the generation of $ZnSiF_6 \cdot 6H_2O$ from $Zn(BF_4)_2 \cdot xH_2O$ in the glass tube under the same condition (slow diffusion of a EtOH solution of $Zn(BF_4)_2 \cdot xH_2O$ into a CH_2Cl_2 blank solution under room temperature) was successfully repeated.

However, it is surprising that the formation of the crystalline materials is difficult starting from $ZnSiF_6 \cdot 6H_2O$ but reproducible from $Zn(BF_4)_2 \cdot xH_2O$ by so-called *in-situ* generation methods.

3.2.3.4 The crystal structure of $E2 \cdot Co(BF_4)_2$

At room temperature, slow diffusion of an EtOH solution of $Co(BF_4)_2 \cdot 6H_2O$ into a $CHCl_3$ solution of tectons **E2** leads to pink prismatic crystals. The structural analysis on single-crystal

revealed the presence of a discrete complex composed of one metallic salts, two organic tecton **E2** and two water molecules with a formula of $\text{Co}(\mathbf{E2})_2(\text{H}_2\text{O})(\text{BF}_4)_2$, which is abbreviated as $\mathbf{E2}\cdot\text{Co}(\text{BF}_4)_2$ (Figure 3-9).

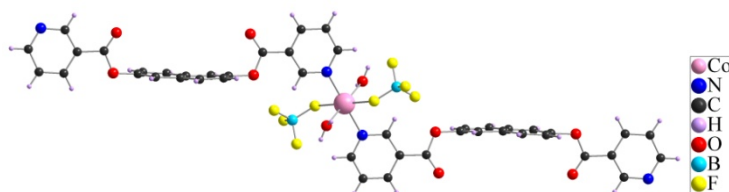


Figure 3-9: The crystal structure of the complex $\mathbf{E2}\cdot\text{Co}(\text{BF}_4)_2$

In the structure, the organic tecton **E2** adopts *syn-syn-anti* conformation (Scheme 3-3b), different from that of the free tecton in crystal. Only one pyridine moiety of each tecton **E2** is found to be coordinated while the other remains unbound. The two pyridine rings are slightly tilted with a small dihedral angle of 6.3° and are nearly perpendicular to the central naphthalene moieties (88.5° and 86.0°). Concerning the cations, each Co^{2+} adopts an octahedral coordination geometry, and is coordinated to the two N atoms of the two organic tectons ($d_{\text{Co-N}} = 2.169 \text{ \AA}$) and two O atoms of the water molecules ($d_{\text{Co-O}} = 2.130 \text{ \AA}$) in the equatorial base of the octahedron, and two F atoms of BF_4^- occupy the left two axial coordination sites ($d_{\text{Co-F}} = 2.012 \text{ \AA}$).

Along the *a* axis, two independent complexes are connected in a head-to-tail fashion through N \cdots F interactions with BF_4^- ($d_{\text{N}\cdots\text{F}} = 2.87 \text{ \AA}$) and π - π interactions between the pyridine rings, which leads to a 2-D staircase like plane (Figure 3-10a). In space, the staircase like planes are stacked closely by weak hydrogen bonds ($d_{\text{O}_2\cdots\text{H}_2} = 2.72 \text{ \AA}$) (Figure 3-10b).

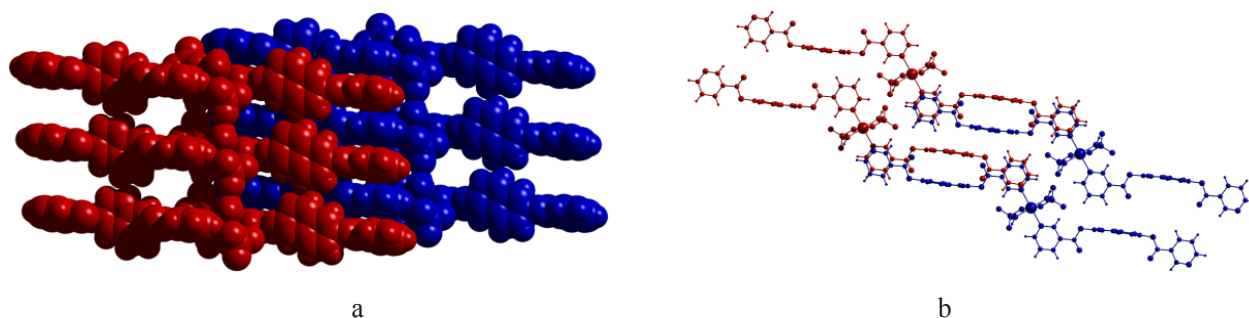


Figure 3-10: the packing of the complex $\mathbf{E2}\cdot\text{Co}(\text{BF}_4)_2$ along the *a* axis (a) and in space (b).

3.2.3.5 The crystal structure of $\mathbf{E2}\cdot\text{Co}(\text{SCN})_2$

Similarly, slow diffusion of an EtOH solution of $\text{Co}(\text{SCN})_2$ into a CHCl_3 solution of tectons **E2** leads to pink needle type crystals. The structural determination revealed that the crystal (monoclinic system, $P21/n$ space group) is composed of two tecton **E2** and one metallic salt with a formula of $\text{Co}(\mathbf{E2})_2(\text{SCN})_2$ (abbreviated as $\mathbf{E2}\cdot\text{Co}(\text{SCN})_2$, Figure 3-11). Similar to the coordination pattern of $\mathbf{E2}\cdot\text{ZnSiF}_6$, each Co^{2+} cation, adopting octahedral coordination geometry, bridges four organic tectons in the equatorial plane through the formation of Co-N bonds ($d_{\text{Co-N}} = 2.20\text{-}2.28 \text{ \AA}$), and the other two axial positions are occupied by two SCN^- anions *via* Zn-N bonds ($d_{\text{Co-N}} = 2.05 \text{ \AA}$) for

charge neutrality.

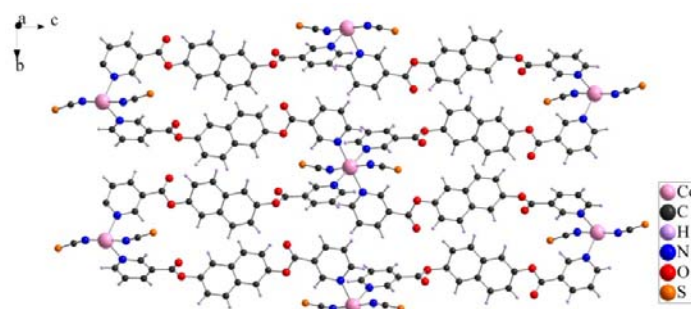


Figure 3-11: The crystal structure of the complex $\mathbf{E2} \cdot \text{Co}(\text{SCN})_2$

Although the organic tecton adopts the same *syn-syn-anti* conformation (Scheme 3-3b), the adjacent two tectons around one central cobalt cation have different distortions with a dihedral angle of 34.9° and 35.7° respectively between the divergent pyridine rings, as well as a dihedral angle of 44.7° and 79.5° between the pyridine ring and naphthalene moiety in one tecton, and 44.1° and 79.5° for another one.

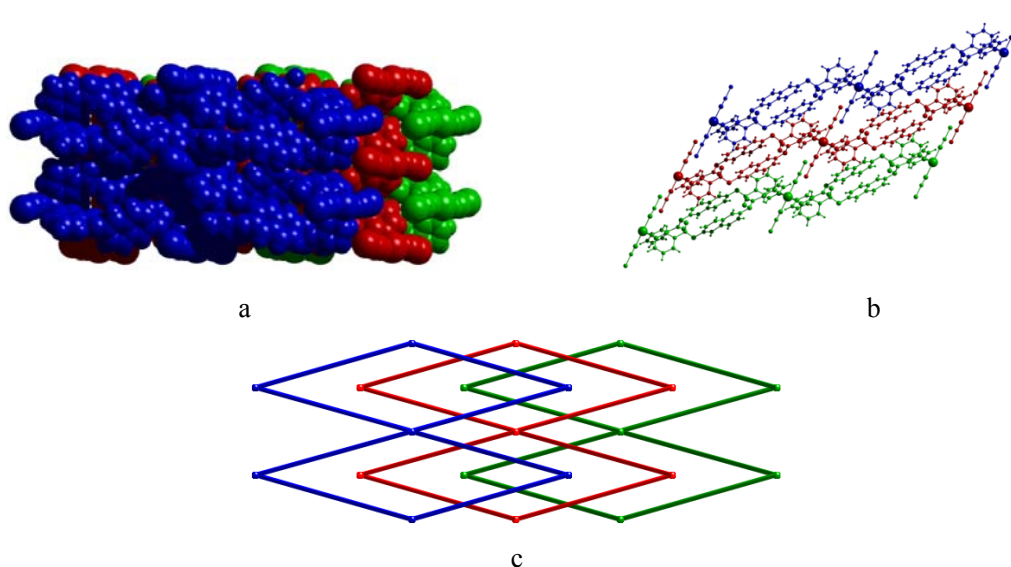


Figure 3-12: the packing of the complex $\mathbf{E2} \cdot \text{Co}(\text{SCN})_2$ along the a axis (a), b axis (b) as well as its topological analysis (c).

Along the axial direction of the metals, the 2-D staircase-like grid networks are somewhat staggered and stack with concave-convex mosaic in space (Figure 3-12). Usually, 2-D grid type networks always lead to the formation of cavities or channels, surprisingly, no cavities are found in this case perhaps due to the staggered arrangement and the compact packing.

3.2.3.6 The crystal structure of $\mathbf{E2} \cdot \text{Cu}(\text{OAc})_2$

Using the same crystallization procedure, the combination of an EtOH solution of $\text{Cu}(\text{OAc})_2$ with a CHCl_3 solution of tectons $\mathbf{E2}$ leads to blue prismatic crystals. The X-ray diffraction on single-crystal revealed that the crystal is composed of one molecule of tecton $\mathbf{E2}$, one

carboxy-bridged dimeric copper unit and one methanol molecule (monoclinic, $C2/c$, $\text{Cu}_2(\mathbf{E2})_2(\text{OAc})\cdot\text{C}_2\text{H}_5\text{OH}$, abbreviated as $\mathbf{E2}\cdot\text{Cu}(\text{OAc})_2$). No specific interactions between the methanol molecules and the other components are detected.

The molecular structure of $\mathbf{E2}\cdot\text{Cu}(\text{OAc})_2$ is a 1-D helical coordination network formed upon bridging of dimeric copper units by tectons $\mathbf{E2}$ (Figure 3-13). Within the molecular chain, tecton $\mathbf{E2}$ adopts *anti-anti-anti* conformation (Scheme 3-3a), as for the free tecton $\mathbf{E2}$ in the solid state. However, the dihedral angle between the naphthalene and pyridine moieties (64.21°) is larger than that of the free tecton $\mathbf{E2}$. As expected, the geometry of the copper centre within the dimer is square based pyramid, with the square base occupied by four oxygen atoms belonging to four acetate groups and the axial position by a nitrogen atom belonging to tecton $\mathbf{E2}$ (Cu-N distances of 2.18 \AA and NCuO angle in the range of 93.5° to 106.8°). The Cu-Cu distance in the dimeric core is 2.68 \AA and the shortest Cu-Cu distance between two dimers in the molecular chain is 18.28 \AA .

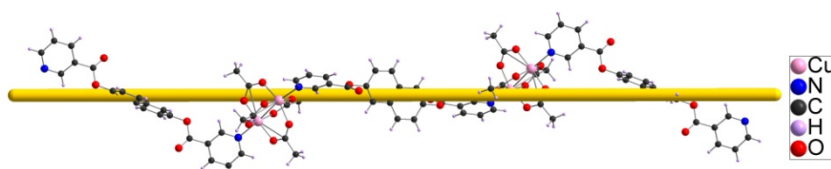


Figure 3-13: The crystal structure of the complex $\mathbf{E2}\cdot\text{Cu}(\text{OAc})_2$. For clarity of helix, a yellow axis is given.

In the plane perpendicular to the c axis, the neighboring two 1-D helical networks are slipped about one helical loop and stacked in a parallel fashion with interweaving π - π interactions of pyridine rings of tectons to form an interwoven 2-D plane (Figure 3-14) with a parallelogram grid ($10.0\text{ \AA} \times 14.6\text{ \AA}$). The neighboring two interwoven planes are slipped about half grid and stacked without any special interactions, leading thus to the generation of 1-D channels (Figure 3-15). The channels are occupied by methanol molecules.

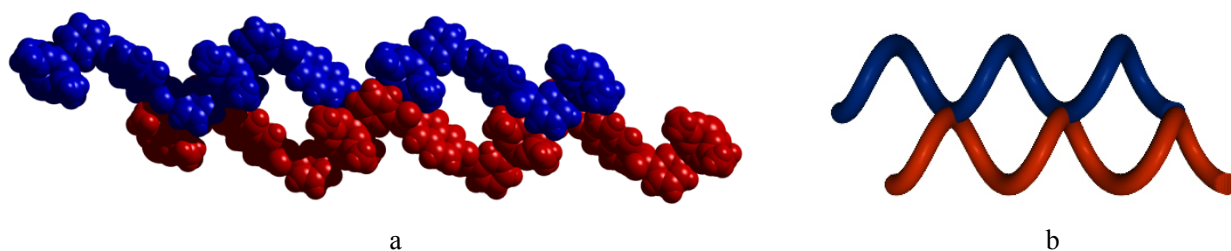


Figure 3-14: The packing of the complex $\mathbf{E2}\cdot\text{Cu}(\text{OAc})_2$ in the ab plane (a) and its topological geometry (b).

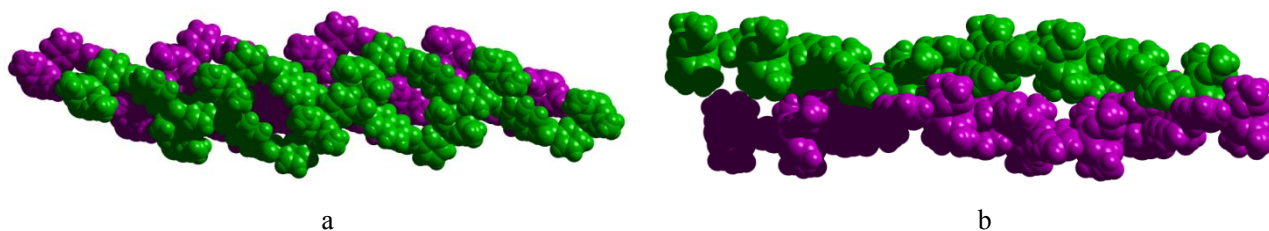


Figure 3-15: The top-view (a) and side view (b) of the packing of the complex $\mathbf{E2}\cdot\text{Cu}(\text{OAc})_2$ along the c axis.

3.2.3.7 The crystal structure of $E2 \cdot HgCl_2$

The colorless prismatic crystals were obtained upon slow diffusion of an EtOH solution of $HgCl_2$ into a $CHCl_3$ solution of tectons **E2**. The X-ray diffraction analysis on single-crystal revealed the formation of a 1-D zigzag coordination network (monoclinic, $P2(1)/n$), which is composed of one tecton **E2** and one $HgCl_2$ ($Hg(E2)Cl_2$, abbreviated as $E2 \cdot HgCl_2$, Figure 3-16a). Within the structure, each organic tecton **E2** adopts a *syn-syn-anti* conformation (Scheme 3-2b), identical to the one observed for $E2 \cdot Co(BF_4)_2$, and the two pyridine rings are slightly tilted with a small dihedral angle of 7.75° and tilted with respect to the central naphthalene moieties with a dihedral angle of 62.7° and 69.9° .

Each central Hg^+ , adopting a distorted tetrahedral coordination geometry ($ClHgCl$, $NHgN$ and $NHgCl$ angle of 157.0° , 119.8° and 94.6° respectively), connected to two pyridine moieties and two halide anions through the $Hg-N$ bonds ($d_{Hg-N} = 2.53 - 2.51 \text{ \AA}$) and $Hg-Cl$ bonds ($d_{Hg-Cl} = 2.35 \text{ \AA}$). Because of the distortions of tecton **E2** and zigzag shape coordination mode, the 1-D coordination network looks like a half-tubular gutter, as shown in Figure 3-16b.

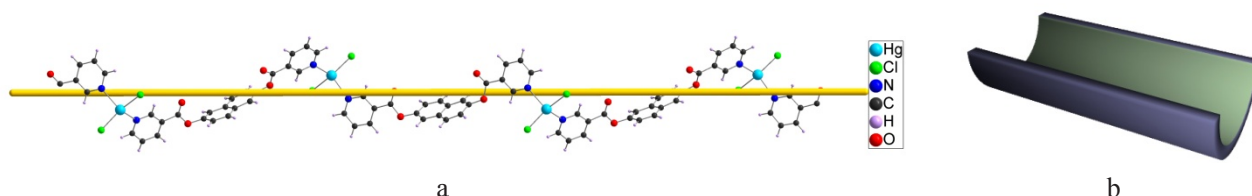


Figure 3-16: The crystal structure of the complex $E2 \cdot HgCl_2$ (a) and schematic representation of its half-tubular shape (b). For clarity of its shape, a yellow axis is given.

Along the b axis, the neighboring two chains are mirror images and slipped about the length of a tecton to stack into a plane with $\pi-\pi$ interactions between the pyridine rings (Figure 3-17) with a distance of 3.41 \AA . In three dimension, the neighbor two layers are stabilized by the weak hydrogen bonds ($d_{C_{H1}-H_{20}} = d_{C_{12}-H_2} = 2.89 \text{ \AA}$).

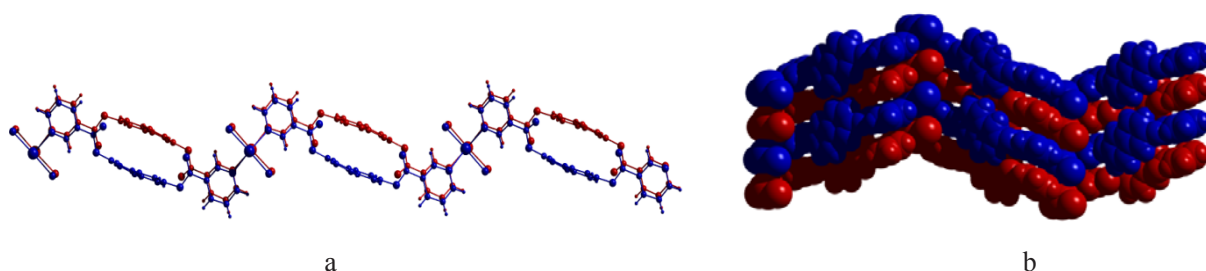


Figure 3-17: The packing of chains along the b axis: views along b axis (a) and along the a axis (b).

3.2.3.8 The comparison of the rotations of tecton **E2** in different crystalline structures

As expected, in the presence of different metallatectons, due to the rotation, the tecton **E2** present different conformations (Table 3-1).

From the compared data given in Table 3-1, it might be concluded that the semi-rigid tecton **E2**

can adjust its conformations during the self-assembly process.

Table 3-1: The comparison of the selected data highlighting the rotations of tecton **E2**

Compounds	Conformations ^[a]	Dihedral angles between two pyridine rings/ $^{\circ}$	Dihedral angles between the pyridine rings and naphthalene moieties/ $^{\circ}$
Free tecton (solid state)	<i>anti-anti-anti</i>	180	50.41
Protonated tecton	<i>anti-anti-anti</i>	180	40.9
E2 ·ZnSiF ₆	<i>anti-anti-anti</i>	180	40.6, 44.6
E2 ·Co(BF ₄) ₂	<i>syn-syn-anti</i>	6.28	88.57, 86.01
E2 ·Co(SCN) ₂	<i>syn-syn-anti</i>	34.94/35.57	44.73, 79.57/44.09, 79.57
E2 ·Cu(OAc) ₂	<i>anti-anti-anti</i>	180	64.21
E2 ·HgCl ₂	<i>syn-syn-anti</i>	7.75	62.76, 69.97

^[a] Schematic representation of the possible conformations referring to [Scheme 3-2](#).

3.2.4. The coordination networks based on other metallatectons and naphthalene based tectons

For the other 9 naphthalene based tectons, a CHCl₃ solution of **E1** or **E3-E10** was layered with DMSO and then an EtOH solution of selected metallatectons (M(BF₄)₂, M(SCN)₂, Cu(OAc), HgCl₂, M = Fe²⁺, Co²⁺, Zn²⁺) was carefully added. Upon slow diffusion, only three combinations (**E8** with Co(SCN)₂, **E9** with Cu(OAc)₂ and **E10** with Co(SCN)₂) generated single crystals suitable for X-ray diffraction studies.

3.2.4.1 The crystal structure of **E8**·Co(SCN)₂

The structural analysis on single-crystal revealed that the needle type crystals (monoclinic system and *C2/c* space group) are composed of 2-D coordination networks with a formula of Co(**E8**)₂(SCN)₂·3H₂O (abbreviated as **E8**·Co(SCN)₂, [Figure 3-18a](#)).

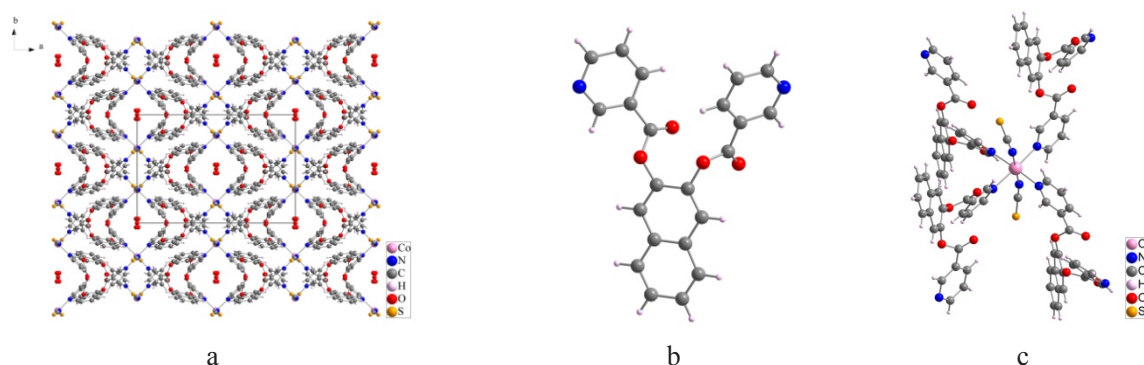


Figure 3-18: The crystal structure of the complex **E8**·Co(SCN)₂ (a) and the independent organic tecton **E8** (b) and coordination pattern for each metal cation (c).

As for **E2**·Co(SCN)₂ network, each Co²⁺ adopts an octahedral coordination geometry, coordinated by four organic tecton **E8** in the square plane and two SCN mono-anions in the axial positions through Co-N bonds ($d_{\text{Co-N}} = 2.21 - 2.22 \text{ \AA}$ for tecton, 2.08 \AA for SCN mono-anion) to form a rhombic grid of $13.0 \text{ \AA} \times 13.0 \text{ \AA}$ ([Figure 3-18c](#)). However, the organic tecton **E8**, adopts a

coplanar zigzag coordinating shape with a dihedral angle of 50.7° and 36.7° between pyridine rings and naphthalene moiety, bridged by two Co^{2+} cations to form the grid plane. With regard to the four tectons around one Co^{2+} cation, the naphthalene moieties of the opposite two are located upward or downward and thus leads to the “burr” plane (Figure 3-18b, c).

In space, the “burs” of the consecutive two planes are inserted into one another without any special interactions, as shown in Figure 3-19. As a result, a 1-D parallelogram channel with the cross section of $9.3 \text{ \AA} \times 9.0 \text{ \AA}$ is formed. The channel is filled with 3 water molecules per cobalt cation without any distinct interactions.

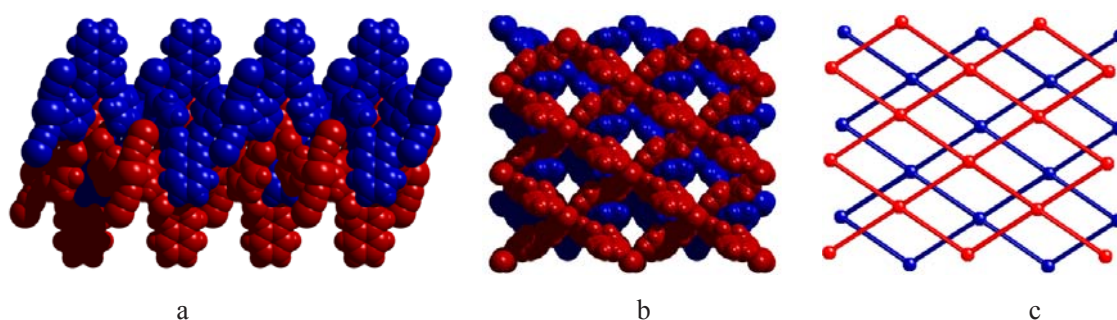


Figure 3-19: the packing of the complex $\text{E8} \cdot \text{Co}(\text{SCN})_2$ along the b axis (a), the c axis (b) as well as its topological geometry (c).

3.2.4.2 The crystal structure of $\text{E9} \cdot \text{Cu}(\text{OAc})_2$

The X-ray diffraction study on single-crystal revealed that the blue prismatic crystal (triclinic, $P-1$) is a classic 1-D zigzag coordination network composed of the V-shape organic tecton linked by linear copper acetate dimers with a formula of $\text{Cu}_2(\text{E9})_2(\text{OAc}) \cdot 1.5\text{H}_2\text{O}$ (abbreviated as $\text{E9} \cdot \text{Cu}(\text{OAc})_2$, Figure 3-20).

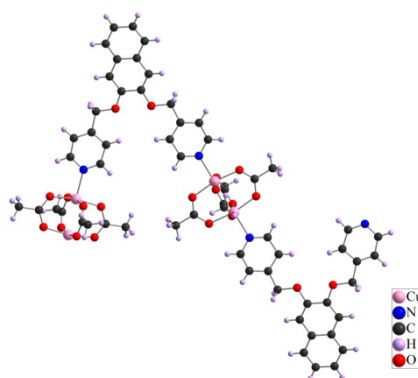


Figure 3-20: The crystal structure of the complex $\text{E9} \cdot \text{Cu}(\text{OAc})_2$.

In the coordination chain, each V-shape tecton E9 bears two nearly parallel pyridine rings with a dihedral angle of 5.2° , and the latter pyridine rings are tilted with respect to the central naphthalene moiety with a dihedral angle of 22.8° and 18.5° respectively. The sharp angle of V shape is equal to 44.9° .

Similar to **E2**·Cu(OAc)₂, each copper acetate dimer adopts square-based pyramidal geometry with the square base occupied by four oxygen atoms belonging to four acetate groups and the axial position by a nitrogen atom belonging to the tecton **E9** (Cu-N distances both are 2.16 Å, NCuO angle in the range of 94.4 ° to 97.0 °). The Cu-Cu distance in the dimeric core is 2.63 Å and the shortest distance between two dimers in the molecular chain is 10.92 Å.

In space, the zigzag chains are stacked with a head-to-tail pattern by strong π - π interactions between pyridine rings and thus lead to a 1-D hexagon channels (Figure 3-21). In the channels, 3 water molecules per copper acetate dimer take up the voids without any special interaction.

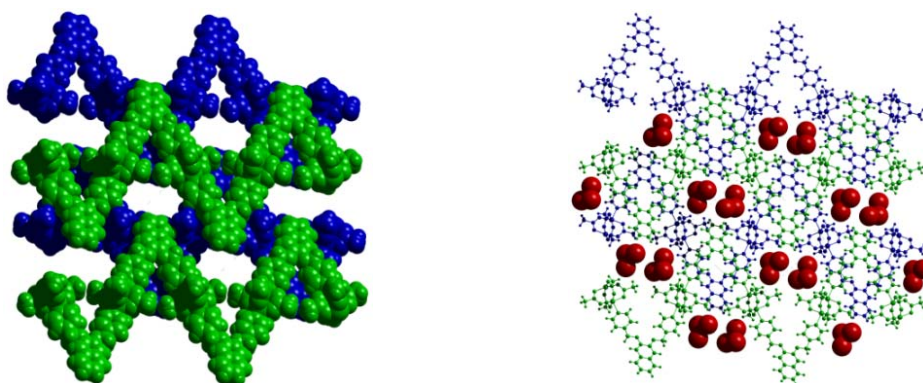


Figure 3-21: The packing of complex **E9**·Cu(OAc)₂ in the space highlighting the stacking mode (a) and the included solvents (b)

3.2.4.3 The crystal structure of **E10**·Co(SCN)₂

The structural determination reveals that the molecular structure of **E10**·Co(SCN)₂ (pink prismatic crystals) can be described as a discrete complex composed of one tecton **E10**, one Co²⁺ cation and two SCN⁻ anions (Figure 3-22). In the structure, the octahedral cobalt dication is surrounded by two N atoms ($d_{\text{Co--N}} = 2.09 - 2.13$ Å) and two O atoms ($d_{\text{Co--O}} = 2.16 - 2.25$ Å) of organic tecton and two N atoms ($d_{\text{Co--N}} = 2.01$ Å) of SCN⁻ anions so as to form a neutral discrete complex. Owing to the chelation of the tecton, the Co--N distances in **E10**·Co(SCN)₂ are slightly shorter than those in the infinite networks described previously (**E2**·Co(SCN)₂ and **E8**·Co(SCN)₂).

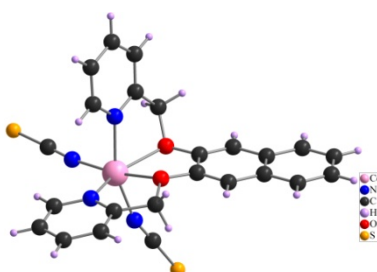


Figure 3-22: The crystal structure of the complex **E10**·Co(SCN)₂.

In space, the packing of the discrete complex is stabilized by the weak C--H--S hydrogen bonds with the distances in the range of 2.90 - 3.00 Å

3.3. The coordination networks based on the spirobiindane core

3.3.1. Design and synthesis of spirobiindane based organic tectons T2

The generation of helical assemblies is a topic of interest. These architectures, discrete or infinite in dimension, may either be purely organic or hybrid in nature engaging both organic parts and metallic centres⁹⁻¹⁷. For the design of infinite helical coordination architectures, one may apply the tectonic approach in designing specific helix inducing tectons (*e.g.* 1,10-binaphthyl, isomannide or calixarene based tectons)¹³⁻¹⁷. Due to the nature of helices, so far most of reported helical coordination assemblies are presented as 1-D networks⁹⁻¹⁷. However, few are involved in the 2-D or 3-D helical networks¹⁸⁻²³.

Design of 3-D coordination networks based on infinite MSiF₆ tecton containing helical channels (Figure 3-33) is one of the objectives of this work. Compared with 1, 1'-binaphthalene, 1,1'-spirobiindane is a conformationally more rigid scaffold. Using it as a core of tecton, a chiral shape with two divergent coordination sites may be designed and thus the formation of helical 3-D architectures (Figure 3-33) may be achieved.

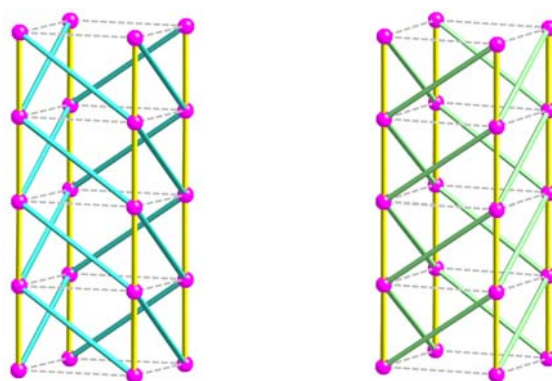
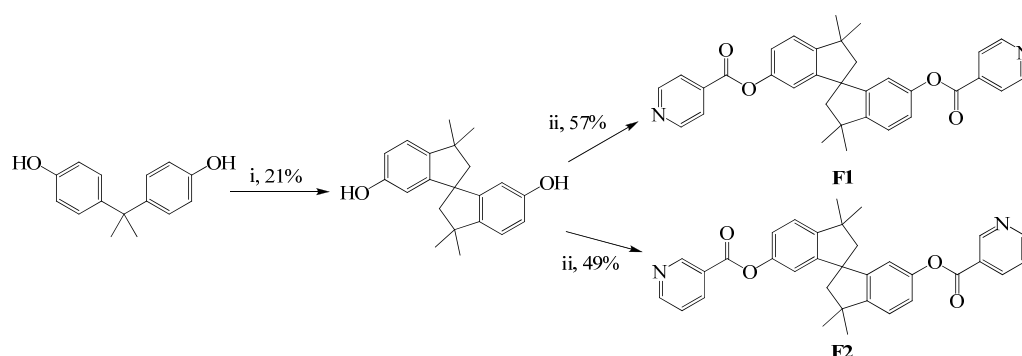


Figure 3-23: Schematic representation of 3-D coordination networks based on ZnSiF₆ pillars containing P (left) or M (right) helical channels.



Scheme 3-3: Reaction conditions: (i) methanesulphonic acid, 135 °C for 3 h; (ii) isonicotinoyl chloride (nicotinoyl chloride), Et₃N, room temperature, 48h.

3,3,3',3'-Tetramethyl-1,1'-spirobisindane-6,6'-diol, which is easily obtained in racemic form, by combining the coordination moieties (pyridine moieties) with its hydroxyl groups *via* the flexible

ester connector³ leads to two isomeric tectons **F1** and **F2**. The starting material 3,3,3',3'-Tetramethyl-1,1'-spirobisindane-6,6'-diol³ was easily available in multi-gram quantities by the one-step acid-mediated rearrangement of bisphenol A. The coordinating groups, *para*- or *meta*-pyridine rings, have been attached using isonicotinoyl chloride or nicotinoyl chloride under basic conditions (triethylamine) and under nitrogen atmosphere in 57 % and 49 % yields respectively (*see experimental part*).

3.3.2. *Attempt to build coordination networks based on MSiF₆ and spirobiindane based tectons*

The formation of coordination networks based on ZnSiF₆ pillar was investigated by slow diffusion of an EtOH solution (1 mL) of infinite inorganic tecton MSiF₆·6H₂O (M = Zn²⁺, Co²⁺, 5 mg) and Zn(BF₄)₂ (5 mg) into a CHCl₃ solution (1 mL) of spirobiindane based organic tectons **F1-F2** (3 mg) respectively at room temperature. Unfortunately, no suitable crystals for X-ray structural studies on single crystal were obtained in spite of many attempts by modifying the solvents (DMSO, CHCl₃/DMSO, CH₂ClCH₂Cl /DMSO). Spirobiindane based organic tectons **F1-F2** are also of interest to be combined other metal complexes such as HgCl₂ for the generation of neutral helical strands.

3.3.3. *The coordination networks based on HgCl₂ and spirobiindane based tectons*

At room temperature, a solution of tectons **F1** or **F2** in CHCl₃ (3 mg) was layered with DMSO (1 mL) and then a solution of HgCl₂ (5 mg) in EtOH (1 mL) was carefully added. Upon slow diffusion, colorless prism-type crystals, insoluble in common solvents, were obtained after several days. In both cases, crystals were analyzed by X-ray diffraction on single crystals (XRD) and by X-ray diffraction on powder (PXRD).

3.3.3.1 *Structural studies of F1·HgCl₂*

For the first combination, the structural study revealed that the crystal (*Triclinic, P-1*) was composed of both enantiomers of **F1** (Figure 3-24a-b) and HgCl₂ with a formula of Hg(**F1**)₂Cl₂ (abbreviated as **F1**·HgCl₂). The interconnection of consecutive tectons **F1** with the same chirality by HgCl₂ leads to the formation of both P and M helical strands (Figure 3-24c-d). For the 1,1'-spirobi(indane) backbone, an angle of 70.7 ° between the two phenyl groups is observed. The Hg²⁺ cation adopts a slightly distorted square pyramidal geometry and its coordination sphere is composed of 2 Cl⁻ anions (d_{Hg-Cl} = 2.34 - 2.35 Å, ClHgCl angle of 167.5 °) and 3 N atoms (d_{Hg-N} = 2.59 - 2.72 Å, NHgN angles of 83.4 ° and 171.4 °) belonging to three different tectons **F1** (Figure 3-24e-f). Among the 3 N atoms present in the coordination sphere of Hg²⁺ cation, two belongs to two consecutive tectons **F1** of the same chirality generating the helical strand (Figure 3-24c-d) and the third one belongs to a second type of tecton **F1** (angle between the two phenyl groups of the 1,1'-spirobi(indane) moiety of 78.8 °) possessing the opposite handedness (Figure 3-24e-f). The latter type behaves as an appended ligand and only one out of the two pyridine units are engaged in the binding of Hg²⁺ cation belonging to the helical strand. This is probably due to the rigidity of the

backbone and to the junction between the scaffold and the pyridyl moiety in position 4. The overall structure is a 1-D interwoven architecture composed of two enantiomorphous helical strands (Figure 3-24g).

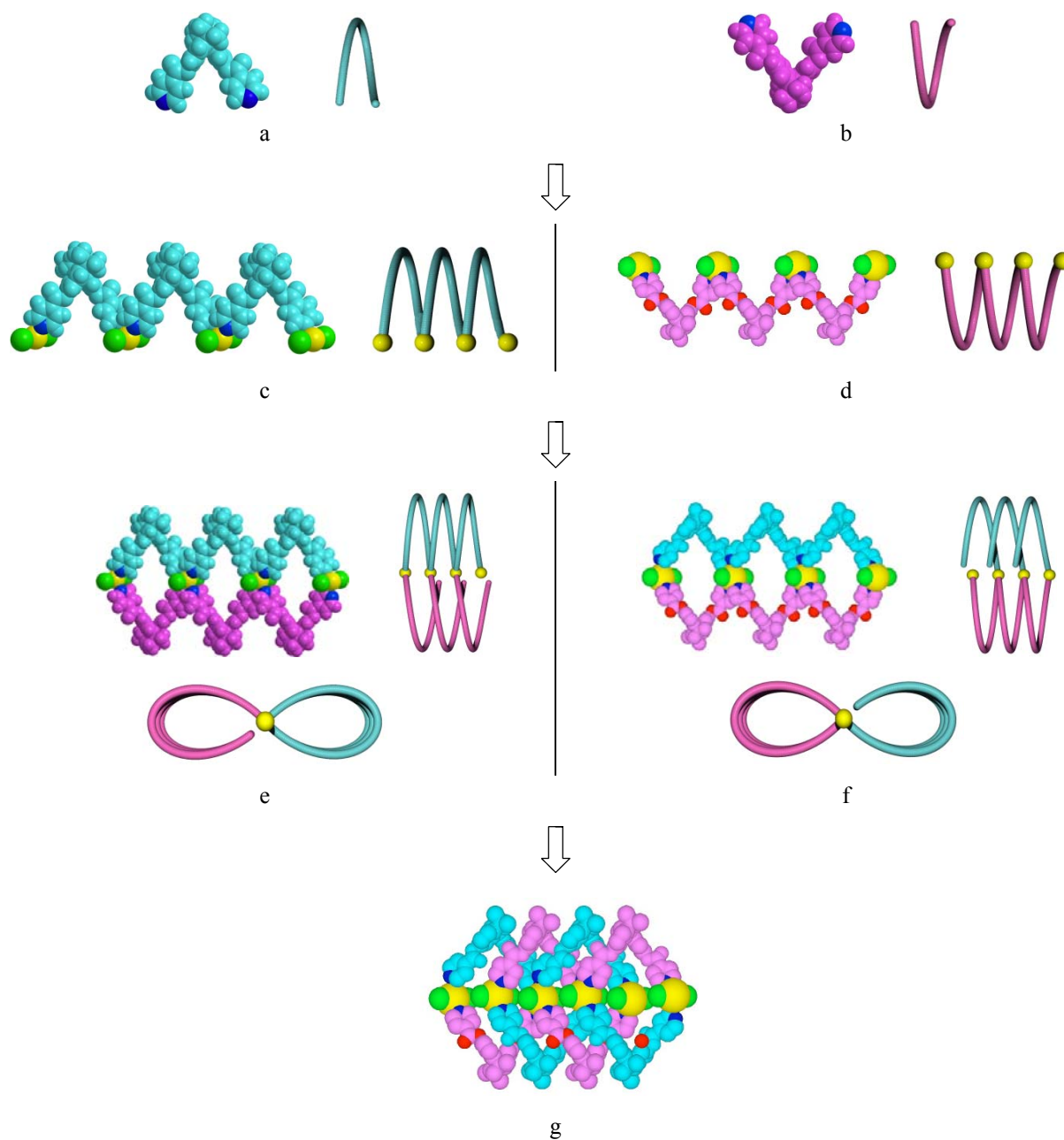


Figure 3-24: Schematic representation of the P (blue) and M (pink) helical configuration adopted by the tecton **F1** (a, b), a portion of the helical strands generated upon bridging of consecutive tectons **F1** by HgCl_2 and their schematic representations (c, d), a portion of the structure of helical strand bearing appended tectons **F1** and their schematic representations (e, f) and a portion of the interwoven architecture (g). H atoms are omitted for clarity.

In space, all the networks are parallel and two neighboring racemic 1-D interwoven networks are staggered and stacked by head-to-tail mode with weak C--H--O hydrogen-bonded interactions ($d_{\text{H--O}} = 2.50 - 2.70 \text{ \AA}$, Figure 3-25). Concerning the packing, each arrangement of given chirality (M helicity) is in contact with four units of the opposite chirality (P helicity). Because of the close

packing by stacking, no cavities are observed and thus no solvent molecule is present in the crystal.

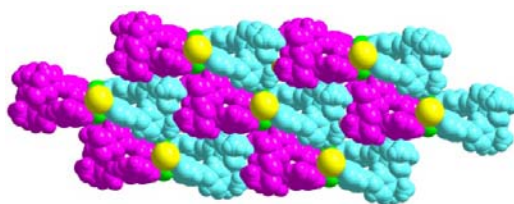


Figure 3-25: The cross section of the packing of $\mathbf{F1}\cdot\text{HgCl}_2$. For clarity, the P (blue) and M (pink) helices are differentiated by color.

3.3.3.2 Structural studies of $\mathbf{F2}\cdot\text{HgCl}_2$

For the second combination, *i.e.* tecton $\mathbf{F2}$ and HgCl_2 , the structural analysis revealed that the crystal (*trigonal*, space group $R\bar{3}c$) is composed of $\mathbf{F2}$, HgCl_2 , 2 H_2O and 2 CHCl_3 solvent molecules with a formula of $6[\text{Hg}(\mathbf{F1})\text{Cl}_2]\cdot 2(\text{CHCl}_3)\cdot 2(\text{H}_2\text{O})$ (abbreviated as $\mathbf{F2}\cdot\text{HgCl}_2$, [Figure 3-26](#)).

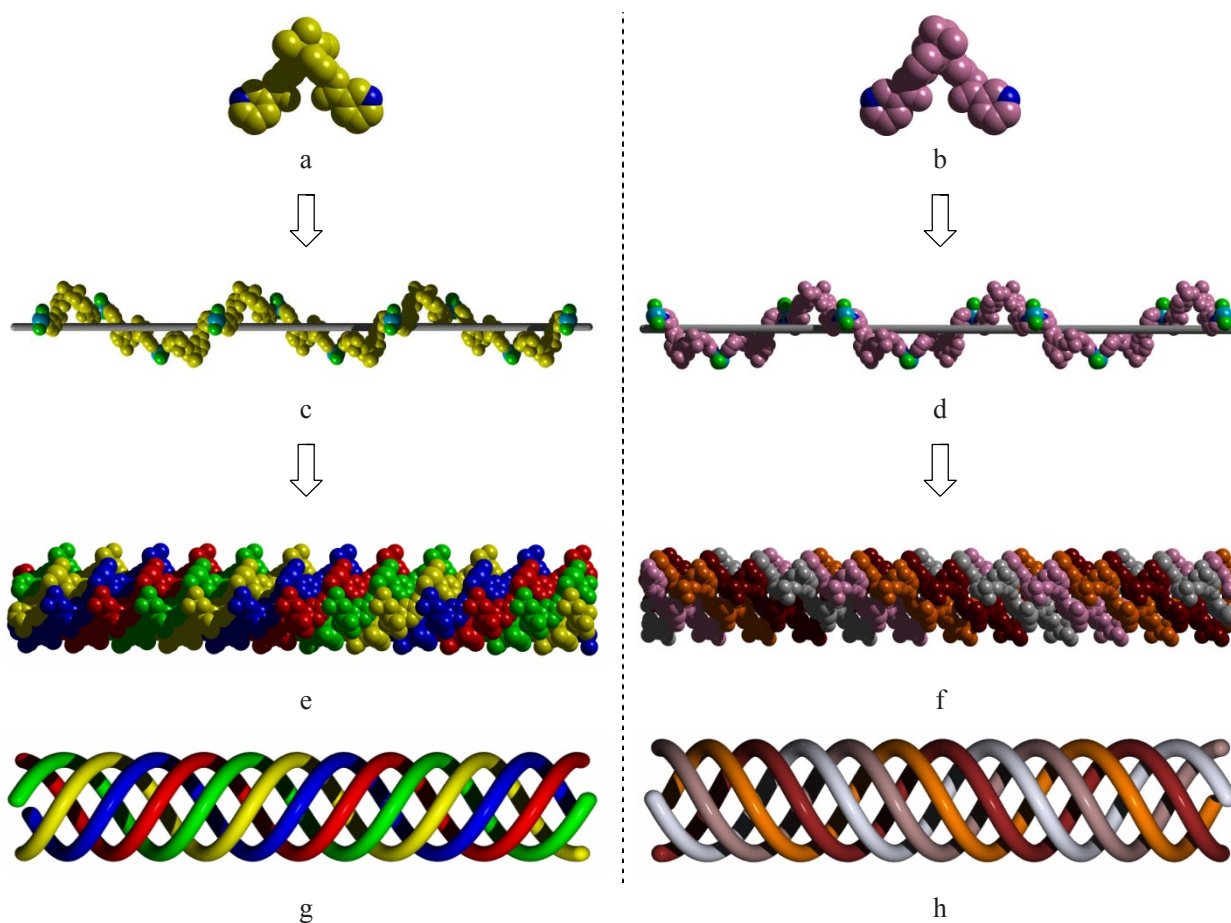


Figure 3-26: A perpendicular view of two enantiomers of the tecton $\mathbf{F2}$ (a, b), a portion of corresponding enantiomerically pure infinite 1-D helical coordination network formed upon bridging of two enantiomers by HgCl_2 (c, d), a portion of the quadruplex stranded helices formed between four single stranded helices through aromatic/aromatic interactions (e, f) and the topological simplification of the quadruplex stranded helices (g, h). For clarity, the H atoms are omitted in all cases.

The organic and inorganic tectons **F2** and HgCl_2 respectively form helical strands (Figure 3-26c-d) with opposite handedness. This is not surprising since for **F2**, a racemic mixture of both enantiomers was used and consequently both *P* and *M* helical strands are found in the crystal. The metric analysis presented here after concerns the strand with *P* helicity. As expected, except for the handedness, the same analysis holds for the other strand. Within the helical strand composed of the same enantiomer, for the central 1,1'-spirobi(indane) scaffold a torsion angle of 87.5° between the two phenyl groups is observed. The two 3-pyridyl units connected to the backbone through ester junctions ($d_{\text{C-O}} = 1.36 \text{ \AA}$ and $d_{\text{C=O}} = 1.20 \text{ \AA}$) are divergently oriented towards the concave face of the scaffold and tilted by 18.7° .

The Hg^{2+} cation adopts a distorted tetrahedral geometry and its coordination sphere is composed of two Cl^- anions ($d_{\text{Hg-Cl}} = 2.34 \text{ \AA}$ and ClHgCl angle of 154.5°) and the two N atoms ($d_{\text{Hg-N}} = 2.45 \text{ \AA}$, NHgN angle of 89.5° and ClHgN angle varying between 97.6° and 100.4°). Owing to the nearly perpendicular disposition of the spiro-annulated rings along the helical axis, the minimum translation unit (one tecton and one HgCl_2) generates a helical rotation angle of 120° and thus the helical pitch of the helix, composed of three translation units, is *ca* 43.47 \AA (Figure 3-26c-d). Probably, as a result of the long pitch, four strands of the same handedness form a quadruple stranded helical arrangement (Figure 3-26e-h) with weak interstrand hydrogen-bonds between nicotinoyl units of different strands (distance between O and C atoms of *ca* 3.14 \AA).

The quadruple stranded helices are not cylindrical but triangular in shape and are packed in a hexagonal fashion with alternated *P* and *M* chirality without any specific interactions between them (Figure 3-27). A view of the cross section parallel to the helical axis of the hexagonal packing of the triangular quadruple helical strands with opposite handedness ($3P$ and $3M$ in alternate disposition), shows that each triangular column of a given chirality is in contact with three columns of the opposite chirality (Figure 3-27b).

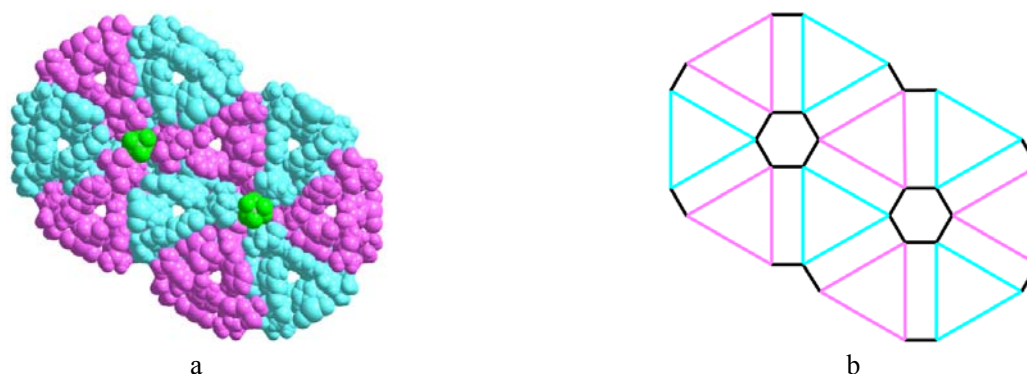


Figure 3-27: The cross section of the packing of **F2**- HgCl_2 trigonal quadruple stranded helices (a) and its schematic representation (b). For clarity, the *P* (blue) and *M* (pink) quadruple stranded helices are differentiated by color. The Cl atoms of CHCl_3 located at the centre of the hexagons are colored in green.

The packing of quadruple helical strands generates two types of channels. The inner triangular channels, with a side length of 8.8 \AA , are empty, whereas the hexagonal channels with a side length

of *ca.* 6.2 Å are found to be filled with two chloroform and two water molecules per mercury cation without any specific interaction with the helical walls. As a result, the included solvents are easily released in the air, which is confirmed by the observation that no solvent loss is found in its TGA trace (Figure 3-29) after the sample standing in air for *ca.* 1h (PXRD recorded time).

3.3.3.3 Stability and thermal properties of spirobiindane based coordination networks

Both coordination networks, **F1**·HgCl₂ and **F2**·HgCl₂, are stable in air. The purity of their crystalline phase was checked by PXRD which revealed a single set of diffraction peaks matching the simulated patterns (Figure 3-28).

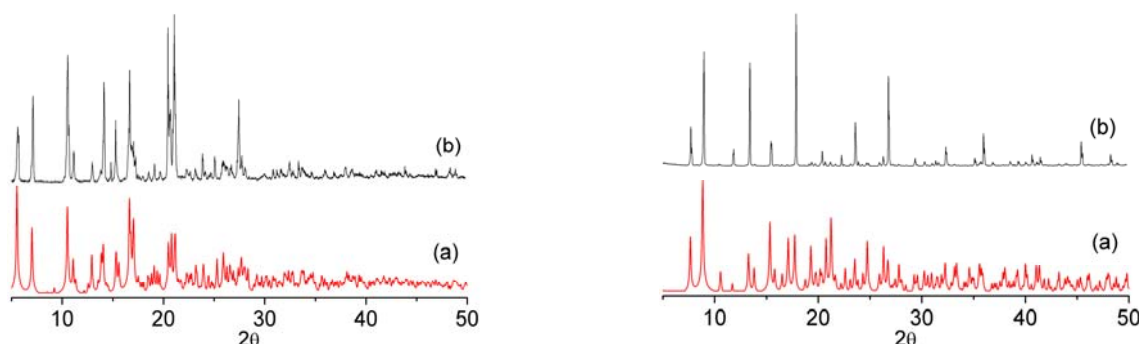


Figure 3-28: Comparison of the simulated (a) and recorded (b) PXRD for the crystalline material of **F1**·HgCl₂ (left) and **F2**·HgCl₂ (right).

The thermal stability of the crystalline materials was investigated by TGA which revealed that whereas **F1**·HgCl₂ is stable up to *ca.* 250 °C, **F2**·HgCl₂ starts to decompose at *ca.* 200 °C (Figure 3-29), without any loss of solvents between 30 °C and 200 °C. No solvent release was observed by TGA analysis of **F2**·HgCl₂.

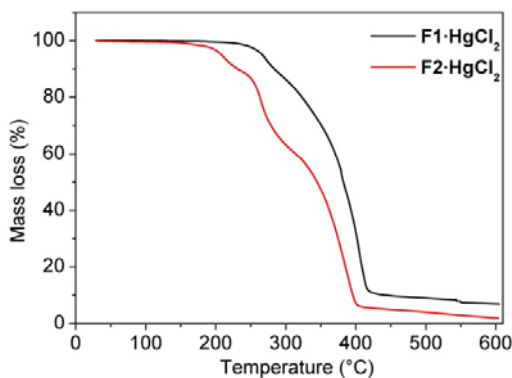


Figure 3-29: The TGA patterns for the two air-stable networks under the N₂ with the rate of 5°C/min. For the latter case, the sample was dried in air for *ca.* 1h.

In conclusion, the 1,10-spirobiindane backbone is a helix directing unit. The combination of racemic pyridine based tectons **F1** and **F2** with HgCl₂, depending on the position of attachment of the coordinating sites to the scaffold, leads to the formation of either a double stranded interwoven helical arrangement or to a quadruple-stranded metallaorganic helix.

3.4. The coordination networks based on the 1,3,5-triazine core

3.4.1. Design and synthesis of 1,3,5-triazine based organic tectons T2

The combination of a tridentate tecton with a square-planar four coordinating metal always leads to an octahedral coordination cage^{5, 24, 25}. For example, a face-driven corner-linked truncated octahedral nanocages, $[\text{Pd}_6\text{L}_8]^{12+}$ ($\text{L} = \text{N}, \text{N}', \text{N}''$ -tris(3-pyridinyl)-1,3,5-benzenetricarboxamide) have been prepared with eight C_3 -symmetric tridentate ligands and six square planar tetratopic palladium(II) ions (Figure 3-30a)²⁴. Considering similar coordination patterns of MSiF_6 who offers four available sites at the corners of a square, we anticipated to bridge the cages (Figure 3-30a, b) as secondary building units (SBUs) by our bridged anion SiF_6^{2-} in six truncated octahedral vertices to form a 3-D coordination network (Figure 3-30c). In order to carry out this design principle, a tridentate tecton 2,4,6-tris(pyridin-4-ylmethylthio)-1,3,5-triazine (**G1**, Scheme 3-4) was prepared according to the literature⁵.

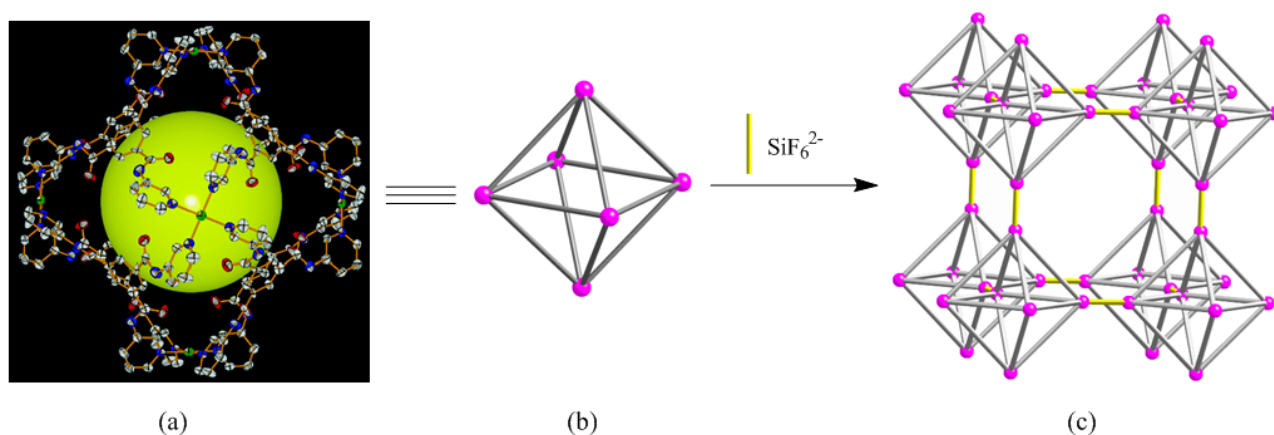
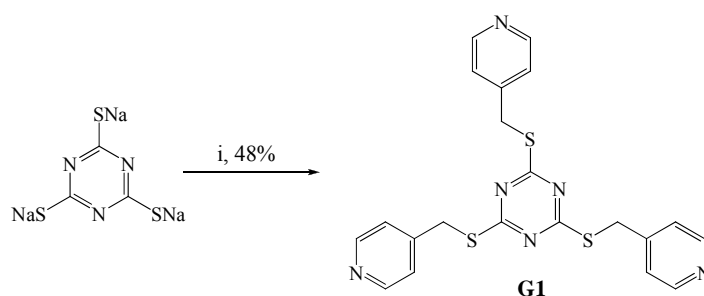


Figure 3-30: Schematic representation of a possible formation of 3-D networks by bridging of $[\text{M}_6\text{L}_8]^{12+}$ cages as SBUs using SiF_6^{2-} anions.



Scheme 3-3: Reaction conditions: (i) K_2CO_3 , 4-bromomethylpyridine, 80°C for 12 h.

3.4.2. Attempt to build coordination networks based on MSiF_6 and 1,3,5-triazine based tecton

Again, upon slow diffusion of an EtOH solution of MSiF_6 ($\text{M} = \text{Zn}^{2+}, \text{Co}^{2+}$, 5 mg) into a CHCl_3 solution (1 mL) of the tecton **G1** (3 mg) at room temperature, no suitable crystals for the X-ray diffraction was obtained in spite of many attempts by modifying the solvents (DMSO, $\text{CHCl}_3/\text{DMSO}$, $\text{CH}_2\text{ClCH}_2\text{Cl}/\text{DMSO}$). Once again, we combined the tecton **G1** with HgCl_2 .

3.4.3. The coordination networks based on HgCl_2 and tecton **G1**

At room temperature, a solution of tecton **G1** in CHCl_3 (3 mg) was layered with DMSO (*ca.* 0.1 mL) and then a solution of HgCl_2 (5 mg) in EtOH (1 mL) was carefully added. Upon slow diffusion, colorless prism-type crystals, insoluble in common solvents, were obtained after several days. The X-ray diffraction analysis on single-crystal revealed the formation of a 1-D nanosized metal-organic tubular chain composed of two tectons **G1**, three HgCl_2 and two water molecules with a formula of $\text{Hg}_3(\mathbf{G1})_2\text{Cl}_6 \cdot 2\text{CHCl}_3$ (abbreviated as $\mathbf{G1} \cdot \text{HgCl}_2$, Figure 3-31).

Within the chain, three Hg^{2+} cations are bridged the Cl^- anions to form a trinuclear cluster. Wherein, two Hg^+ cations, adopt a slightly distorted square pyramidal geometry, occupied by one capped Cl^- anion ($d_{\text{Hg}-\text{Cl}} = 2.57\text{\AA}$) and two bridged Cl^- anions ($d_{\text{Hg}-\text{Cl}} = 2.58, 2.86\text{\AA}$) in the equatorial triangular plane. However, the central cation adopts an octahedral geometry with the equatorial square plane occupied by four bridged Cl^- anions ($d_{\text{Hg}-\text{N}} = 2.76, 2.86\text{\AA}$). As a result, as shown in Figure 3-31a, each trinuclear unit, offering six free coordination sites at the axial positions, are connected by the organic tectons *via* $\text{Hg}-\text{N}$ bonds ($d_{\text{Hg}-\text{N}} = 2.21 - 2.31\text{\AA}$) affording thus a tubular chain with a parallelogram cavities of *ca.* $12.8 \times 6.8\text{\AA}$ filled by chloroform molecules (Figure 3-31b).

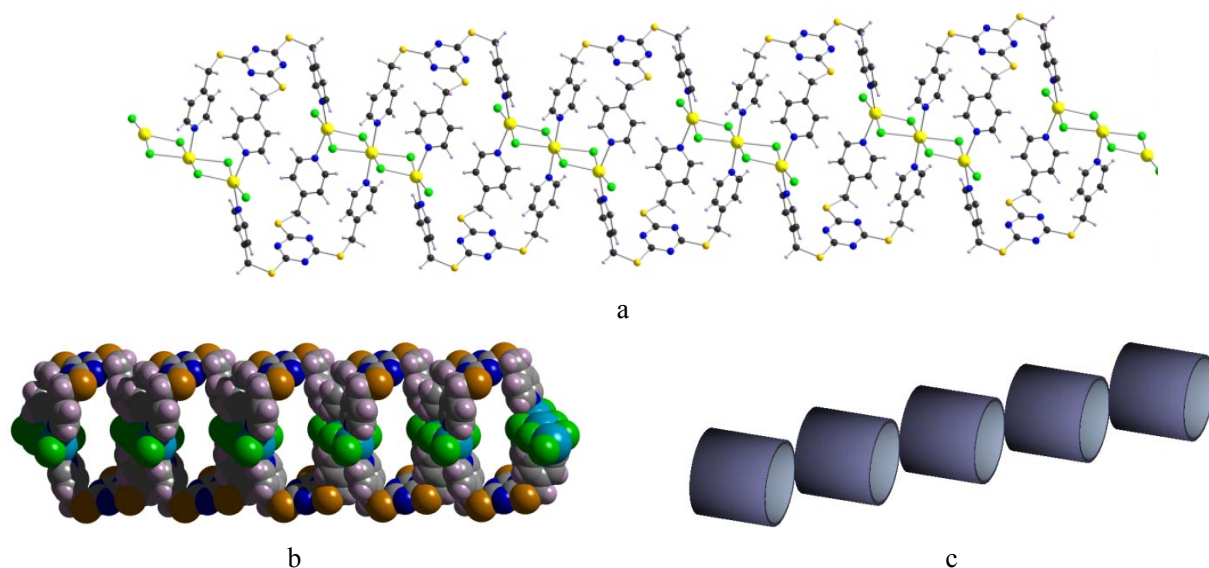


Figure 3-31: The crystal structure of $\mathbf{G1} \cdot \text{HgCl}_2$: a portion of 1-D nanosized metal-organic tubular chain in ball and stick mode (a) and space-filling mode (b), as well as its schematic representation (c).

Each tridentate tectons **G1** adopts a “Y” shape geometry, bridging two consecutive trinuclear clusters by a head-to-tail mode. As shown in Figure 3-31a, if two pyridine moieties of **G1** in one side (head) are coordinated to one central and one extreme Hg^{2+} cation, one pyridine unit in another side (tail) ring will coordinate to another extreme Hg^{2+} cation of the consecutive unit. As a result, the consecutive two coordination tubes are parallel but slipped (Figure 3-31c).

Along the axial direction of Hg^{2+} cation, the adjacent two metal-organic tubular chains are

stacked closely to form a 2-D plane through the π - π interactions between the 1,3,5-triazine rings with a distance of 3.34 Å, near the thickness value for normal aromatic system (*ca.* 3.4Å). The 2-D planes are stacked with concave-convex mosaic in the space without any specific interactions.

3.5. Conclusions

In this chapter, we have extended our investigations to semi-rigid naphthalene, spirobiindane and 1,3,5-triazine based tectons. The semi restriction of the conformational space of the organic tectons afforded only a transformed cuboid 3-D architecture based on SiF_6^{2-} pillars. ZnSiF_6 unit was generated *in-situ* from $\text{Zn}(\text{BF}_4)_2$. Owing to the different distortions and thus different lengths of organic tectons, the architecture is a four-component parallelepiped.

In the meantime, in order to give an explanation on the difficulty encountered during the crystallization processes engaging semi-rigid tectons and ZnSiF_6 , a series of 1-D and 2-D networks with novel topology and geometry have been generated using other metallatectons.

References

1. B. J. O'Keefe, P. J. Steel, *CrystEngComm*, **2007**, 9: 222–227.
2. S. Banfi, L. Carlucci, E. Caruso, G. Ciani, D. M. Proserpio, *J. Chem. Soc., Dalton Trans.*, **2002**, 2714–2721.
3. A. M. Kendhale, R. Gonnade, P. R. Rajamohanam, H. J. Hofmann, G. J. Sanjayan, *Chem. Commun.*, **2008**, 2541-2543.
4. B. F. Abrahams, D. J. Price, R. Robson, *Angew. Chem. Int. Ed.*, **2006**, 45: 806-810.
5. M. Hong, Y. Zhao, W. Su, R. Cao, M. Fujita, Z. Zhou, A. S. C. Chan, *J. Am. Chem. Soc.*, **2000**, 122: 4819-4820
6. D. B. Cordes, C. V. K. Sharma, R. D. Rogers, *Crystal Growth & Design*, **2007**, 7: 1943-1945.
7. H. Casellas, A. Pevec, B. Kozlevcar, P. Gamez, J. Reedijk, *Polyhedron*, **2005**, 24: 1549-1554.
8. C. H. Springsteen, R. D. Sweeder, R. L. LaDuca, *Crystal Growth & Design*, **2006**, 6: 2308-2314.
9. C. Piguet, G. Bernardinelli, G. Hopfgartner, *Chem. Rev.*, **1997**, 97: 2005-2062.
10. M. Albrecht, *Chem. Rev.*, **2001**, 101: 3457-3498.
11. L. Han, M. Hong, *Inorg. Chem. Commun.*, **2005**, 8: 406-419.
12. D. Bradshaw, J. B. Claridge, E. J. Cussen, T. J. Prior, M. J. Rosseinsky, *Acc. Chem. Res.*, **2005**, 38: 273-282.
13. Y. Cui, S. J. Lee, W. B. Lin, *J. Am. Chem. Soc.*, **2003**, 125: 6014-6015.
14. J. Heo, Y.-M. Jeon, C. A. Mirkin, *J. Am. Chem. Soc.*, **2007**, 129: 7712-7713.
15. C. D. Wu, W. Lin, *Angew. Chem. Int. Ed.*, **2005**, 44: 1958-1961.

16. P. Grosshans, A. Jouaiti, V. Bulach, J.M. Planeix, M. W. Hosseini, J.F. Nicoud, *Chem. Commun.*, **2003**, 1336-1337.
17. W. Jaunky, M. W. Hosseini, J.-M. Planeix, A. De Cian, N. Kyritsakas, J. Fischer, *Chem. Commun.*, **1999**, 2313-2314.
18. G. O. Lloyd, J. L. Atwood, L. J. Barbour, *Chem. Commun.*, **2005**, 1845-1847.
19. X. Li, B.-L. Wu, W. Liu, H.-Y. Zhang, *Inorg. Chem. Commun.*, **2008**, 11, 1308-1311.
20. Y. Hu, G. Li, X. Liu, B. Hu, M. Bi, Lu Gao, Z. Shi, S. Feng, *CrystEngComm*, **2008**, 10, 888-893.
21. D. R. Xiao, Y. G. Li, E. B. Wang, L. L. Fan, H. Y. An, Z. M. Su, L. Xu, *Inorg. Chem.*, **2007**, 46, 4158-4166.
22. C. Livage, N. Guillou, P. Rabu, P. Pattison, J. Marrot, G. Férey, *Chem. Commun.*, **2009**, 4551-4553.
23. J. Zhang, R. Liu, P. Feng, X. Bu, *Angew. Chem. Int. Ed.*, **2007**, 46, 8388-8391.
24. D. Moon, S. Kang, J. Park, K. Lee, R. P. John, H. Won, G. H. Seong, Y. S. Kim, G. H. Kim, H. Rhee, M. S. Lah, *J. Am. Chem. Soc.*, **2006**, 128, 3530-3531
25. J. Park, S. Hong, D. Moon, M. Park, K. Lee, S. Kang, Y. Zou, R. P. John, G. H. Kim, M. S. Lah, *Inorg. Chem.*, **2007**, 46, 10208-10213.

**CHAPTER IV : DESIGN AND STUDY OF THE
COORDINATION NETWORKS BASED ON FLEXIBLE
ORGANIC TECTONS AND ZINC
HEXAFLUOROSILICATE PILLARS**

Chapter IV: Design and Study of the Coordination Networks Based on Flexible Organic Tectons and ZnSiF_6 Pillars

This chapter is dedicated to the combination of flexible organic tectons T2 with ZnSiF_6 infinite tecton T1. In order to control the size and the shape of the networks, a series of flexible organic tectons of different length with different cores bearing two pyridines oriented in a divergent fashion were designed, prepared and studied.

4.1. Introduction

In Chapter II, we have shown that ZnSiF_6 could be regarded as an infinite inorganic tecton (Figure 3-1a) offering in a regular fashion (every *ca.* 7.5 Å) square planar tetratopic coordination nodes along the pillar. In this Chapter, we will extend this concept to flexible tectons T2. Indeed, by exploiting the flexibility of the organic tecton, either 1-D (Figure 3-1b) or 2-D (Figure 3-1c) architectures with inner cavities may be designed. There are many reports¹⁻⁵ on 1-D ringed coordination chains (Figure 4-1a) resulting from combinations of flexible organic tectons bearing two divergently oriented pyridines with metal cations such as Co^{2+} , Cu^{2+} and Zn^{2+} adopting octahedral coordination geometry. In this chapter, we will use the infinite ZnSiF_6 pillar to interconnect ringed chain or coordination cages into a “flat” cable-like tubular plane (Figure 4-1b).

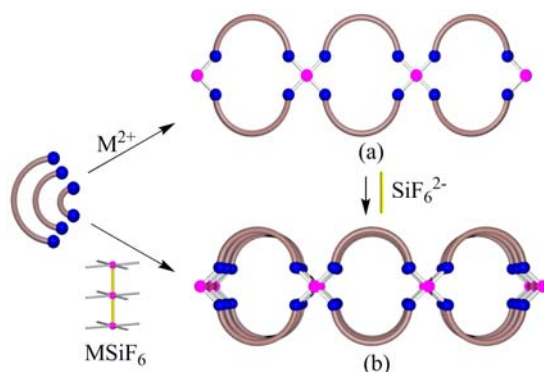


Figure 4-1: Schematic representation of formation of a tubular plane or caged chain from flexible tectons and ZnSiF_6 .

Depending on the nature of flexible tectons T2 (core and denticity), this chapter will be subdivided into five parts based on five series tectons, as described below.

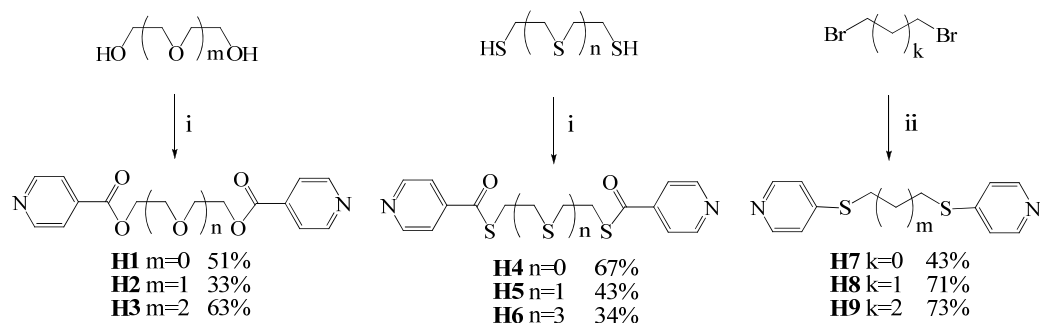
4.2. Construction and modulation of tubular 2-D coordination networks

4.2.1. Design and synthesis of the flexible organic tectons T2

Dealing with the flexible core, oligoethylene glycol and oligoethylene thioglycols are good candidates because of their conformational flexibility and length controllability by the number of glycol (thioglycol) unit used. Thus, tectons **H1-H9** (Scheme 4-1) were designed and prepared. For these tectons, the coordinating site is a 4-pyridyl unit. Based on the nature of the junction between

the pyridyl unit and the spacer controlling the rigidity of the building block, tectons **H1-H9** may be divided into two classes A (ester) and B (ether).

Tectons **H1-H6** were prepared by treating glycols or thioglycols of different length with the hydrochloride salt of isonicotinoyl chloride in the presence of Et_3N at room temperature and in dry THF.⁸⁻⁹ Tectons **H7-H9** were obtained in high yield upon reacting 4-mercaptopyridine with α,ω -alkyl dihalides (ethyl for **H7**, propyl for **H8** and butyl for **H9**) in THF and in the presence of K_2CO_3 (see Experimental section).⁶



Scheme 4-1: Reaction conditions: (i) isonicotinoyl chloride, Et_3N , THF, room temperature, 48h; (ii) K_2CO_3 , 4-mercaptopyridine, THF under N_2 for 48h.

4.2.2. Structural studies of tubular 2-D coordination networks

The same methodology as the one used for build cuboid networks (Chapter II) was used here. In crystallization tubes, upon slow diffusion of an EtOH solution of $\text{ZnSiF}_6 \cdot 6\text{H}_2\text{O}$ into a CHCl_3 solution of tectons **H1-H9**, colorless crystalline materials were obtained after several days. However, only crystals containing **H4**, **H5**, **H7** and **H9** were found to be suitable for X-ray diffraction technique on single crystals. For other combinations, in spite of many attempts, crystals obtained were twinned.

The X-ray diffraction study revealed that all four crystals (**H4**· ZnSiF_6 , **H5**· ZnSiF_6 , **H7**· ZnSiF_6 and **H9**· ZnSiF_6) are composed of organic tecton, infinite inorganic tecton ZnSiF_6 and solvent molecules. Selected crystallographic parameters listed in Table 4-1.

Table 4-1: Selected crystallographic parameters for tubular 2-D coordination networks

Compound	Chemical formula	Crystal system	Space group	a(Å)	b(Å)	c(Å)	α (deg)	β (deg)	γ (deg)
H4 · ZnSiF_6	$[\text{Zn}(\text{H4})_2\text{SiF}_6] \cdot 2(\text{C}_2\text{H}_6\text{O}) \cdot \text{CHCl}_3$	monoclinic	<i>C2/c</i>	22.512	14.527	15.235	90	112.227	90
H5 · ZnSiF_6	$[\text{Zn}(\text{H5})_2\text{SiF}_6]_2(\text{SQUEEZE})$	Triclinic	<i>P-1</i>	13.180	15.835	28.830	99.98	94.883	106.023
H7 · ZnSiF_6	$[\text{Zn}(\text{H7})_2\text{SiF}_6] \cdot \text{CHCl}_3$	monoclinic	<i>C2/c</i>	21.687	7.621	24.163	90	114.128	90
H9 · ZnSiF_6	$[\text{Zn}(\text{H9})_2\text{SiF}_6] (\text{SQUEEZE})$	monoclinic	<i>C2/c</i>	21.649	7.708	28.670	90	111.545	90

As expected from the design principle mentioned above, the combination of the flexible organic tectons (**H4**, **H5**, **H7** or **H9**) with an infinite inorganic tecton ZnSiF_6 leads to the formation of neutral flat cable-like 2-D tubular planes (Figure 4-2). In all four cases, the combination of Zn^{2+}

with SiF_6^{2-} leads to the formation of a 1-D network resulting from the bridging of Zn^{2+} cations by the SiF_6^{2-} anions through Zn-F bonds ($d_{\text{Zn-F}}$ in the range of 2.08 - 2.18 Å, details listed in Table 4-2). For the SiF_6^{2-} moiety, the Si-F bond distances for the F atoms located at the square base of the octahedron in the range of 1.65 - 1.68 Å is shorter than those for the F atoms occupying the apical positions ($d_{\text{Si-F}}$ in the range of *ca* 1.71 - 1.74 Å). The zinc cation adopts also the Oh geometry with its coordination sphere composed of two F and four N atoms. The two F atoms are located at the apical positions and the remaining four sites in the equatorial plane are occupied by four pyridine units belonging to four different organic tecton ($d_{\text{Zn-N}}$ in the range of *ca* 2.11 - 2.18 Å). Whereas in the case of **H4** (Figure 4-2a) and **H5** (Figure 4-2b), a puckered rod is obtained (FZnF angle of 180° but ZnFSi angle of 174.5° and 171.4° respectively), for the other two structures based on **H7** (Figure 4-2c) and **H9** (Figure 4-2d), the formation of linear pillars is observed (both FZnF and ZnFSi angle of 180°). Within the 1-D networks, the distance between consecutive Zn^{2+} cations varies between *ca* 7.52 and 7.71 Å (Table 4-3).

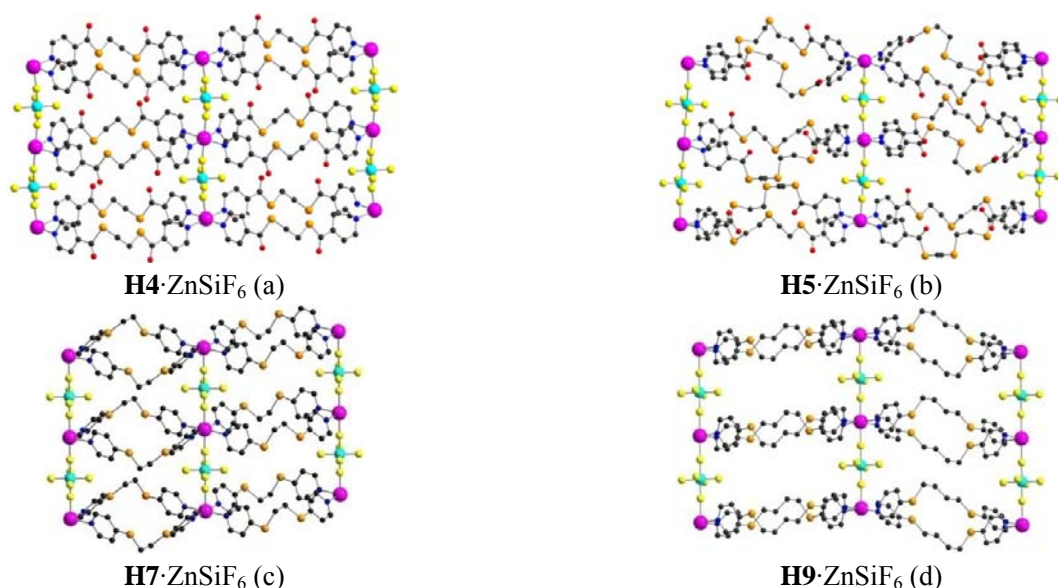


Figure 4-2: Portions of X-ray structures of the metallacrown 2-D tubular planes **H4**·ZnSiF₆ (a), **H5**·ZnSiF₆ (b), **H7**·ZnSiF₆ (c) and **H9**·ZnSiF₆ (d). H atoms are omitted for the clarity.

Table 4-2: Selected bonds and angles for tubular 2-D coordination networks

Compound	Zn-F(SiF_6^{2-}) distances/Å	Zn-N distances/Å	Si-F (unbound) distances/Å	Si-F (bridge) distances/Å	N-Zn-N angles/°	F-Zn-F angles/°
H4 ·ZnSiF ₆	2.082	2.137, 2.165	1.655	1.737	90.69	180
H5 ·ZnSiF ₆	2.097-2.150	2.154, 2.179	1.660-1.668	1.713-1.722	89.57	180
H7 ·ZnSiF ₆	2.078-2.092	2.107-2.182	1.660, 1.665	1.723, 1.728	91.10	180
H9 ·ZnSiF ₆	2.119, 2.138	2.114, 2.157	1.659, 1.678	1.724,	89.39	180

As expected from the design of tectons **H4**, **H5**, **H7** and **H9**, based on flexible spacers capable of adopting a curved conformation but not allowing biting on the same metal centre, the interconnection of consecutive pillars leads to the formation of 2-D tubular architectures

schematically presented in Figure 3-1c. Alternatively, the 2-D coordination networks may be described as catenated cationic [2+2] metallamacrocycles (2 Zn^{2+} cations and two ligands) forming a 1-D networks interconnected by SiF_6^{2-} anions. The size of the metallamacrocycles ([30]MC for **H4** and **H9**, [36]MC for **H5** and [26]MC for **H7**), reflected by the distance between the two endocyclic Zn^{2+} cations (14.53 Å, 16.50 Å, 12.09 Å and 14.51 Å for **H4**, **H5**, **H7** and **H9** respectively, Table 4-3), is controlled by the nature of the tectons adopting a *gauche* conformation (Figure 4-3). As the result of the design of the system, imposing the parallel arrangement of metallamacrocycles by the use of the square planar base of the octahedron around the Zn^{2+} cation, the channels are parallel to the pillars axis. The channels are filled by the solvent molecules (CHCl_3 for **H7**, CHCl_3 and EtOH for **H4**, **H5** and **H9**) without any specific interactions with the tubular channels. Whereas for structures engaging tectons **H4** and **H7**, the solvent molecules could be located, in the case of **H5** and **H9**, the solvent molecules were found to be disordered and could not be refined and the SQUEEZE command was used.

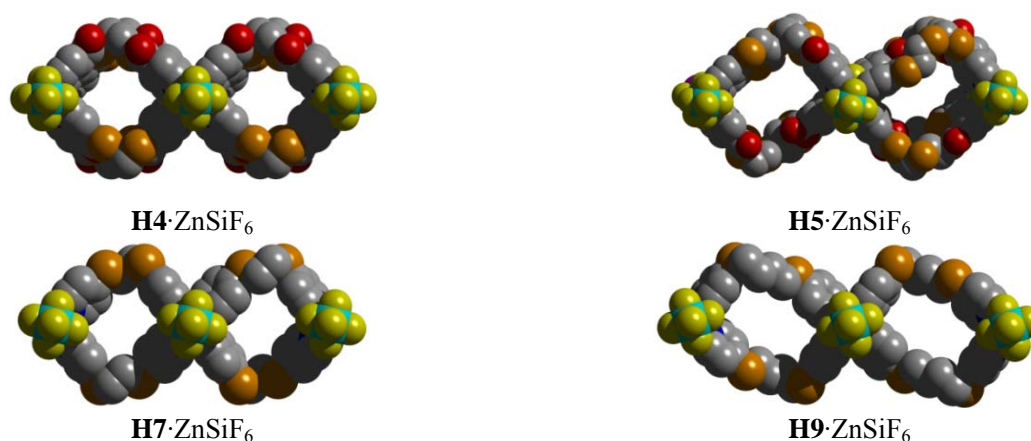


Figure 4-3: Portions of X-ray structures of the metallacrown 2-D tubular planes **H4**·ZnSiF₆, **H5**·ZnSiF₆, **H7**·ZnSiF₆ and **H9**·ZnSiF₆ showing the modulation of the size of the cuboid tubes by the lengths of the organic tectons.

Table 4-3: Comparison of parameters and porous data for tubular 2-D coordination networks

Compound	H4 ·ZnSiF ₆	H5 ·ZnSiF ₆	H7 ·ZnSiF ₆	H9 ·ZnSiF ₆
Distance between two consecutive ZnSiF ₆ pillars/Å	14.53	16.50	12.09	14.51
Side lengths of rectangle in cross sections /Å×Å	8.99×10.14	9.05×12.69	7.48×8.89	7.48×11.27
Distance between two consecutive Zn ²⁺ along pillar /Å	7.62	7.52	7.62	7.71
Distance between two consecutive plane centers/Å	10.42	11.40	9.90	9.99
Solvent accessible void volume/Å ³	1670.4	2181.3	1128.0	1626.9
Unit cell volume/ Å ³	4612.3	5640.6	3644.8	4450.1
Occupancy percents/%	36.2	38.7	30.9	36.6

For all four networks, the flat cable-like tubular planes are stacked through the *concave-convex* mosaic along the perpendicular direction of ZnSiF₆ pillars (Figure 4-4) with a distance between two

consecutive plane centers is *ca.* 10.41 Å, 11.40 Å, 9.90 Å and 9.99 Å for **H4**, **H5**, **H7** and **H9** respectively (Table 4-3). Along the direction of ZnSiF_6 pillars, for **H5**· ZnSiF_6 , the consecutive planes are slipped by *ca.* 2.53 Å which corresponds to *ca.* one third of the distance between two consecutive zinc atoms leading thus to a “ABC” packing (Figure 4-4e). As the consequence of the packing of the 2-D networks, the crystal presents only tubular channels along the pillars. However, for **H4**· ZnSiF_6 , **H7**· ZnSiF_6 and **H9**· ZnSiF_6 , the consecutive planes are slipped by *ca.* 3.82 Å which corresponds to *ca.* half of the distance between two consecutive zinc atoms resulting in a “ABA” packing (Figure 4-4 b and Figure 4-5b and d), which also results in tubular channels along the pillars.

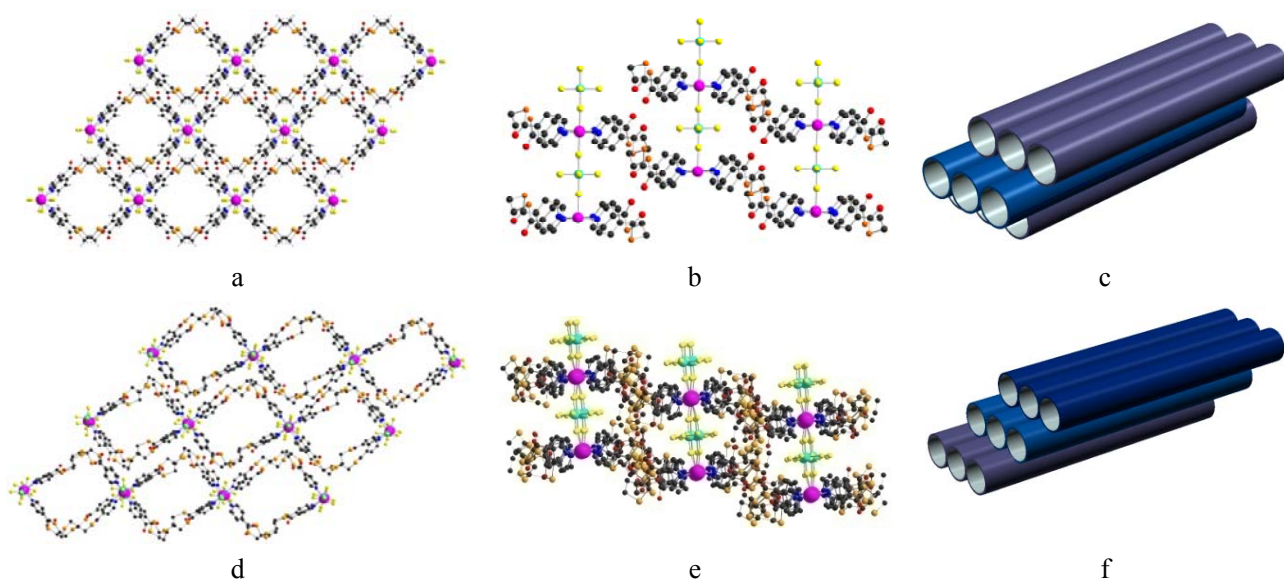


Figure 4-4: The packing of flat cable-like 2-D tubular networks for **H4**· ZnSiF_6 (a, b) and **H5**· ZnSiF_6 (d, e)) along the perpendicular direction and parallel direction of ZnSiF_6 pillars as well as their schematic representations (c, f)

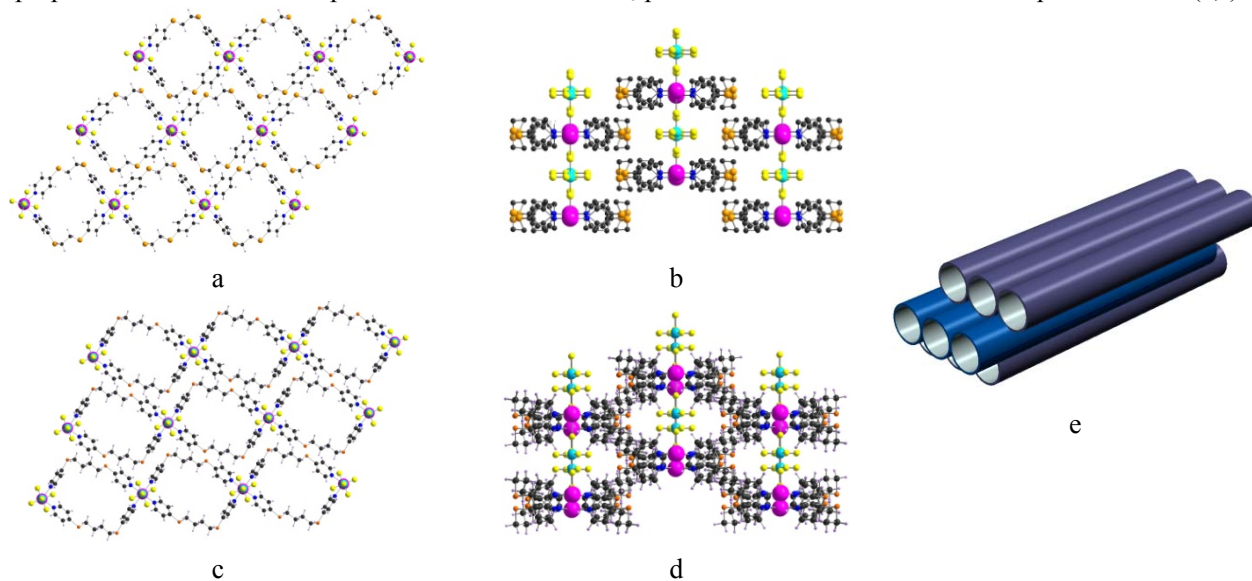


Figure 4-5: The packing of flat cable-like 2-D tubular networks obtained for **H7**· ZnSiF_6 (a, b) and **H9**· ZnSiF_6 (c, d)) along the perpendicular direction and parallel direction of ZnSiF_6 pillars as well as their schematic representations

4.2.3. Stability and thermal properties of tubular 2-D coordination networks

Owing to the difference in the length of the tectons, the four structures differ evidently by the side lengths of rectangle in the cross sections (about 8.99 x 10.14 Å for **H4**·ZnSiF₆, 9.05 x 12.69 Å for **H5**·ZnSiF₆, 7.48 x 8.89 Å for **H7**·ZnSiF₆, and 7.48 x 11.27 Å for **H9**·ZnSiF₆ respectively, Table 4-3) and the distance between consecutive zinc cations in cross sections (14.53 Å, 16.22 Å, 12.09 Å and 14.51 Å respectively). Consequently, by modulating the length of the organic moiety, the shape of the cuboid tubes as well as the size of their cavities can be tuned. The potential solvent accessible volume, calculated with the Platon software¹⁰, are 1670, 2181, 1128 and 1626 Å³, thus 36.2%, 38.7%, 30.9% and 36.6% of the total unit cell volume for **H4**·ZnSiF₆, **H5**·ZnSiF₆, **H7**·ZnSiF₆ and **H9**·ZnSiF₆ respectively. These values are significantly smaller than those of the cuboid 3-D networks obtained by same methods in Chapter II.

Among the four combinations, **H5**·ZnSiF₆ is rather unstable in air and upon removal of the solvent molecules they irreversibly collapse in a few seconds. The purity of the other three crystalline phases was established by PXRD (Figure 4-6) which revealed **H4**·ZnSiF₆, **H7**·ZnSiF₆, **H9**·ZnSiF₆ form pure phases, *i.e.* matching between observed and simulated diffraction patterns.

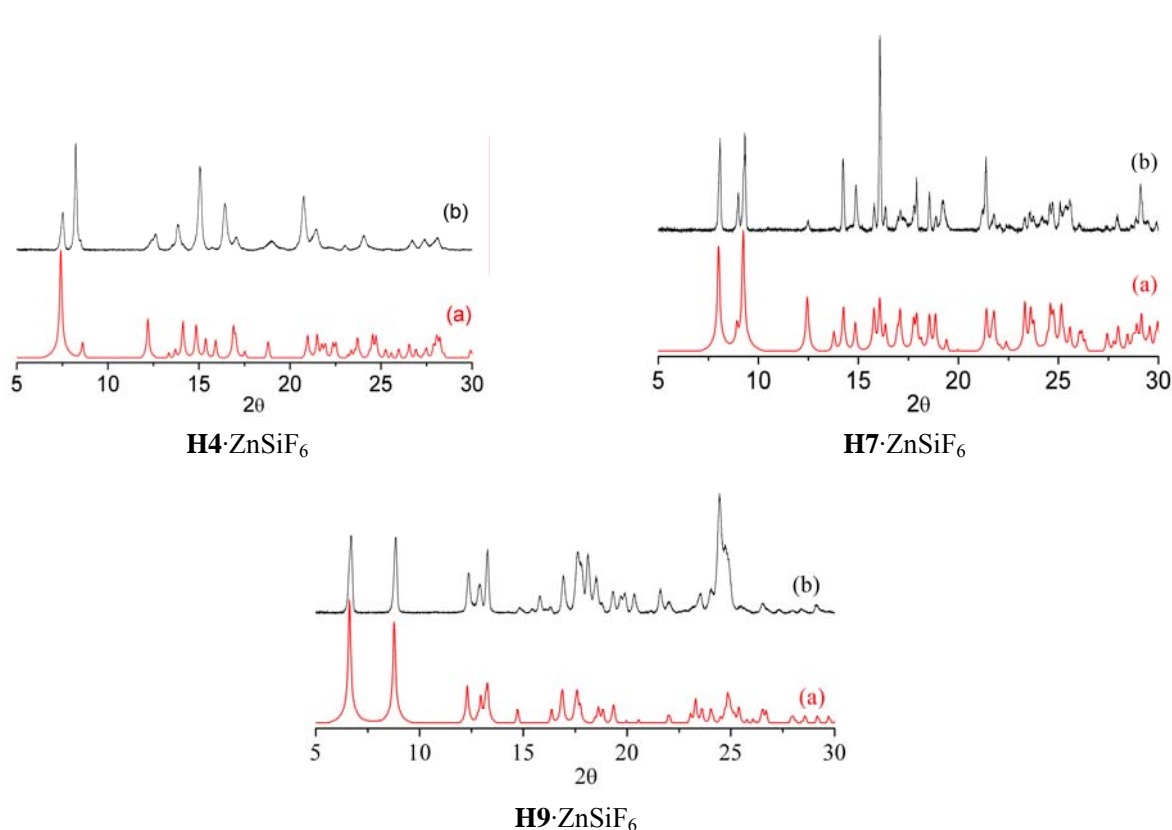


Figure 4-6 Comparison of the recorded (a) and simulated PXRD patterns (b) for **H4**·ZnSiF₆, **H7**·ZnSiF₆ and **H9**·ZnSiF₆.

The thermal stabilities of the air stable crystalline materials were investigated by TGA measurements (Figure 4-7) which revealed the loss of solvent molecules (alcohol and chloroform)

between 30 and 150 °C prior to decomposition of the samples, which appeared at *ca.* 180 °C for **H4**·ZnSiF₆ and 200 °C for **H7**·ZnSiF₆ and **H9**·ZnSiF₆.

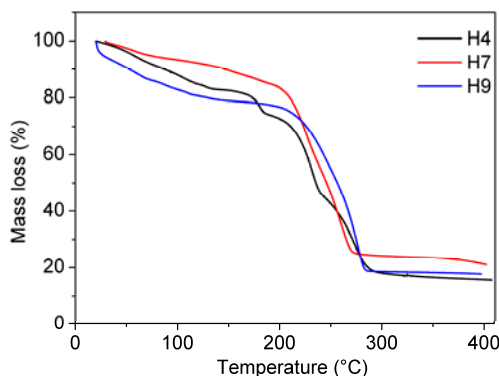


Figure 4-7 The TGA traces for the three air-stable networks **H4**·ZnSiF₆, **H7**·ZnSiF₆ and **H9**·ZnSiF₆ under N₂ with the speed of 5°C/min.

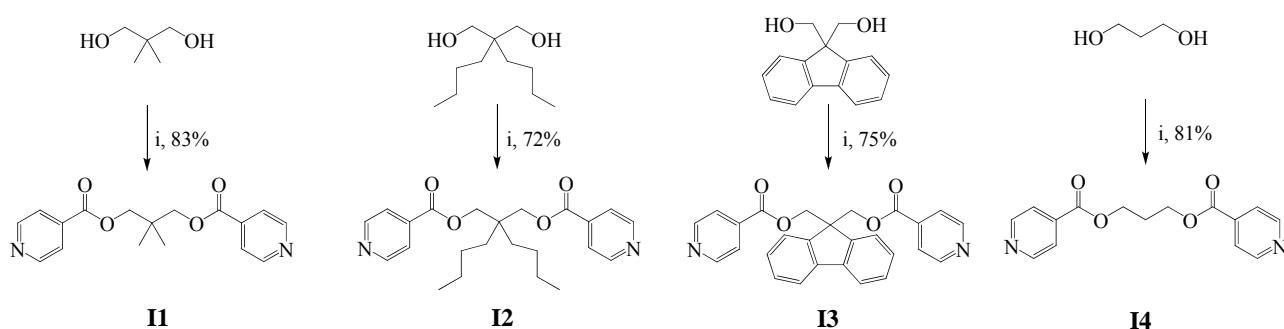
In conclusion, we have demonstrated that the combination of flexible bismonodentate organic tectons bearing two pyridines oriented in a divergent fashion with ZnSiF₆ units forming a single stranded pillar, leads, by design, to the formation of 2-D coordination networks based on the interconnection of zinc metallacrown of various size by SiF₆²⁻ groups. The packing of the sheets generates crystals offering only tubular channels oriented along the pillars axis. The shape as well as the size of the tubular channels may be modulated by the nature of the metallathiacrown ethers through the choice of the organic tectons. Extension to other functionalized flexible tectons will be discussed below.

4.3. Functionalization of tubular 2-D coordination networks

4.3.1. Design and Synthesis of functionalized flexible organic tectons T2

As stated above, owing to its serrate surface, the cable-like tubular 2-D coordination network **H4**·ZnSiF₆ is stacked with *concave-convex* mosaic and thus presents only tubular channels with imposed orientation along the pillars axis. Indeed, its serration may be truncated by incorporating substituent within the framework of the flexible organic tecton.

In order to functionalize the tectons, a core with tertiary carbon containing symmetrical substituents is required. Thus, tectons **I1-I3** with tertiary carbon as well as **I4** with primary carbon for comparison were designed and prepared (Scheme 4-2). For these tectons, the spacer is the 1,3-propanediol fragment and the coordinating site is a 4-pyridyl unit connected by an ester type junction. These compounds were prepared in high yield (75% - 90%) and large quantity by treating at room temperature and in dry THF, the corresponding diol with the hydrochloride salt of isonicotinoyl chloride in the presence of Et₃N (*see experimental parts*).



Scheme 4-2: Reaction conditions: (i) isonicotinoyl chloride, Et_3N , THF, room temperature, 48h

4.3.2. Structural studies of functionalized 2-D tubular coordination networks

Again, upon slow diffusion of an EtOH solution of $\text{ZnSiF}_6 \cdot 6\text{H}_2\text{O}$ into a CHCl_3 solution of the organic tecton (**I1-I4**), colorless crystalline materials were obtained in crystallization tubes after several days. Whereas for compounds **I4**, in spite of many attempts, the solid obtained was polycrystalline, for the other three combinations with **I1-I4** single crystals (**I2**· ZnSiF_6 , **I2**· ZnSiF_6 and **I3**· ZnSiF_6) were obtained and analyzed by X-ray diffraction technique on single crystals, which revealed that they are all composed of organic tecton, infinite inorganic tecton ZnSiF_6 and solvent molecules (Table 4-4).

Table 4-4: Selected crystallographic parameters for functionalized tubular 2-D coordination networks

Compound	Chemical formula	Crystal system	Space group	a(Å)	b(Å)	c(Å)	α (deg)	β (deg)	γ (deg)
I1 · ZnSiF_6	$[\text{Zn}(\mathbf{I1})_2\text{SiF}_6] \cdot 2(\text{CHCl}_3)$	Triclinic	<i>P</i> -1	7.60	12.17	16.12	108.16	97.99	102.01
I2 · ZnSiF_6	$[\text{Zn}(\mathbf{I2})_2\text{SiF}_6]$ (SQUEEZE)	Monoclinic	<i>P2</i> (1)/ <i>c</i>	15.37	34.56	12.63	90	104.565	90
I3 · ZnSiF_6	$[\text{Zn}(\mathbf{I3})_2\text{SiF}_6]$ (SQUEEZE)	Triclinic	<i>P</i> -1	7.64	12.72	18.49	81.70	80.949	76.46

As expected from the choice of the inorganic tecton (ZnSiF_6) and the design of the organic tectons **I1**, **I2** and **I3**, in all three cases structurally investigated the formation of 2-D tubular coordination networks with the bulky groups oriented towards outside (methyl for **I1**· ZnSiF_6 , *n*-butyl for **I2**· ZnSiF_6 , and 9H-fluorene for **I3**· ZnSiF_6 , Figure 4-8) is observed. Again, in all three cases, the combination of Zn^{2+} with SiF_6^{2-} leads to the formation of 1-D pillars resulting from the bridging of Zn^{2+} cations by the SiF_6^{2-} anions through Zn-F bonds ($d_{\text{Zn-F}}$ in the range of 2.09 - 2.15 Å, details listed in Table 4-5). Along the pillars, the zinc dications, which are coordinated by four pyridine units belonging to four different organic tectons in the equatorial plane *via* Zn-N bonds, are regularly distributed with a distance from *ca* 7.61 to 7.69 Å (Table 4-6).

Table 4-5: Selected bonds and angles for functionalized tubular 2-D coordination networks

Compound	Zn-F(SiF_6^{2-}) distances/Å	Zn-N distances/Å	Si-F (unbound) distances/Å	Si-F (bridge) distances/Å	N-Zn-N angles/ $^\circ$	F-Zn-F angles/ $^\circ$
I1 · ZnSiF_6	2.094	2.145, 2.169	1.660, 1.671	1.712	89.3	180
I2 · ZnSiF_6	2.124, 2.145	2.078, 2.108	1.644-1.685	1.724	88.1, 89.5	178.4
I3 · ZnSiF_6	2.105	2.144, 2.166	1.653, 1.660	1.719	89.7	180

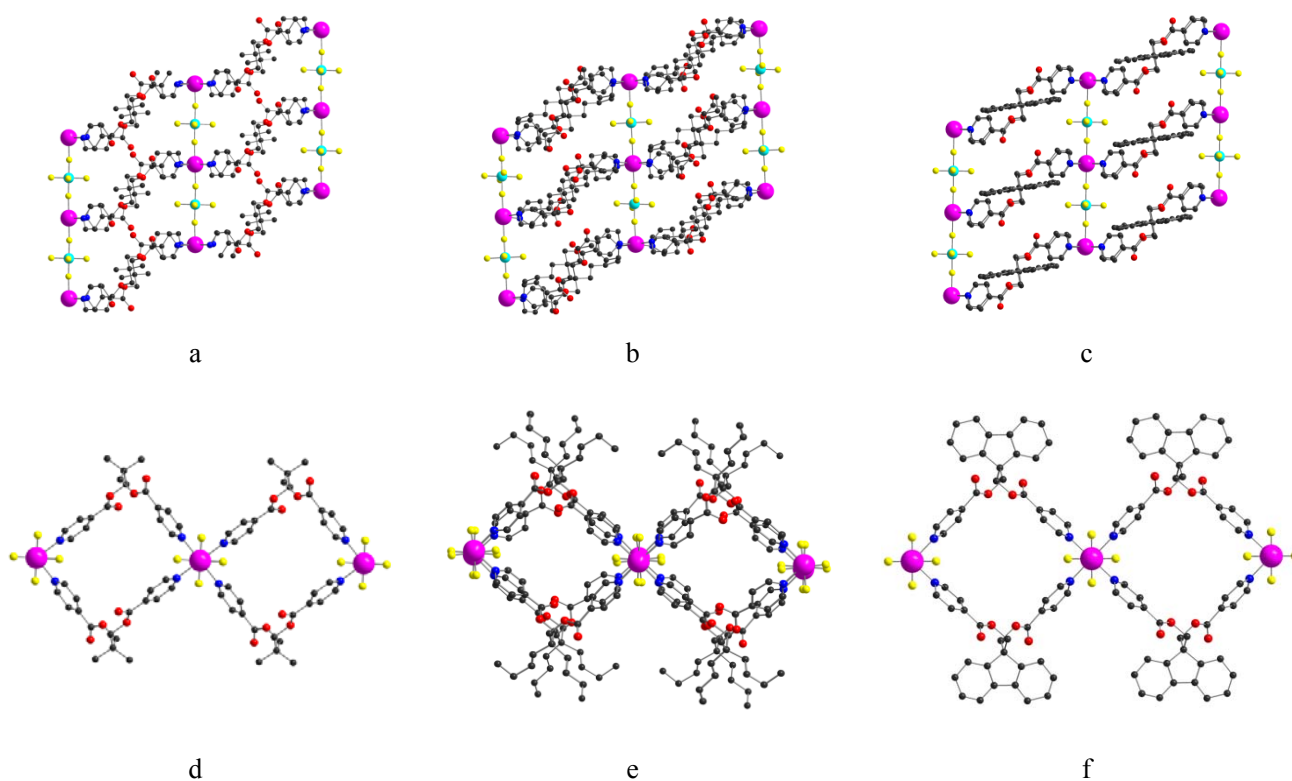


Figure 4-8: Portions of X-ray structures of the functionalized 2-D tubular coordination networks **I1**·ZnSiF₆ (a, d), **I2**·ZnSiF₆ (b, e) and **I3**·ZnSiF₆ (c, f) views perpendicular and parallel to the direction of ZnSiF₆ pillars. H atoms are omitted for the clarity.

However, owing to the presence of the tertiary carbon in the flexible chain, the organic tectons adopt an inclined pattern to interconnect the consecutive pillars (**Figure 4-9**). Alternatively, the consecutive pillars are slipped. Due to the restriction of the organic tecton length, the consecutive pillars are slipped by *ca* 3.82 Å, which corresponds to *ca* half of the distance between two consecutive zinc atoms (**Figure 4-8d, e and f**). In the three architectures, the outer functionalized groups spread around the tubes. The inclined interconnections are mainly attributed to the diamondoid shape of tertiary carbon in spacer.

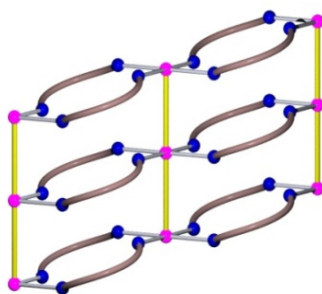


Figure 4-9 Schematic representation of a 2-D tubular architecture with inclining interconnection resulting from the combination of ZnSiF₆ with flexible organic tectons containing tertiary carbon **I1**, **I2** and **I3**.

Similarly, the 2-D coordination networks may also be described as [2+2] metallamacrocycles (2 Zn²⁺ cations and two ligands) forming a 1-D staircase-like networks interconnected by SiF₆²⁻ anions. The size of the metallamacrocycles ([32]MC) is reflected by the distance between the two

endocyclic Zn^{2+} cations which fluctuates between 11.53Å and 12.30Å (Table 4-6) and is controlled by the curvature of the tectons adopting a *gauche* conformation (Figure 4-3). As the result of the design of the system, imposing the parallel arrangement of metallamacrocycles by the use of the square planar base of the octahedron around the Zn^{2+} cation, the channels are parallel to the pillars axis. The channels are filled with solvent molecules (CHCl_3 for **I1**, CHCl_3 and EtOH for **I2** and **I3**) through H-bond interactions (C--H--F) between the solvents and the tubular channels. For structures engaging tectons **I2** and **I3**, the solvent molecules were found to be disordered and could not be refined and the SQUEEZE command was used for the refinement of structure.

Table 4-6: Comparison of parameters and porous data for functionalized tubular 2-D coordination networks

Compound	I1 ·ZnSiF ₆	I2 ·ZnSiF ₆	I3 ·ZnSiF ₆
Distance between two consecutive ZnSiF ₆ pillars/Å	11.91	11.53	12.30
Side lengths of rectangle in cross sections /Å×Å	7.26×9.20	7.75×8.15	8.59×8.81
Distance between two consecutive Zn ²⁺ along pillar /Å	7.61	7.69	7.65
Distance between two consecutive plane centers/Å	14.95	17.27	18.14
Solvent accessible void volume/Å ³	551.8	2185.6	733.1
Unit cell volume/ Å ³ [*]	1355.2	6499.7	1717.4
Occupancy percents/%	40.7	33.6	42.7

[*] Calculated with the Platon software¹⁰

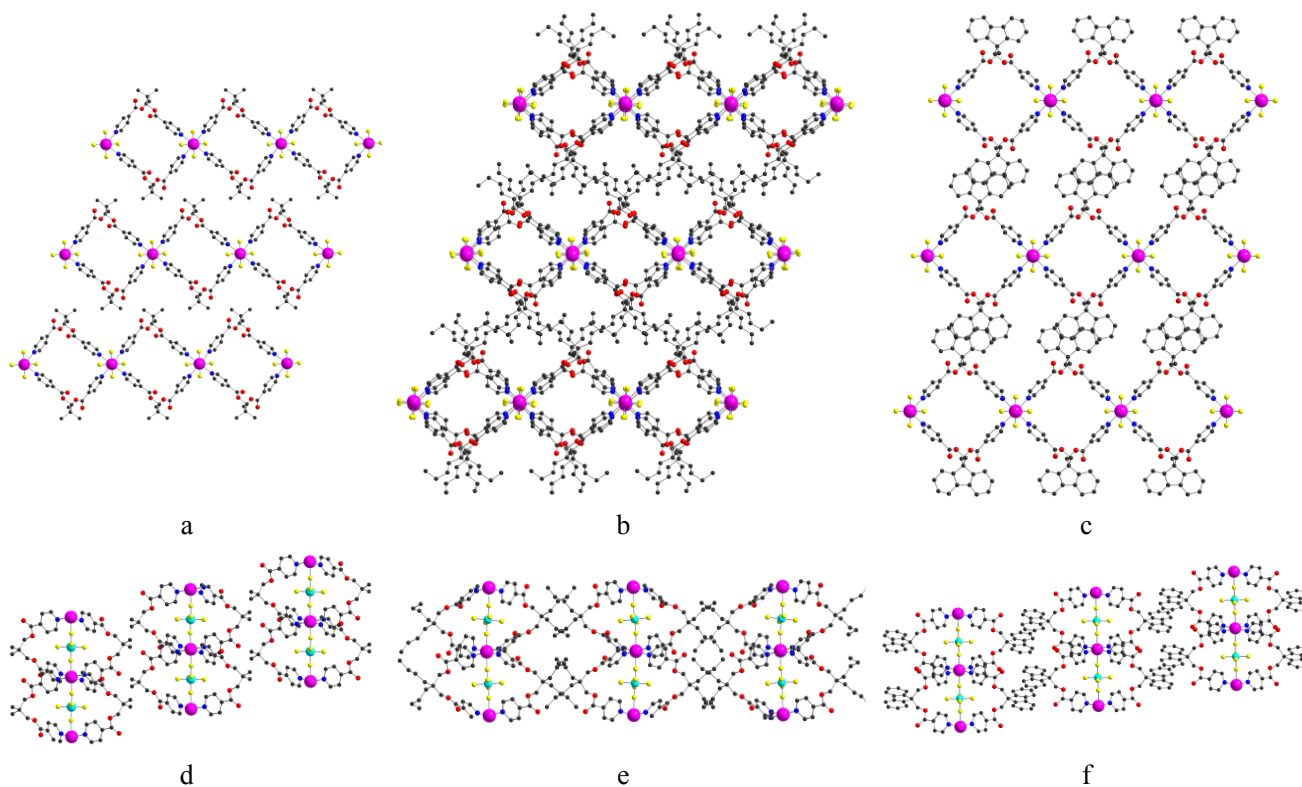


Figure 4-10: The packing of the functionalized 2-D tubular coordination networks **I1**·ZnSiF₆ (a, d), **I2**·ZnSiF₆ (b, e) and **I3**·ZnSiF₆ (c, f) views perpendicular and parallel to the direction of ZnSiF₆ pillars. H atoms are omitted for the clarity.

In the perpendicular direction to ZnSiF_6 pillars, for $\mathbf{I1}\cdot\text{ZnSiF}_6$ and $\mathbf{I2}\cdot\text{ZnSiF}_6$, although two consecutive tubular 2-D planes are slipped in order to position the *concaves* portion of one plane with respect to the *convex* area of the other (Figure 4-10a, b), they are inserted into one another distinctly for the introduction of the outer functionalized groups. For $\mathbf{I3}\cdot\text{ZnSiF}_6$, two neighboring planes are only slightly slipped with *ca.* 1/7 distance of two consecutive ZnSiF_6 in the plane ($12.4 \text{ \AA}/7 = 1.77 \text{ \AA}$) leading thus to π - π stacking of 9H-fluorene (3.88 \AA , Figure 4-10c). Distances between Zn cations in neighboring coordination networks are 14.95 \AA , 17.27 \AA and 18.14 \AA for the three networks respectively (Table 4-6). Herein, the different packing observed for $\mathbf{I3}\cdot\text{ZnSiF}_6$ with respect to the other two networks may be attributed to π - π interactions between 9H-fluorene units.

Along the direction of ZnSiF_6 pillars, for $\mathbf{I1}\cdot\text{ZnSiF}_6$ and $\mathbf{I3}\cdot\text{ZnSiF}_6$, the consecutive planes are slipped by *ca.* 3.82 \AA which corresponds to *ca.* half of the distance between two consecutive zinc atoms with a “ABA” mode of packing (Figure 4-10d, f). For the $\mathbf{I2}\cdot\text{ZnSiF}_6$, however, owing to the isolating role played by the extra alkyl groups, preventing the slippage, the consecutive planes are totally parallel (Figure 4-10e).

4.3.3. Stability of functionalized tubular 2-D coordination networks

Owing to the incompact packing of all three networks resulting from the presence of the outer functionalized groups, the potential solvent accessible volume, calculated using the Platon software¹⁰, are 551.8, 2185.6 and 733.1 \AA^3 , corresponding to 40.7%, 33.6% and 42.7% of the total unit cell volume for $\mathbf{I1}\cdot\text{ZnSiF}_6$, $\mathbf{I2}\cdot\text{ZnSiF}_6$ and $\mathbf{I3}\cdot\text{ZnSiF}_6$ respectively (Table 4-6). The relatively small void observed for $\mathbf{I2}\cdot\text{ZnSiF}_6$ is because the cavity generated by packing is filled by the large butyl substituents.

Introduction of groups at the periphery of the tecton leads to loose packing and consequently, the stability of these three compounds are rather poor in air and upon removal of the solvent molecules. Indeed, they irreversibly collapse in a few seconds. For that reason, we could not further study their thermal stabilities.

In conclusion, the combination of functionalized flexible organic tectons with an inorganic ZnSiF_6 pillar leads to the formation of functionalized 2-D coordination networks based on the inclined interconnection of ZnSiF_6 pillars by organic tecton T2. Extension to other functionalized (chiral) flexible tectons with infinite tecton ZnSiF_6 will be discussed below.

4.4. Design and Construction of helical 2-D tubular coordination networks

4.4.1. Design and synthesis of chiral flexible organic tectons T2

The formation of a helical 2-D network with the topology shown in Figure 4-11b have been demonstrated already in our laboratory upon combining a chiral flexible organic tecton ((1S,2S)-cyclohexane-1,2- diyldiisonicotinate) with $\text{Cu}(\text{NO}_3)_2$ by self-assembly process.⁸ Its helical pitch is *ca.* 9.0 \AA , slightly larger than the distance (*ca.* 7.6 \AA) between two consecutive Zn^{2+} cations

in the infinite ZnSiF_6 pillar. Considering the flexibility of the network imposed by the flexible tecton, we envisaged to interconnect this type of arrangement by ZnSiF_6 pillars into a rigid helical 2-D network (Figure 4-11c).

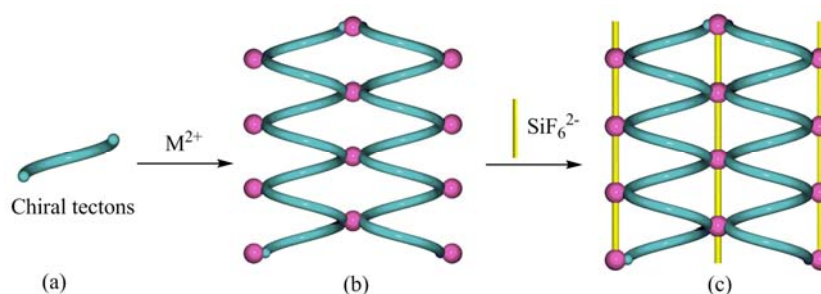
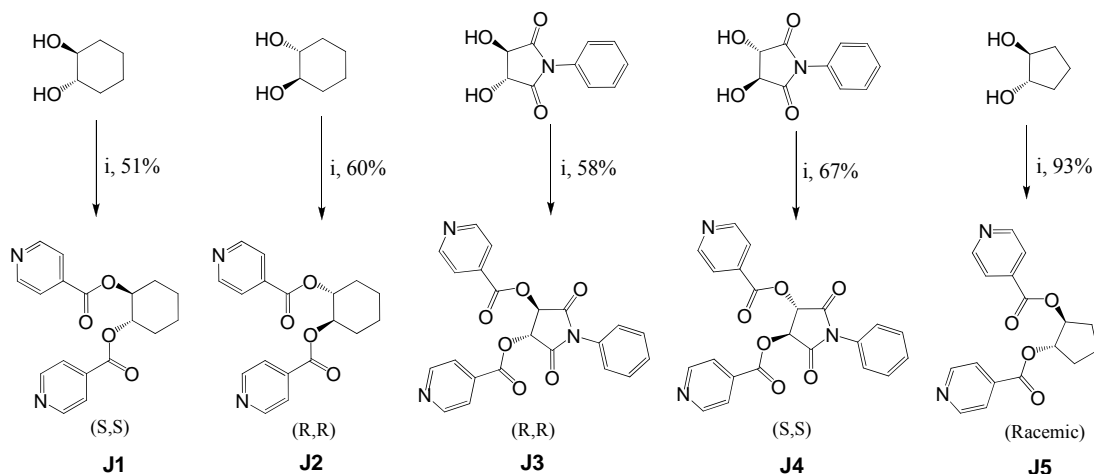


Figure 4-11: Schematic representation of the generation of a rigid helical 2-D network using a flexible tecton and ZnSiF_6 .

Dealing with the chiral core, both suitable chirality and pitch are required. Thus, tectons **J1-J4** presenting a similar core were designed and prepared (Scheme 4-3). For comparison, the racemic **J5** tecton was also prepared.



Scheme 4-3: Reaction conditions: (i) isonicotinoyl chloride, Et_3N , THF, room temperature, 48h

All tectons are obtained in high yields from the corresponding 1,2-diol derivatives and isonicotinoyl chloride hydrochloride salt at room temperature in dry THF and in the presence of Et_3N . The starting materials (3S,4S) or (3R,4R)-N-phenyl-3,4-dihydroxy-2,5-dioxopyrrolidine were prepared following reported procedures starting from the corresponding enantiomerically pure tartaric acid and aniline using Dean-Stark elimination of water (the reaction was completed when the theoretical amount of water was collected)¹¹. The (1S,2S), (1R,2R)-cyclohexane-1,2-diol and trans-cyclopentane-1,2-diol are commercially available (see experimental parts).

4.4.2. Structural studies of helical 2-D tubular coordination networks

Upon slow diffusing the EtOH solution of ZnSiF_6 (5 mg) into a CHCl_3 solution (1 mL) for **J1-J2** and **J4-J5** (3 mg) or $\text{CH}_2\text{ClCH}_2\text{Cl}$ solution (1 mL) for **J3** (3 mg) with a layer of DMSO (ca.

0.1 mL) respectively at room temperature, colorless crystalline materials were obtained in the crystallization tubes. Combinations based on the first four enantiomerically pure tectons **J1-J4** gave single crystals which were studied by X-ray diffraction on single crystal. Crystals obtained for the combination based on the racemic tecton **J5** were twinned and no satisfied diffraction data could be collected.

As expected from the design principle, owing to the nature of the up and down coordination sites in chiral tectons, the X-ray diffraction study revealed that the combinations of tectons **J1-J4**, crystals based on **J1** and **J2** (crystal system *orthorhombic* and space group *C222(1)* and on **J3** and **J4** (*monoclinic* and *C2*) (details listed in Table 4-7) contain tubular 2-D coordination networks with enantiomerically pure P or M helical walls (Figure 4-12). The handedness of tubular walls is originated from the chirality of the organic tectons, and thus the crystals based on **J1** and **J3** are P helical while the other two are of M handedness. From their crystallographic parameters, **J1**·ZnSiF₆ and **J2**·ZnSiF₆ are identified as perfect isostructures. However, for **J3**·ZnSiF₆ and **J4**·ZnSiF₆, owing to different crystallization condition, they appeared not to be isostructural. An attempt to crystallize both enantiomers under the same condition is in progress.

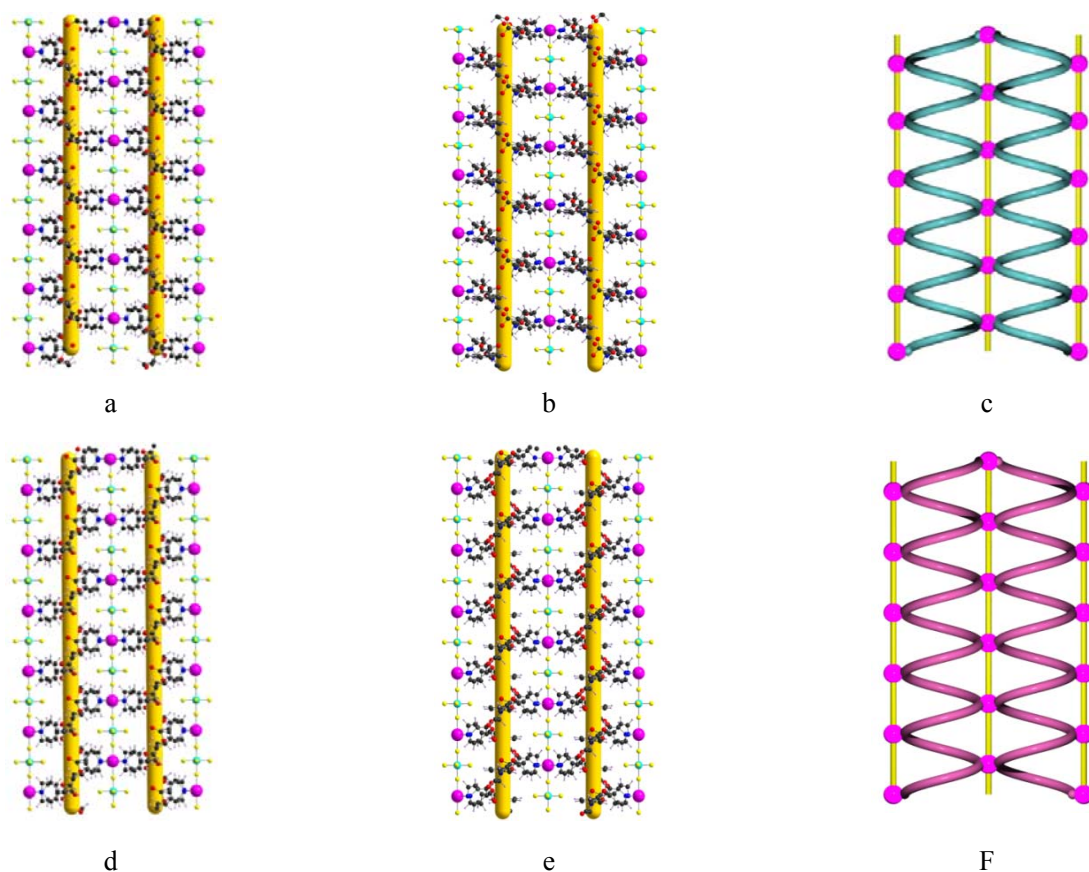


Figure 4-12 Portions of X-ray structures of the 2-D helically tubular coordination networks **J1**·ZnSiF₆ (a), **J2**·ZnSiF₆ (d), **J3**·ZnSiF₆ (b) and **J4**·ZnSiF₆ (e) views perpendicular to the direction of ZnSiF₆ pillars and their schematic representation with P and M helices (c, f). For clarity, in a, b, d and e, a yellow cylinder was added at the center of each tube.

Table 4-7: Selected crystallographic parameters for helically tubular 2-D coordination networks

Compound	Chemical formula	Crystal system	Space group	a(Å)	b(Å)	c(Å)	α (deg)	β (deg)	γ (deg)
J1 ·ZnSiF ₆	[Zn(J1) ₂ SiF ₆] ₂ ·2(CH ₃ OH)	Orthorhombic	C222(1)	7.669	21.030	28.373	90	90	90
J2 ·ZnSiF ₆	Zn(J2) ₂ SiF ₆ (SQUEEZE)	Orthorhombic	C222(1)	7.673	21.001	28.370	90	90	90
J3 ·ZnSiF ₆	[Zn(J3) ₂ SiF ₆] ₂ ·5(C ₂ H ₅ OH)·H ₂ O	Monoclinic	C2	24.063	7.631	16.339	90	99.928	90
J4 ·ZnSiF ₆	Zn(J4) ₂ SiF ₆ (SQUEEZE)	Monoclinic	C2	23.387	7.625	16.571	90	100.07	90

In all four cases, the consecutive Zn²⁺ cations are bridged by the SiF₆²⁻ anions through Zn-F bonds ($d_{\text{Zn-F}}$ in the range of 2.05 - 2.13 Å, Table 4-8) to form a 1-D pillars. For the SiF₆²⁻ moieties, the Si-F bond distances for the unbounded F atoms are in the range of 1.65 - 1.69 Å which is shorter than those for the bounded F atoms ($d_{\text{Si-F}}$ in the range of *ca* 1.71 - 1.74 Å). The zinc cation adopts an octahedral geometry with its coordination sphere composed of two apically positioned F atoms and four N atoms in the equatorial plane with a Zn-N bond ($d_{\text{Zn-N}}$ in the range of *ca* 2.13 - 2.17 Å). In all four cases, the formation of linear pillars is observed (FZnF angle of nearly 180°) and the distance between consecutive Zn²⁺ cations varies between *ca.* 7.63 and 7.67 Å within the 1-D networks (Table 4-9). The pitch of the four helical architectures is in the 7.63-7.67 Å range, considerably smaller than that of the non-pillared analogues (9.0 Å) obtained by combining the tecton **J1** and Cu(NO₃)₂.⁸

Table 4-8: Selected bonds and angles for 2-D helically tubular coordination networks

Compound	Zn-F(SiF ₆ ²⁻) distances/Å	Zn-N distances/Å	Si-F (unbound) distances/Å	Si-F (bridge) distances/Å	N-Zn-N angles/°	F-Zn-F angles/°
J1 ·ZnSiF ₆	2.09	2.14/2.16	1.66-1.68	1.74	89.1/90.6	177.0
J2 ·ZnSiF ₆	2.09	2.16/2.14	1.65-1.69	1.74	89.6	177.6
J3 ·ZnSiF ₆	2.07/2.13	2.13/2.15	1.65-1.67	1.71	89.5-90.5	179.4
J4 ·ZnSiF ₆	2.05-2.12	2.13-2.17	1.65-1.66	1.72-1.74	89.4-90.6	180.0

Based on flexible spacers capable of adopting a curved conformation but not allowing biting on the same metal centre, the interconnection of consecutive pillars leads to the formation of 2-D rectangular tubular architectures (Figure 4-13). As for tectons **I1-I3**, the tectons **J1-J4** adopt an inclined pattern to interconnect consecutive pillars. But owing to the enantiomerically pure nature of the tecton, four tectons around each tectons (up and down spread to four directions) are formed 2-D flat cable like molecular planes with helical tubes of the same chirality. Due to the shorter length of the organic tecton, the consecutive pillars are slipped by 3.82 Å, which corresponds to *ca* half of the distance between two consecutive zinc atoms (Figure 4-12).

Alternatively, the 2-D coordination networks may be described as single-stranded helically rectangular tubes interconnected by ZnSiF₆ pillars. The tube type channels are filled with solvent molecules (Table 4-7). For structures engaging tectons **J2** and **J4**, the solvent molecules were found to be disordered and could not be refined and thus SQUEEZE command was used for the

refinement of structure. The size of the helical tubes is reflected by the distance between the two consecutive ZnSiF_6 pillars which is 10.51 Å, 10.50 Å, 12.03 Å and 11.69 Å for tectons **J1**-**J4** respectively (Table 4-9). The slightly difference between **J3**· ZnSiF_6 and **J4**· ZnSiF_6 may be due to their different crystallization conditions and thus inclusion of different solvents, but this difference will be further investigated. Indeed, attempts to crystallize them under similar conditions are in progress.

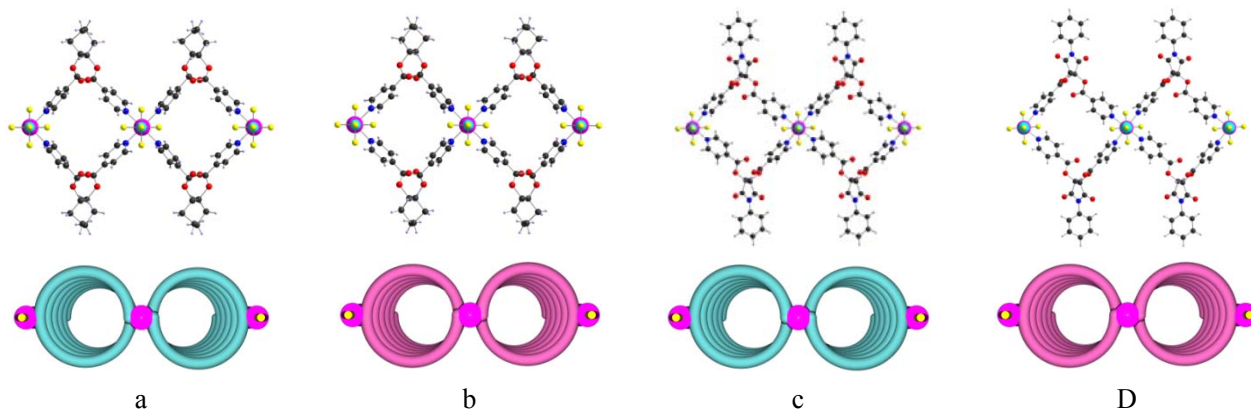


Figure 4-13 Portions of X-ray structures of the 2-D helically tubular coordination networks viewed along the direction of ZnSiF_6 pillars and their schematic representations: **J1**· ZnSiF_6 (a), **J2**· ZnSiF_6 (b), **J3**· ZnSiF_6 (c) and **J4**· ZnSiF_6 (d).

Table 4-9: Comparison of parameters and porous data for tubular 2-D coordination networks

Compound	J1 · ZnSiF_6	J2 · ZnSiF_6	J3 · ZnSiF_6	J4 · ZnSiF_6
Distance between two consecutive ZnSiF_6 pillars/Å	10.51	10.50	12.03	11.69
Distance between two consecutive Zn^{2+} along pillar /Å	7.670	7.673	7.632	7.625
Distance between two consecutive plane centers/Å	14.19	14.19	16.09	16.32
Solvent accessible void volume/Å ³	958.3	962.5	1021.6	990.7
Unit cell volume/ Å ³	4576.5	4571.6	2955.4	2909.3
Occupancy percents/%	20.9	21.1	34.6	34.1

With respect to the packing, for both isomers **J1**· ZnSiF_6 and **J2**· ZnSiF_6 , the neighboring two helical planes are stacked into the closest packing through the *concave-convex* mosaic (Figure 4-14a-b) along the perpendicular direction to ZnSiF_6 pillars. But for **J3**· ZnSiF_6 and **J4**· ZnSiF_6 , although the same *concave* and *convex* mosaic is obtained, they are only slightly slipped with *ca.* 1/4 distance (*ca.* 3 Å) of two consecutive ZnSiF_6 pillars in the same plane (Figure 4-14e). Because **J1**· ZnSiF_6 and **J2**· ZnSiF_6 form perfect isostructures, the distance between the centers of consecutive helical planes is the same (14.19 Å and 14.19 Å respectively). Whereas those of **J3**· ZnSiF_6 and **J4**· ZnSiF_6 (16.09 Å and 16.32 Å respectively) are different due to their different crystallographic parameters.

Along the direction of ZnSiF_6 pillars, for all four networks, the consecutive planes are inserted through the *concave-convex* mosaic at the corner of helical chains (Figure 4-14 c and d) and they

are not slipped, which is different from the packing of **H1**·ZnSiF₆ and **I1**·ZnSiF₆. In addition, in all four cases, the crystal presents only tubular channels with helical walls along the pillars.

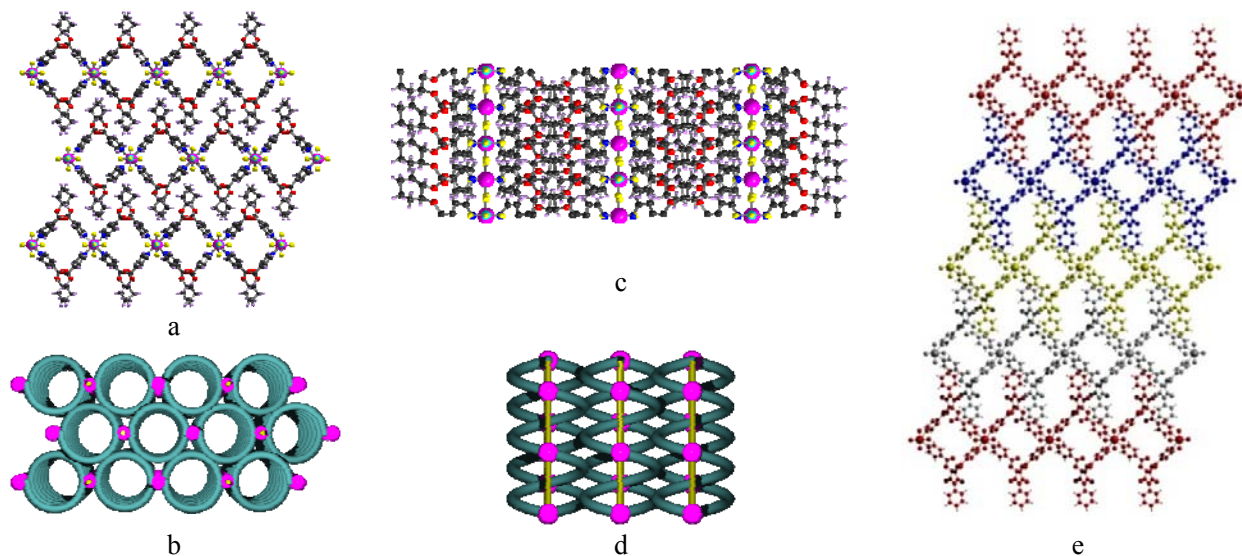


Figure 4-14 The packing of the 2-D helically tubular coordination networks **J1**·ZnSiF₆ (a, c), and **J3**·ZnSiF₆ (e) views perpendicular and parallel to the direction of ZnSiF₆ pillars and their schematic representations.

The bad quality for the crystals for the racemic tecton **J5** or the racemic mixture of tecton **J1** (50%) and **J2** (50%) may be attributed to the two possible organizations within the coordination networks or in the packing (Figure 4-15).

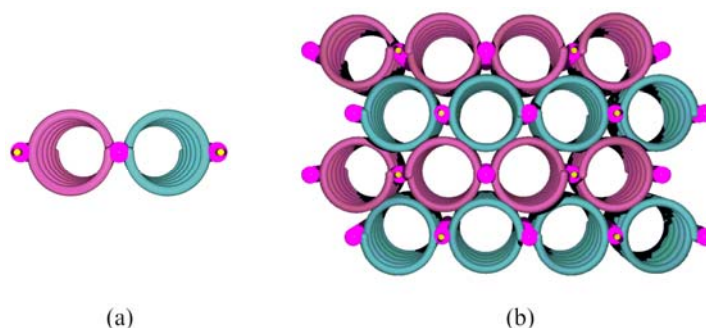


Figure 4-15: Schematic representation of the two possible 2-D tubular architectures composed of racemic P and M helices.

4.4.3. Stability and thermal properties of helical 2-D tubular coordination networks

The potential solvent accessible volume, calculated using the Platon software¹³, are 958.3 Å³, 962.5 Å³, 1021.6 Å³ and 990.7 Å³, corresponding to 20.9%, 21.1%, 34.6% and 34.1% of the total unit cell volume for **J1**·ZnSiF₆ (4576.5 Å³), **J2**·ZnSiF₆ (4571.6 Å³), **J3**·ZnSiF₆ (2955.4 Å³) and **J4**·ZnSiF₆ (2909.3 Å³) respectively (Table 4-9).

All four crystals are stable in air and thus their purity was controlled by X-ray diffraction on powder (Figure 4-16). The latter technique revealed that all four crystalline materials are pure phases, *i.e.* matching between observed and simulated peaks. As expected, for the first couple of isomeric networks **J1**·ZnSiF₆ and **J2**·ZnSiF₆, owing to their identical metrics, their recorded and

simulated PXRD patterns are the same. However, for the second couple (**J3**·ZnSiF₆ and **J4**·ZnSiF₆), their recorded PXRD are slightly different because of their slightly different crystallographic parameters. This again will be investigated upon crystallization of both enantiomers under identical conditions. Work towards this goal is currently under progress.

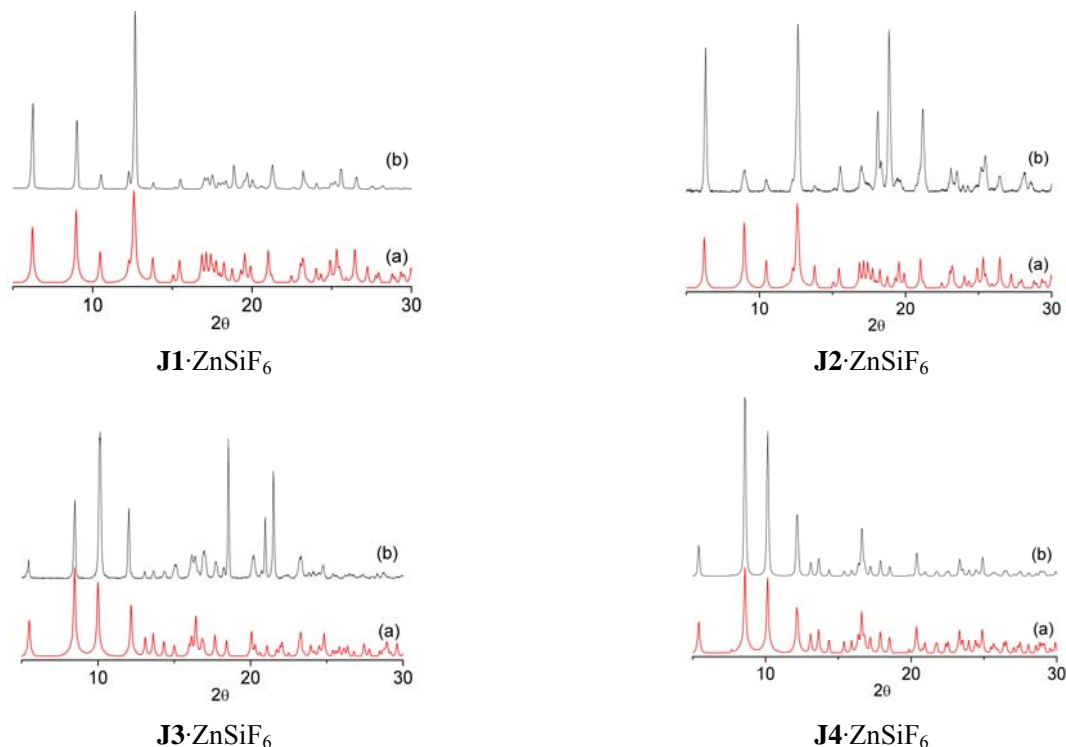


Figure 4-16: Comparison of the simulated (a) and recorded PXRD patterns (b) for helically tubular 2-D networks.

For these four crystals, they are all rather stable in air and their thermal stability under nitrogen atmosphere was investigated by TGA measurements (Figure 4-17) which revealed the loss of solvent molecules (alcohol, water and chloroform) between 80 and 120 °C prior to decompositions of the samples which appeared at *ca.* 180 °C for **J1**·ZnSiF₆ and **J2**·ZnSiF₆ and at 160 °C for **J3**·ZnSiF₆ and **J4**·ZnSiF₆. Owing to the disorder observed, the nature of the solvent molecules in **J2**·ZnSiF₆ and **J4**·ZnSiF₆ cannot be defined by X-crystal diffraction and the thermal analysis revealed that the solvent molecules can not be of high boiling point.

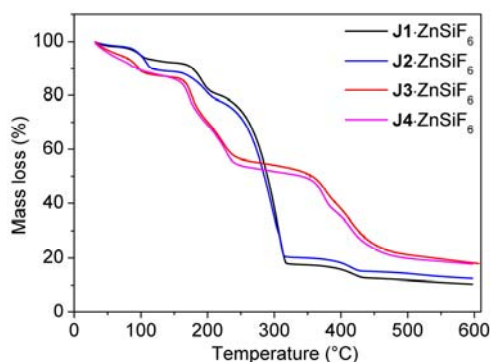


Figure 4-17: The TGA traces for two couples of isomeric helical networks under the N₂ with the speed of 5 °C/min.

In conclusion, the combination of chiral flexible tectons with an infinite tecton ZnSiF_6 lead to the formation of 2-D helically tubular coordination networks based on the chaining of single-stranded helices (enantiomerically P or M chirality) by ZnSiF_6 pillars. Extension to other shapes (*e.g.* nano-cages) obtained by chaining processes using the infinite tecton ZnSiF_6 will be discussed below.

4.5. From discrete molecular cages to the infinite caged chains

4.5.1. Design and synthesis of the flexible organic tectons (T2) of specific lengths

By controlling the length of organic tectons, the coordination cages bearing two tetrapotic coordination planes (Figure 4-18a) have been demonstrated⁶⁻⁷ upon combining the tectons with octahedral coordination metal cations (Co^{2+} , Cu^{2+} and Zn^{2+}) and capped Cl^- anions. In this work, we would like to chain such macrotetracyclic cages by SiF_6^{2-} anion through the combination of the organic tectons of suitable length with an infinite tecton ZnSiF_6 (Figure 4-18b).

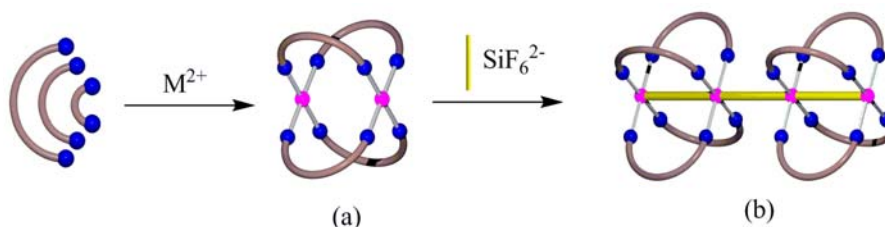
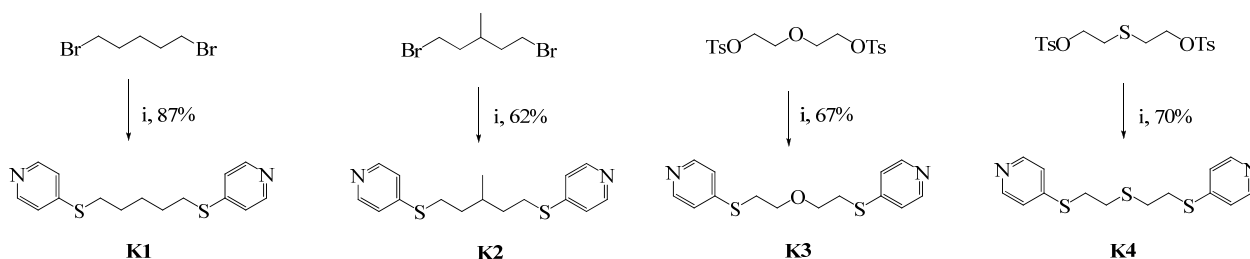


Figure 4-18: Schematic representation of the generation of a 1-D caged chain from a flexible tecton of suitable length and ZnSiF_6 .

As flexible organic tecton bearing two monodentate coordinating sites on each end, tectons **K1-K4** (Scheme 4-3) were designed and prepared. The choice of these tectons was motivated by the previous observation on the formation of a discrete binuclear coordination cage, $\{[\text{Zn}(\mathbf{K1})_2(\text{H}_2\text{O})_2](\text{ClO}_4)_2\}_2$ with a Zn-Zn distance of 8.1 Å,⁶ which should fit the predefined distance of *ca.* 7.6 Å between consecutive Zn^{2+} cations in the infinite ZnSiF_6 pillar. Tectons **K1-K4** differ only by the nature of the spacer connecting the two 4-thiapyridyl units. Whereas for tectons **K1** and **K2**, the spacer is a hydrocarbon chain, for the other two, the spacer is either $(\text{CH}_2)_2\text{-O-(CH}_2)_2$ or $(\text{CH}_2)_2\text{-S-(CH}_2)_2$ fragment. In all four cases, the junction between 4-thiapyridyl units is of the thioether type. The synthesis of **K1** had been previously reported⁶ and for the other three compounds, it was straightforward.



Scheme 4-4: Reaction conditions: (i) K_2CO_3 , 4-mercaptopyridine, THF under N_2 for 48h.

Following the published procedure⁶, tectons **K1-K2** were obtained upon reacting a THF solution of 4-mercaptopyridine with α,ω -alkyl dihalides (*n*-pentyl for **K1** and 3-methyl-pentyl for **K2**) in the presence of K_2CO_3 . Tectons **K3-K4** were prepared in 45% and 54% yields under same condition from 4-mercaptopyridine and the corresponding bis(4-methylbenzene- sulfonate) obtained from their diol and tosyl chloride in the presence of Et_3N (*see experimental parts*).

4.5.2. Structural studies of 1-D caged chain

In crystallization tubes, upon slow diffusion of an EtOH solution of $ZnSiF_6 \cdot 6H_2O$ (5 mg) into a $CHCl_3$ solution (1 mL) of tecton **K1-K4** (3 mg) with a buffered layer of DMSO (ca. 0.1 mL), colorless crystalline materials were obtained after several days. However, the quality of the crystals containing tectons **K2-K4** is quite poor and could not be improved in spite of many attempts. Thus, only the first combination is analyzed by X-ray diffraction technique on single crystals, which revealed that the crystal is tetragonal with space group $I4/m$ and consists of organic tecton **K1** and infinite $ZnSiF_6$ pillar with a formula of $[Zn(\mathbf{K1})_2SiF_6] \cdot 2(C_2H_6O)$ (abbreviated as **K1**· $ZnSiF_6$, Figure 4-19).

As expected from the design principle, the combination of infinite inorganic tecton $ZnSiF_6$ with organic tecton **K1** leads to the formation of a 1-D shashlik like coordination network (Figure 4-19a) resulting from the interconnection between binuclear coordination cages $[Zn_2(\mathbf{K1})_4(SiF_6)]^{2+}$ and linear SiF_6^{2-} anions. To the best of our knowledge, this is the first example on the 1-D organization of coordination cages.

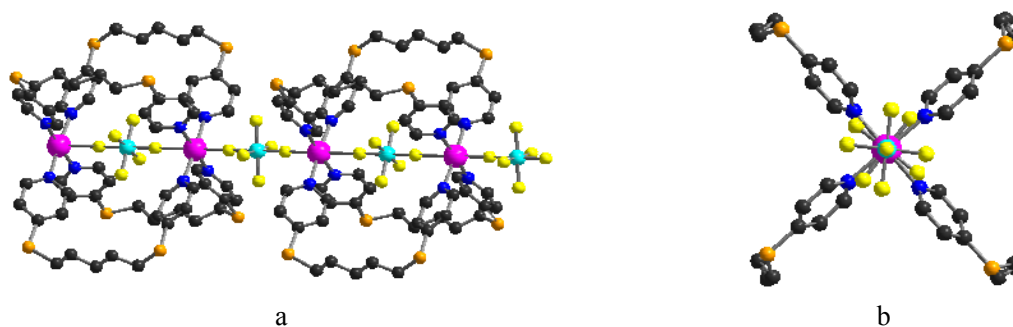


Figure 4-19: Portions of X-ray structures of the 1-D caged chain **K1**· $ZnSiF_6$ views perpendicular (a) and along the direction of $ZnSiF_6$ pillars (b). For clarity, the H atoms are omitted.

For the binuclear coordination cages, each zinc cation adopts a slightly distorted octahedral geometry with its coordination sphere composed of two F and four N atoms, wherein the angles of N-Zn-N and F-Zn-N are in the range from 87.7° to 92.3° deviating most from 90° by 2.3° . The two F atoms of two SiF_6^{2-} anions are located at the apical positions and the remaining four sites in the equatorial plane are occupied by four pyridine units belonging to four different organic tectons (d_{Zn-N} in the range of ca 2.07 - 2.17 Å). As expected from the design of the tecton **K1**, adopting a curved conformation but not allowing biting on the same metal centre, interconnection of two zinc cations leads to the formation of quadruple stranded cationic cages. To reduce steric hindrance, the

adjacent coordinated pyridyl rings are inclined to each other with the dihedral angle of 80.3° , while the coordinated pyridyl rings in the symmetrical positions are parallel to each other. In the cage, the $\text{Zn}\cdots\text{Zn}$ distance is 8.4 \AA , a bit larger than the reported isolated cages (8.1 \AA) from the same tectons **K1** and zinc cations but in the presence of uncoordinated ClO_4^- anion⁶. Thus, the coordination of SiF_6^{2-} anions leads to the expansion of the coordination cages.

In the center of each cage, an octahedral SiF_6^{2-} anion is found to be selected through weak coordination and hydrogen bonds (Figure 4-20). For the encapsulated SiF_6^{2-} moiety, the axial two F atoms are coordinated to the zinc cations with Zn-F bonds of 2.47 \AA , much longer than those for the bridged SiF_6^{2-} anions in the 3-D ZnSiF_6 pillared networks ($2.07 - 2.12 \text{ \AA}$). Conversely, the Si-F bond distances (1.62 \AA) for the F atoms located at the square base of the octahedron are slightly shorter. In addition, strong H-F hydrogen bonds are observed between the equatorial four F atoms of encapsulated SiF_6^{2-} anion and surrounding four organic tectons with distances in the range of $2.45 - 2.47 \text{ \AA}$.

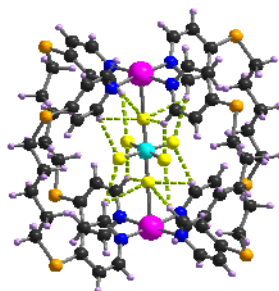


Figure 4-20: Schematic representation of four possible 1-D coordination networks from ZnSiF_6 pillars.

The exposed coordination sites of the quadruple stranded coordination cages are connected along the c axis by the bridged SiF_6^{2-} anions through Zn-F bonds ($d_{\text{Zn-F}} = 2.07 \text{ \AA}$) leading thus to a 1-D neutral coordination network (Figure 4-19a). Wherein, the bond lengths of Zn-F, Si-F (bridged), Si-F (unbound) and thus the close $\text{Zn}\cdots\text{Zn}$ distance between two neighboring cages (7.6 \AA) are in normal range for the ZnSiF_6 pillared networks.

Owing to the unequal SiF_6^{2-} anions in the ZnSiF_6 pillars, the distance between two consecutive zinc cations are alternated with 8.4 \AA and 7.6 \AA . In addition, the stagger angles between the zinc cation octahedron and SiF_6^{2-} octahedron are alternated with 11.8° and 42.5° (Figure 4-19b).

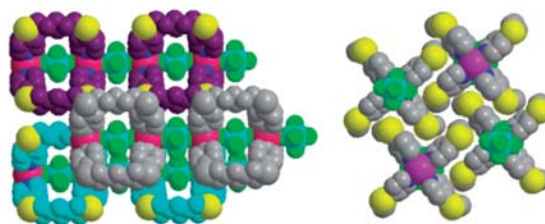


Figure 4-21: the packing of **K1**· ZnSiF_6 viewed perpendicular (a) and along the direction of ZnSiF_6 pillar. For clarity, the adjacent chains are differentiated with color and solvents are omitted.

In space, along the direction of ZnSiF_6 pillar, the two adjacent 1-D shashlik-like caged chains

are parallel and slipped about a distance of one cage so as to achieve the close packing (Figure 4-21). Owing to the separation and partial filling of voids by encapsulated SiF_6^{2-} anions, four small cavities occupied by ethanol molecules around each coordination cages are observed.

4.5.3. Stability and thermal properties of 1-D caged chain

The crystal $\text{K1}\cdot\text{ZnSiF}_6$ is rather stable in air and thus the purity of the generated solid $\text{K1}\cdot\text{ZnSiF}_6$ was investigated by X-ray diffraction on powder (Figure 4-22). The latter technique revealed that the crystalline material forms a pure phase, *i.e.* matching between observed and simulated peaks.

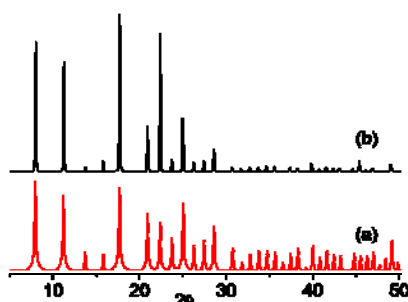


Figure 4-22: The Comparison of the simulated (a) and recorded (b) PXRD patterns for powdered $\text{K1}\cdot\text{ZnSiF}_6$

The thermal stability of $\text{K1}\cdot\text{ZnSiF}_6$ was investigated under nitrogen atmosphere using the TGA technique (Figure 4-23), which reveals one regime between 100 °C and 150 °C prior to decomposition of the sample, which appeared at *ca.* 230 °C. The first loss of mass corresponds to the release of the ethanol molecules and about 15% solvent proportion is close to the theoretical porosity ($792.0 \text{ \AA}^3/4045.3 \text{ \AA}^3 = 19.6\%$) calculated by PLATON software¹³. The slightly higher observed temperature than the boiling point of ethanol is attributed to the close cavities and hydrogen bonded interactions between networks and solvent molecules.

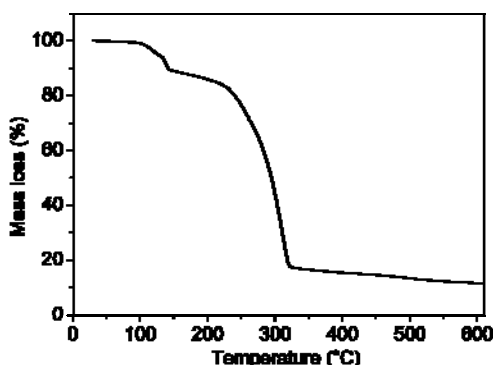


Figure 4-23: The TGA trace for $\text{K1}\cdot\text{ZnSiF}_6$ under the N_2 with the rate of 5°C/min.

In conclusion, the combination of a flexible tecton of specific length with an infinite tecton ZnSiF_6 lead to a 1-D shashlik like coordination network based on the chaining of the binuclear macrotetracyclic cages by ZnSiF_6 pillars. Extension to other coordination shape (*e.g.* 2-D planes) connected by the infinite tecton ZnSiF_6 will be discussed below.

4.6. From 2-D to 3-D tubular coordination networks

4.6.1. Design and synthesis of the multi-dentate flexible tectons

All the examples discussed above were based on bidentate tectons bearing two monodentate coordinating sites at the extremities of a backbone. We have also explored the possibility of using multi-dentate flexible tectons (Figure 4-24a). Some examples^{8,12-15} of 2-D coordination networks (Figure 4-24b) have been published upon combining multi-dentate flexible organic tectons with octahedral metal cations (Co^{2+} , Cu^{2+} and Zn^{2+}) in the presence of capping Cl^- anion. Our aim was to connect macrotetracyclic cages by SiF_6^{2-} anion with the help of multi-dentate flexible tectons (Figure 4-24c).

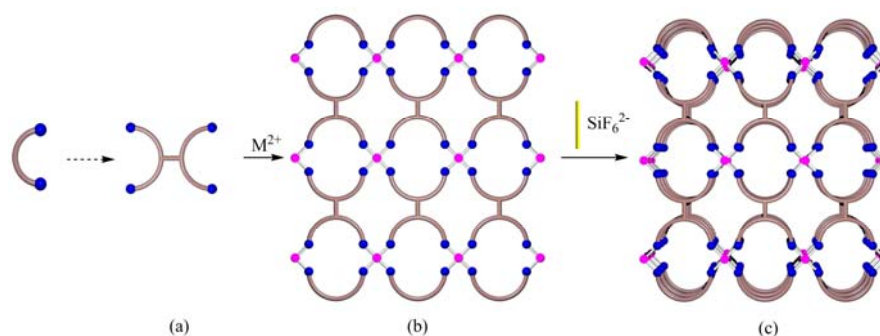
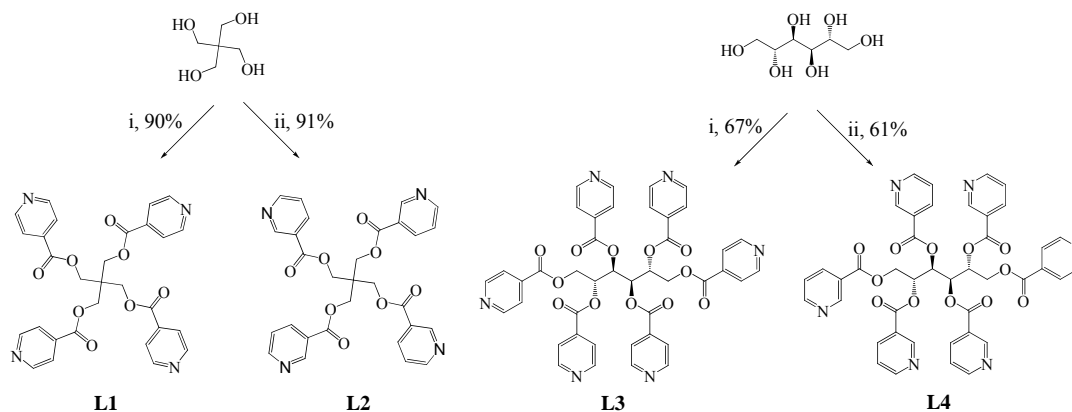


Figure 4-24: Schematic representation of the generation of a 3-D network using multi-dentate tectons and ZnSiF_6 .

In order to better coordinate to the infinite inorganic tecton ZnSiF_6 (four available site for each Zn^{2+} cation) in plane, the even number of denticity for the organic tectons is required. Thus, four organic tectons **L1-L4** (Scheme 4-5) based on flexible spacers bearing four or six pyridine (3-pyridine or 4-pyridine) groups at their extremities were designed and prepared. Tectons **L1** and **L3** differ from **L2** and **L4** with respect to the position of coordinating site within the pyridine unit. Whereas for tectons **L1** and **L2**, the spacer is an achiral connector, for the other two, the spacer is a chiral fragment. In all four cases, the junction between pyridine units and the backbone is of the ester type. The synthesis of isomeric **L1** and **L2** has been previously reported and their combinations with NiCl_2 leading to 2-D planes have been demonstrated.¹⁴



Scheme 4-5: Reaction conditions: (i) isonicotinoyl chloride, Et_3N , THF, room temperature, 48h; (ii) nicotinoyl chloride, Et_3N , THF, room temperature, 48h.

Following the published procedure¹⁴, tectons **L3-L4** were obtained in one step from the D-mannitol and *isonicotinoyl* (or *nicotinoyl*) chloride hydrochloride salt at room temperature in dry THF in the presence of Et₃N (*see experimental parts*).

4.6.2. Structural studies of 3-D tubular coordination networks

At room temperature, a solution of **L1-L4** in CHCl₃ (3 mg) was layered with DMSO (*ca.* 0.1 mL) and then a solution of ZnSiF₆ (5 mg) in EtOH (1 mL) was carefully added. Only in the case of the tecton **L1**, colorless crystals insoluble in common solvents were obtained after several days and analyzed by X-ray diffraction on a single crystal (**L1**·ZnSiF₆, Table 4-10). Unfortunately, due to its weak diffracting power (ratio observed/unique reflections = 26%), the structural study could not be achieved. In order to increase the diffraction power, the formation of the cobalt analogue (**L1**·CoSiF₆) was attempted. Using the same procedure, the EtOH solution of ZnSiF₆ was replaced by MeOH solution of CoSiF₆. The diffracting power in that case was indeed improved (ratio observed/unique reflections = 43%).

Table 4-10: Selected crystallographic parameters for 3-D tubular coordination networks

Compound	Chemical formula	Crystal system	Space group	a(Å)	b(Å)	c(Å)	α(deg)	β(deg)	γ(deg)
L1 ·ZnSiF ₆	[Zn ₂ (L1) ₂ (SiF ₆) ₂] ²⁻ (SQUEEZE)	Tetragonal	P-4c2	16.682	16.682	27.249	90	90	90
L1 ·CoSiF ₆	[Co ₂ (L1) ₂ (SiF ₆) ₂] ²⁻ (SQUEEZE)	Tetragonal	P-4c2	16.507	16.507	26.939	90	90	90

The structural analysis revealed that the two crystalline materials are isostructural and composed of one **L1**, two M²⁺ dications, three SiF₆²⁻ anions and solvent molecules. Due to disorder, not all solvents could be refined and thus SQUEEZE command was used for refinement. As a result, the H⁺ in the networks could not be fixed and only 3-D skeletons containing negative rectangle tubular channels are shown (Figure 4-25).

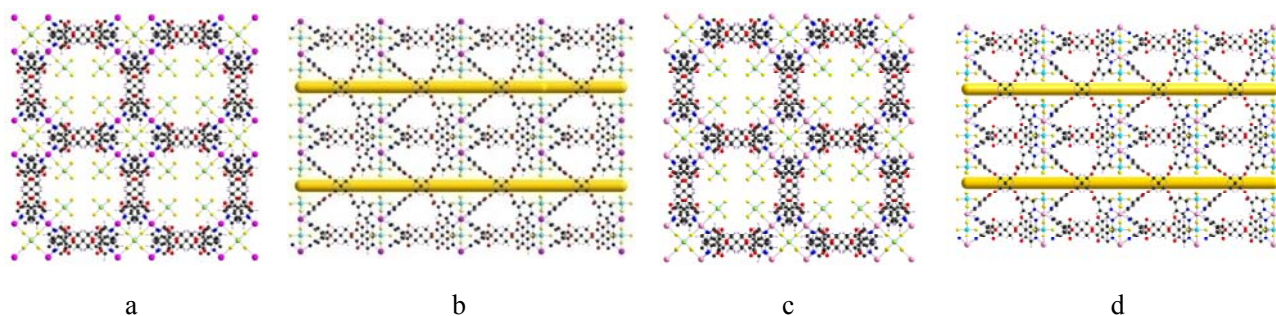


Figure 4-25: Portions of X-ray structures of two 3-D tubular coordination networks viewed along (a: **L1**·ZnSiF₆, c: **L1**·CoSiF₆) and perpendicular to the direction of channels (b: **L1**·ZnSiF₆, d: **L1**·CoSiF₆). For clarity, a yellow cylinder was added at the center of each channel in (b) and (d).

In both structures, each M²⁺ cation adopts a slightly distorted octahedral coordination geometry (NMN and FMF angles only deviating slightly from 90° and 180°, Table 4-11), connected by four different organic tectons through the formation of M-N ($d_{M-N} = 1.93/2.13$ Å) bonds in the

equatorial plane around the metal and the other two positions are occupied by the SiF_6^{2-} counter-anion ($d_{\text{Si-F}} = 1.62 - 1.68 \text{ \AA}$ for unbound fluorine atoms and $d_{\text{Si-F}} = 1.71 - 2.08 \text{ \AA}$ for bridging F atoms) *via* M-F bonds ($d_{\text{M-F}} = 1.85 - 2.13 \text{ \AA}$). Different from the infinite pillar MSiF_6 described above, in both case, two M^{2+} cations are bridged by one SiF_6^{2-} anion and then capped by two SiF_6^{2-} anions to form an anionic dinuclear pillar (Figure 3-26a).

Table 4-11: Selected bonds for the two isostructural coordination networks

Compound	M-F (bridged) distances/ \AA	M-F (capped) distances/ \AA	M-N distances/ \AA	Si-F (bridged) distances/ \AA	Si-F (capped) distances/ \AA	Si-F (unbound) distances/ \AA	N-Zn-N angles/ $^\circ$	F-Zn-F angles/ $^\circ$
L1 ·ZnSiF ₆	2.069	2.130	2.125-2.128	1.734	1.710	1.623-1.680	90	180
L1 ·CoSiF ₆	1.849	1.934	2.110-2.126	1.849	2.078	1.663	91.9	180

For the organic tectons, each **L1** adopts a distorted diamond type conformation with MCM (C atom is the center tertiary carbon) angles of 85.0° , 105.2° , 84.9° and 105.2° respectively in zinc case and 85.4° , 104.8° , 84.9° and 104.8° respectively in cobalt case. The organic tecton is connected to four different M^{2+} dications. As shown in Figure 3-26b, for four equatorial 4N planes of the four metal atoms around each organic tecton, plane *a* and *b* as well as plane *c* and *d* are parallel with the same distance of 12.48 \AA and 12.38 \AA for zinc and cobalt networks respectively. As a result, the four metal atoms are perpendicularly spread at the four corners (Figure 4-26c) to connect with organic tectons to form the 3-D tubular framework (Figure 4-25). Among four truncated rectangle tubes, the two face-to-face are bridged by one SiF_6^{2-} anion.

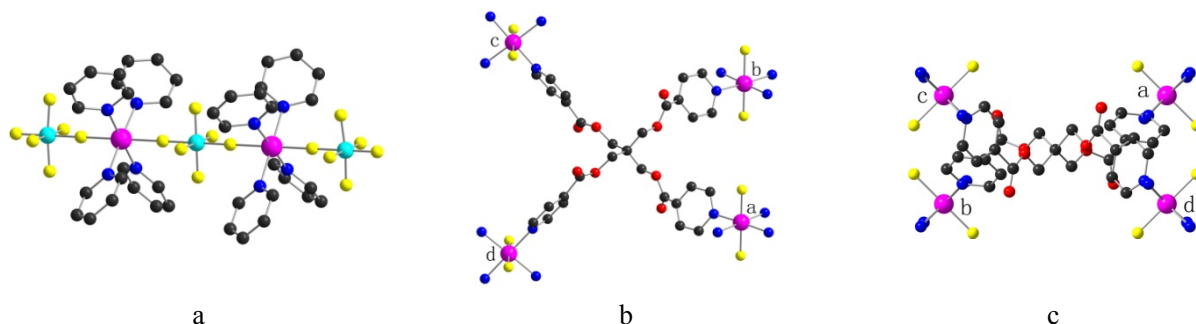


Figure 4-26: Portions of X-ray structures of **L1**·ZnSiF₆ showing the coordination pattern of two Zn^{2+} cations (a), the configuration of organic tecton viewed along b (b) and c axis (c). For clarity, the H atoms are omitted.

The comparison of crystallographic parameters observed for **L1**·ZnSiF₆ and **L1**·CoSiF₆ shows that the bond lengths M-F and M-N for **L1**·ZnSiF₆ are smaller than those for **L1**·CoSiF₆ (Table 4-11). However, the bond lengths of Si-F for the former are found to be increased. As a result, the distance between two consecutive metal atoms in the dinuclear pillar is 7.566 \AA and the diagonal two metal distances of channels are 15.778 \AA , slightly lower than those for **L1**·ZnSiF₆ (7.728 \AA and 15.865 \AA respectively).

4.6.3. Stability and thermal properties of 3-D tubular coordination networks

Both crystals are rather stable in air. The purity of the crystal batches is checked by X-ray

diffraction on powder at room temperature, which revealed only one phase, *i.e.* the matching between the recorded and simulated PXRD patterns (Figure 4-27).

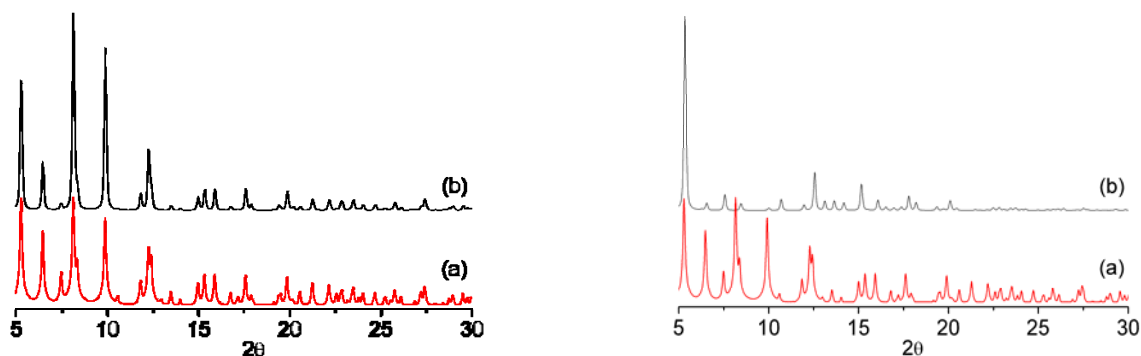


Figure 4-27: The Comparison of the simulated (a) and recorded (b) PXRD patterns for powdered $L1 \cdot ZnSiF_6$ (left) and $L1 \cdot CoSiF_6$ (right).

The thermal stability of both isostructural networks was investigated by TGA technique (Figure 4-28), which revealed the loss of solvent molecules between 30 °C and 180 °C for zinc specie and between 30 °C and 220 °C for cobalt one prior to decompositions of the samples, which appeared at *ca.* 180 °C and 230 °C respectively. Due to the unknown ratio of solvent by X-ray diffraction, we were not able to calculate the amount of solvents from TGA measurements.

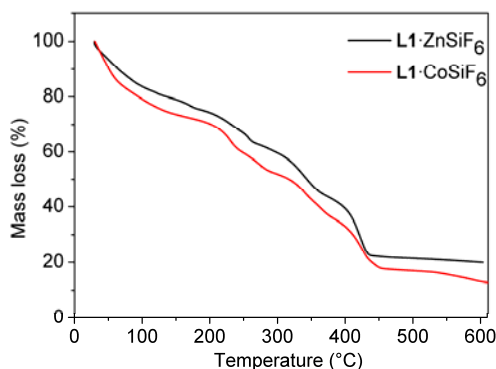


Figure 4-28: The TGA patterns for $L1 \cdot ZnSiF_6$ and $L1 \cdot CoSiF_6$ under the N_2 with the rate of 5°C/min.

4.7. Conclusions

In this chapter, we have demonstrated a series of 1-D to 3-D coordination networks based on flexible tectons and an infinite inorganic tecton $ZnSiF_6$. Depending on the nature of the flexible spacer (core), the topology, dimensionality, size as well as thermal properties of the networks could be modulated.

- ✧ By introduction of different spacers, one may control the interconnection pattern (perpendicular, inclined or helical) between consecutive $ZnSiF_6$ pillars in 2-D tubular networks. Therein, the organic tectons bearing only primary carbon atoms always lead to perpendicular interconnection patterns whereas those containing tertiary carbon atoms generate inclined patterns. Finally, the chiral organic tectons lead to the helical interconnection patterns. For all

these architectures, the shape as well as the size of the tubular channels has been modulated by the length of the organic tecton.

- ✧ By design of the flexible organic tectons of specific length (*ca.* 7.6 Å), a peculiar 1-D shashlik like coordination network composed of interconnected binuclear zinc macrotetracyclic cages by SiF_6^{2-} anions was demonstrated.
- ✧ By increasing the denticity of the flexible organic tectons, a series of isostructural 3-D coordination networks containing negative rectangle tubular channels were built. Wherein, the ZnSiF_6 (or CoSiF_6) do not behave as an infinite pillar but rather as dinuclear anionic unit.

References

1. C. Merz, M. Desciak, C. O'Brien, R. L. LaDuca, R. C. Finn, R. S. Rarig, J. A. Zubieta, *Inorg. Chim. Acta*, **2004**, 357: 3331-3335.
2. L. Carlucci, G. Ciani, D. M. Proserpio, S. Rizzato, *Cryst. Eng. Comm.*, **2003**, 5: 190-199.
3. T. M. Bujici, X. -T. Wang, S. -J. Li, C. Wang, *Z. Kristallogr. -New Crystal Structures*, **2003**, 218: 148-150.
4. K. J. Nordell, J. D. Hammond, M. D. Smith, *Acta Crystallogr. Sect. E*, **2003**, 59: m852-854.
5. C-L. Chen, J.-Y. Zhang, C.-Y. Su, *Eur. J. Inorg. Chem.*, **2007**, 19: 2997-3010.
6. Y. -B. Xie, J. -R. Li, C. Zhang, X. -H. Bu, *Crystal Growth & Design*, **2005**, 5: 1743-1749.
7. B. Wu, D. Yuan, B. Lou, L. Han, C. Liu, C. Zhang, M. Hong, *Inorg. Chem.*, **2005**, 44: 9175-9184.
8. P. Grosshans, *PhD thesis*, Universite Louis Paster de Strasbourg, **2005**.
9. D. Pocic, *PhD thesis*, Universite Louis Paster de Strasbourg, **2005**.
10. A. L. Spek, Platon, The University of Utrecht, Utrecht, The Netherlands, **1999**
11. A. M. d'A. Rocha Gonsalves, M. E. S. Serra, D. Murtinho, V. F. Silva, A. Matos Beja, J. A. Paixão, M. Ramos Silva, L. Alte da Veiga, *J. Mol. Catal. A: Chem.*, **2003**, 195: 1-9.
12. K. Nättinen, P. E. N. Bairos, P. J. Seppälä, K. Rissanen, *Eur. J. Inorg. Chem.*, **2005**, 2819-2825.
13. K. Nättinen, K. Rissanen, *Inorg. Chem.*, **2003**, 42: 5126-5134
14. P. Grosshans, A. Jouaiti, M. W. Hosseini, N. Kyritsakas, *New J. Chem.*, **2003**, 27: 793-797.
15. L.-C. Song, G. X. Jin, W.-X. Zhang, Q.-M. Hu, *Chin. J. Chem.*, **2005**, 23: 1065-1070.

**CHAPTER V: GENERAL CONCLUSIONS AND
PERSPECTIVES**

Chapter V: General Conclusions and Perspectives

Coordination networks or metal-organic frameworks (MOFs) with inner cavities have attracted considerable interest because of their ability to encapsulate and exchange guest molecules and to catalyze chemical reactions.¹⁻⁷ Most of these potential applications directly depend on the type, shape and size of the cavity. As an intrinsic property of MOFs, their cavities are mostly filled by solvent molecules and/or counter-anions. In order to avoid such self-inclusion of counter-anions, the use of coordinating anions seems interesting. So far, the vast majority of reported examples deal with coordinating organic anions, such as carboxylate, sulfonate, dipyrin and Imidazolate.⁴⁻⁵ Bridging inorganic anions may also be of interest for the design of porous crystals based on coordination networks. This approach has been explored in only few reports⁸⁻¹⁰. For example, SiF_6^{2-} anion is an interesting bridging unit for the design of porous MOFs¹¹. Indeed, its combination with dications such as Zn^{2+} , Co^{2+} , Cu^{2+} and organic tectons leads to the formation of pillar based architectures resulting from the bridging of metal centres through the two fluorine atoms occupying the axial positions¹²⁻¹⁹. In terms of design strategy, instead of looking at MSiF_6 as two separated entities, one may consider the pillar as an infinite tecton.

In this PhD work, we have focused on the design and study of the coordination networks with inner cavities based on SiF_6^{2-} and Zn^{2+} as linear pillars. We have combined the latter with a variety of rigid and flexible organic tectons and studied the structure of the crystalline materials generated.

First of all, we have explored rigid linear bidentate organic tectons of different length bearing two *para*-pyridyl units oriented in a divergent fashion. Upon combining these organic tectons with an infinite inorganic pillar type tecton (ZnSiF_6), 3-D cuboid type architectures have been designed (Figure 5-1a-b) and generated. We have demonstrated that the cross section of the faces, the size of the channels, the interpenetration as well as the thermal stability may be tuned by the length of the organic tectons. In order to improve the stability of such architectures, the same strategy was applied using other metal cations (such as Co^{2+} , Figure 5-1a), functionalizing organic tectons (Figure 5-1c) or designing new tectons serving as diagonal connectors for cuboid architecture (Figure 5-1d).

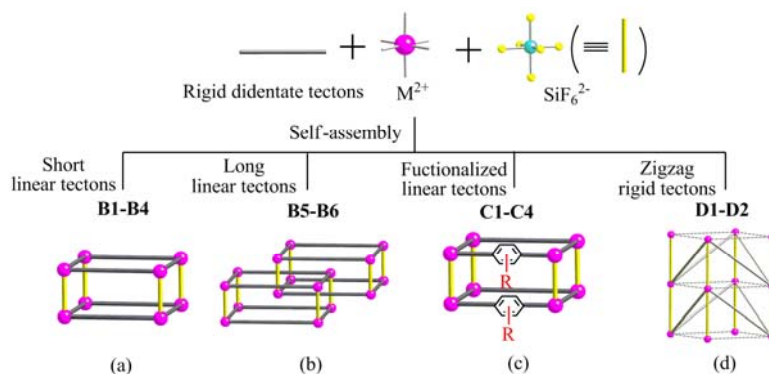


Figure 5-1: Schematic representation of 3-D coordination networks resulting from the combinations of MSiF_6 with different rigid organic tectons.

Secondly, we have extended our investigations to semi-rigid naphthalene, spirobiindane and 1,3,5-triazine based tectons. The restriction of the conformation space of the organic tecton afforded only a transformed cuboid 3-D architecture by similar self-assembly processes during which ZnSiF_6 are generated *in-situ* from $\text{Zn}(\text{BF}_4)_2$. Owing to different distortions and thus different lengths of organic tectons, the architecture is a four-component parallelepiped (Figure 5-2).

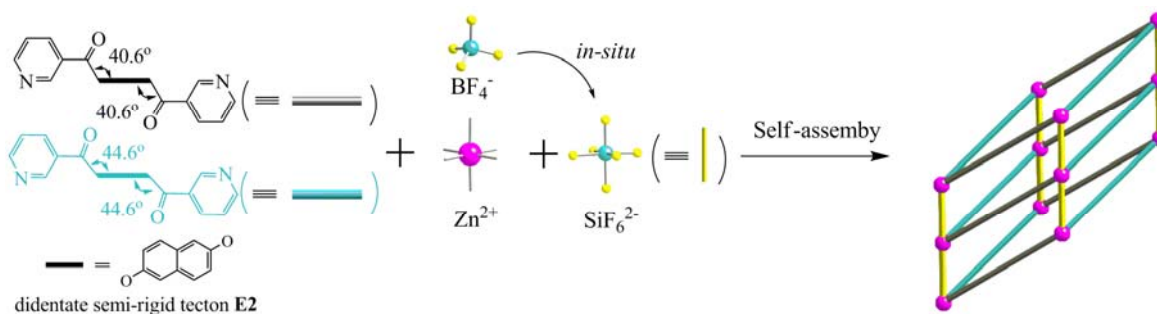


Figure 5-2: Schematic representation of one 3-D parallelepiped architecture resulting from the combination of ZnSiF_6 with naphthalene based semi-rigid tecton **E2**.

Thirdly, we have explored the influence of flexible didentate organic tectons. A series of flat cable-like tubular 2-D coordination networks have been obtained by combining bidentate flexible tectons with ZnSiF_6 (Figure 5-3a-c). It was found that the coordination pattern (perpendicular, inclined or helical) and geometry depend on the nature of the spacer connecting the two coordinating sites within the organic tectons. Organic tectons for which the spacer only contains methylene groups lead to the perpendicular coordination patterns (Figure 5-3a) whereas those containing tertiary carbon centres form inclined patterns (Figure 5-3b). Finally, chiral organic tectons lead to the helical coordination patterns (Figure 5-3c). For all these architectures, the shape as well as the size of the tubular channels can be modulated by the length and nature of the organic tecton.

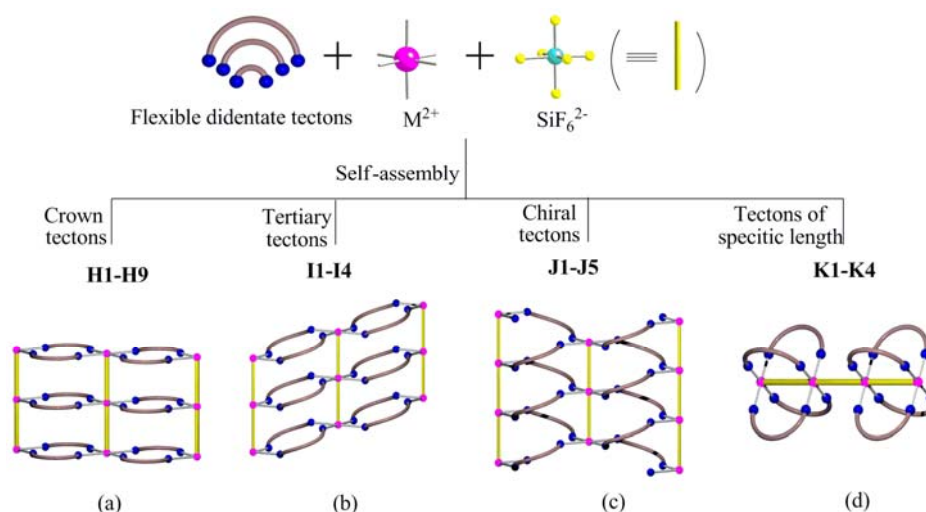


Figure 5-3: Schematic representation of 1-D and 2-D architectures resulting from the combination of ZnSiF_6 with different flexible organic tectons.

When using a flexible bidentate organic tecton of a specific length (*ca.* 7.6 Å), a 1-D shashlik type coordination network based on the interconnection of binuclear zinc macrotetracyclic cages has been generated (Figure 5-3d). To the best of our knowledge, this is the first example of such an organization *via* coordination bonds.

Finally, by increasing the denticity of organic tectons, in the presence of zinc or cobalt, isostructural 3-D coordination frameworks offering negative channels were generated using a flexible tetra-dentate tecton **L1** (Figure 5-4). However, much to our surprise, in these cases, ZnSiF_6 or CoSiF_6 forms a dinuclear anionic unit instead of a neutral infinite pillar.

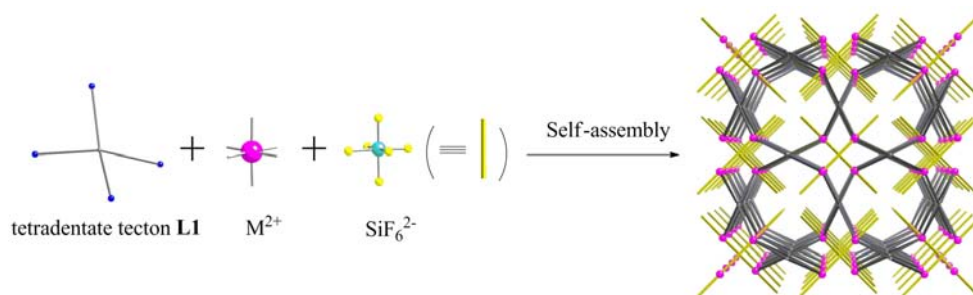


Figure 5-4: Schematic representation of 3-D coordination networks resulting from the combination of MSiF_6 with flexible tetra-dentate organic tecton **L1**.

Overall, the results described in this work showed that SiF_6^{2-} can be an attractive building block for the construction of porous coordination networks. As during the last years an increasing number of supramolecular structures incorporating SiF_6^{2-} pillars have been reported¹⁰, one can reasonably assume that the field will continue to attract interest in the next years, and that several new and interesting SiF_6^{2-} pillar based coordination networks will be reported.

Although the construction of crystalline architectures with different topology and geometry based on SiF_6^{2-} pillars have been well demonstrated, several improvements as listed below:

- ✧ For the coordination networks based on SiF_6^{2-} pillars found in this works, their stability concerning the solvents release under pumping and heating should be investigated and improved. Furthermore, the uptake and release of guest molecules (solvents or gas) and the selectivity of the process must be further investigated.
- ✧ The use of a tecton serving as a diagonal connector has been shown to improve the stability of non-interpenetrating cuboid 3-D coordination networks. Thus, design new rigid tecton based on this principle seems interesting to be developed. In particular, the 3-D helical networks (Figure 3-23) from the chiral tectons are anticipated to display a better stability.
- ✧ Considering the stability of interpenetrated architectures investigated in this work, the improvement of their porosity by increasing the length of spacer between two extreme pyridine units is advisable.

- ✧ Concerning the networks based on flexible tectons, it is interesting to design new tectons with increased denticity so as to connect the tubular 2-D networks, in particular helical tubes into 3-D architectures.

Despite of many difficulties encountered in the control and prediction of the final networks using the molecular tectonics strategy, several design principles have been successfully applied to build new architectures, in particular based on rigid tectons.

References

1. B. F. Abrahams, B. F. Hoskins, R. Robson, *J. Am. Chem. Soc.*, **1991**, 113: 3606-3607.
2. A. J. Blake, N. R. Champness, P. Hubberstey, W.-S. Li, M. A. Withersby, M. Schröder, *Coord. Chem. Rev.*, **1999**, 183: 117-138.
3. B. Moulton, M. J. Zaworotko, *Chem. Rev.*, **2001**, 101: 1629-1658.
4. M. Eddaoudi, D. B. Moler, H. Li, B. Chen, T. M. Reineke, M. O'Keeffe, O. M. Yaghi, *Acc. Chem. Res.*, **2001**, 34: 319-330.
5. G. F. Swiegers, T. J. Malefetse, *Chem. Rev.*, **2000**, 100: 3483-3538.
6. S. Kitagawa, R. Kitaura, S. Noro, *Angew. Chem., Int. Ed.*, **2004**, 43: 2334-2375.
7. G. Férey, *Chem. Soc. Rev.*, **2008**, 37: 191-214.
8. J. L. Manson, M. M. Conner, J. A. Schlueter, T. Lancaster, *et al*, *Chem. Commun.*, **2006**, 4894-4896.
9. S.I., Noro, S. Kitagawa, M. Kondo, K. Seki, *Angew. Chem. Int. Ed.*, **2000**, 39: 2081-2084.
10. K. Uemura, A. Maeda, T. K. Maji, P. Kanoo, H. Kita, *Eur. J. Inorg. Chem.* **2009**, 16: 2329-2337.
11. S. Ray, A. Zalkin and D. H. Templeton, *Acta Crystallogr., Sect. B: Struct. Crystallogr. Cryst. Chem.*, **1973**, 29: 2741-2747.
12. S.I., Noro, S. Kitagawa, M. Kondo, K. Seki, *Angew. Chem. Int. Ed.*, **2000**, 39: 2081-2084.
13. S.I., Noro, R. Kitaura, M. Kondo, S. Kitagawa, *et al*, *J. Am. Chem. Soc.*, **2002**, 124: 2568-2583.
14. A. J. Norquist, K. R. Heier, C. L. Stern, K. R. Poeppelmeier, *Inorg. Chem.*, **1998**, 37: 6494-6501.
15. R. A. J. Driessen, F. B. Hulsbergen, W. J. Vermin, J. Reedijk, *Inorg. Chem.*, **1982**, 21: 3594-3597.
16. F. S. Keij, R. A. G. De Graaff, J. G. Haasnoot, J. Reedijk, *Inorg. Chim. Acta*, **1989**, 156: 65-70.
17. S. Subramanian, M. J. Zaworotko, *Angew. Chem. Int. Ed.*, **1995**, 34: 2127-2129.

18. M.C. Suen, J.C. Wang, *Struct. Chem.*, **2006**, 17: 315-322.
19. M.C. Suen, Z.K. Chan, J. D. Chen, J.C. Wang, C. H. Hung, *Polyhedron*, **2006**, 25: 2325-2332.

CHAPTER VI: EXPERIMENTAL PART

Chapter VI: Experimental Part

6.1. General

6.1.1. Solvents and Reagents

All the commercially available solvents and reagents were purchased and used without any further purification except for special clarification. Tetrahydrofuran (THF), dichloromethane and diethyl ether were dried over Na and then distilled under nitrogen. N, N-Dimethylformamide (DMF), acetonitrile and ethanol were dried over 3 Å molecular sieve and then distilled under nitrogen.

6.1.2. Instruments

Single crystal X-ray diffraction experiments were carried out on a Bruker APEX8 CCD diffractometer equipped with an oxford Cryosystem liquid N₂ device at 173(2)K, using graphite monochromated Mo-K α radiation ($\lambda = 0.71073$ Å). The structures were solved using SHELXS-97 and refined by full matrix least-squares on F₂ using SHELXL-97 with anisotropic thermal parameters for all non hydrogen atoms. The hydrogen atoms were introduced at calculated positions and not refined (riding model).

The powder X-ray diffraction (PXRD) patterns were recorded on Bruker D8 ADVANCE diffractometer using Cu-K α radiation ($\lambda = 1.5406$ Å) at 40 kV and 40 mA with a scanning range between 3.8 and 30° by a scan step size of 2°/min. For comparison, the simulated PXRD patterns were calculated using the Mercury software.

¹H NMR and ¹³C-NMR spectra were recorded at room temperature on a Bruker AVANCE 300 (300 MHz) spectrometer, using the deuterated solvent as the lock and residual solvent as the internal reference. For ¹H-NMR spectra, chemical shifts were referenced to the residual proton peak of the solvent: CDCl₃ (7.26 ppm), (CD₃)₂SO (2.50 ppm) and CD₃OD (3.31 ppm). And for ¹³C-NMR spectra, the C atom of the solvent was used as reference: CDCl₃ (77.0 ppm), (CD₃)₂SO (39.0 ppm) and CD₃OD (49.1 ppm). The following abbreviations for specifying the multiplicity of ¹H-NMR signal in this manuscript are defined as follows: s = singlet, d = doublet, t = triplet, dd = doublet of doublets, m = multiplet and br = broad; (Units: δ (ppm), J (Hz)).

Melting points were measured in capillary on Stuart Scientific Melting Point SMP-1 apparatus with a rate of 5 °C/min.

Thermo gravimetric analysis (TGA) were performed on Pyris 6 TGA Lab System (Perkin-Elmer), using a N₂ flow of 20 ml/min and a heat rate of 5 °C/ min.

Elemental analyses were performed by the Service de Microanalyses de la Federation de Recherché de Chimie de Université de Strasbourg.

6.2. Syntheses of Organic Tectons

6.2.1. The reported tectons

Among the organic tectons used in this work, 4-pyridinemethanol (**A1**), 4-pyridineethanol (**A2**), isonicotinamide (**A3**), 4-aminopyridine (**A4**), 9-aminoacridine (**A5**), pyrazine (**B1**) and 4,4'-bipyridine (**B2**) were commercial products. 24 tectons listed in Table 6-1 were synthesized according to the published procedure and their spectra data were in agreement with reported data.

Table 6-1: The number, structure, name and reference of the reported tectons in this manuscript

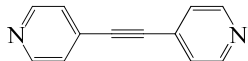
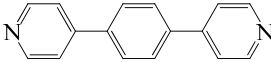
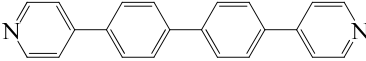
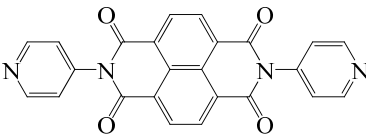
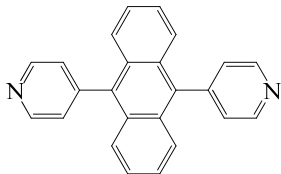
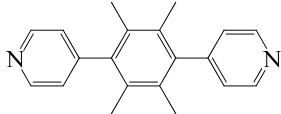
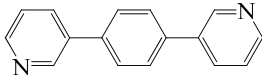
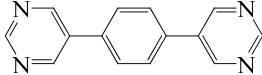
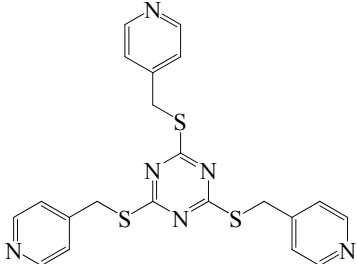
Number	Structure	Name	Reference
B3		1,2-di(pyridin-4-yl)ethyne	[1]
B4		1,4-bis(4-pyridyl)benzene	[2]
B6		4,4'-bis(4-pyridyl)biphenyl	[3]
B7		N,N'-Di-(4-pyridyl)-1,4,5,8-naphthalenetetracarboxydiimide	[4]
C1		1,4-bis(4-pyridyl)anthracene	[2]
C3		2,3,5,6-tetramethyl-1,4-bis(4-pyridyl)benzene	[11]
D1		1,4-bis(3-pyridyl)benzene	[5]
D2		1,4-bis(3,5-pyrimidyl)benzene	[6]
G1		2,4,6-tris(pyridin-4-ylmethylthio)-1,3,5-triazine	[7]

Table 6-1: The number, structure, name and reference of the reported tectons in this manuscript (Continue)

Number	Structure	Name	Reference
H1		ethane-1,2-diyl diisonicotinate	[10]
H2		2,2'-oxybis(ethane-2,1-diyl) diisonicotinate	[10]
H3		2,2'-(ethane-1,2-diylbis(oxy))bis(ethane-2,1-diyl) diisonicotinate	[10]
H4		S,S'-ethane-1,2-diyl dipyridine-4-carbothioate	[9]
H5		S,S'-2,2'-thiobis(ethane-1,2-diyl) dipyridine-4-carbothioate	[9]
H6		S,S'-2,2'-(ethane-1,2-diylbis(sulfanediyl)) bis(ethane-2,1-diyl)dipyridine-4-carbothioate	[9]
H7		1,2-bis(pyridin-4-ylthio)ethane	[8]
H8		1,3-bis(pyridin-4-ylthio)propane	[8]
H9		1,4-bis(pyridin-4-ylthio)butane	[8]
I3		(9H-fluorene-9,9-diyl)bis(methylene) diisonicotinate	[10]
K1		1,5-bis(pyridin-4-ylthio)pentane	[8]
J1		(1S,2S)-cyclohexane-1,2-diyl diisonicotinate	[10]
J2		(1R,2R)-cyclohexane-1,2-diyl diisonicotinate	[10]

Table 6-1: The number, structure, name and reference of the reported tectons in this manuscript (Continue)

Number	Structure	Name	Reference
L1		2,2-bis(isonicotinoyloxymethyl)propane-1,3-diyl diisonicotinate	[10]
L2		2,2-bis(nicotinoyloxymethyl)propane-1,3-diyl dinicotinate	[10]

6.2.2. The unreported tectons

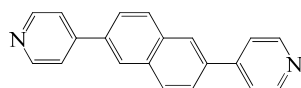
6.2.2.1 Rigid organic tectons

The precursor 1,4-dibromo-*p*-xylene was commercially available and 1,4-dibromo-2,5-di(*n*-propoxy)benzene was obtained following the published procedure¹².

General method for the syntheses of organic tectons B5, C2 and C4: Under nitrogen, a mixture of 4-pyridylboronic acid (4.4 mmol), corresponding dibromo aromatic compounds (2 mmol), Cs₂CO₃ (4.4 mmol) and [Pd(PPh₃)₄] (0.06 mmol) in deoxygenated DMF (20 mL) was stirred at 100 °C for 48h. After cooling to room temperature, the solvents were removed under vacuum and the residue thus obtained was washed twice with 100 mL of chloroform. After removal of the chloroform, the resulting mass was purified by column chromatography [SiO₂, CHCl₃] affording a white crystalline products.

2,6-bis(4-pyridyl)naphthalene (0.495g, 87%): m. p. > 250°C (sublimed)

¹H-NMR (CDCl₃, 300MHz, 298K): δ (ppm) = 8.72-8.74(dd, 4H, J = 2.7, 1.8), 8.17-8.18(d, 2H, J = 1.5), 8.05-8.07(m, 2H), 7.81-7.84(dd, 2H, J = 6.9, 1.8), 7.67-7.69(dd, 4H, J = 3.0, 1.5). ¹³C-NMR (CDCl₃, 75MHz, 25°C): δ(ppm) = 157.7, 155.5, 153.5, 150.0, 129.6, 126.3, 125.4, 121.9.

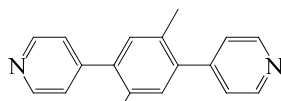


B5

Elemental analysis (C₂₀H₁₄N₂) :

Calculated (%) : C : 85.08, H:5.00, N:9.92

Measured (%): C : 85.31, H:4.82, N: 9.74

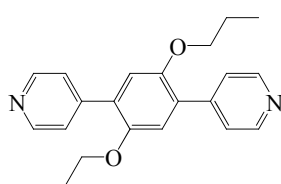
**C2**

2,5-dimethyl-1,4-bis(4-pyridyl)benzene (0.298g, 57%): m. p. >230°C (sublimed)
¹H-NMR (CDCl₃, 300MHz, 298K): δ(ppm) = 8.66-8.68(dd, 4H, J = 2.7, 1.5), 7.29-7.31(dd, 4H, J = 2.7, 1.8), 7.15(s, 2H), 2.29(s, 6H). ¹³C-NMR (CDCl₃, 75MHz, 25°C): δ(ppm) = 149.5, 149.2, 139.1, 132.7, 131.5, 124.1, 19.7.

Elemental analysis (C₁₈H₁₆N₂):

Calculated (%): C : 83.04, H :6.19, N:10.76

Measured (%): C : 83.31, H :6.25, N:10.84

**C4**

2,5-dipropoxyl-1,4-bis(4-pyridyl)benzene (0.283g, 40%): m. p. >200°C (sublimed)
¹H-NMR (CDCl₃, 300MHz, 298K): δ(ppm) = 8.64-8.66(d, 4H, J = 5.7), 7.52- 7.54(m, 4H), 6.99 (s, 2H), 3.90-3.94 (m, 4H), 1.68-1.77 (m, 4H), 0.93-0.98(m, 6H). ¹³C-NMR (CDCl₃, 75MHz, 25°C): δ(ppm) = 149.4, 145.8, 124.2, 115.4, 71.1, 22.6, 10.6.

Elemental analysis (C₂₂H₂₄N₂O₂):

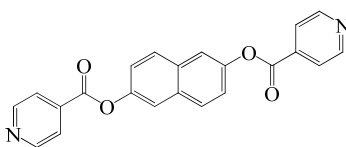
Calculated (%): C : 75.83, H :6.94, N:8.04

Measured (%): C : 75.33, H :6.94, N:8.07

6.2.2.2 Semi-rigid tectons

Dihydroxynaphthalene analogues were commercially available. However, 3,3,3',3'-tetramethyl-1,1'-spirobisindane-6,6'-diol and 1,5-bis(bromomethyl)naphthalene were synthesized following the published procedure¹³⁻¹⁴.

General method for the syntheses of organic tectons E1-E8, F1 and F2: Under nitrogen and at room temperature, to a degassed solution of diol (5 mmol) in dry THF (20 ml), the hydrochloride salt of isonicotinoyl chloride (10 mmol) was added and the mixture was stirred at room temperature for 15 min. Et₃N (5 ml) was added to the mixture and stirring was further continued for two days. After evaporation to dryness, a saturated aqueous solution of Na₂CO₃ (40 ml) was added to the residue and the mixture extracted with CHCl₃ (3 x 30 ml). The organic solvent was removed and the residue purified by column chromatography [SiO₂, CHCl₃] affording the pure products as white crystals.

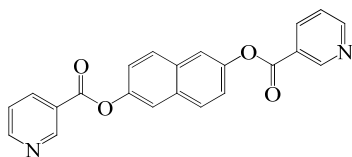
**E1**

naphthalene-2,6-diyl diisonicotinate (1.43g, 77%): m. p. = 241-243°C
¹H-NMR (300 MHz, 298K, CDCl₃): δ (ppm) = 7.39-7.43 (dd, 2H, J = 6.6, 2.4), 7.76-7.77(d, 2H, J = 2.7), 7.91-7.94 (d, 2H, J = 6.0), 8.05-8.07 (dd, 4H, J = 2.7, 1.8), 8.89-8.91 (dd, 4H, J = 2.7, 1.8); ¹³C-NMR (75 MHz, 298K, CDCl₃): δ [ppm] = 118.7, 121.8, 123.2, 129.5, 131.9, 136.7, 148.3, 150.9, 163.9.

Elemental analysis (C₂₂H₁₄N₂O₄·0.5H₂O):

Calculated (%): C : 69.65, H :3.99, N:7.38

Measured (%): C : 70.94, H :3.93, N:7.45

**E2**

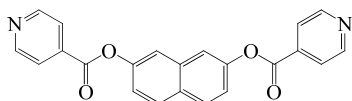
naphthalene-2,6-diyl dinicotinate (1.09g, 59%): m. p. = 206-208°C

$^1\text{H-NMR}$ (300 MHz, 298K, CDCl_3): δ (ppm) = 7.41-7.44 (dd, 2H, $J = 6.6, 2.1$), 7.48-7.53 (m, 2H), 7.77(d, 2H, $J = 2.4$), 7.91-7.94 (d, 2H, $J = 5.7$), 8.49-8.52 (m, 2H), 8.88-8.90 (dd, 4H, $J = 3.3, 1.8$), 9.45-9.46 (dd, 4H, $J = 1.5, 0.6$); $^{13}\text{C-NMR}$ (75 MHz, 298K, CDCl_3): δ [ppm] = 118.8, 121.9, 123.5, 125.5, 129.4, 131.9, 137.6, 148.2, 151.5, 154.1, 164.0.

Elemental analysis ($\text{C}_{22}\text{H}_{14}\text{N}_2\text{O}_4 \cdot 0.5\text{H}_2\text{O}$) :

Calculated (%): C : 69.65, H :3.99, N:7.38

Measured (%): C : 70.63, H :3.88, N:7.35

**E3**

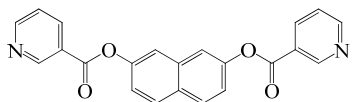
naphthalene-2,7-diyl diisonicotinate (1.05g, 57%): m. p. = 234-236°C

$^1\text{H-NMR}$ (CDCl_3 , 300MHz, 298K): δ (ppm) = 8.88-8.90 (dd, 2H, $J = 3.0, 1.5$), 8.04-8.06 (dd, 2H, $J = 2.4, 1.8$), 7.96-7.99 (d, 2H, $J = 9.0$), 7.71-7.72 (d, 2H, $J = 2.1$), 7.37-7.40 (dd, 2H, $J = 6.6, 2.1$). $^{13}\text{C-NMR}$ (75 MHz, 298K, CDCl_3): δ [ppm] = 165.2, 153.9, 149.3, 137.8, 129.6, 124.3, 123.3, 115.2, 107.8.

Elemental analysis ($\text{C}_{22}\text{H}_{14}\text{N}_2\text{O}_4$) :

Calculated (%): C : 71.35, H :3.81, N:7.56

Measured (%): C : 71.61, H :3.88, N:7.43

**E4**

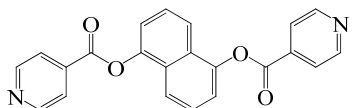
naphthalene-2,7-diyl dinicotinate (0.886g, 48%): m. p. = 208-211°C

$^1\text{H-NMR}$ (CDCl_3 , 300MHz, 298K): δ (ppm) = 9.45-9.46(d, 2H, $J = 1.5$), 8.87-8.88(d, 2H, $J = 1.5$), 8.48-8.52(dd, 2H, $J = 2.1, 1.5$), 7.95-9.98(d, 2H, $J = 9.0$), 7.72 (s, 2H), 7.48-7.52 (m, 2H), 7.37-7.41 (dd, 2H, $J = 6.9, 2.1$). $^{13}\text{C-NMR}$ (CDCl_3 , 75MHz, 25°C): δ (ppm) = 163.9, 154.1, 151.4, 148.9, 137.7, 129.6, 123.5, 121.1, 118.6.

Elemental analysis ($\text{C}_{22}\text{H}_{14}\text{N}_2\text{O}_4 \cdot 0.5\text{H}_2\text{O}$) :

Calculated (%): C : 69.65, H :3.99, N:7.38

Measured (%): C : 70.29, H :3.87, N:7.43

**E5**

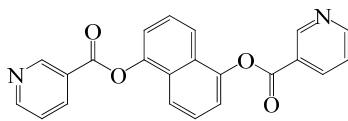
naphthalene-1,5-diyl diisonicotinate (1.256g, 68%): m. p. = 233-236°C

$^1\text{H-NMR}$ (CDCl_3 , 300MHz, 298K): δ (ppm) = 8.86-8.89 (dd, 2H, $J = 3.0, 1.5$), 8.02-8.04 (dd, 2H, $J = 2.4, 1.8$), 7.88-7.91(m, 2H), 7.55-7.57 (m, 2H), 7.45-7.48(m, 2H). $^{13}\text{C-NMR}$ (75 MHz, 298K, CDCl_3): δ [ppm] = 165.2, 152.4, 149.3, 137.8, 128.6, 124.3, 123.3, 115.2, 109.8.

Elemental analysis ($\text{C}_{22}\text{H}_{14}\text{N}_2\text{O}_4 \cdot 0.5\text{H}_2\text{O}$) :

Calculated (%): C : 69.65, H :3.99, N:7.38

Measured (%): C : 70.63, H :3.88, N:7.35

**E6**

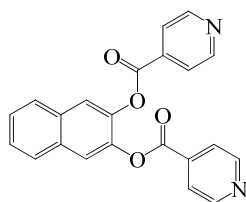
naphthalene-1,5-diyl dinicotinate (1.016g, 55%): m. p. = 212-214°C

¹H-NMR (CDCl₃, 300MHz, 298K): δ(ppm) = 9.55-9.55(m, 2H), 8.92-8.94(dd, 2H, J = 3.0, 1.8), 8.57-8.59 (m, 2H), 7.88-7.91(m, 2H), 7.55-7.57 (m, 2H), 7.45-7.48(m, 2H). ¹³C-NMR (CDCl₃, 75MHz, 25°C): δ(ppm) = 163.7, 154.3, 151.4, 146.5, 137.8, 128.2, 126.3, 125.3, 123.6, 119.6, 119.1.

Elemental analysis (C₂₂H₁₄N₂O₄) :

Calculated (%): C : 71.35, H :3.81, N:7.56

Measured (%): C : 71.63, H :3.87, N:7.39

**E7**

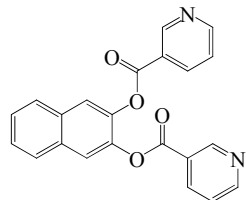
naphthalene-2,3-diyl diisonicotinate (1.515g, 82%): m. p. = 230-233°C

¹H-NMR (CDCl₃, 300MHz, 298K): δ(ppm) = 8.75-8.78(dd, 4H, J = 2.7, 1.8), 7.87-7.90(m, 8H), 7.550-7.582 (dd, 2H, J = 3.6, 2.7). ¹³C-NMR (CDCl₃, 75MHz, 25°C): δ(ppm) = 163.0, 150.9, 140.4, 135.8, 131.7, 127.6, 126.9, 122.9, 121.1.

Elemental analysis (C₂₂H₁₄N₂O₄) :

Calculated (%): C : 71.35, H :3.81, N:7.56

Measured (%): C : 70.62, H :3.95, N:7.47

**E8**

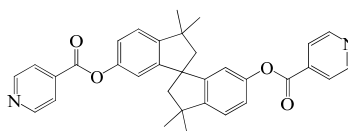
naphthalene-2,3-diyl dinicotinate (0.887g, 48%): m. p. = 211-214°C

¹H-NMR (CDCl₃, 300MHz, 298K): δ(ppm) = 9.28-9.29(dd, 2H, J =1.2, 0.9), 8.76-8.79(dd, 2H, J = 3.0, 1.8), 8.33-8.35 (d, 2H, J = 8.1), 7.86-7.87 (d, 4H, J = 3.0), 7.54-7.57 (dd, 2H, J = 3.3, 3.3), 7.34-7.39(m, 2H). ¹³C-NMR (CDCl₃, 75MHz, 25°C): δ(ppm) = 163.1, 154.2, 151.2, 140.6, 137.5, 131.7, 127.6, 126.8, 124.7, 123.5, 121.2.

Elemental analysis (C₂₂H₁₄N₂O₄·0.5H₂O) :

Calculated (%): C : 69.65, H :3.99, N:7.38

Measured (%): C : 71.33, H :4.24, N:7.18

**F1**

3,3,3',3'-tetramethyl-2,2',3,3'-tetrahydro-1,1'-spirobi[indene]-6,6'-diyl

diisonicotinate (1.48g, 57%): m. p. = 230-231°C

¹H-NMR (300 MHz, 298K, CDCl₃): δ [ppm] = 1.27-1.41 (d, 12H, J = 12), 2.30-2.45 (dd, 4H, J = 19.5, 13.2), 6.68 (d,2H, J = 2.4), 7.1 (dd, 2H, J = 6, 2.1), 7.24 (m, 2H), 8.0 (dd, 4H, J = 3.0, 1.5), 8.8 (dd, 2H, J = 2.7, 1.5); ¹³C-NMR (75 MHz, 298K, CDCl₃): δ [ppm] = 30.2, 43.3, 57.6, 59.4, 116.9, 120.4, 122.9, 123.1, 127.9, 149.9, 150.3, 150.8, 151.7, 163.9.

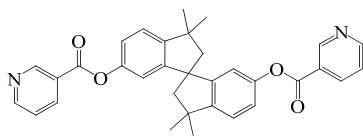
Elemental analysis (C₃₃H₃₀N₂O₄) :

Calculated (%): C : 76.43, H :5.83, N:5.40

Measured (%): C : 74.73, H :5.67, N:5.23

3,3,3',3'-tetramethyl-2,2',3,3'-tetrahydro-1,1'-spirobi[indene]-6,6'-diyl**dinicotinate** (1.27g, 49%): m. p. = 235-238°C

¹H-NMR (300 MHz, 298K, CDCl₃): δ [ppm] = 1.38-1.42 (d, 12H, J = 12), 2.31-2.46 (dd, 4H, J = 16.8, 13.2), 6.69 (d, 2H, J = 2.1), 7.07-7.10 (dd, 2H, J = 6, 2.1), 7.21-7.24 (d, 2H, J = 8.4), 7.40-7.44 (m, 2H), 8.37-8.41 (m, 2H), 8.81-8.83(m, 2H), 9.33-9.34(m, 2H); ¹³C-NMR (75 MHz, 298K, CDCl₃): δ [ppm] = 30.3, 43.3, 57.6, 59.4, 117.1, 120.6, 122.9, 123.4, 125.6, 137.5, 150.0, 150.1, 151.7, 153.9, 164.0.

**F2**Elemental analysis (C₃₃H₃₀N₂O₄) :

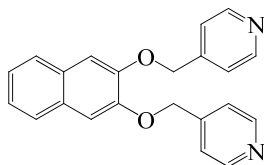
Calculated (%): C : 76.43, H : 5.83, N:5.40

Measured (%): C : 75.36, H : 5.87, N:5.66

General method for the syntheses of organic tectons F9 and F10: Under nitrogen and at room temperature, to a degassed solution of diol (5 mmol) in dry DMF (20 ml), the hydro bromide salt of 4-(bromomethyl)pyridine or 2-(bromomethyl)pyridine (10 mmol) and K₂CO₃ (20 mmol) were added and the mixture was stirred at room temperature for two days. After evaporation to dryness, the residue was dissolve in 200 mL of water and the mixture extracted with CHCl₃ (3 x 30 ml). The organic solvent was removed and the residue purified by column chromatography [SiO₂, CHCl₃] affording the pure products as white powders.

2,3-bis(pyridin-4-ylmethoxy)naphthalene (0.530g, 31%): m. p. = 223-225°C

¹H-NMR (CDCl₃, 300MHz, 298K): δ(ppm) = 8.63-8.65(dd, 4H, J = 3.0, 1.8), 7.63-7.67(m, 2H), 7.44-7.46 (m, 4H), 7.33-7.36 (m, 2H), 7.18 (s, 2H), 5.31 (s, 4H), ¹³C-NMR (CDCl₃, 75MHz, 25°C): δ(ppm) = 150.0, 146.0, 129.3, 126.4, 124.8, 121.3, 109.1, 68.9.

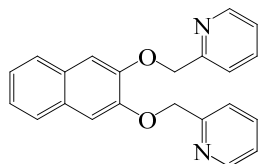
**E9**Elemental analysis (C₂₂H₁₈N₂O₂) :

Calculated (%): C : 77.17, H : 5.30, N:8.18

Measured (%): C : 76.72, H : 5.20, N:8.03

2,3-bis(pyridin-2-ylmethoxy)naphthalene (1.52g, 89%): m. p. = 221-224°C

¹H-NMR (CDCl₃, 300MHz, 298K): δ(ppm) = 8.62-8.64(m, 2H), 7.61- 7.71 (m, 6H), 7.29-7.32 (m, 2H), 7.21-7.24 (m, 4H), 5.44 (s, 4H), ¹³C-NMR (CDCl₃, 75MHz, 25°C): δ(ppm) = 155.0, 149.3, 148.3, 136.3, 129.3, 124.4, 121.3, 109.1, 69.3.

**E10**Elemental analysis (C₂₂H₁₈N₂O₂) :

Calculated (%): C : 77.17, H : 5.30, N:8.18

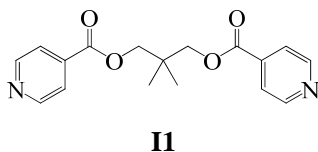
Measured (%): C : 77.01, H : 5.31, N:8.23

6.2.2.3 Flexible tectons

1,3-propanediol, 2,2'-dimethyl-1,3-propanediol, 2,2'-dibutyl-1,3-propanediol as well as trans-cyclopentane-1,2-diol, 2-(hydroxymethyl)-2-ethyl-1,3-propanediol, D(+)-mannitol and 2,2'-oxybis(ethane-2,1-diyl) bis(4-methylbenzenesulfonate) were commercially available. However, (3S, 4S)-N-phenyl-3, 4-dihydroxy-2,5-dioxopyrrolidines, (3R, 4R)-N-phenyl-3,4-dihydroxy-2,5-dioxopyrrolidines and 2,2'-thiobis(ethane-2,1-diyl) bis(4-methylbenzenesulfonate) were synthesized following the published procedure¹⁵⁻¹⁶.

General method for the syntheses of organic tectons **I1**, **I2**, **I4**, **K3**, **K4**, **K5**, **L1** and **L3**:

Under nitrogen and at room temperature, to a degassed solution of alcohol (5 mmol) in dry THF (20 ml), the hydrochloride salt of isonicotinoyl chloride (10 mmol for **I1**, **I2**, **I4**, **K3**, **K4** and **K5**, 15 mmol for **L1** and 25 mmol for **L3**) was added and the mixture was stirred at room temperature for 15 min. Et₃N (5 ml) was added to the mixture and stirring was further continued for two days. After evaporation to dryness, a saturated aqueous solution of Na₂CO₃ (40 ml) was added to the residue and the mixture extracted with CHCl₃ (3 x 30 ml). The organic solvent was removed and the residue purified by column chromatography [SiO₂, CHCl₃] affording the pure products as a colorless oil or as a powder.



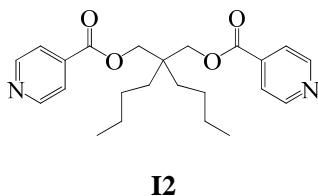
2,2-dimethylpropane-1,3-diyl diisonicotinate (1.31g, 83%): m. p. = 53°C

¹H-NMR (300 MHz, 298K, CDCl₃): δ (ppm) = 8.72-7.74 (dd, 4H, J = 2.7, 1.5), 7.77-7.79(dd, 4H, J = 2.7, 1.5), 4.23 (s, 4H), 1.14 (s, 6H); ¹³C-NMR (75 MHz, 298K, CDCl₃): δ [ppm] = 164.8, 150.6, 137.0, 122.7, 70.2, 35.3, 21.9.

Elemental analysis (C₁₇H₁₈N₂O₄·0.5H₂O) :

Calculated (%) : C : 63.15, H :5.92, N:8.66

Measured (%): C : 62.67, H :5.75, N:8.43



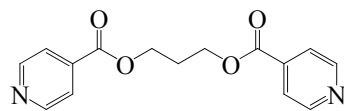
2,2-dibutylpropane-1,3-diyl diisonicotinate (white oil, 1.44g, 72%):

¹H-NMR (300 MHz, 298K, CDCl₃): δ (ppm) = 8.71-7.73 (dd, 4H, J = 3.0, 1.5), 7.74-7.76(dd, 4H, J = 3.0, 1.5), 4.27(s, 4H), 1.25-1.47 (m, 6H), 0.85-0.89 (m, 6H); ¹³C-NMR (75 MHz, 298K, CDCl₃): δ [ppm] = 164.8, 150.7, 137.1, 122.8, 67.5, 40.0, 31.2, 24.8, 23.3, 14.1.

Elemental analysis (C₂₃H₃₀N₂O₄) :

Calculated (%) : C : 69.32, H :7.59, N:7.03

Measured (%): C : 69.17, H :7.75, N:7.00

**I4**

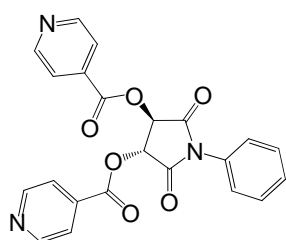
propane-1,3-diyl diisonicotinate (white oil, 2.16g, 81%):

$^1\text{H-NMR}$ (CDCl_3 , 300MHz, 298K): δ (ppm) = 8.74-8.77(m, 4H), 7.80-7.84 (m, 4H), 4.51-4.55(m, 4H), 2.24-2.32(m, 3H). $^{13}\text{C-NMR}$ (CDCl_3 , 75MHz, 25°C): δ (ppm) = 165.0, 150.7, 137.0, 122.8, 62.3, 28.0.

Elemental analysis ($\text{C}_{15}\text{H}_{14}\text{N}_2\text{O}_4$):

Calculated (%): C : 62.93, H :4.93, N:9.79

Measured (%): C : 62.56, H :4.85, N:9.60



(R,R)

J3

(3R,4R)-N-phenyl-3,4-isonicotinoyl-2,5-dioxopyrrolidines (1.21g, 58%):

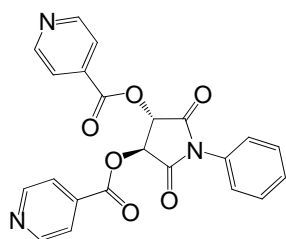
m. p. >200°C (decomposed)

$^1\text{H-NMR}$ (300 MHz, 298K, CDCl_3): δ (ppm) = 8.85-8.87 (d, 4H, J = 6.0) ; 7.78-7.91 (dd, 4H, J = 3.0, 1.2) ; 7.41-7.54 (m, 5H), 6.08 (s, 2H); $^{13}\text{C-NMR}$ (75 MHz, 298K, CDCl_3): δ [ppm] = 73.7; 123.1; 126.1; 129.5; 129.5; 135.2; 150.9; 164.4; 167.5.

Elemental analysis ($\text{C}_{22}\text{H}_{15}\text{N}_3\text{O}_6$):

Calculated (%): C : 63.31, H :3.62 , N:10.07

Measured (%): C : 64.23, H :3.82, N : 9.64



(S,S)

J4

(3S,4S)-N-phenyl-3,4-isonicotinoyl-2,5-dioxopyrrolidines (1.40g, 67%): m.

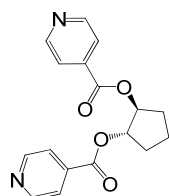
p. >200°C (decomposed)

$^1\text{H-NMR}$ (300 MHz, 298K, CDCl_3): δ (ppm) = 8.85- 8.87 (d, 4H, J =6.0), 7.91-7.93 (dd, 4H, J = 2.7, 1.8) ; 7.26-7.55 (m, 5H), 6.08 (s, 2H); $^{13}\text{C-NMR}$ (75 MHz, 298K, CDCl_3): δ [ppm] = 73.7; 123.1; 126.1; 129.5; 135.1; 150.9; 164.4; 167.5.

Elemental analysis ($\text{C}_{22}\text{H}_{15}\text{N}_3\text{O}_6$):

Calculated (%): C : 63.31, H :3.62 , N:10.07

Measured (%): C : 64.21, H :3.83, N : 9.58



(Racemic)

J5

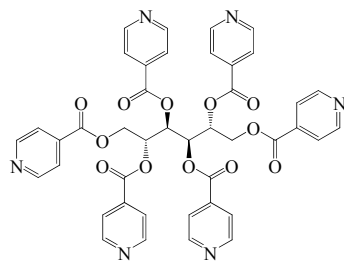
trans-cyclopentane-1,2-diyl diisonicotinate (1.50g, 93%): mp = 45°C

$^1\text{H-NMR}$ (CDCl_3 , 300MHz, 298K): δ (ppm) = 8.75-8.78 (m, 4H), 7.79-7.83(m, 4H), 5.46-5.51(m, 2H), 2.15-2.37 (m, 4H), 1.79-1.99 (m, 2H); $^{13}\text{C-NMR}$ (75 MHz, 298K, CDCl_3): δ [ppm] = 164.4, 150.6, 137.1, 122.8, 80.2, 30.4, 21.6.

Elemental analysis ($\text{C}_{17}\text{H}_{18}\text{N}_2\text{O}_4 \cdot 0.5\text{CH}_3\text{OH}$):

Calculated (%): C : 64.01, H :5.53, N:8.53

Measured (%): C : 64.43, H :5.52, N:8.33

**L3**

(2R,3R,4R,5R)-hexane-1,2,3,4,5,6-hexayl hexaisonicotinate (2.74g, 67%):

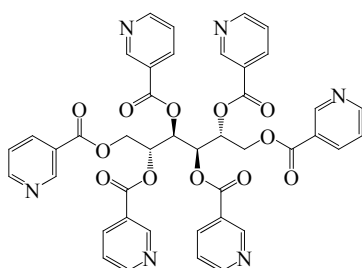
m. p. >200°C (decomposed)

¹H-NMR (300 MHz, 298K, CDCl₃): δ (ppm) = 8.68-8.85 (m, 12H), 7.67-7.80(m, 12H), 6.14-6.17(d, 2H, J = 7.2), 5.76-5.81(m, 2H), 4.87-4.92 (dd, 2H, J =9.9, 3.0), 4.48-4.54 (dd, 4H, J = 6.9, 5.7); ¹³C-NMR (75 MHz, 298K, CDCl₃): δ [ppm] = 164.5, 164.1, 163.9, 151.1, 150.9, 150.8, 136.0, 135.9, 135.2, 122.7, 122.6, 69.8, 69.2, 62.6.

Elemental analysis (C₄₂H₃₂N₆O₁₂·2H₂O) :

Calculated (%) : C : 59.43, H :4.28, N:9.90

Measured (%): C : 59.01, H :4.26, N:9.77

**L4**

(2R,3R,4R,5R)-hexane-1,2,3,4,5,6-hexayl hexanicotinate (2.48g, 61%):

m. p. >200°C (decomposed)

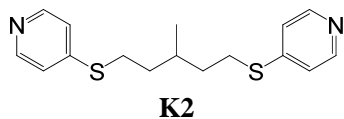
¹H-NMR (300 MHz, 298K, CDCl₃): δ (ppm) = 9.24-9.25 (d, 6H, J = 2.1), 8.77-8.80 (dd, 6H, J =3.0, 1.8), 8.29-8.33 (m, 6H), 7.37-7.41 (m, 6H), 5.76-5.81(m, 2H), 4.87-4.92 (dd, 2H, J =9.9, 3.0), 4.48-4.54 (dd, 4H, J = 6.9, 5.7); ¹³C-NMR (75 MHz, 298K, CDCl₃): δ [ppm] = 165.2, 153.6, 153.1, 151.0, 136.0, 135.9, 135.2, 122.7, 122.6, 69.8, 69.2, 62.6.

Elemental analysis (C₄₂H₃₂N₆O₁₂·1H₂O) :

Calculated (%) : C : 60.72, H :4.13, N:10.12

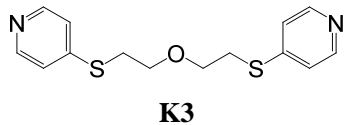
Measured (%): C : 59.81, H :4.20, N:10.27

General method for the syntheses of organic tectons J2, J3 and J4: Under argon and at room temperature, 4-mercaptopyridine (1.22 g, 11 mmol) and K₂CO₃ in excess (4.64 g, 33.4 mmol) were dissolved in acetonitrile (50 mL). To the stirred mixture, 5 mmol 1,5-dibromo-3-methylpentane for **J2**, 2,2'-oxybis(ethane-2,1-diyl) bis(4-methylbenzenesulfonate) for **J3** and 2,2'-thiobis(ethane-2,1-diyl) bis(4-methylbenzenesulfonate) for **J4** was added. The solution was heated to reflux over night. The mixture was cooled to RT and filtrated. Solvent was removed under reduced pressure. CH₂Cl₂ (50 mL) was added to the residue and then purified by column chromatography (SiO₂) with CH₂Cl₂ as eluents. The pure final product was obtained as yellowish oil.

**K2**

3-methyl-1,5-bis(pyridin-4-ylthio)pentane (yellowish oil, 0.94g, 62%):

¹H-NMR (300 MHz, 298K, CDCl₃): δ [ppm] = 0.95-0.96 (m, 3H), 1.65-1.75 (m, 5H), 2.94-2.97 (m, 4H), 7.47-7.59 (dd, 4H, J = 3, 1.5), 8.64-8.66 (dd, 4H, J = 3, 1.8); ¹³C-NMR (75 MHz, 298K, CDCl₃): δ [ppm] = 22.6, 31.3, 33.5, 34.1, 120.4, 149.3.



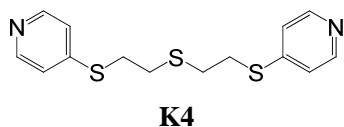
1,5-bis(pyridin-4-ylthio)ethoxyethane (yellowish oil, 0.98g, 67%):

$^1\text{H-NMR}$ (300 MHz, 298K, DMSO- d_6): δ [ppm] = 3.23-3.27 (m, 4H), 3.67-3.71 (m, 4H), 7.27-7.29 (dd, 4H, $J = 3, 1.8$), 8.34-8.36 (dd, 4H, $J = 3, 1.5$); $^{13}\text{C-NMR}$ (75 MHz, 298K, DMSO- d_6): δ [ppm] = 40.2, 68.7, 121.0, 148.6, 149.6.

Elemental analysis ($\text{C}_{14}\text{H}_{16}\text{N}_2\text{OS}_2$) :

Calculated (%): C : 57.50, H : 5.52, N:9.58

Measured (%): C : 57.21, H : 5.83, N:9.58



1,5-bis(pyridin-4-ylthio) diethylsulfane (yellowish oil, 1.08g, 70%):

$^1\text{H-NMR}$ (300 MHz, 298K, CDCl_3): δ [ppm] = 3.13-3.25 (m, 4H), 3.72-3.74(m, 4H), 7.26-7.29 (dd, 4H, $J = 3.6, 2.4$), 8.37-8.40 (dd, 4H, $J = 3.6, 1.5$); $^{13}\text{C-NMR}$ (75 MHz, 298K, CDCl_3): δ [ppm] = 33.2, 40.1, 121.2, 149.4, 149.6.

Elemental analysis ($\text{C}_{14}\text{H}_{16}\text{N}_2\text{S}_3$) :

Calculated (%): C : 54.51, H : 5.23, N:9.08

Measured (%): C : 54.44, H : 5.24, N:9.12

6.3. Crystallization and crystallographic data

6.3.1. General condition and method

The solvents involving in crystallization are analytical reagents and used without purification:

Ethanol (Aldrich -99.8%)

Methanol (Aldrich-99.8%)

Chloroform (Fluka-99%)

Dichloromethane (Fluka-99.5%)

1,2-Dichloroethane (Aldrich-99.5%)

Dimethylsulfoxide (Fluka-99.5%)

1,1,2,2-tetrachloroethane (Aldrich-99.5%)

General method for the crystallization (Figure 6-1): In a crystallization tube (height = 15 cm, diameter = 0.4 cm), slow diffusion of an ethanol (or methanol) solution (*ca.* 1 mL) of metal salt (5 mg) into the chloroform or 1,2-Dichloroethane or 1,1,2,2-tetrachloroethane or DMSO solution (1 mL) of the tectons (3 mg) with a buffered layer of DMSO (*ca.* 0.1 mL) or ethanol (*ca.* 0.1 mL) affords crystals after few days.

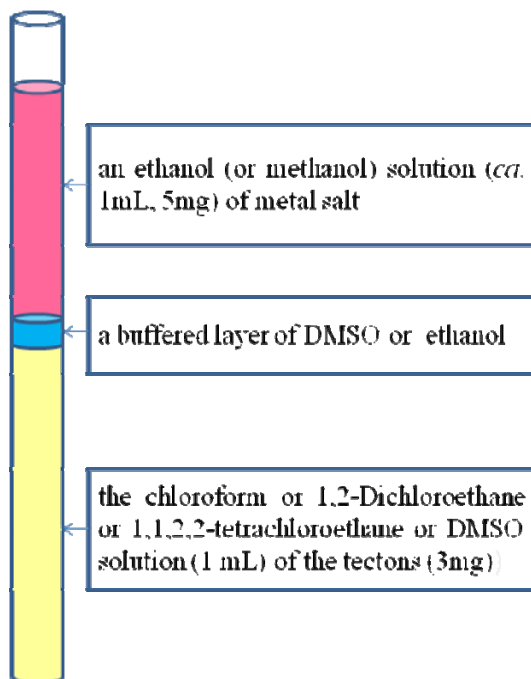
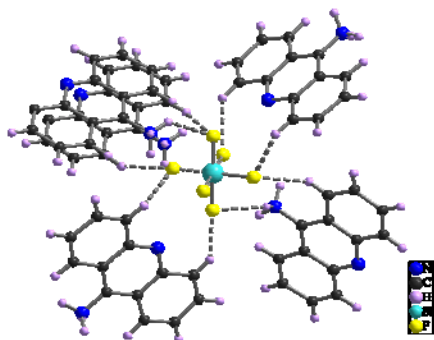


Figure 6-1: Schematic representation of crystallization method used.

6.3.2. The crystallographic data for the products for preparative experiments

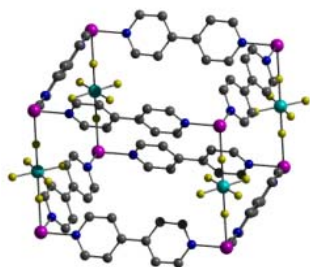


Product 1: A5·H₂SiF₆

Crystallization Method: In a crystallization tube (height = 15 cm, diameter = 0.4 cm), slow diffusion of an ethanol solution (*ca.* 1 mL, 5 mg) of ZnSiF₆·6H₂O into the chloroform solution (1 mL) of the 9-aminoacridine (A5, 3 mg) with a buffered layer of ethanol (*ca.* 0.1 mL) affords colorless crystals after few days.

Crystallographic data (Lab code: s1408):

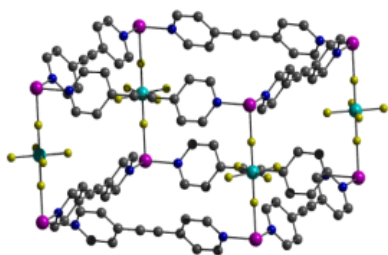
Empirical formula	2(C ₁₃ H ₁₁ N ₂), F ₆ Si	Absorption coefficient	0.174 mm ⁻¹
Formula weight	532.57	F(000)	548
Temperature	173(2) K	Theta range for data collection	1.28 to 27.47°.
Wavelength	0.71073 Å	Index ranges	-7<=h<=6, -17<=k<=17, -20<=l<=20
Crystal system	Monoclinic	Reflections collected	18910
Space group	P2(1)	Independent reflections	5180 [R(int) = 0.0354]
a(Å)	5.3977(4)	Completeness to theta	99.3 %
b(Å)	13.5424(14)	Absorption correction	Semi-empirical from equivalents
c(Å)	15.9120(17) Å	Max. and min. transmission	0.9914 and 0.9828
α(deg)	90	Refinement method	Full-matrix least-squares on F ²
β(deg)	92.136(2)	Data / restraints / parameters	5180 / 1 / 336
γ(deg)	90	Goodness-of-fit on F ²	1.051
V(Å ³)	1162.32(19) Å ³	Final R indices [I>2σ(I)]	R1 = 0.0437, wR2 = 0.1203
Z	2	R indices (all data)	R1 = 0.0508, wR2 = 0.1296
Color	colorless	Absolute structure parameter	0.14(14)
Crystal size	0.10 x 0.07 x 0.05 mm ³	Largest diff. peak and hole	0.427 and -0.431 e.Å ⁻³
Density (calculated)	1.522 mg/m ³		

6.3.3. *The crystallographic data for the networks from rigid organic tectons***Product 2: B2·ZnSiF₆**

Crystallization Method: In a crystallization tube (height = 15 cm, diameter = 0.4 cm), slow diffusion of an ethanol solution (*ca.* 1 mL, 5 mg) of ZnSiF₆·6H₂O into the chloroform solution (1 mL) of the 4,4-bipyridine (**B2**, 3 mg) with a buffered layer of ethanol (*ca.* 0.1 mL) affords colorless crystals after few days.

Crystallographic data (Lab code: s1267):

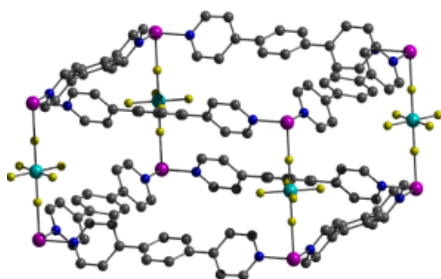
Empirical formula	4(C ₂₀ H ₁₆ F ₆ N ₄ SiZn), 36(H ₂ O)	Absorption coefficient	0.718 mm ⁻¹
Formula weight	2727.89	F(000)	1408
Temperature	173(2) K	Theta range for data collection	2.54 to 27.49°
Wavelength	0.71073 Å	Index ranges	-17<=h<=18, -20<=k<=11, -19<=l<=19
Crystal system	Tetragonal	Reflections collected	6674
Space group	I4/mcm	Independent reflections	1229 [R(int) = 0.0383]
a(Å)	16.0491(8)	Completeness to theta	98.8 %
b(Å)	16.0491(8)	Absorption correction	Semi-empirical from equivalents
c(Å)	15.3683(16)	Max. and min. transmission	0.9582 and 0.9188
α(deg)	90	Refinement method	Full-matrix least-squares on F ²
β(deg)	90	Data / restraints / parameters	1229 / 0 / 70
γ(deg)	90	Goodness-of-fit on F ²	1.141
V(Å ³)	3958.5(5) Å ³	Final R indices [I>2σ(I)]	R1 = 0.0982, wR2 = 0.2976
Z	1	R indices (all data)	R1 = 0.1193, wR2 = 0.3261
Color	colorless	Largest diff. peak and hole	1.882 and -1.640 e.Å ⁻³
Crystal size	0.12 x 0.08 x 0.06 mm ³		
Density (calculated)	1.144 mg/m ³		

**Product 3: B3·ZnSiF₆**

Crystallization Method: In a crystallization tube (height = 15 cm, diameter = 0.4 cm), slow diffusion of an ethanol solution (*ca.* 1 mL, 5 mg) of ZnSiF₆·6H₂O into the chloroform solution (1 mL) of the 1,2-di(pyridin-4-yl)ethyne (**B3**, 3 mg) with a buffered layer of ethanol (*ca.* 0.1 mL) affords colorless crystals after few days.

Crystallographic data (Lab code: s1268):

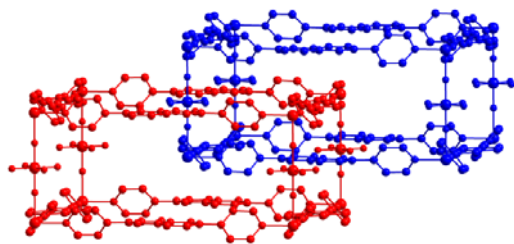
Empirical formula	C ₂₄ H ₁₆ F ₆ N ₄ SiZn·3(CHCl ₃)	Absorption coefficient	0.898 mm ⁻¹
Formula weight	925.97	F(000)	1840
Temperature	173(2) K	Theta range for data collection	1.47 to 27.59°
Wavelength	0.71073 Å	Index ranges	-25 ≤ h ≤ 25, -22 ≤ k ≤ 25, -18 ≤ l ≤ 19
Crystal system	Tetragonal	Reflections collected	22910
Space group	I4/mcm	Independent reflections	1813 [R(int) = 0.0852]
a(Å)	19.5940(3)	Completeness to theta	99.3 %
b(Å)	19.5940(3)	Absorption correction	Semi-empirical from equivalents
c(Å)	15.0666(5)	Max. and min. transmission	0.9398 and 0.8999
α(deg)	90	Refinement method	Full-matrix least-squares on F ²
β(deg)	90	Data / restraints / parameters	1813 / 3 / 75
γ(deg)	90	Goodness-of-fit on F ²	1.214
V(Å ³)	5784.4(2)	Final R indices [I > 2σ(I)]	R1 = 0.1100, wR2 = 0.2972
Z	4	R indices (all data)	R1 = 0.1511, wR2 = 0.3005
Color	colorless	Largest diff. peak and hole	1.428 and -0.912 e.Å ⁻³
Crystal size	0.12 x 0.10 x 0.07 mm ³		
Density (calculated)	1.063 mg/m ³		

**Product 4: B4·ZnSiF₆**

Crystallization Method: In a crystallization tube (height = 15 cm, diameter = 0.4 cm), slow diffusion of an ethanol solution (*ca.* 1 mL, 5 mg) of ZnSiF₆·6H₂O into the chloroform solution (1 mL) of the 1,4-bis(4-pyridyl)benzene (**B4**, 3 mg) with a buffered layer of ethanol (*ca.* 0.1 mL) affords colorless crystals after few days.

Crystallographic data (Lab code: s1215):

Empirical formula	4(C ₃₂ H ₂₄ FN ₄ SiZn)· 8(CHCl ₃)·H ₂ O	Absorption coefficient	0.605 mm ⁻¹
Formula weight	3787.12	F(000)	1912
Temperature	173(2) K	Theta range for data collection	1.31 to 27.49°
Wavelength	0.71073 Å	Index ranges	-11 ≤ h ≤ 28, -28 ≤ k ≤ 27, -7 ≤ l ≤ 19
Crystal system	Tetragonal	Reflections collected	10236
Space group	I4/mcm	Independent reflections	2262 [R(int) = 0.1045]
a(Å)	22.0593(13)	Completeness to theta	99.1 %
b(Å)	22.0593(13)	Absorption correction	Semi-empirical from equivalents
c(Å)	15.0937(18)	Max. and min. transmission	0.9762 and 0.9646
α(deg)	90	Refinement method	Full-matrix least-squares on F ²
β(deg)	90	Data / restraints / parameters	2262 / 2 / 90
γ(deg)	90	Goodness-of-fit on F ²	1.261
V(Å ³)	7344.8(11) Å ³	Final R indices [I > 2σ(I)]	R1 = 0.1001, wR2 = 0.3255
Z	1	R indices (all data)	R1 = 0.1669, wR2 = 0.3575
Color	colorless	Extinction coefficient	0.0106(19)
Crystal size	0.06 x 0.06 x 0.04 mm ³	Largest diff. peak and hole	1.460 and -0.859 e.Å ⁻³
Density (calculated)	0.856 mg/m ³		

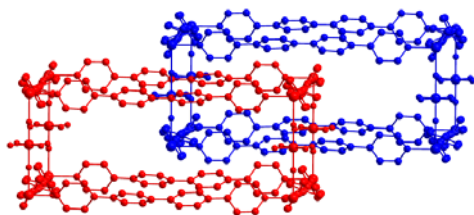


Product 5: B5·ZnSiF₆

Crystallization Method: In a crystallization tube (height = 15 cm, diameter = 0.4 cm), slow diffusion of an ethanol solution (*ca.* 1 mL, 5 mg) of ZnSiF₆·6H₂O into the DMSO solution (1 mL) of the 2,6-bis(4-pyridyl)naphthalene (**B5**, 3 mg) with a buffered layer of ethanol (*ca.* 0.1 mL) affords colorless crystals after few days.

Crystallographic data (Lab code: s1204):

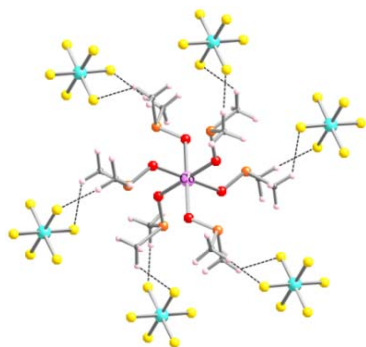
Empirical formula	C ₄₀ H ₂₈ F ₆ N ₄ SiZn·2(C ₂ H ₆ OS)·C ₂ H ₆ O	Absorption coefficient	0.695 mm ⁻¹
Formula weight	974.45	F(000)	2016
Temperature	173(2) K	Theta range for data collection	2.90 to 27.54°
Wavelength	0.71073 Å	Index ranges	-23 ≤ h ≤ 23, -23 ≤ k ≤ 21, -19 ≤ l ≤ 19
Crystal system	Tetragonal	Reflections collected	61009
Space group	P4/ncc	Independent reflections	2759 [R(int) = 0.0547]
a(Å)	17.7892(3)	Completeness to theta	99.9 %
b(Å)	17.7892(3)	Absorption correction	Semi-empirical from equivalents
c(Å)	15.0473(3)	Max. and min. transmission	0.9150 and 0.872
α(deg)	90	Refinement method	Full-matrix least-squares on F ²
β(deg)	90	Data / restraints / parameters	2759 / 5 / 170
γ(deg)	90	Goodness-of-fit on F ²	1.064
V(Å ³)	4761.80(15) Å ³	Final R indices [I > 2σ(I)]	R1 = 0.0663, wR2 = 0.1993
Z	4	R indices (all data)	R1 = 0.0776, wR2 = 0.2118
Color	colorless	Largest diff. peak and hole	1.057 and -1.075 e.Å ⁻³
Crystal size	0.15 x 0.18 x 0.13 mm ³		
Density (calculated)	1.359 mg/m ³		

**Product 6: B6·ZnSiF₆**

Crystallization Method: In a crystallization tube (height = 15 cm, diameter = 0.4 cm), slow diffusion of an ethanol solution (*ca.* 1 mL, 5 mg) of ZnSiF₆·6H₂O into 1,1,2,2-tetrachloroethane solution (1 mL) of the 4,4'-bis(4-pyridyl)biphenyl (**B6**, 3 mg) with a buffered layer of ethanol (*ca.* 0.1 mL) affords colorless crystals after few days.

Crystallographic data (Lab code: s1257):

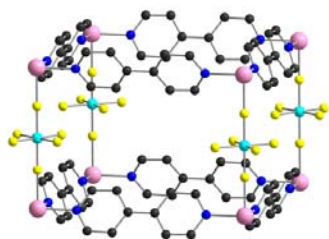
Empirical formula	C ₄₄ H ₃₂ F ₆ N ₄ SiZn·4(C ₂ H ₂ Cl ₄)	Absorption coefficient	1.189 mm ⁻¹
Formula weight	1495.54	F(000)	3000
Temperature	173(2) K	Theta range for data collection	2.04 to 27.47°
Wavelength	0.71073 Å	Index ranges	-12 ≤ h ≤ 25, -16 ≤ k ≤ 23, -10 ≤ l ≤ 19
Crystal system	Tetragonal	Reflections collected	15382
Space group	P4/ncc	Independent reflections	3429 [R(int) = 0.0458]
a(Å)	19.9188(3)	Completeness to theta	98.4 %
b(Å)	19.9188(3)	Absorption correction	Semi-empirical from equivalents
c(Å)	15.2892(6)	Max. and min. transmission	0.9005 and 0.8705
α(deg)	90	Refinement method	Full-matrix least-squares on F ²
β(deg)	90	Data / restraints / parameters	3429 / 0 / 184
γ(deg)	90	Goodness-of-fit on F ²	1.065
V(Å ³)	6066.1(3) Å ³	Final R indices [I > 2σ(I)]	R1 = 0.0537, wR2 = 0.1370
Z	4	R indices (all data)	R1 = 0.0862, wR2 = 0.1700
Color	colorless	Largest diff. peak and hole	1.071 and -0.606 e.Å ⁻³
Crystal size	0.12 x 0.09 x 0.09 mm ³		
Density (calculated)	1.638 mg/m ³		

**Product 7:** CoSiF₆·6DMSO

Crystallization Method: In a crystallization tube (height = 15 cm, diameter = 0.4 cm), slow diffusion of a methanol solution (*ca.* 1 mL, 3 mg) of CoSiF₆·6H₂O into the 1,2-Dichloroethane solution (1 mL) of the 4,4-bipyridine (**B2**, 3 mg) with a buffered layer of DMSO (*ca.* 0.1 mL) affords red crystals after few days.

Crystallographic data (Lab code: s1686):

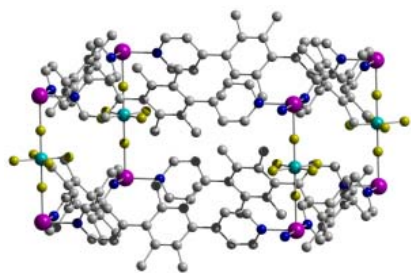
Empirical formula	C ₁₄ H ₄₄ CoF ₆ O ₈ S ₆ Si	Absorption coefficient	1.052 mm ⁻¹
Formula weight	733.87	F(000)	383
Temperature	173(2) K	Theta range for data collection	2.23 to 27.48°
Wavelength	0.71073 Å	Index ranges	-12 ≤ h ≤ 12, -12 ≤ k ≤ 9, -12 ≤ l ≤ 9
Crystal system	Rhombohedral	Reflections collected	7560
Space group	R-3	Independent reflections	1207 [R(int) = 0.0236]
a(Å)	9.32630(10)	Completeness to theta	100.0 %
b(Å)	9.32630(10)	Absorption correction	None
c(Å)	9.32630(10)	Max. and min. transmission	0.9021 and 0.8754
α(deg)	81.3960(10)	Refinement method	Full-matrix least-squares on F ²
β(deg)	81.3960(10)	Data / restraints / parameters	1207 / 0 / 72
γ(deg)	81.3960(10)	Goodness-of-fit on F ²	1.093
V(Å ³)	786.301(15) Å ³	Final R indices [I > 2σ(I)]	R1 = 0.0209, wR2 = 0.0556
Z	1	R indices (all data)	R1 = 0.0222, wR2 = 0.0565
Color	red	Largest diff. peak and hole	0.221 and -0.263 e.Å ⁻³
Crystal size	0.13 x 0.12 x 0.10 mm ³		
Density (calculated)	1.550 mg/m ³		

**Product 8: B2·CoSiF₆**

Crystallization Method: In a crystallization tube (height = 15 cm, diameter = 0.4 cm), slow diffusion of an ethanol solution (*ca.* 1 mL, 3 mg) of CoSiF₆·6H₂O into the chloroform solution (1 mL) of the 4,4-bipyridine (**B2**, 3 mg) with a buffered layer of ethanol (*ca.* 0.1 mL) affords red crystals after few days.

Crystallographic data (Lab code: s1698):

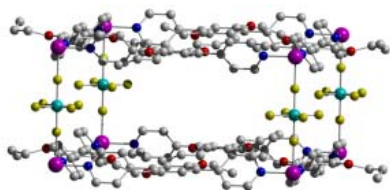
Empirical formula	C ₄₀ H ₃₂ Co ₂ F ₁₂ N ₈ Si ₂	Absorption coefficient	0.508 mm ⁻¹
Formula weight	1026.78	F(000)	1036
Temperature	173(2) K	Theta range for data collection	2.54 to 27.55°
Wavelength	0.71073 Å	Index ranges	0 ≤ h ≤ 14, 0 ≤ k ≤ 20, 0 ≤ l ≤ 19
Crystal system	Tetragonal	Reflections collected	1225
Space group	I4/mcm	Independent reflections	5690 [R(int) = 0.0560]
a(Å)	16.0244(6)	Completeness to theta	99.0 %
b(Å)	16.0244(6)	Absorption correction	Semi-empirical from equivalents
c(Å)	15.1565(12)	Max. and min. transmission	0.9750 and 0.9509
α(deg)	90	Refinement method	Full-matrix least-squares on F ²
β(deg)	90	Data / restraints / parameters	1225 / 0 / 42
γ(deg)	90	Goodness-of-fit on F ²	1.129
V(Å ³)	3891.9(4) Å ³	Final R indices [I > 2σ(I)]	R1 = 0.0714, wR2 = 0.1940
Z	2	R indices (all data)	R1 = 0.0911, wR2 = 0.2006
Color	red	Largest diff. peak and hole	1.156 and -0.890 e.Å ⁻³
Crystal size	0.10 x 0.06 x 0.05 mm ³		
Density (calculated)	0.876 mg/m ³		

**Product 9: C₂·ZnSiF₆**

Crystallization Method: In a crystallization tube (height = 15 cm, diameter = 0.4 cm), slow diffusion of an ethanol solution (*ca.* 1 mL, 5 mg) of ZnSiF₆·6H₂O into the chloroform solution (1 mL) of the 2,5-dimethyl-1,4-bis(4-pyridyl)benzene (**C2**, 3 mg) with a buffered layer of ethanol (*ca.* 0.1 mL) affords colorless crystals after few days.

Crystallographic data (Lab code: s1316):

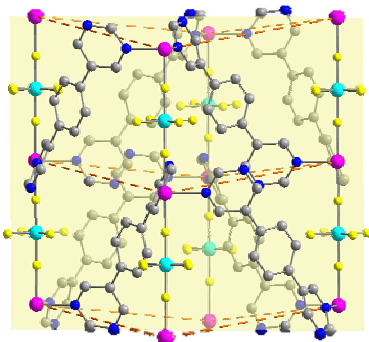
Empirical formula	C ₃₆ H ₃₂ F ₆ N ₄ SiZn	Absorption coefficient	0.379 mm ⁻¹
Formula weight	728.12	F(000)	1496
Temperature	173(2) K	Theta range for data collection	1.30 to 27.72°
Wavelength	0.71073 Å	Index ranges	0 ≤ h ≤ 20, 0 ≤ k ≤ 28, 0 ≤ l ≤ 19
Crystal system	Tetragonal	Reflections collected	26661
Space group	I4/mcm	Independent reflections	2319 [R(int) = 0.0400]
a(Å)	22.0788(13)	Completeness to theta	99.4 %
b(Å)	22.0788(13)	Absorption correction	Semi-empirical from equivalents
c(Å)	15.119(2)	Max. and min. transmission	0.9776 and 0.9630
α(deg)	90	Refinement method	Full-matrix least-squares on F ²
β(deg)	90	Data / restraints / parameters	2319 / 0 / 79
γ(deg)	90	Goodness-of-fit on F ²	1.044
V(Å ³)	7370.2(13) Å ³	Final R indices [I > 2σ(I)]	R1 = 0.0764, wR2 = 0.1931
Z	4	R indices (all data)	R1 = 0.1079, wR2 = 0.2022
Color	colorless	Largest diff. peak and hole	1.367 and -0.466 e.Å ⁻³
Crystal size	0.10 x 0.08 x 0.06 mm ³		
Density (calculated)	0.656 mg/m ³		

Product 10: C4·ZnSiF₆

Crystallization Method: In a crystallization tube (height = 15 cm, diameter = 0.4 cm), slow diffusion of an ethanol solution (*ca.* 1 mL, 5 mg) of ZnSiF₆·6H₂O into the chloroform solution (1 mL) of the 2,5-dipropoxyl-1,4-bis(4-pyridyl)benzene (**C4**, 3 mg) with a buffered layer of ethanol (*ca.* 0.1 mL) affords colorless crystals after few days.

Crystallographic data (Lab code: s1309):

Empirical formula	C ₄₄ H ₄₈ F ₆ N ₄ O ₄ SiZn	Absorption coefficient	0.391 mm ⁻¹
Formula weight	904.32	F(000)	1880
Temperature	173(2) K	Theta range for data collection	1.31 to 27.55°
Wavelength	0.71073 Å	Index ranges	-19 ≤ h ≤ 20, 0 ≤ k ≤ 28, 0 ≤ l ≤ 19
Crystal system	Tetragonal	Reflections collected	32315
Space group	I4/m	Independent reflections	4433 [R(int) = 0.0594]
a(Å)	22.0582(2)	Completeness to theta	99.8 %
b(Å)	22.0582(2)	Absorption correction	Semi-empirical from equivalents
c(Å)	15.1797(3)	Max. and min. transmission	0.9694 and 0.9546
α(deg)	90	Refinement method	Full-matrix least-squares on F ²
β(deg)	90	Data / restraints / parameters	4433 / 0 / 132
γ(deg)	90	Goodness-of-fit on F ²	1.132
V(Å ³)	7385.90(17) Å ³	Final R indices [I > 2σ(I)]	R1 = 0.0784, wR2 = 0.2572
Z	4	R indices (all data)	R1 = 0.0945, wR2 = 0.2716
Color	colorless	Largest diff. peak and hole	1.694 and -0.988 e.Å ⁻³
Crystal size	0.12 x 0.09 x 0.08 mm ³		
Density (calculated)	0.813 mg/m ³		

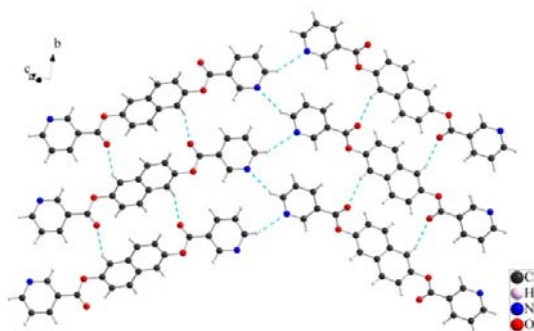
**Product 11: D2·ZnSiF₆**

Crystallization Method: In a crystallization tube (height = 15 cm, diameter = 0.4 cm), slow diffusion of an ethanol solution (*ca.* 1 mL, 5 mg) of ZnSiF₆·6H₂O into the 1,2-Dichloroethane solution (1 mL) of the 1, 4-bis(3,5-pyrimidyl)benzene (**D2**, 3 mg) with a buffered layer of ethanol (*ca.* 0.1 mL) affords colorless crystals after few days.

Crystallographic data (Lab code: s1650):

Empirical formula	C ₂₈ H ₂₀ F ₆ N ₈ SiZn·3(C ₂ H ₄ Cl ₂)	Absorption coefficient	1.137
Formula weight	972.84	F(000)	1968
Temperature	173(2) K	Theta range for data collection	2.54-27.52°
Wavelength	0.71073 Å	Index ranges	-20 ≤ h ≤ 19, -18 ≤ k ≤ 18, -18 ≤ l ≤ 19
Crystal system	Tetragonal	Reflections collected	19668
Space group	P4/ncc	Independent reflections	2253 [R(int) = 0.0244]
a(Å)	16.0415(2)	Completeness to theta	99.6 %
b(Å)	16.0415(2)	Absorption correction	Semi-empirical from equivalents
c(Å)	15.1959(3)	Max. and min. transmission	0.9145 and 0.9453
α(deg)	90	Refinement method	Full-matrix least-squares on F ²
β(deg)	90	Data / restraints / parameters	2092 / 0 / 135
γ(deg)	90	Goodness-of-fit on F ²	1.097
V(Å ³)	3910.36(10)	Final R indices [I > 2σ(I)]	R1 = 0.0620, wR2 = 0.1786
Z	4	R indices (all data)	R1 = 0.0655, wR2 = 0.1824
Color	colorless	Largest diff. peak and hole	0.786 and -2.178 e.Å ⁻³
Crystal size	0.08x 0.07 x 0.05 mm ³		
Density (calculated)	1.652 mg/m ³		

6.3.4. The crystallographic data for the networks from semi-rigid organic tectons



Product 12: E2

Crystallization Method: evaporation of the $\text{CHCl}_3/\text{EtOH}$ solution of naphthalene-2,6-diyl dinicotinate (**E2**, 5 mg) at room temperature affords colorless crystals after few days.

Crystallographic data (Lab code: s1080):

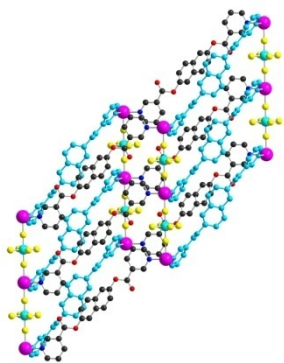
Empirical formula	$\text{C}_{22}\text{H}_{14}\text{N}_2\text{O}_4$	Absorption coefficient	0.101 mm^{-1}
Formula weight	370.35	F(000)	384
Temperature	173(2) K	Theta range for data collection	1.50 to 27.72°
Wavelength	0.71073 Å	Index ranges	$-17 \leq h \leq 7$, $-6 \leq k \leq 8$, $-10 \leq l \leq 12$
Crystal system	Monoclinic	Reflections collected	5383
Space group	P2(1)/c	Independent reflections	1958 [R(int) = 0.0640]
a(Å)	13.710(3)	Completeness to theta	97.6 %
b(Å)	6.306(2)	Absorption correction	Semi-empirical from equivalents
c(Å)	9.989(3)	Max. and min. transmission	0.9950 and 0.9940
α (deg)	90	Refinement method	Full-matrix least-squares on F^2
β (deg)	98.91(2)	Data / restraints / parameters	1958 / 0 / 127
γ (deg)	90	Goodness-of-fit on F^2	1.030
V(Å ³)	853.3(4) Å ³	Final R indices [$I > 2\sigma(I)$]	R1 = 0.0928, wR2 = 0.2101
Z	2	R indices (all data)	R1 = 0.1767, wR2 = 0.2545
Color	colorless	Largest diff. peak and hole	0.384 and -0.417 e.Å ⁻³
Crystal size	0.06 x 0.06 x 0.05 mm ³		
Density (calculated)	1.441 mg/m ³		

Product 13: E2·HBF₆

Crystallization Method: In a crystallization tube (height = 15 cm, diameter = 0.4 cm), slow diffusion of an ethanol solution (*ca.* 1 mL, 5 mg) of Fe(BF₄)₂ into the chloroform solution (1 mL) of the naphthalene-2,6-diyl dinicotinate (**E2**, 3 mg) with a buffered layer of ethanol (*ca.* 0.1 mL) affords colorless crystals after *ca.* one month.

Crystallographic data (Lab code: s1194):

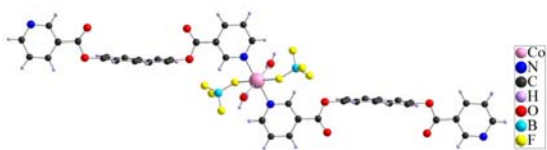
Empirical formula	C ₂₂ H ₁₆ N ₂ O ₄ ·2(BF ₄)	Absorption coefficient	0.151 mm ⁻¹
Formula weight	545.99	F(000)	552
Temperature	173(2) K	Theta range for data collection	2.25 to 27.54°
Wavelength	0.71073 Å	Index ranges	-8<=h<=8, -14<=k<=14, -19<=l<=18
Crystal system	Monoclinic	Reflections collected	8468
Space group	P2(1)/c	Independent reflections	2602 [R(int) = 0.0322]
a(Å)	6.7216(4)	Completeness to theta	99.4 %
b(Å)	11.5023(5)	Absorption correction	Semi-empirical from equivalents
c(Å)	15.0186(7)	Max. and min. transmission	0.9851 and 0.9792
α(deg)	90	Refinement method	Full-matrix least-squares on F ²
β(deg)	102.078(2)	Data / restraints / parameters	2602 / 0 / 172
γ(deg)	90	Goodness-of-fit on F ²	1.079
V(Å ³)	1135.44(10) Å ³	Final R indices [I>2σ(I)]	R1 = 0.0471, wR2 = 0.0868
Z	2	R indices (all data)	R1 = 0.0697, wR2 = 0.1013
Color	colorless	Largest diff. peak and hole	0.269 and -0.257 e.Å ⁻³
Crystal size	0.14 x 0.12 x 0.10 mm ³		
Density (calculated)	1.597 mg/m ³		

**Product 14: E2·ZnSiF₆**

Crystallization Method: In a crystallization tube (height = 15 cm, diameter = 0.4 cm), slow diffusion of an ethanol solution (*ca.* 1 mL, 5 mg) of Zn(BF₄)₂ into the chloroform solution (1 mL) of the naphthalene-2,6-diyl dinicotinate (**E2**, 3 mg) with a buffered layer of ethanol (*ca.* 0.1 mL) affords colorless crystals after *ca.* one month.

Crystallographic data (Lab code: s1073):

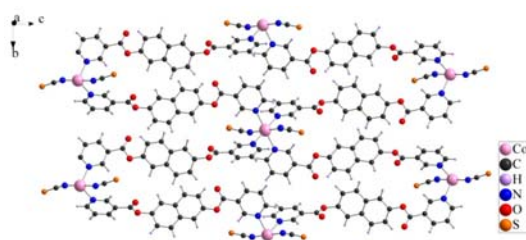
Empirical formula	C ₄₄ H ₂₈ F ₆ N ₄ O ₈ SiZn·CH ₂ Cl ₂ ·H ₂ O	Absorption coefficient	0.781 mm ⁻¹
Formula weight	1051.11	F(000)	534
Temperature	173(2) K	Theta range for data collection	1.56 to 27.52°
Wavelength	0.71073 Å	Index ranges	-10 ≤ h ≤ 10, -14 ≤ k ≤ 14, -17 ≤ l ≤ 17
Crystal system	Triclinic	Reflections collected	18893
Space group	P-1	Independent reflections	5123 [R(int) = 0.0264]
a(Å)	7.7996(4)	Completeness to theta	99.1 %
b(Å)	11.1030(5)	Absorption correction	Semi-empirical from equivalents
c(Å)	13.5616(7)	Max. and min. transmission	0.9121 and 0.8722
α(deg)	85.018(2)	Refinement method	Full-matrix least-squares on F ²
β(deg)	74.024(2)	Data / restraints / parameters	5123 / 2 / 318
γ(deg)	83.203(2)	Goodness-of-fit on F ²	1.070
V(Å ³)	1119.31(10) Å ³	Final R indices [I > 2σ(I)]	R1 = 0.0619, wR2 = 0.1900
Z	1	R indices (all data)	R1 = 0.0794, wR2 = 0.2080
Color	colorless	Largest diff. peak and hole	1.664 and -0.731 e.Å ⁻³
Crystal size	0.18 x 0.14 x 0.12 mm ³		
Density (calculated)	1.559 mg/m ³		

Product 15: E2·Co(BF₄)₂

Crystallization Method: In a crystallization tube (height = 15 cm, diameter = 0.4cm), slow diffusion of an ethanol solution (*ca.* 1 mL, 5 mg) of Co(BF₄)₂ into the chloroform solution (1 mL) of the naphthalene-2,6-diyldinicotinate (**E2**, 3 mg) with a buffered layer of ethanol (*ca.* 0.1 mL) affords purple crystals after few days.

Crystallographic data (Lab code: s1089):

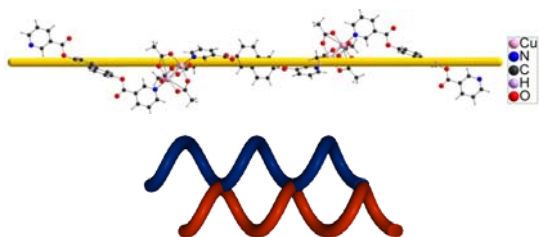
Empirical formula	C ₄₄ H ₃₂ B ₂ CoF ₈ N ₄ O ₁₀	Absorption coefficient	0.522 mm ⁻¹
Formula weight	1009.29	F(000)	513
Temperature	173(2) K	Theta range for data collection	2.73 to 28.50°
Wavelength	0.71073 Å	Index ranges	-10 ≤ h ≤ 10, -8 ≤ k ≤ 10, -26 ≤ l ≤ 25
Crystal system	Triclinic	Reflections collected	7992
Space group	P-1	Independent reflections	5078 [R(int) = 0.0271]
a(Å)	7.4551(2)	Completeness to theta	97.8 %
b(Å)	7.5910(3)	Absorption correction	Semi-empirical from equivalents
c(Å)	18.5773(6)	Max. and min. transmission	0.9694 and 0.9497
α(deg)	82.541(2)	Refinement method	Full-matrix least-squares on F ²
β(deg)	84.273(2)	Data / restraints / parameters	5078 / 1 / 317
γ(deg)	81.838(3)	Goodness-of-fit on F ²	1.242
V(Å ³)	1028.31(6) Å ³	Final R indices [I > 2σ(I)]	R1 = 0.0822, wR2 = 0.2090
Z	1	R indices (all data)	R1 = 0.1329, wR2 = 0.2357
Color	purple	Largest diff. peak and hole	1.363 and -1.055 e.Å ⁻³
Crystal size	0.10 x 0.08 x 0.06 mm ³		
Density (calculated)	1.630 mg/m ³		

Product 16: E2·Co(SCN)₂

Crystallization Method: In a crystallization tube (height = 15 cm, diameter = 0.4cm), slow diffusion of an ethanol solution (*ca.* 1 mL, 5 mg) of Co(SCN)₂ into the chloroform solution (1 mL) of the naphthalene-2,6-diyl dinicotinate (**E2**, 3 mg) with a buffered layer of ethanol (*ca.* 0.1 mL) affords purple crystals after few days.

Crystallographic data (Lab code: s1221):

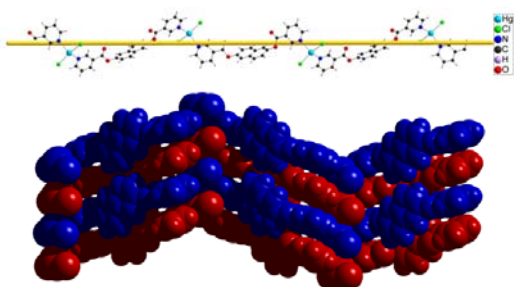
Empirical formula	C ₄₆ H ₂₈ CoN ₆ O ₈ S ₂	Absorption coefficient	0.582 mm ⁻¹
Formula weight	915.79	F(000)	938
Temperature	173(2) K	Theta range for data collection	1.61 to 27.00°
Wavelength	0.71073 Å	Index ranges	-11 ≤ h ≤ 20, -13 ≤ k ≤ 13, -16 ≤ l ≤ 16
Crystal system	Monoclinic	Reflections collected	10935
Space group	P2(1)/n	Independent reflections	4302 [R(int) = 0.0564]
a(Å)	16.7026(15)	Completeness to theta	96.1 %
b(Å)	10.1637(11)	Absorption correction	Semi-empirical from equivalents
c(Å)	13.6381(15)	Max. and min. transmission	0.9771 and 0.9659
α(deg)	90	Refinement method	Full-matrix least-squares on F ²
β(deg)	117.101(3)	Data / restraints / parameters	4302 / 14 / 220
γ(deg)	90	Goodness-of-fit on F ²	1.073
V(Å ³)	2061.0(4) Å ³	Final R indices [I > 2σ(I)]	R1 = 0.1293, wR2 = 0.3757
Z	2	R indices (all data)	R1 = 0.1941, wR2 = 0.4000
Color	purple	Largest diff. peak and hole	1.502 and -1.333 e.Å ⁻³
Crystal size	0.06 x 0.05 x 0.04 mm ³		
Density (calculated)	1.476 mg/m ³		

Product 17: E2·Cu(OAc)₂

Crystallization Method: In a crystallization tube (height = 15 cm, diameter = 0.4 cm), slow diffusion of an ethanol solution (*ca.* 1 mL, 5 mg) of Cu(OAc)₂ into the chloroform solution (1 mL) of the naphthalene-2,6-diyl dinicotinate (**E2**, 3 mg) with a buffered layer of ethanol (*ca.* 0.1 mL) affords blue crystals after few days.

Crystallographic data (Lab code: s1078):

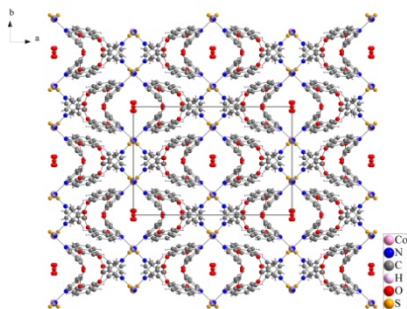
Empirical formula	2(C ₁₅ H ₁₃ CuNO ₆)·C ₂ H ₆ O	Absorption coefficient	1.396 mm ⁻¹
Formula weight	779.68	F(000)	1600
Temperature	173(2) K	Theta range for data collection	2.25 to 27.10°.
Wavelength	0.71073 Å	Index ranges	-26<=h<=24, -9<=k<=15, -11<=l<=18
Crystal system	Monoclinic	Reflections collected	6747
Space group	C2/c	Independent reflections	3501 [R(int) = 0.0385]
a(Å)	20.157(4)	Completeness to theta	100.0 %
b(Å)	12.194(3)	Absorption correction	Semi-empirical from equivalents
c(Å)	14.569(3)	Max. and min. transmission	0.8730 and 0.8394
α(deg)	90	Refinement method	Full-matrix least-squares on F ²
β(deg)	116.222(5)	Data / restraints / parameters	3501 / 1 / 222
γ(deg)	90	Goodness-of-fit on F ²	1.036
V(Å ³)	3212.6(12) Å ³	Final R indices [I>2σ(I)]	R1 = 0.0719, wR2 = 0.2075
Z	4	R indices (all data)	R1 = 0.1064, wR2 = 0.2398
Color	blue	Largest diff. peak and hole	1.530 and -1.292 e.Å ⁻³
Crystal size	0.13 x 0.12 x 0.10 mm ³		
Density (calculated)	1.612 mg/m ³		

**Product 18: E2·HgCl₂**

Crystallization Method: In a crystallization tube (height = 15 cm, diameter = 0.4 cm), slow diffusion of an ethanol solution (*ca.* 1 mL, 5 mg) of HgCl₂ into the chloroform solution (1 mL) of the naphthalene-2,6-diyl dinicotinate (**E2**, 3 mg) with a buffered layer of ethanol (*ca.* 0.1 mL) affords colorless crystals after few days.

Crystallographic data (Lab code: s1137):

Empirical formula	C ₂₂ H ₁₄ Cl ₂ HgN ₂ O ₄	Absorption coefficient	8.044 mm ⁻¹
Formula weight	641.84	F(000)	1224
Temperature	173(2) K	Theta range for data collection	2.68 to 27.81°
Wavelength	0.71073 Å	Index ranges	-9<=h<=9, -10<=k<=10, -45<=l<=44
Crystal system	Monoclinic	Reflections collected	20237
Space group	P2(1)/n	Independent reflections	4643 [R(int) = 0.0846]
a(Å)	7.4417(4)	Completeness to theta	98.7 %
b(Å)	7.7800(4)	Absorption correction	Semi-empirical from equivalents
c(Å)	34.5453(16)	Max. and min. transmission	0.6892 and 0.3783
α(deg)	90	Refinement method	Full-matrix least-squares on F ²
β(deg)	96.18(1)	Data / restraints / parameters	4643 / 0 / 280
γ(deg)	90	Goodness-of-fit on F ²	1.034
V(Å ³)	1988.41(17) Å ³	Final R indices [I>2σ(I)]	R1 = 0.0361, wR2 = 0.0639
Z	4	R indices (all data)	R1 = 0.0698, wR2 = 0.0717
Color	colorless	Largest diff. peak and hole	1.124 and -1.364 e.Å ⁻³
Crystal size	0.15 x 0.05 x 0.05 mm ³		
Density (calculated)	2.144 mg/m ³		

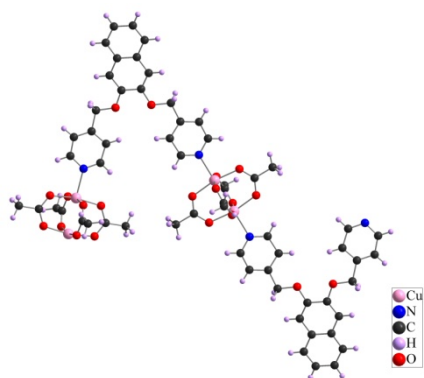


Product 19: E8·Co(SCN)₂

Crystallization Method: In a crystallization tube (height = 15 cm, diameter = 0.4 cm), slow diffusion of an ethanol solution (*ca.* 1 mL, 5 mg) of Co(SCN)₂ into the chloroform solution (1 mL) of the naphthalene-2,3-diyl dinicotinate (**E8**, 3 mg) with a buffered layer of ethanol (*ca.* 0.1 mL) affords purple crystals after few days.

Crystallographic data (Lab code: s1097):

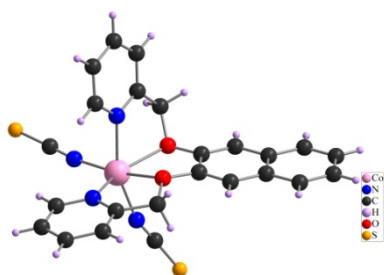
Empirical formula	C ₄₆ H ₂₈ CoN ₆ O ₈ S ₂ ·3(H ₂ O)	Absorption coefficient	0.552 mm ⁻¹
Formula weight	969.84	F(000)	1996
Temperature	173(2) K	Theta range for data collection	1.70 to 27.52°
Wavelength	0.71073 Å	Index ranges	-28<=h<=19, -18<=k<=18, -18<=l<=18
Crystal system	Monoclinic	Reflections collected	17739
Space group	C2/c	Independent reflections	5065 [R(int) = 0.0345]
a(Å)	21.580(3)	Completeness to theta	99.7 %
b(Å)	14.5260(9)	Absorption correction	Semi-empirical from equivalents
c(Å)	14.3519(17)	Max. and min. transmission	0.9676 and 0.9267
α(deg)	90	Refinement method	Full-matrix least-squares on F ²
β(deg)	100.726(2)	Data / restraints / parameters	5065 / 0 / 300
γ(deg)	90	Goodness-of-fit on F ²	1.047
V(Å ³)	4420.4(8) Å ³	Final R indices [I>2σ(I)]	R1 = 0.0604, wR2 = 0.2098
Z	4	R indices (all data)	R1 = 0.0810, wR2 = 0.2306
Color	purple	Largest diff. peak and hole	1.273 and -0.758 e.Å ⁻³
Crystal size	0.14 x 0.10 x 0.06 mm ³		
Density (calculated)	1.457 mg/m ³		

**Product 20: E9·Cu(OAc)₂**

Crystallization Method: In a crystallization tube (height = 15 cm, diameter = 0.4cm), slow diffusion of an ethanol solution (*ca.* 1 mL, 5 mg) of Cu(OAc)₂ into the chloroform solution (1 mL) of the 2,3-bis(pyridin-4-ylmethoxy)naphthalene (**E9**, 3 mg) with a buffered layer of ethanol (*ca.* 0.1 mL) affords blue crystals after few days.

Crystallographic data (Lab code: s1110):

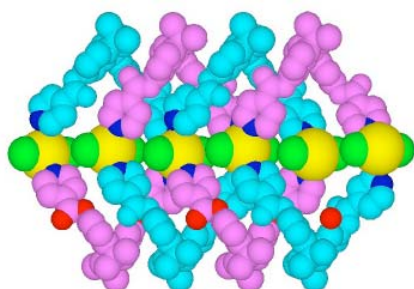
Empirical formula	C ₃₀ H ₃₀ Cu ₂ N ₂ O ₁₀ ·1.5(H ₂ O)	Absorption coefficient	1.238 mm ⁻¹
Formula weight	740.66	F(000)	762
Temperature	173(2) K	Theta range for data collection	2.65 to 27.65°.
Wavelength	0.71073 Å	Index ranges	-10<=h<=10, -18<=k<=18, -19<=l<=19
Crystal system	Triclinic	Reflections collected	21364
Space group	P-1	Independent reflections	8120 [R(int) = 0.0924]
a(Å)	8.088(2)	Completeness to theta	96.6 %
b(Å)	14.618(5)	Absorption correction	Semi-empirical from equivalents
c(Å)	15.431(5)	Max. and min. transmission	0.9407 and 0.8862
α(deg)	93.226(16)	Refinement method	Full-matrix least-squares on F ²
β(deg)	91.82(2)	Data / restraints / parameters	8120 / 0 / 428
γ(deg)	98.21(2)	Goodness-of-fit on F ²	1.000
V(Å ³)	1801.5(10) Å ³	Final R indices [I>2σ(I)]	R1 = 0.1034, wR2 = 0.2512
Z	2	R indices (all data)	R1 = 0.2667, wR2 = 0.3180
Color	blue	Largest diff. peak and hole	1.158 and -1.326 e.Å ⁻³
Crystal size	0.10 x 0.06 x 0.05 mm ³		
Density (calculated)	1.365 mg/m ³		

**Product 21: E10·Co(SCN)₂**

Crystallization Method: In a crystallization tube (height = 15 cm, diameter = 0.4cm), slow diffusion of an ethanol solution (*ca.* 1 mL, 5 mg) of Co(SCN)₂ into the chloroform solution (1 mL) of 2,3-bis(pyridin-2-ylmethoxy)naphthalene (**E10**, 3 mg) with a buffered layer of ethanol (*ca.* 0.1 mL) affords purple crystals after few days.

Crystallographic data (Lab code: s1086):

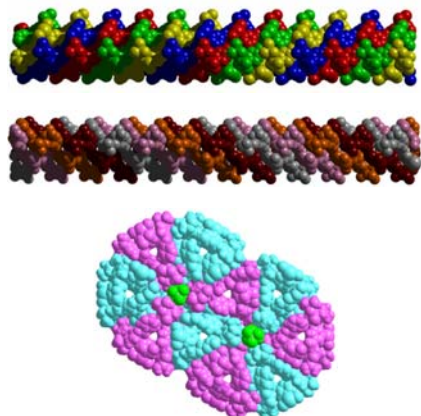
Empirical formula	C ₂₄ H ₁₈ CoN ₄ O ₂ S ₂	Absorption coefficient	0.940 mm ⁻¹
Formula weight	517.47	F(000)	530
Temperature	173(2) K	Theta range for data collection	2.84 to 27.53°
Wavelength	0.71073 Å	Index ranges	-10<=h<=10, -13<=k<=13, -19<=l<=19
Crystal system	Triclinic	Reflections collected	19681
Space group	P-1	Independent reflections	5314 [R(int) = 0.0295]
a(Å)	8.4246(3)	Completeness to theta	98.6 %
b(Å)	10.1647(3)	Absorption correction	Semi-empirical from equivalents
c(Å)	15.2104(4)	Max. and min. transmission	0.8719 and 0.8343
α(deg)	109.3951(9)	Refinement method	Full-matrix least-squares on F ²
β(deg)	93.8721(10)	Data / restraints / parameters	5314 / 0 / 298
γ(deg)	104.7862(10)	Goodness-of-fit on F ²	1.050
V(Å ³)	1171.24(6) Å ³	Final R indices [I>2σ(I)]	R1 = 0.0327, wR2 = 0.0763
Z	2	R indices (all data)	R1 = 0.0529, wR2 = 0.0814
Color	purple	Largest diff. peak and hole	0.332 and -0.411 e.Å ⁻³
Crystal size	0.20 x 0.16 x 0.15 mm ³		
Density (calculated)	1.467 mg/m ³		

**Product 22: F1·HgCl₂**

Crystallization Method: In a crystallization tube (height = 15 cm, diameter = 0.4cm), slow diffusion of an ethanol solution (*ca.* 1 mL, 5 mg) of HgCl₂ into the chloroform solution (1 mL) of 3,3,3',3'-tetramethyl-2,2',3,3'-tetrahydro-1,1'-spirobi[indene]-6,6'-diyldiisonicotinate (**F1**, 3 mg) with a buffered layer of ethanol (*ca.* 0.1 mL) affords colorless crystals after few days.

Crystallographic data (Lab code: s1512):

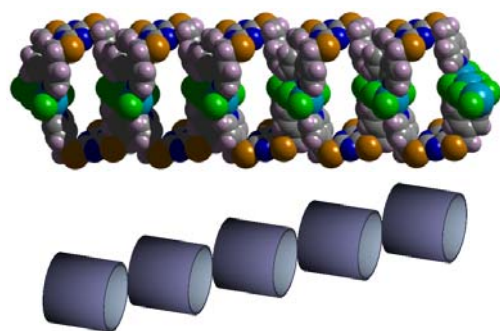
Empirical formula	C ₆₆ H ₆₀ Cl ₂ HgN ₄ O ₈	Absorption coefficient	2.822 mm ⁻¹
Formula weight	1308.67	F(000)	1324
Temperature	173(2) K	Theta range for data collection	1.59 to 27.58°
Wavelength	0.71073 Å	Index ranges	-17<=h<=17, -18<=k<=14, -22<=l<=22
Crystal system	Triclinic	Reflections collected	20466
Space group	P-1	Independent reflections	12910 [R(int) = 0.0379]
a(Å)	13.1808(12)	Completeness to theta	96.7 %
b(Å)	14.0766(12)	Absorption correction	Semi-empirical from equivalents
c(Å)	17.3666(15)	Max. and min. transmission	0.8489 and 0.7282
α(deg)	67.326(2)	Refinement method	Full-matrix least-squares on F ²
β(deg)	89.185(2)	Data / restraints / parameters	12910 / 0 / 732
γ(deg)	76.700(3)	Goodness-of-fit on F ²	1.062
V(Å ³)	2883.5(4) Å ³	Final R indices [I>2σ(I)]	R1 = 0.0622, wR2 = 0.1613
Z	2	R indices (all data)	R1 = 0.0888, wR2 = 0.1738
Color	colorless	Largest diff. peak and hole	1.543 and -0.920 e.Å ⁻³
Crystal size	0.12 x 0.07 x 0.06 mm ³		
Density (calculated)	1.507 mg/m ³		

**Product 23: F2·HgCl₂**

Crystallization Method: In a crystallization tube (height = 15 cm, diameter = 0.4 cm), slow diffusion of an ethanol solution (*ca.* 1 mL, 5 mg) of HgCl₂ into the chloroform solution (1 mL) of 3,3,3',3'-tetramethyl-2,2',3,3'-tetrahydro-1,1'-spirobi[indene]-6, 6'-diylidnicotinate (**F2**, 3 mg) with a buffered layer of ethanol (*ca.* 0.1 mL) affords colorless crystals after few days.

Crystallographic data (Lab code: s1570):

Empirical formula	6(C ₃₃ H ₃₀ Cl ₂ HgN ₂ O ₄)·2(CHCl ₃)·2(H ₂ O)	Absorption coefficient	4.878 mm ⁻¹
Formula weight	4983.25	F(000)	7344
Temperature	173(2) K	Theta range for data collection	2.04 to 27.54°
Wavelength	0.71073 Å	Index ranges	-50 ≤ h ≤ 52, -51 ≤ k ≤ 51, -14 ≤ l ≤ 12
Crystal system	Hexagonal	Reflections collected	120760
Space group	R-3c	Independent reflections	3864 [R(int) = 0.0305]
a(Å)	39.9988(10)	Completeness to theta	99.8 %
b(Å)	39.9988(10)	Absorption correction	Semi-empirical from equivalents
c(Å)	10.8667(3)	Max. and min. transmission	0.7925 and 0.6412
α(deg)	90	Refinement method	Full-matrix least-squares on F ²
β(deg)	90	Data / restraints / parameters	3864 / 0 / 207
γ(deg)	120	Goodness-of-fit on F ²	1.088
V(Å ³)	15056.4(7) Å ³	Final R indices [I > 2σ(I)]	R1 = 0.0285, wR2 = 0.0750
Z	3	R indices (all data)	R1 = 0.0414, wR2 = 0.0881
Color	colorless	Largest diff. peak and hole	2.182 and -0.931 e.Å ⁻³
Crystal size	0.10 x 0.06 x 0.05 mm ³		
Density (calculated)	1.649 mg/m ³		

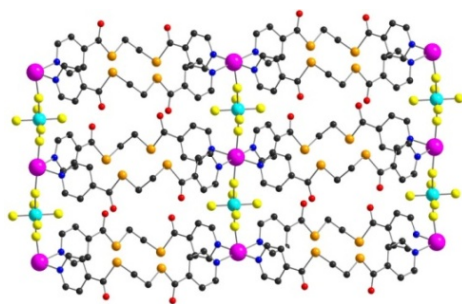
**Product 24:** G1·HgCl₂

Crystallization Method: In a crystallization tube (height = 15 cm, diameter = 0.4 cm), slow diffusion of an ethanol solution (*ca.* 1 mL, 5 mg) of HgCl₂ into the chloroform solution (1 mL) of 2,4,6-tris(pyridin-4-ylmethylthio)-1,3,5-triazine (**G1**, 3 mg) with a buffered layer of DMSO (*ca.* 0.1 mL) affords colorless crystals after few days.

Crystallographic data (Lab code: s1455):

Empirical formula	C ₄₂ H ₃₆ Cl ₆ Hg ₃ N ₁₂ S ₆ ·2(CHCl ₃)	Absorption coefficient	8.620 mm ⁻¹
Formula weight	1954.39	F(000)	926
Temperature	173(2) K	Theta range for data collection	2.54 to 27.58°
Wavelength	0.71073 Å	Index ranges	-12 ≤ h ≤ 12, -16 ≤ k ≤ 16, -17 ≤ l ≤ 17
Crystal system	Triclinic	Reflections collected	45474
Space group	P-1	Independent reflections	6699 [R(int) = 0.0465]
a(Å)	9.3686(2)	Completeness to theta	98.4 %
b(Å)	12.7382(2)	Absorption correction	Semi-empirical from equivalents
c(Å)	13.2586(3)	Max. and min. transmission	0.4794 and 0.3783
α(deg)	108.0051(9)	Refinement method	Full-matrix least-squares on F ²
β(deg)	95.7681(8)	Data / restraints / parameters	6699 / 0 / 349
γ(deg)	98.5890(10)	Goodness-of-fit on F ²	1.044
V(Å ³)	1469.70(5) Å ³	Final R indices [I > 2σ(I)]	R1 = 0.0324, wR2 = 0.0665
Z	1	R indices (all data)	R1 = 0.0448, wR2 = 0.0729
Color	colorless	Largest diff. peak and hole	1.411 and -1.244 e.Å ⁻³
Crystal size	0.14 x 0.10 x 0.10 mm ³		
Density (calculated)	2.208 mg/m ³		

6.3.5. The crystallographic data for the networks from flexible organic tectons

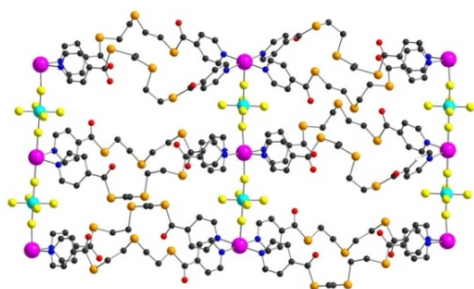


Product 25: H₄·ZnSiF₆

Crystallization Method: In a crystallization tube (height = 15 cm, diameter = 0.4 cm), slow diffusion of an ethanol solution (*ca.* 1 mL, 5 mg) of ZnSiF₆·6H₂O into the chloroform solution (1 mL) of the S,S'-ethane-1,2-diyl dipyridine-4-carbothioate (**H4**, 3 mg) with a buffered layer of ethanol (*ca.* 0.1 mL) affords colorless crystals after few days.

Crystallographic data (Lab code: s1286):

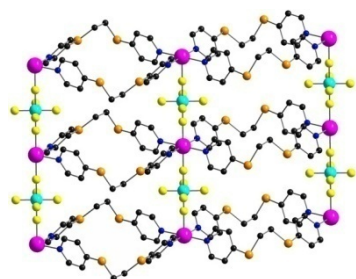
Empirical formula	C ₂₈ H ₂₄ F ₆ N ₄ O ₄ S ₄ SiZn·2(C ₂ H ₆ O) ·0.25(C ₄ H ₄ Cl ₁₂)	Absorption coefficient	0.888
Formula weight	921.96	F(000)	1876
Temperature	173(2) K	Theta range for data collection	1.71 to 27.51°
Wavelength	0.71073 Å	Index ranges	-29<=h<=20, -18<=k<=18, -14<=l<=19
Crystal system	Monoclinic	Reflections collected	15152
Space group	C2/c	Independent reflections	5237 [R(int) = 0.0413]
a(Å)	22.512(2)	Completeness to theta	98.6%
b(Å)	14.5274(17)	Absorption correction	Semi-empirical from equivalents
c(Å)	15.2352(16)	Max. and min. transmission	0.8784 and 0.9165
α(deg)	90	Refinement method	Full-matrix least-squares on F ²
β(deg)	112.227(3)	Data / restraints / parameters	5237 / 2 / 280
γ(deg)	90	Goodness-of-fit on F ²	1.020
V(Å ³)	4612.2(8)	Final R indices [I>2σ(I)]	R1 = 0.1157, wR2 = 0.3446
Z	4	R indices (all data)	R1 = 0.1365, wR2 = 0.3703
Color	colorless	Largest diff. peak and hole	1.313 and -0.816 e.Å ⁻³
Crystal size	0.15 x 0.12 x 0.10 mm ³		
Density (calculated)	1.328mg/m ³		

**Product 26: H5·ZnSiF₆**

Crystallization Method: In a crystallization tube (height = 15 cm, diameter = 0.4 cm), slow diffusion of an ethanol solution (*ca.* 1 mL, 5 mg) of ZnSiF₆·6H₂O into the chloroform solution (1 mL) of the S,S'-2,2'-thiobis(ethane-1,2-diyl) dipyridine-4-carbothioate (**H5**, 3 mg) with a buffered layer of ethanol (*ca.* 0.1 mL) affords colorless crystals after few days.

Crystallographic data (Lab code: s1290):

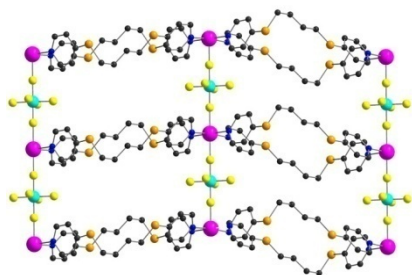
Empirical formula	C ₆₄ H ₆₄ F ₁₂ N ₈ O ₈ S ₁₂ Si ₂ Zn ₂	Absorption coefficient	0.728 mm ⁻¹
Formula weight	1872.87	F(000)	1912
Temperature	173(2) K	Theta range for data collection	1.37 to 27.68°
Wavelength	0.71073 Å	Index ranges	-17 ≤ h ≤ 17, -20 ≤ k ≤ 20, 0 ≤ l ≤ 37
Crystal system	Triclinic	Reflections collected	63726
Space group	P-1	Independent reflections	25498 [R(int) = 0.0811]
a(Å)	13.1804(4)	Completeness to theta	96.7 %
b(Å)	15.8350(5)	Absorption correction	Semi-empirical from equivalents
c(Å)	28.8368(8)	Max. and min. transmission	0.9374 and 0.9049
α(deg)	99.985(2)	Refinement method	Full-matrix least-squares on F ²
β(deg)	94.883(2)	Data / restraints / parameters	25498 / 4 / 950
γ(deg)	106.023(2)	Goodness-of-fit on F ²	1.004
V(Å ³)	5640.6(3)	Final R indices [I > 2σ(I)]	R1 = 0.0819, wR2 = 0.1862
Z	2	R indices (all data)	R1 = 0.1337, wR2 = 0.2060
Color	Colorless	Largest diff. peak and hole	2.241 and -1.286 e.Å ⁻³
Crystal size	0.14 x 0.12 x 0.09 mm ³		
Density (calculated)	1.103 mg/m ³		

**Product 27: H7·ZnSiF₆**

Crystallization Method: In a crystallization tube (height = 15 cm, diameter = 0.4cm), slow diffusion of an ethanol solution (*ca.* 1 mL, 5 mg) of ZnSiF₆·6H₂O into the chloroform solution (1 mL) of the 1,2-bis(pyridin-4-ylthio)ethane (**H7**, 3 mg) with a buffered layer of ethanol (*ca.* 0.1 mL) affords colorless crystals after few days.

Crystallographic data (Lab code: s1339):

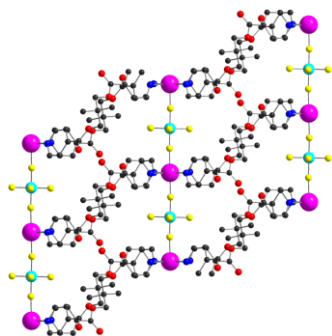
Empirical formula	C ₂₅ H ₂₅ Cl ₃ F ₆ N ₄ S ₄ SiZn	Absorption coefficient	1.210 mm ⁻¹
Formula weight	823.54	F(000)	1664
Temperature	173(2) K	Theta range for data collection	2.88 to 27.56°.
Wavelength	0.71073 Å	Index ranges	-28 ≤ h ≤ 28, -9 ≤ k ≤ 9, -31 ≤ l ≤ 31
Crystal system	Monoclinic	Reflections collected	31145
Space group	C2/c	Independent reflections	4174 [R(int) = 0.0612]
a(Å)	21.6873(6)	Completeness to theta	99.4 %
b(Å)	7.6211(2)	Absorption correction	Semi-empirical from equivalents
c(Å)	24.1630(7)	Max. and min. transmission	0.9420 and 0.8886
α(deg)	90	Refinement method	Full-matrix least-squares on F ²
β(deg)	114.128(3)	Data / restraints / parameters	4174 / 3 / 214
γ(deg)	90	Goodness-of-fit on F ²	1.035
V(Å ³)	3644.78(19)	Final R indices [I > 2σ(I)]	R1 = 0.0694, wR2 = 0.2006
Z	4	R indices (all data)	R1 = 0.0888, wR2 = 0.2214
Color	Colorless	Largest diff. peak and hole	1.340 and -0.849 e.Å ⁻³
Crystal size	0.10 x 0.07 x 0.05 mm ³		
Density (calculated)	1.501 mg/m ³		

**Product 28: H₉·ZnSiF₆**

Crystallization Method: In a crystallization tube (height = 15 cm, diameter = 0.4 cm), slow diffusion of an ethanol solution (*ca.* 1 mL, 5 mg) of ZnSiF₆·6H₂O into the chloroform solution (1 mL) of the 1,4-bis(pyridin-4-ylthio)butane (**H₉**, 3 mg) with a buffered layer of ethanol (*ca.* 0.1 mL) affords colorless crystals after few days.

Crystallographic data (Lab code: s1540):

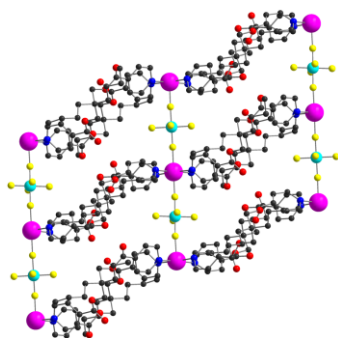
Empirical formula	C ₂₈ H ₃₂ F ₆ N ₄ S ₄ SiZn	Absorption coefficient	0.811 mm ⁻¹
Formula weight	760.28	F(000)	1560
Temperature	173(2) K	Theta range for data collection	1.53 to 27.50°
Wavelength	0.71073 Å	Index ranges	-28 ≤ h ≤ 26, 0 ≤ k ≤ 9, 0 ≤ l ≤ 37
Crystal system	Monoclinic	Reflections collected	12211
Space group	C2/c	Independent reflections	4889 [R(int) = 0.0342]
a(Å)	21.6498(14)	Completeness to theta	96.7 %
b(Å)	7.7080(5)	Absorption correction	Semi-empirical from equivalents
c(Å)	28.670(2)	Max. and min. transmission	0.9683 and 0.9454
α(deg)	90	Refinement method	Full-matrix least-squares on F ²
β(deg)	111.5450(10)	Data / restraints / parameters	4889 / 0 / 201
γ(deg)	90	Goodness-of-fit on F ²	1.075
V(Å ³)	4450.1(5)	Final R indices [I > 2σ(I)]	R1 = 0.0585, wR2 = 0.1894
Z	4	R indices (all data)	R1 = 0.0737, wR2 = 0.2005
Color	Colorless	Largest diff. peak and hole	1.217 and -0.950 e.Å ⁻³
Crystal size	0.07 x 0.06 x 0.04 mm ³		
Density (calculated)	1.135 mg/m ³		

**Product 29:** I1·ZnSiF₆

Crystallization Method: In a crystallization tube (height = 15 cm, diameter = 0.4 cm), slow diffusion of an ethanol solution (*ca.* 1 mL, 5 mg) of ZnSiF₆·6H₂O into the chloroform solution (1 mL) of the 2,2-dimethylpropane-1,3-diyl diisonicotinate (**I1**, 3 mg) with a buffered layer of ethanol (*ca.* 0.1 mL) affords colorless crystals after few days.

Crystallographic data (Lab code: s1518):

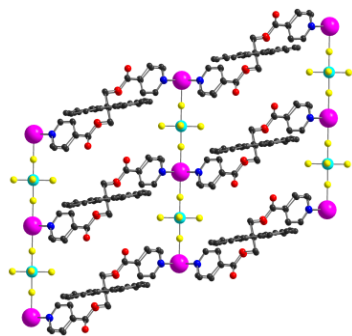
Empirical formula	C ₃₄ H ₃₆ F ₆ N ₄ O ₈ SiZn·2(CHCl ₃)	Absorption coefficient	0.836 mm ⁻¹
Formula weight	1074.86	F(000)	546
Temperature	173(2) K	Theta range for data collection	1.83 to 27.00°
Wavelength	0.71073 Å	Index ranges	-9 ≤ h ≤ 9, -15 ≤ k ≤ 14, 0 ≤ l ≤ 21
Crystal system	Triclinic	Reflections collected	10205
Space group	P-1	Independent reflections	5728 [R(int) = 0.0367]
a(Å)	7.6090(13)	Completeness to theta	96.7 %
b(Å)	12.179(3)	Absorption correction	Semi-empirical from equivalents
c(Å)	16.128(3)	Max. and min. transmission	0.9516 and 0.9137
α(deg)	108.161(6)	Refinement method	Full-matrix least-squares on F ²
β(deg)	97.995(8)	Data / restraints / parameters	5728 / 0 / 286
γ(deg)	102.016(6)	Goodness-of-fit on F ²	1.211
V(Å ³)	1355.1(4) Å ³	Final R indices [I > 2σ(I)]	R1 = 0.1088, wR2 = 0.2448
Z	1	R indices (all data)	R1 = 0.1355, wR2 = 0.2847
Color	colorless	Largest diff. peak and hole	1.660 and -0.889 e.Å ⁻³
Crystal size	0.11 x 0.07 x 0.06 mm ³		
Density (calculated)	1.317 mg/m ³		

**Product 30:** $\text{I2} \cdot \text{ZnSiF}_6$

Crystallization Method: In a crystallization tube (height = 15 cm, diameter = 0.4 cm), slow diffusion of an ethanol solution (*ca.* 1 mL, 5 mg) of $\text{ZnSiF}_6 \cdot 6\text{H}_2\text{O}$ into the chloroform solution (1 mL) of the 2,2-dibutylpropane-1,3-diyl diisonicotinate (**I2**, 3 mg) with a buffered layer of ethanol (*ca.* 0.1 mL) affords colorless crystals after few days.

Crystallographic data (Lab code: e1632):

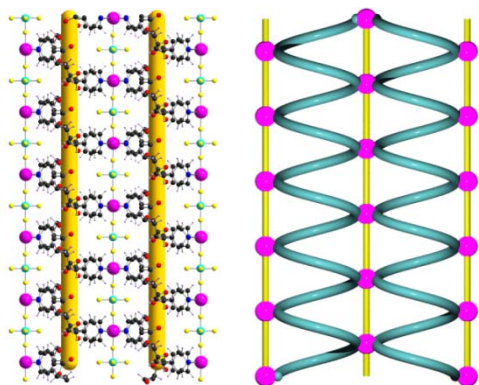
Empirical formula	$\text{C}_{46}\text{H}_{60}\text{F}_6\text{N}_4\text{O}_8\text{SiZn}$	Absorption coefficient	0.454 mm^{-1}
Formula weight	1004.44	F(000)	2104
Temperature	173(2) K	Theta range for data collection	1.77 to 27.53°
Wavelength	0.71073 Å	Index ranges	$-19 \leq h \leq 18$, $0 \leq k \leq 44$, $0 \leq l \leq 16$
Crystal system	Monoclinic	Reflections collected	13643
Space group	P21/c	Independent reflections	13643 [R(int) = 0.0000]
a(Å)	15.3799(14)	Completeness to theta	91.1 %
b(Å)	34.561(3)	Absorption correction	None
c(Å)	12.6340(10)	Max. and min. transmission	0.9732 and 0.9475
α (deg)	90	Refinement method	Full-matrix least-squares on F^2
β (deg)	104.565(3)	Data / restraints / parameters	13643 / 0 / 602
γ (deg)	90	Goodness-of-fit on F^2	1.667
V(Å ³)	6499.7(9) Å ³	Final R indices [$I > 2\sigma(I)$]	R1 = 0.1698, wR2 = 0.4491
Z	4	R indices (all data)	R1 = 0.2027, wR2 = 0.4713
Color	colorless	Largest diff. peak and hole	4.803 and -1.914 e.Å ⁻³
Crystal size	0.12 x 0.06 x 0.06 mm ³		
Density (calculated)	1.026 mg/m ³		

**Product 31: I3·ZnSiF₆**

Crystallization Method: In a crystallization tube (height = 15 cm, diameter = 0.4cm), slow diffusion of an ethanol solution (*ca.* 1 mL, 5 mg) of ZnSiF₆·6H₂O into the chloroform solution (1 mL) of the (9H-fluorene-9,9-diyl)bis(methylene) diisonicotinate (**I3**, 3 mg) with a buffered layer of ethanol (*ca.* 0.1 mL) affords colorless crystals after few days.

Crystallographic data (Lab code: s1637):

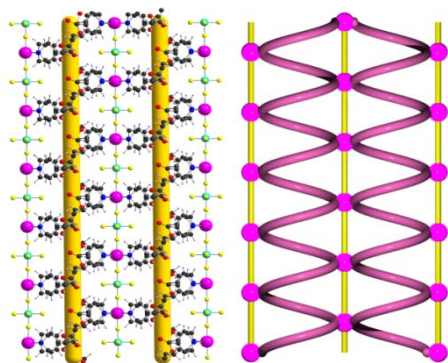
Empirical formula	C ₅₄ H ₄₀ F ₆ N ₄ O ₈ SiZn	Absorption coefficient	0.435 mm ⁻¹
Formula weight	1080.36	F(000)	554
Temperature	173(2) K	Theta range for data collection	1.89 to 27.00°.
Wavelength	0.71073 Å	Index ranges	-9<=h<=9, -16<=k<=16, 0<=l<=23
Crystal system	Triclinic	Reflections collected	15716
Space group	P-1	Independent reflections	7128 [R(int) = 0.0279]
a(Å)	7.6475(3)	Completeness to theta	99.0 %
b(Å)	12.7299(4)	Absorption correction	Semi-empirical from equivalents
c(Å)	18.4901(7)	Max. and min. transmission	0.9828 and 0.9619
α(deg)	81.705(2)	Refinement method	Full-matrix least-squares on F ²
β(deg)	80.949(2)	Data / restraints / parameters	7128 / 0 / 337
γ(deg)	76.461(2)	Goodness-of-fit on F ²	1.033
V(Å ³)	1717.38(11) Å ³	Final R indices [I>2σ(I)]	R1 = 0.0970, wR2 = 0.2515
Z	1	R indices (all data)	R1 = 0.1070, wR2 = 0.2618
Color	colorless	Largest diff. peak and hole	1.460 and -0.884 e.Å ⁻³
Crystal size	0.09 x 0.06 x 0.04 mm ³		
Density (calculated)	1.045 mg/m ³		

**Product 32: J1·ZnSiF₆**

Crystallization Method: In a crystallization tube (height = 15 cm, diameter = 0.4 cm), slow diffusion of an ethanol solution (*ca.* 1 mL, 5 mg) of ZnSiF₆·6H₂O into the chloroform solution (1 mL) of (1S,2S)-cyclohexane-1,2-diyl diisonicotinate (**J1**, 3 mg) with a buffered layer of ethanol (*ca.* 0.1 mL) affords colorless crystals after few days.

Crystallographic data (Lab code: s1345):

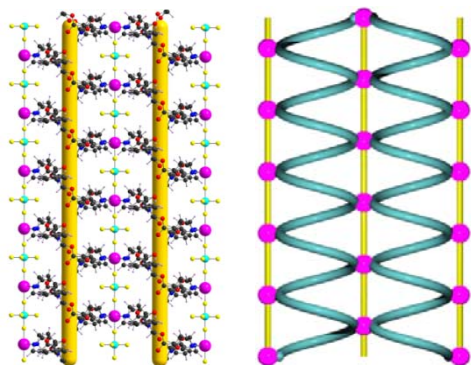
Empirical formula	2(C ₃₆ H ₃₆ F ₆ N ₄ O ₈ SiZn)·2(CH ₃ OH)	Absorption coefficient	0.638 mm ⁻¹
Formula weight	1784.38	F(000)	1840
Temperature	173(2) K	Theta range for data collection	1.44 to 27.50°
Wavelength	0.71073 Å	Index ranges	-9 ≤ h ≤ 9, -27 ≤ k ≤ 27, -36 ≤ l ≤ 26
Crystal system	Orthorhombic	Reflections collected	23640
Space group	C222(1)	Independent reflections	5232 [R(int) = 0.0479]
a(Å)	7.6698(4)	Completeness to theta	99.7 %
b(Å)	21.0303(11)	Absorption correction	Semi-empirical from equivalents
c(Å)	28.3731(11)	Max. and min. transmission	0.9688 and 0.9540
α(deg)	90	Refinement method	Full-matrix least-squares on F ²
β(deg)	90	Data / restraints / parameters	5232 / 10 / 226
γ(deg)	90	Goodness-of-fit on F ²	1.214
V(Å ³)	4576.5(4) Å ³	Final R indices [I > 2σ(I)]	R1 = 0.1400, wR2 = 0.3148
Z	2	R indices (all data)	R1 = 0.1842, wR2 = 0.4087
Color	colorless	Absolute structure parameter	0.002(3)
Crystal size	0.08 x 0.06 x 0.05 mm ³	Largest diff. peak and hole	2.666 and -1.661 e.Å ⁻³
Density (calculated)	1.295 mg/m ³		

**Product 33: J2·ZnSiF₆**

Crystallization Method: In a crystallization tube (height = 15 cm, diameter = 0.4 cm), slow diffusion of an ethanol solution (*ca.* 1 mL, 5 mg) of ZnSiF₆·6H₂O into the chloroform solution (1 mL) of (1R,2R)-cyclohexane-1,2-diyl diisonicotinate (**J2**, 3 mg) with a buffered layer of ethanol (*ca.* 0.1 mL) affords colorless crystals after few days.

Crystallographic data (Lab code: s1360):

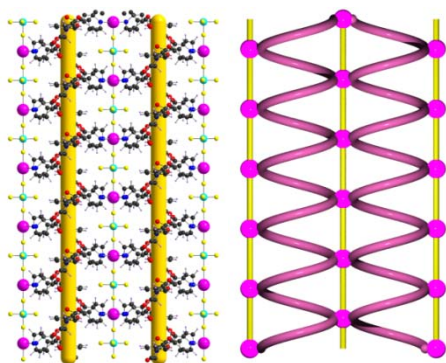
Empirical formula	C ₃₆ H ₃₆ F ₆ N ₄ O ₈ SiZn	Absorption coefficient	0.635 mm ⁻¹
Formula weight	860.15	F(000)	1768
Temperature	173(2) K	Theta range for data collection	1.44 to 27.50°.
Wavelength	0.71073 Å	Index ranges	-9<=h<=9, 0<=k<=27, 0<=l<=36
Crystal system	Orthorhombic	Reflections collected	14563
Space group	C222(1)	Independent reflections	5241 [R(int) = 0.0345]
a(Å)	7.6731(5)	Completeness to theta	99.9 %
b(Å)	21.0006(13)	Absorption correction	Semi-empirical from equivalents
c(Å)	28.3703(19)	Max. and min. transmission	0.9690 and 0.9510
α(deg)	90	Refinement method	Full-matrix least-squares on F ²
β(deg)	90	Data / restraints / parameters	5241 / 17 / 214
γ(deg)	90	Goodness-of-fit on F ²	1.265
V(Å ³)	4571.6(5) Å ³	Final R indices [I>2σ(I)]	R1 = 0.1145, wR2 = 0.2374
Z	4	R indices (all data)	R1 = 0.1441, wR2 = 0.2638
Color	colorless	Absolute structure parameter	0.03(1)
Crystal size	0.08 x 0.06 x 0.05 mm ³	Largest diff. peak and hole	1.528 and -1.468 e.Å ⁻³
Density (calculated)	1.250 mg/m ³		

**Product 34:** J3·ZnSiF₆

Crystallization Method: In a crystallization tube (height = 15 cm, diameter = 0.4 cm), slow diffusion of an ethanol solution (*ca.* 1 mL, 5 mg) of ZnSiF₆·6H₂O into the CH₂ClCH₂Cl solution (1 mL) of (3R,4R)-N-phenyl-3,4-isonicotinoyl-2,5-dioxopyrrolidines (**J3**, 3 mg) with a buffered layer of ethanol (*ca.* 0.1 mL) affords colorless crystals after few days.

Crystallographic data (Lab code: s1571):

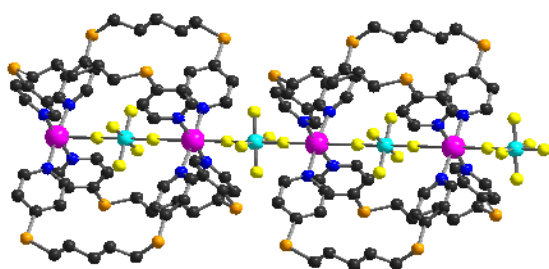
Empirical formula	2(C ₄₄ H ₃₀ F ₆ N ₆ O ₁₂ SiZn)·5(C ₂ H ₆ O)·H ₂ O	Absorption coefficient	0.519 mm ⁻¹
Formula weight	2332.76	F(000)	1200
Temperature	173(2) K	Theta range for data collection	1.72 to 27.62°
Wavelength	0.71073 Å	Index ranges	-31 ≤ h ≤ 31, -8 ≤ k ≤ 9, -21 ≤ l ≤ 20
Crystal system	Monoclinic	Reflections collected	24061
Space group	C2	Independent reflections	6428 [R(int) = 0.0304]
a(Å)	24.0625(16)	Completeness to theta	99.2 %
b(Å)	7.6315(4)	Absorption correction	Semi-empirical from equivalents
c(Å)	16.3387(10)	Max. and min. transmission	0.9745 and 0.9547
α(deg)	90	Refinement method	Full-matrix least-squares on F ²
β(deg)	99.928(3)	Data / restraints / parameters	6428 / 5 / 375
γ(deg)	90	Goodness-of-fit on F ²	1.028
V(Å ³)	2955.4(3) Å ³	Final R indices [I > 2σ(I)]	R1 = 0.0542, wR2 = 0.1541
Z	1	R indices (all data)	R1 = 0.0625, wR2 = 0.1602
Color	colorless	Absolute structure parameter	0.023(2)
Crystal size	0.09 x 0.07 x 0.05 mm ³	Largest diff. peak and hole	1.091 and -0.373 e.Å ⁻³
Density (calculated)	1.311 mg/m ³		

**Product 35: J4·ZnSiF₆**

Crystallization Method: In a crystallization tube (height = 15 cm, diameter = 0.4 cm), slow diffusion of an ethanol solution (*ca.* 1 mL, 5 mg) of ZnSiF₆·6H₂O into the chloroform solution (1 mL) of (3S,4S)-N-phenyl-3,4-isonicotinoyl-2,5-dioxopyrrolidines (**J4**, 3 mg) with a buffered layer of ethanol (*ca.* 0.1 mL) affords colorless crystals after few days.

Crystallographic data (Lab code: s1382):

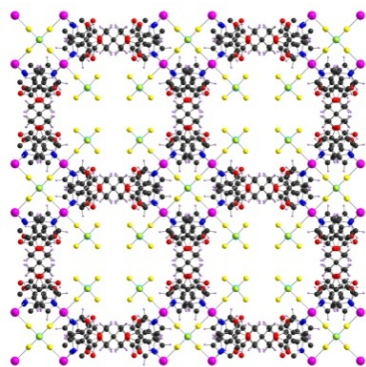
Empirical formula	C ₄₄ H ₃₀ F ₆ N ₆ O ₁₂ SiZn	Absorption coefficient	0.516 mm ⁻¹
Formula weight	1042.20	F(000)	1060
Temperature	173(2) K	Theta range for data collection	1.25 to 27.54°
Wavelength	0.71073 Å	Index ranges	-29<=h<=29, -9<=k<=9, 0<=l<=21
Crystal system	Monoclinic	Reflections collected	13609
Space group	C2	Independent reflections	5723 [R(int) = 0.0546]
a(Å)	23.3869(7)	Completeness to theta	94.7 %
b(Å)	7.6246(3)	Absorption correction	Semi-empirical from equivalents
c(Å)	16.5705(6)	Max. and min. transmission	0.9697 and 0.9406
α(deg)	90	Refinement method	Full-matrix least-squares on F ²
β(deg)	100.067(2)	Data / restraints / parameters	5723 / 1 / 318
γ(deg)	90	Goodness-of-fit on F ²	1.026
V(Å ³)	2909.29(18) Å ³	Final R indices [I>2σ(I)]	R1 = 0.0678, wR2 = 0.1700
Z	2	R indices (all data)	R1 = 0.0994, wR2 = 0.1874
Color	colorless	Absolute structure parameter	0.039(19)
Crystal size	0.12 x 0.09 x 0.06 mm ³	Largest diff. peak and hole	0.403 and -0.872 e.Å ⁻³
Density (calculated)	1.190 mg/m ³		

**Product 36: K1·ZnSiF₆**

Crystallization Method: In a crystallization tube (height = 15 cm, diameter = 0.4 cm), slow diffusion of an ethanol solution (*ca.* 1 mL, 5 mg) of ZnSiF₆·6H₂O into the chloroform solution (1 mL) of the 1,5-bis(pyridin-4-ylthio)pentane (**K1**, 3 mg) with a buffered layer of ethanol (*ca.* 0.1 mL) affords colorless crystals after few days.

Crystallographic data (Lab code: s1481):

Empirical formula	C ₃₀ H ₃₆ F ₆ N ₄ S ₄ SiZn·2(C ₂ H ₆ O)	Absorption coefficient	0.907 mm ⁻¹
Formula weight	880.46	F(000)	1832
Temperature	173(2) K	Theta range for data collection	1.81 to 27.55°
Wavelength	0.71073 Å	Index ranges	-16 ≤ h ≤ 20, -20 ≤ k ≤ 15, -20 ≤ l ≤ 20
Crystal system	Tetragonal	Reflections collected	10010
Space group	I4/m	Independent reflections	2417 [R(int) = 0.0644]
a(Å)	15.930(2)	Completeness to theta	99.3 %
b(Å)	15.930(2)	Absorption correction	Semi-empirical from equivalents
c(Å)	15.941(4)	Max. and min. transmission	0.9228 and 0.9148
α(deg)	90	Refinement method	Full-matrix least-squares on F ²
β(deg)	90	Data / restraints / parameters	2417 / 12 / 133
γ(deg)	90	Goodness-of-fit on F ²	1.002
V(Å ³)	4045.3(12) Å ³	Final R indices [I > 2σ(I)]	R1 = 0.0491, wR2 = 0.1194
Z	4	R indices (all data)	R1 = 0.1147, wR2 = 0.1495
Color	colorless	Largest diff. peak and hole	1.249 and -0.803 e.Å ⁻³
Crystal size	0.10 x 0.09 x 0.09 mm ³		
Density (calculated)	1.446 mg/m ³		

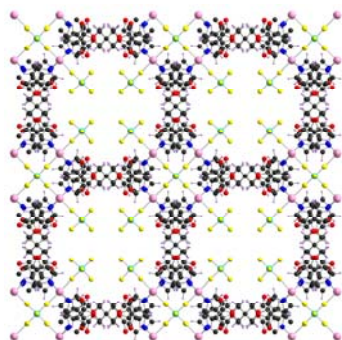


Crystallographic data (Lab code: s1308):

Empirical formula	$C_{58}H_{48}F_{18}N_8O_{14}Si_3Zn_2$	Absorption coefficient	0.393 mm^{-1}
Formula weight	1638.05	F(000)	1656
Temperature	173(2) K	Theta range for data collection	1.22 to 27.50°
Wavelength	0.71073 Å	Index ranges	$0 \leq h \leq 21, 0 \leq k \leq 21, 0 \leq l \leq 35$
Crystal system	Tetragonal	Reflections collected	21625
Space group	P-4c2	Independent reflections	8636 [R(int) = 0.1403]
a(Å)	16.6826(6)	Completeness to theta	99.7 %
b(Å)	16.6826(6)	Absorption correction	Semi-empirical from equivalents
c(Å)	27.249(2)	Max. and min. transmission	0.9806 and 0.9693
α (deg)	90	Refinement method	Full-matrix least-squares on F^2
β (deg)	90	Data / restraints / parameters	8636 / 12 / 146
γ (deg)	90	Goodness-of-fit on F^2	1.169
V(Å ³)	7583.7(7) Å ³	Final R indices [$I > 2\sigma(I)$]	R1 = 0.1355, wR2 = 0.2998
Z	2	R indices (all data)	R1 = 0.2239, wR2 = 0.3331
Color	colorless	Absolute structure parameter	0.05(2)
Crystal size	0.08 x 0.05 x 0.05 mm ³	Largest diff. peak and hole	1.259 and -1.550 e.Å^{-3}
Density (calculated)	0.717 mg/m ³		

Product 37: L1·ZnSiF₆

Crystallization Method: In a crystallization tube (height = 15 cm, diameter = 0.4 cm), slow diffusion of an ethanol solution (*ca.* 1 mL, 5 mg) of ZnSiF₆·6H₂O into the chloroform solution (1 mL) of 2,2-bis(isonicotinoyloxymethyl)propane-1,3-diyl diisonicotinate (**L1**, 3 mg) with a buffered layer of DMSO (*ca.* 0.1 mL) affords colorless crystals after few days.

**Product 38: L1·CoSiF₆**

Crystallization Method: In a crystallization tube (height = 15 cm, diameter = 0.4 cm), slow diffusion of a methanol solution (*ca.* 1 mL, 3 mg) of CoSiF₆ into the chloroform solution (1 mL) of 2,2-bis(isonicotinoyloxymethyl)propane-1,3-diyl diisonicotinate (**L1**, 3 mg) with a buffered layer of DMSO (*ca.* 0.1 mL) affords purple crystals after few days.

Crystallographic data (Lab code: e1798):

Empirical formula	C ₂₉ H ₂₄ F ₉ N ₄ O ₇ Si _{1.5} Co	Absorption coefficient	0.305 mm ⁻¹
Formula weight	812.59	F(000)	1644
Temperature	173(2) K	Theta range for data collection	1.90 to 27.78°
Wavelength	0.71073 Å	Index ranges	0 ≤ h ≤ 21, 0 ≤ k ≤ 21, 0 ≤ l ≤ 34
Crystal system	Tetragonal	Reflections collected	28509
Space group	P-4c2	Independent reflections	7002 [R(int) = 0.1160]
a(Å)	16.5070(6)	Completeness to theta	92.0 %
b(Å)	16.5070(6)	Absorption correction	Semi-empirical from equivalents
c(Å)	26.939(2)	Max. and min. transmission	0.9849 and 0.9760
α(deg)	90	Refinement method	Full-matrix least-squares on F ²
β(deg)	90	Data / restraints / parameters	7002 / 18 / 146
γ(deg)	90	Goodness-of-fit on F ²	1.180
V(Å ³)	7340.4(7) Å ³	Final R indices [I > 2σ(I)]	R1 = 0.1724, wR2 = 0.3868
Z	4	R indices (all data)	R1 = 0.2221, wR2 = 0.4230
Color	purple	Absolute structure parameter	0.00
Crystal size	0.08 x 0.05 x 0.05 mm ³	Largest diff. peak and hole	2.179 and -1.119 e.Å ⁻³
Density (calculated)	0.735 mg/m ³		

6.4. References

1. M. Tanner, A. Ludi, *Chimia*, **1980**, 34: 23-24.
2. K. Biradha and M. Fujita, *J. Chem. Soc., Dalton Trans.*, **2000**, 3805-3810.
3. K. Biradha and M. Fujita, *Chem. Commun.*, **2001**, 15-16.
4. P. H. Dinolfo, M. E. Williams, C. L. Stern, J. T. Hupp, *J. Am. Chem. Soc.*, **2004**, 126: 12989-13001.
5. D. K. Chand, K. Biradha, M. Kawano, S. Sakamoto, K. Yamaguchi, M. Fujita, *Chem. Asian. J.*, **2006**, 1: 82-90.
6. J.-P. Bourgeois, M. Fujita, M. Kawano, S. Sakamoto, K. Yamaguchi, *J. Am. Chem. Soc.*, **2003**, 125: 9260-9261.
7. M. Hong, Y. Zhao, W. Su, R. Cao, M. Fujita, Z. Zhou, A. S. C. Chan, *J. Am. Chem. Soc.*, **2000**, 122: 4819-4820.
8. Y. -B. Xie, J. -R. Li, C. Zhang, X. -H. Bu, *Crystal Growth & Design*, **2005**, 5: 1743-1749.
9. D. Pocic, *PhD thesis*, Université Louis Pasteur de Strasbourg, **2005**.
10. P. Grosshans, *PhD thesis*, Université Louis Pasteur de Strasbourg, **2005**.
11. K. Yamashita, K. Sato, M. Kawano, M. Fujita, *New J. Chem.*, **2009**, 33: 264 - 270.
12. H. Meier, D. Ickenroth, U. Stalmach, K. Koynov, A. Bahtiar, C. Bubeck, *Eur. J. Org. Chem.* **2001**, 4431-4443.
13. A. M. Kendhale, R. Gonnade, P. R. Rajamohanam, H. J. Hofmann, G. J. Sanjayan, *Chem. Commun.*, **2008**, 2541-2543.
14. R. Y. Zou, F. B. Xu, Q. S. Li, Z. Z. Zhang, *Acta Crystallogr.* **2003**, E59: o1451- o1452.
15. A. M. d'A. Rocha Gonsalves, M. E. S. Serra, D. Murtinho, V. F. Silva, A. Matos Beja, J. A. Paixão, M. Ramos Silva, L. Alte da Veiga, *J. Mol. Catal. A: Chem.*, **2003**, 195: 1-9.
16. S. Samanta, *PhD thesis*, Georgia Institute of Technology, **2007**.

PUBLICATIONS

Publications

A) PUBLICATIONS

1. **M. J. Lin**, A. Jouaiti, N. Kyritsakas, M. W. Hosseini, "Molecular tectonics: from 1-D interwoven racemic chains to quadruple stranded helices", *ChemCommun.*, **2010**, 115-117. ([download.pdf](#)). (*Enhanced HTML article*)
2. **M. J. Lin**, A. Jouaiti, D. Pocic, N. Kyritsakas, J. M. Planeix, M. W. Hosseini, "Molecular tectonics: tubular crystals with controllable channel size and orientation", *ChemCommun.*, **2010**, 112-114. ([download.pdf](#)). (*Enhanced HTML article*)
3. **M. J. Lin**, A. Jouaiti, N. Kyritsakas, M. W. Hosseini, "Molecular tectonics: chaining cages into a 1-D coordination network", *CrystEngCommun.*, **2010**, 12, 67-69. ([download.pdf](#)). (*hot paper*)
4. **M. J. Lin**, A. Jouaiti, N. Kyritsakas, M. W. Hosseini, "Molecular tectonics: modulation of size and shape of cuboid 3-D coordination networks", *CrystEngCommun.*, **2009**, 11, 189-191. ([download .pdf](#))

B) MANUSCRIPTS IN PREPARATION

1. **M. J. Lin**, A. Jouaiti, P. Grosshans, N. Kyritsakas, M. W. Hosseini, "Molecular tectonics: Tubular 2-D coordination networks with enantiomerically pure single-stranded helical walls"
2. **M. J. Lin**, A. Jouaiti, N. Kyritsakas, M. W. Hosseini, "Molecular tectonics: 2-D and 3-D tubular coordination networks"

C) CONFERENCE

1. **M. J. Lin**, A. Jouaiti, M. W. Hosseini, "Porous Metal-Organic Framework Based on SiF_6 Pillars", *4th FuMaSSEC Workshop*, Barcelona, Spain, Apr. 18-21, **2009**. (Oral presentation)
2. **M. J. Lin**, A. Jouaiti, N. Kyritsakas, M. W. Hosseini, "Porous Metal-Organic Frameworks Based on SiF_6^{2-} Pillars ", *1st International Conference on Metal-Organic Frameworks and Open Framework Compounds*, Augsburg, Germany, Oct. 8-10, **2008**. (Poster presentation)
3. **M. J. Lin**, A. Jouaiti, N. Kyritsakas, M. W. Hosseini, "Porous Metal-Organic Frameworks Based on SiF_6^{2-} Pillars ", *2nd Karlsruhe-Strasbourg bilateral meetings on progress in Supramolecular Chemistry*, Karlsruhe, Germany, Dec. 5, **2008**. (Oral presentation)
4. **M. J. Lin**, A. Jouaiti, M. W. Hosseini, "Progress in Coordination Networks Based on SiF_6 Pillars", *3rd FuMaSSEC Workshop*, Nottingham, UK, Jul. 7-8, **2008**. (Oral presentation)
5. **M. J. Lin**, A. Jouaiti, M. W. Hosseini, "Naphthalene Based Coordination Networks ", *2nd FuMaSSEC Workshop*, Strasbourg, France, Jan. 15-16, **2008**. (Oral presentation)

Abstract

In this PhD work, the strategy called *molecular tectonic*, which combines molecular recognition processes with iterative self-assembly events, has been used for the design and formation of coordination networks in the solid state.

With the aim of forming porous materials in the crystalline state offering tailored cavities, the self-assembly strategy based on combinations of SiF_6^{2-} anion, Zn^{2+} dication and a variety of bridging organic ligand has been studied. Depending on the nature (rigidity, length, chirality and denticity) of the bridged organic tectons, the formation of 1-D, 2-D and 3-D architectures offering inner cavities and different topologies was demonstrated. The new generated architectures have been characterized by physical-chemical methods, including XRD techniques (Single crystal and Powder). The stability of the coordination networks is improved by several approaches, including using different metal cations, functionalizing rigid organic tectons, designing new rigid tectons serving as diagonal of the formed cuboid 3-D architecture as well as controlling the packing of 2-D networks.

Key words

Supramolecular chemistry, molecular tectonics, coordination network, self-assembly, molecular recognition, inorganic anions, SiF_6^{2-} pillar, porosity, Structure analysis

Résumé

Dans ce travail, la stratégie dite de *tectonique moléculaire*, qui combine la reconnaissance moléculaire avec le processus itératif d'auto-assemblage, a été utilisée pour la conception et la création de réseaux moléculaires de coordination à l'état solide.

Dans le but de former des matériaux poreux à l'état cristallin offrant des cavités de tailles modulable, la stratégie d'auto-assemblage basée sur des combinaisons de l'anion SiF_6^{2-} , du dication Zn^{2+} et une variété de tectons organique pontant a été étudiée. Selon la nature (rigidité, la longueur, la chiralité et le nombre de pôle coordinant) du tecton pontant organique utilisé, la formation de réseaux moléculaires 1-D, 2-D et 3-D offrant des cavités intérieures et de topologies différentes a été démontrée. Les nouvelles architectures formées ont été caractérisées par des méthodes physico-chimiques, y compris les techniques de diffraction RX (monocristal et poudre). La stabilité des réseaux de coordination est améliorée par plusieurs approches, notamment en utilisant d'autres métaux, par la fonctionnalisation des tectons organiques, par la conception de nouveaux tectons rigides adoptant une position diagonale dans une architecture de forme cuboïde ainsi que par le contrôle de l'empilement des réseaux moléculaires 2-D.

Mots clés

Chimie supramoléculaire, tectonique moléculaire, réseau de coordination, auto-assemblage, reconnaissance moléculaire, anions inorganiques, SiF_6^{2-} pilier, porosité, analyse structurale